Summer 7-13-2014

Designing Transition Metal Surfaces for Their Adsorption Properties and Chemical Reactivity

Matthew M. Montemore
University of Colorado Boulder, montemor@colorado.edu

Designing Transition Metal Surfaces for their Adsorption Properties and Chemical Reactivity

by

Matthew M. Montemore

BA, Grinnell College, 2009

MS, University of Colorado Boulder, 2011

A thesis submitted to the

Faculty of the Graduate School of the

University of Colorado in partial fulfillment

of the requirements for the degree of

Doctor of Philosophy

Department of Mechanical Engineering

2014

This thesis entitled:
Designing Transition Metal Surfaces for their Adsorption Properties and Chemical Reactivity
written by Matthew M. Montemore
has been approved for the Department of Mechanical Engineering

J. Will Medlin

John W. Daily

Date

The final copy of this thesis has been examined by the signatories, and we find that both the content and the form meet acceptable presentation standards of scholarly work in the above mentioned discipline.

Montemore, Matthew M. (PhD, Mechanical Engineering)

Designing Transition Metal Surfaces for their Adsorption Properties and Chemical Reactivity

Thesis directed by Prof. J. Will Medlin

Many technological processes, such as catalysis, electrochemistry, corrosion, and some materials synthesis techniques, involve molecules bonding to and/or reacting on surfaces. For many of these applications, transition metals have proven to have excellent chemical reactivity, and this reactivity is strongly tied to the surface's adsorption properties. This thesis focuses on predicting adsorption properties for use in the design of transition metal surfaces for various applications.

First, it is shown that adsorption through a particular atom (e.g, C or O) can be treated in a unified way. This allows predictions of all C-bound adsorbates from a single, simple adsorbate, such as CH_3. In particular, consideration of the adsorption site can improve the applicability of previous approaches, and gas-phase bond energies correlate with adsorption energies for similarly bound adsorbates.

Next, a general framework is presented for understanding and predicting adsorption through any atom. The energy of the adsorbate's highest occupied molecular orbital (HOMO) determines the strength of the repulsion between the adsorbate and the surface. Because adsorbates with similar HOMO energies behave similarly, their adsorption energies correlate. This can improve the efficiency of predictions, but more importantly it constrains catalyst design and suggests strategies for circumventing these constraints. Further, the behavior of adsorbates with dissimilar HOMO energies varies in a systematic way, allowing predictions of adsorption energy differences between any two adsorbates. These differences are also useful in surface design.

In both of these cases, the dependence of adsorption energies on surface electronic properties is explored. This dependence is used to justify the unified treatments mentioned above, and is used to gain further insight into adsorption. The properties of the surface's d band and p band control variations in adsorption energy, as does the strength of the adsorbate-surface coupling. A single

equation, with only a single adsorbate-dependent fitting parameter as well as a few universal fitting parameters, is developed that can predict the adsorption energy of any radical on any close-packed transition metal surface. The surface electronic properties that are input into this equation can be estimated based on the alloy structure of the surface, improving prospects for high-throughput screening and rational catalyst design.

The methods discussed in this thesis are used to design a novel catalyst for ethylene epoxidation, which is experimentally synthesized and tested. Initial tests indicate that this catalyst may have improved selectivity over pure Ag.

Dedication

To all the giants, both in science and in my life, on whose shoulders I am standing.

Acknowledgements

They say it takes a village to raise a child, and it also seems to take one to earn a PhD. I owe a huge debt of gratitude to all those who have listened to me hash out my ideas, those who have given me ideas, and those who have gently nudged me back on the right path when I was getting too far out there. This includes the entire Medlin group, particularly Simon Pang, Tania Tauer, Meghana Rangan, Rhea Williams, and Carolyn Schoenbaum. I've also greatly enjoyed collaborating with and learning from Mike Griffin, Troy Gould, Alia Lubers, Allison Robinson, and Lucas Ellis. Of course, Will Medlin has been my guiding light throughout this whole grad school thing, and I couldn't have asked for a better advisor. I deeply appreciate the support of friends and family, including my parents, Virginia Anderson, and Janet McCombs. I'd also like to thank my committee: Rishi Raj, Charles Musgrave, Sehee Lee, and particularly my coadvisor John Daily. The staffs of both the Mechanical Engineering and Chemical Engineering departments, particularly Sharon Anderson, have been nothing but helpful and fun throughout my time here. I appreciate the support from the National Science Foundation and the Colorado Center for Biorefining and Biofuels. Finally, I'd like to thank all the great teachers I've had over the years, both in and out of school, especially Mr. Martin (second grade), Mr. Runyan (high school calculus), and Paul Tjossem (my undergraduate advisor).

Contents

Chapter

Tables

Table

Figures

Figure

Chapter 1

Introduction

1.1 Motivation

1.1.1 Technologies Involving Adsorption on Transition Metals

This thesis is focused on the bonding of various molecules to transition metal surfaces. Not only does this provide insight into the nature of chemical bonding, but it is applicable to many technologies. Adsorption plays a vital role in many processes, including corrosion and oxidation of materials, graphene deposition, and surface functionalization (e.g., coating particles to make them biocompatible). The most important application, however, is the use of surfaces as catalysts. In short, this thesis is a study of the adsorption properties of transition metals, primarily intended to aid in the design of catalytic surfaces.

Catalysis forms a large part of the global economy, generating about $900 billion in products every year [1]. Since most modern products involve synthetic materials, and catalysis is used to create many of these materials, catalysis is interwoven into many industries. Broadly, fuels and chemicals are the largest applications, although there are many other examples, including the catalytic converters found in most cars. The Haber-Bosch process, which involves heterogeneous catalysis and is used in the synthesis of fertilizer, has been called the most important invention of the 20th century [2], as it has allowed for significant increases in crop yields.

Catalysis also plays a key role in many clean energy technologies. For example, one of the primary impediments to the commercialization of hydrogen fuel cells is that they require expensive

Pt-based catalysts. Replacing Pt with a cheaper or more effective material could significantly reduce their cost. For biofuels and biochemicals, one of the primary technological challenges is selectively converting feedstocks, which often have a variety of multifunctional components, into desired products. In general, an effective catalyst can dramatically improve the energy efficiency of a process by reducing the amount of heat necessary or reducing the need for separation steps.

Many of these processes use a heterogeneous catalyst, meaning that the catalyst is in a different phase than the reactants and products. Most often, this involves gaseous or liquid reactants and a solid catalyst. Heterogeneous catalysis does not require a step to separate the catalyst from the products, which is beneficial as separations are often expensive and energy intensive. Heterogenous catalysts are usually transition metals or transition metal compounds (e.g., oxides or sulfides), and transition metals are the focus of this thesis. To increase the surface area of the catalyst, it is usually synthesized as nanoparticles dispersed on a porous support, such as Al_2O_3. Microporous materials, such as zeolites, may also be used as catalysts, but these are not discussed in this work.

Much of the work presented in this thesis will be fundamental and general, with applications to a wide variety of technologies and processes. However, for concreteness we will briefly describe a few specific applications.

Hydrogen fuel cells generate electricity by converting H_2 and O_2 into H_2O, and are potentially a clean way of producing power. At the cathode, O_2 is reduced by protons to form H_2O. It has proven difficult to design an inexpensive material that catalyzes this reaction and is stable in the harsh, electrochemical conditions [3]. As Pt is one of the few materials that is an effective cathode, much of the research has focused on understanding why it works well and modifying it to improve its performance.

The synthesis of hydrocarbon fuels from CO_2 provides a possible route to an environmentally benign transportation system with relatively little change to the current infrastructure. It has been known for decades that this reaction can be done electrochemically [4]. However, the process suffers from poor selectivity and poor activity, and has only recently gained significant research attention.

Cu is the best monometallic catalyst, and has received the highest amount of research.

Fischer-Tropsch synthesis has long been used to convert synthesis gas (CO and H_2) into hydrocarbon fuels. It has more recently been proposed as part of a series of reactions to convert biomass into fuels. It is a notoriously complex reaction, as a large number of products are formed [5, 6]. The primary considerations are breaking the C−O bond and growing the hydrocarbon chain (i.e., producing primarily long hydrocarbons and little methane). The most effective catalytic materials are Fe, Co, and Ru.

Ethylene epoxidation, which involves the conversion of ethylene into ethylene oxide, is a widely used industrial process. Most materials will catalyze both the combustion of ethylene and its conversion to ethylene oxide, and hence selectivity is the primary consideration. Currently, Ag (with promotors) is used in this process, and this reaction has been intensively studied [7]. Due to the widespread use of this process, it is still an area of active research, and further improvements in the catalysts are highly desirable.

1.1.2 Difficulties in Designing Transition Metal Surfaces for Chemistry

Because of the technological and scientific importance of surface reactions, much research has been devoted to the design of surfaces with desirable properties. However, several factors impede the design of the optimal surface: the complexity of the system, the difficulties for experimental probes, the large design space, and the difficulty of high-throughput screening.

A catalytic surface under reaction conditions is dynamic and complex. At first blush, it may seem simple: reactants adsorb from the gas or liquid phase, react, and desorb as products. However, each adsorbed species interacts with the surface as well as other adsorbed species (through both direct interactions and surface-mediated interactions), and the surface's electronic and geometric properties are changed by the presence of adsorbates. Subsurface oxygen, carbon, or hydrogen may also form. The motion of the atoms is likely to be many orders of magnitude faster than the elementary steps of the chemical reactions, which in turn are often fast compared to macroscopic timescales. There are also temperature and pressure effects, support effects, and the effect of the

size and shape of the nanoparticles (which may change under reaction conditions).

This complexity makes it difficult to gain an atomic-level, mechanistic understanding of a surface reaction. Experimental measurements are impeded by the high pressure, complex morphology of a supported catalyst, and the small length scales. Theoretical approaches are impeded by the large number of atoms and the difference in timescale between vibrational motion and chemical reaction. When it comes to the length scale, experimental and theoretical approaches have opposite problems: it is difficult to experimentally measure quantities on the atomic scale, while it is difficult to include a large number of atoms in a theoretical framework. Hence, the approaches are highly complementary, and using both experimental and theoretical frameworks is often much more powerful than either alone.

Even if a reaction is well-understood, it can be difficult to apply this understanding to the large combinatorial space of possible surfaces. Even if only a single bimetallic structure is considered, such as a monolayer of metal A on metal B, there are hundreds of possible permutations of different transition metals, and in many cases these do not act as weighted averages of the constituent pure metals. Accounting for different structures and the possibility of combining more than two metals, the combinatorial space quickly becomes enormous, on the order of 10^4 or 10^5 different surfaces. Aside from the metallic surface itself, the support, promoters, and the reaction conditions can all affect catalytic performance.

In principle, high-throughput screening can be applied without a strong understanding of a reaction. However, high-throughput screening is also a challenge for catalytic systems, although there have been significant strides in this area. Synthesizing, characterizing, and testing a catalyst is generally a fairly expensive and time-consuming process. Directly computing rates using quantum calculations can be done, but this is too slow to be used for high-throughput screening.

1.1.3 Approaches to Studying Surface Reactions

Traditionally, studies of catalysts have involved characterizing the material and measuring its catalytic performance. However, these studies do not often provide sufficient insight into materials

design. Because of the importance and complexity of reactive surfaces, several approaches have been used to gain the kind of understanding needed for design. These approaches include studies of model systems, improved experimental probes, and computational techniques.

One approach is to reduce the complexity of the system. So-called surface science approaches study a single crystal with a single exposed facet (e.g., Pt(111)), pump down the atmosphere to ultrahigh vacuum ($\approx 10^{-10}$ Torr), and dose a well-controlled amount of reactant. This allows the use of various surface level spectroscopies and allows many factors to be controlled, giving a much clearer picture of the molecules on the surface. These techniques can give information on the elementary steps and reaction pathways [8, 9].

Recently, techniques have become available that allow surfaces to be studied in conditions closer to those experienced during reaction. For example, sum frequency generation is a vibrational spectroscopy that allows inspection of the surface species even under relatively high pressure [10, 11]. Similarly, ambient pressure x-ray photoelectron spectroscopy, performed at a synchrotron, can give surface-sensitive information at higher pressures [11, 12]. These techniques provide new insight into how surfaces and surface species behave under reaction conditions.

Computational studies have become an important part of catalysis and surface science. With the advent of powerful computers and efficient techniques such as density functional theory, the calculation of the properties of simple surface systems has become routine. Because these calculations give detailed, atomic-level insight into reactions, they can be powerful complements to experiments [13]. By calculating the energetics of various intermediates and transition states, predictions can be made of reaction pathways and key intermediates.

1.1.4 Approaches to Surface Design

Even if a reaction is fairly well understood, this understanding must still be translated into design principles or paradigms. This can be highly reaction dependent. For example, the orientation of an adsorbate may play a large role in the selectivity of a particular reaction [14], but in other cases there is no orientation effect. Even so, several general strategies have emerged.

Experimental high-throughput screening can be powerful in certain cases [15]. For example, by synthesizing a so-called composition-spread alloy film, the composition space for a particular set of 2 or 3 metals can be quickly explored [16]. Dozens of materials can be tested fairly efficiently using array channel microreactors [17] or by detecting products using laser ionization [18]. However, it is simply not possible to test every potential catalyst using experimental methods, and strategies to direct these searches are necessary. Further, potentially useful catalysts can be missed in the mass of data if there is no direction to the search, and catalyst lifetime is difficult to screen using these methods.

Computationally, multi-scale modeling can be used to bridge the gap between quantum chemical calculations and macroscopic behavior [19]. Multi-scale approaches range from fairly simple kinetic models, such as the mean-field approximation, to computationally intensive Monte Carlo simulations. These approaches are often necessary to translate quantum chemical calculations into catalytic performance. However, they can require significant computational effort.

Perhaps the most successful paradigm in surface design has been the identification of simple descriptors that correlate with catalytic performance. For example, an adsorption energy or electronic property may be used to much more quickly gain a rough idea of a surface's reactivity. These descriptors may be identified using multi-scale modeling, but once they are identified they are often used as standalone design parameters. This paradigm is a large part of the motivation for the current thesis.

1.1.5 The Current Approach: Importance of Adsorption Strength for Predicting Surface Reactivity

It has become clear that the link between adsorption energies and catalytic performance can often dramatically improve the prospects for designing and screening surfaces. Designing a surface for its adsorption properties is generally much simpler than attempting to directly consider the catalytic performance, and calculating an adsorption energy is orders of magnitude faster than calculating a reaction rate.

Adsorption energies have been shown to predict catalytic performance in a wide variety of cases. This is most obvious in catalytic or electrocatalytic reactions that follow the Sabatier principle [20]. As can be seen in Fig. 1.1, the best catalyst is often the one that binds the relevant adsorbates with an intermediate adsorption strength. The usual reasoning is that if adsorbates bind too strongly, they will crowd and poison the surface. If they bind too weakly, the activation energies will be high and the rate will slow. The Sabatier principle has been shown to hold for a wide variety of simple reactions [21–28].

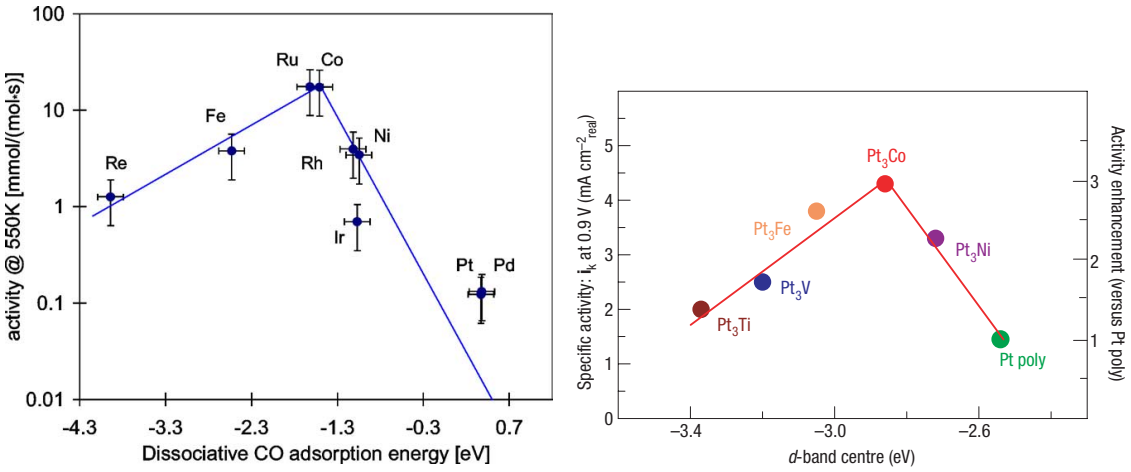

(a) (b)

Figure 1.1: Volcano plots depicting the Sabatier principle, which states that the most active catalyst binds the relevant intermediates moderately. In both cases, the x-axis is a measure of adsorption energy and the y-axis is a measure of catalytic activity. a) CO methanation, from Ref. 29. b) Electrochemical oxygen reduction, from Ref. 30.

Part of the reason that adsorption energies can predict catalytic performance is because activation energies, which largely control rates, are correlated with adsorption energies—this is the reason that surfaces that adsorb intermediates weakly have high barriers. These correlations, called Brønsted-Evans-Polanyi (BEP) relations, have been observed for many reactions, and some examples are shown in Fig. 1.2. Further details on the link between adsorption properties and reactivity are given in Chapter 2.

While simple design parameters are desirable and often effective, in some cases these

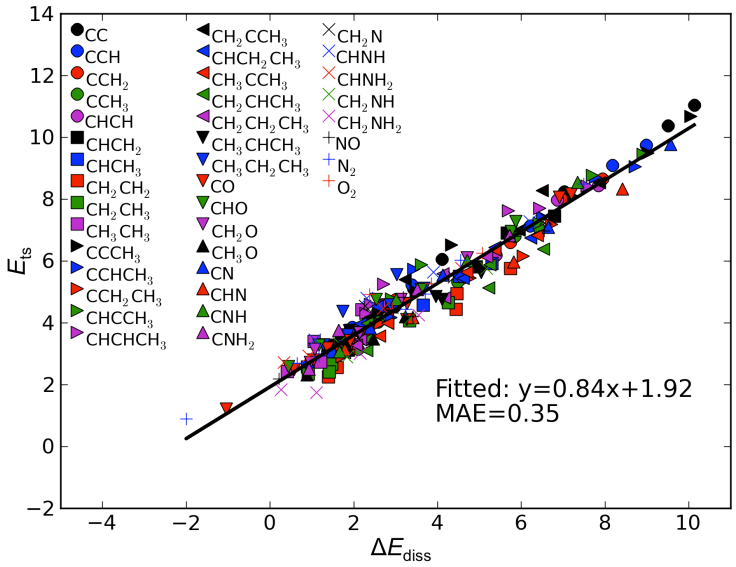

Figure 1.2: BEP relations for a variety of dissociation reactions, demonstrating that activation energies can be estimated from adsorption energies. From Ref. 31.

parameters have been taken too literally. For example, the average energy of the d electrons is often used to predict adsorption energies, but it has been shown that this quantity is not enough to predict catalytic performance when considering a variety of metals [32]. One of the goals of the current work is to improve the applicability and accuracy of simple ideas that have been developed previously. In particular, scaling relations and the d-band model, both of which pervade theoretical catalysis and surface science, are extended to account for more factors.

1.2 Roadmap

Broadly, this work seeks to understand and predict adsorption energies. We will begin with a study of adsorption through C atoms, and provide a unified framework for understanding and predicting adsorption energies for adsorption through a single type of atom (Chapters 4-7). Next, we look at relationships between adsorption through different types of atoms (Chapters 7-8). Finally, we seek to apply this to the design of catalytic surfaces (Chapter 7) and to dramatically increase the efficiency of predictions (Chapter 8). The structure of this thesis is shown in Fig. 1.3.

More specifically, chapters 4-6 have two primary goals: detailed studies of hydrocarbon adsorption on transition metals, and the development of a model for predicting adsorption energies of many hydrocarbons from that of methyl. The model becomes more general as it evolves through these chapters, although the descriptions of the adsorption systems become less detailed. The dependence of hydrocarbon adsorption on surface electronic structure is mentioned in these chapters, but it is not fully explored until chapters 7-8. These chapters explain how the adsorption energies of a variety of adsorbates depend on electronic structure properties. Again, later chapters become more general, but less detailed for individual systems. The dependence of adsorption energies on electronic structure is used to derive simple relationships between the adsorption energies of any two adsorbates. Chapter 7 also includes an application of the methods from the rest of thesis to ethylene epoxidation, where a TiAg catalyst is designed and experimentally tested. Chapter 8 also shows how adsorption energies can be estimated very efficiently.

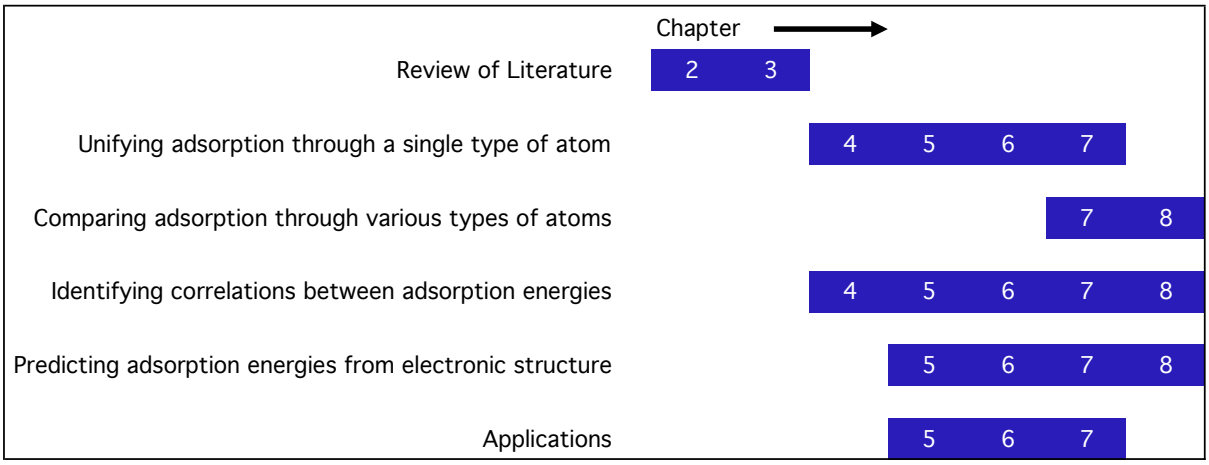

Figure 1.3: A schematic showing which topics are covered in which chapters of this thesis.

Chapter 2

Literature Review: Scaling Relations Between Adsorption Energies for Computational Screening and Design of Catalysts

2.1 Abstract

Adsorption energies have significant value as predictors of catalytic performance. An important method of increasing efficiency of adsorption energy calculations is to employ scaling relations, which are linear relationships between adsorption energies of similar adsorbates. They are most commonly used to unify the description of adsorbates that bind to the surface through a particular type of atom. In this work, we review the development and applications of scaling relations. Scaling relations have been observed for a variety of adsorbates bonding through C, O, H, N, and S atoms to the surfaces of transition metals, oxides, nitrides, sulfides, carbides, and nanoparticles. They can be used to increase the efficiency of predictions, simplify descriptions of surface reactivity, and sometimes to derive limits on the effectiveness of a catalyst. Because scaling relations can impose a significant limitation on catalyst design, it is also useful to explore how to design active sites that significantly deviate from them. We discuss applications to a variety of processes, including methane reforming and synthesis, alcohol decomposition and synthesis, electrochemical systems, and conversion of biomass derivatives.

2.2 Introduction

Many promising technologies for clean energy sources and carriers could significantly benefit from improvements in the performance of certain catalytic and electrochemical processes. However,

designing surfaces for their chemical properties has traditionally relied largely on trial-and-error approaches. More effective design paradigms and efficient screening methods could have broad impacts, and therefore have received significant attention from the research community.

The surface of a heterogenous catalyst is a complex system, with a variety of adsorbed intermediates interacting with the catalyst. As such, these systems can be difficult to model in their entirety using theoretical approaches. Nevertheless, theoretical work has provided deep insight into many surface reactions. One important insight is that trends in catalytic performance often can be predicted from adsorption energies of reaction intermediates or their proxies [29, 33].

Due to the importance of adsorption energies and the computational expense of quantum mechanical calculations, methods for increasing the efficiency of adsorption energy estimation are highly desirable. A popular method is the use of scaling relations, which are linear relationships between adsorption energies of related chemical species. Scaling relations allow predictions of adsorption energies of several species on a particular surface based on the adsorption energy of a single species on that surface. (Figure 2.1 provides an example of how scaling relations can be applied to methane reforming.) Therefore, they can be used to significantly increase the efficiency of calculations. They are even more useful when combined with kinetic approaches to simplify the description of the catalytic performance of a surface, often reducing it to just a few adsorption energies. This gives a simple, intuitive understanding of how to design catalytic surfaces, and greatly improves the prospects of high-throughput screening.

In this review, we discuss the development and application of scaling relations. First, we discuss the motivations for scaling relations and prior, related work. We then discuss the simple formulation developed by Abild-Peterson et. al [35] and various methods for applying scaling relations to complex adsorbates. Proposed explanations for scaling relations are also discussed. Since changes in the adsorption environment can affect the accuracy and generality of scaling relations, the following section is devoted to the behavior of scaling relations on different surfaces, as well as methods for correcting for geometric variations. We next review the application of scaling relations to various reactions. Finally, we discuss reported failures of scaling relations, as well as

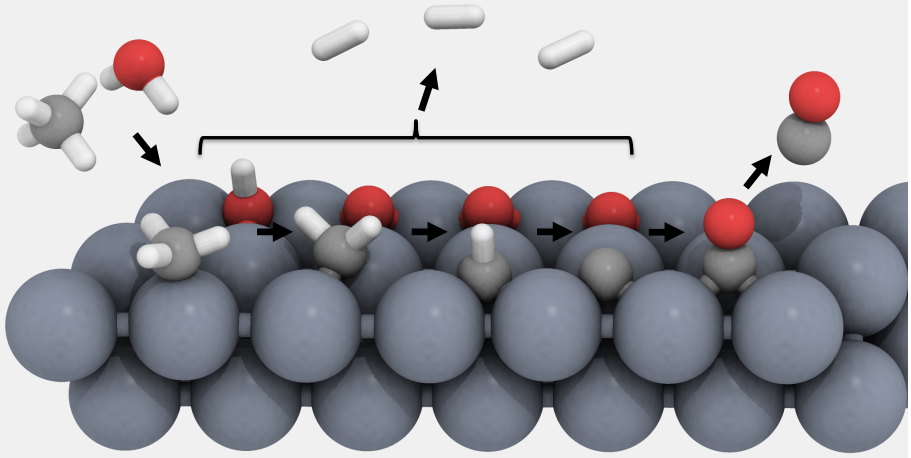

Figure 2.1: A schematic of methane steam reforming ($CH_4 + H_2O \longrightarrow 3\,H_2 + CO$), based on a proposed mechanism [34]. Using scaling relations, the adsorption energies of CH_x and CO can be predicted from the adsorption energy of C, and OH can be predicted from O. Applying BEP relations and a microkinetic model to these results, catalytic performance for this reaction can be approximately described using only the C and O adsorption energies.

possible strategies for deviating from scaling relations when this is desirable.

2.3 Motivation for Scaling Relations

The primary motivation for scaling relations is the importance of adsorption energies in controlling surface reaction pathways. Catalytic performance can be predicted by applying a microkinetic model to the potential energy surface of a reaction; hence, performance can be predicted if the adsorption energies (stable states) and activation energies (saddle points) are known. Since activation energies can be estimated from adsorption energies using linear relationships, knowledge of the proper adsorption energies is often sufficient to allow predictions of trends in catalytic performance. This critical importance of adsorption energies is what makes scaling relations powerful tools for studying catalysis.

The linear relationships between adsorption energies and activation energies are known as Brønsted-Evans-Polanyi (BEP) or transition state scaling (TSS) relations, depending on their form [25, 29, 36–41]. BEP relations, which predate scaling relations, predict activation energies

from reaction energies, while TSS relations, which have been developed more recently, predict activation energies from a single adsorption energy. They are closely related, as both predict adsorption energies as linear combinations of adsorption energies [42, 43]. BEP relations can be applied to predictions from scaling relations, while TSS relations essentially treat the transition state as an adsorbate and more directly apply the concepts from scaling relations. For simple reactions, BEP relations can be used to derive volcano plots [29], which indicate that the optimal catalyst has a moderate adsorption strength for key intermediates. TSS and BEP relations may share an underlying explanation with scaling relations. However, for simplicity this review focuses on (adsorbate) scaling relations, and we refer readers interested in estimating activation energies to other work [24, 31, 42, 44].

Scaling relations have two primary, complementary uses. First, they can be used to rapidly compute the adsorption energies of many adsorbates based on a single adsorbate, reducing computational cost. Thus, scaling relations are commonly employed in efforts aimed at computational design of catalysts, where a large number of surfaces are to be evaluated for improved performance, and it is therefore necessary to reduce computational expense by minimizing the number of required adsorption energy calculations. Second, scaling relations can provide insight into which elementary steps control catalytic performance, as well as which adsorption energies affect these elementary steps. Because they provide analytical relationships between adsorption energies, they can often simplify descriptions of reactivity. Additionally, the relations provide fundamental insight into how molecular structure controls adsorption strength.

Prior to the development of a simple, intuitive formulation of scaling relations in 2007, several studies noted some of the same concepts, including linear relationships between adsorption energies of similar adsorbates. A study of hydrocarbons on late transition metals developed a group additivity method and found that the adsorption energy was approximately proportional to the number of bonds to the surface [45]. A study of trends in reactivity for several reactions found that the energy of adsorption through X atoms (X = C, S, O) on a transition metal M could be predicted by the energy of formation of the bulk MX species. For example, ethylene and benzene adsorption

energies were found to be linearly correlated with carbide formation energies [46]. Studies of water electrolysis found that the adsorption energies of O, OH, and OOH were linearly correlated on metal[47] and oxide[48] surfaces. The unity bond-index quadratic exponential potential (UBI-QEP) method [49], a phenomenological model based on the conservation of a bond index, also preceded the development of scaling relations, and the two formalisms have some similarities. UBI-QEP is generally used to estimate surface energetics to inputs into a kinetic model, as many energies are often needed in these cases. While UBI-QEP allows predictions of many surface phenomena, including diffusion barriers, activation energies, and adsorbate-adsorbate interactions, in this work we focus on its predictions of adsorption energies. We compare UBI-QEP and scaling relations below in Section 2.5.

2.4 Development of Scaling Relations

2.4.1 Scaling Relations for AH_x

The seminal paper on scaling relations gave a simple formulation for linear relationships between adsorption energies of simple hydrides with the same central atom [35]. The adsorption energy of the species AH_x (A = C, N, O or S) was written as

$$E_{\mathrm{ads}}(\mathrm{AH_x}) = \gamma E_{\mathrm{ads}}(\mathrm{A}) + \xi, \tag{2.1}$$

where ξ and γ were fit to adsorption energy data, and γ was found to be approximately

$$\gamma = \frac{(x_{\mathrm{max}} - x)}{x_{\mathrm{max}}}, \tag{2.2}$$

where x_{max} is the maximum number of H atoms that can stably bond to A in the gas phase (4 for C, 3 for N, 2 for O and S). The data and fits are shown in Fig. 2.2, and the mean absolute error of the fits is 0.13 eV. Conceptually, γ is the number of dangling bonds in AH_x divided by the total number of bonds A can form. (More generally, it will be the number of dangling bonds in the predicted species divided by the number of dangling bonds in the predictor species.) Hence, after fitting, knowledge of the adsorption energy of an atomic species allows estimation of the adsorption

energies of its hydrides. This formulation has intuitive power because it conceptualizes adsorption energies in terms of the coordinative unsaturation of the adsorbate. For example, OH has 1/2 as many dangling bonds as O. Therefore, when a change in surface increases $E_{\mathrm{ads}}(\mathrm{O})$ by ΔE, $E_{\mathrm{ads}}(\mathrm{OH})$ will increase by approximately $1/2\Delta E$. However, this intuition only applies to changes in adsorption energy, and not to other quantities such as the site preference (see Section 2.6).

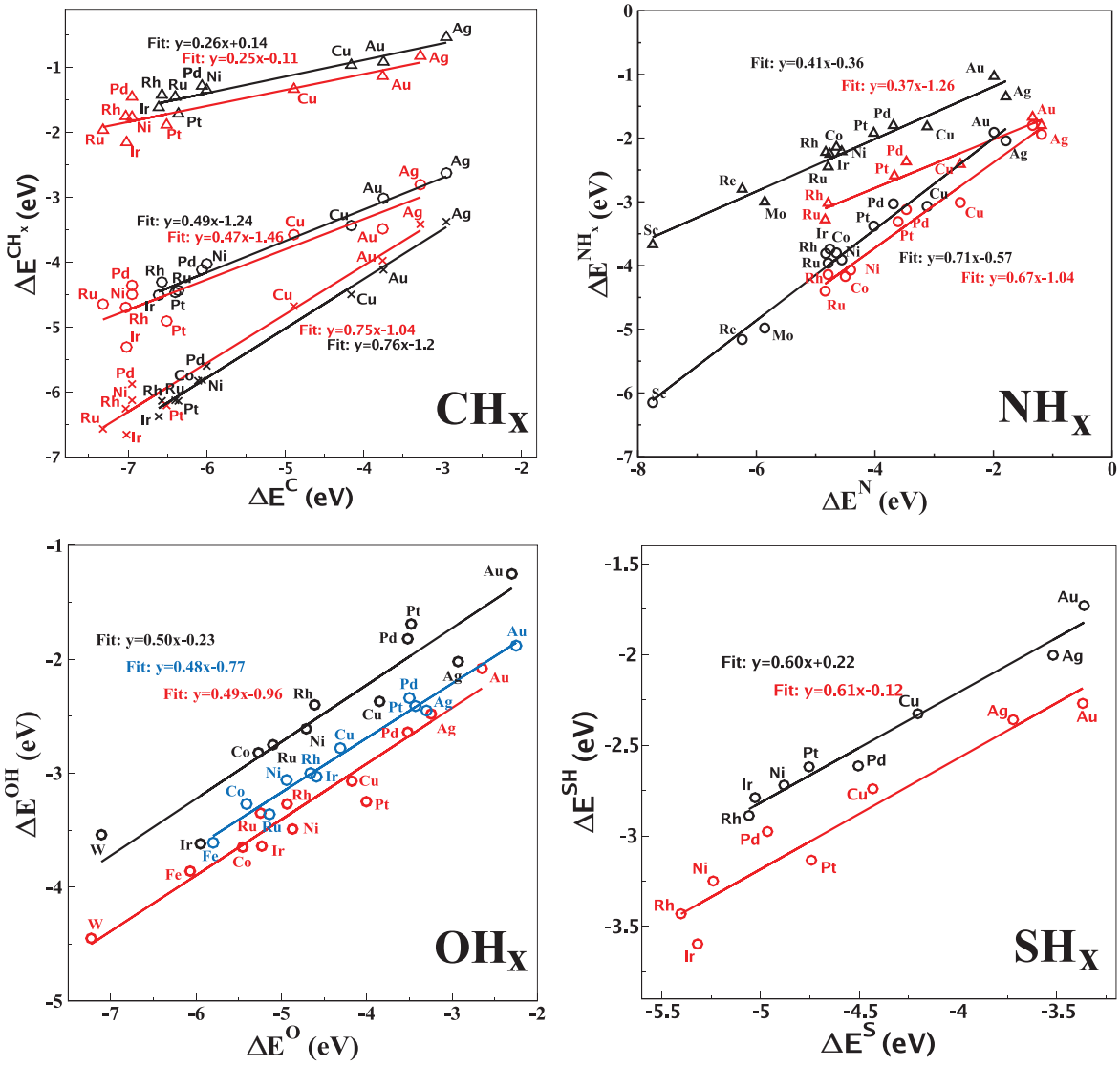

Figure 2.2: Scaling relations for CH_x, OH_x, NH_x, and SH_x on close-packed (black), stepped (red), and fcc(100) (blue) surfaces. Reprinted from Ref. 35.

Equation (2.1) can be rearranged to allow the use of a reference metal [35, 50]:

$$E_{\mathrm{ads}}(\mathrm{AH_x/M_2}) = E_{\mathrm{ads}}(\mathrm{AH_x/M_1}) + \gamma(E_{\mathrm{ads}}(\mathrm{A/M_2}) - E_{\mathrm{ads}}(\mathrm{A/M_1})). \tag{2.3}$$

Hence, if the adsorption energy of $\mathrm{AH_x}$ on $\mathrm{M_1}$, $E_{\mathrm{ads}}(\mathrm{AH_x/M_1})$, is known, one can simply add the scaled difference in the adsorption energies of A on $\mathrm{M_1}$ and $\mathrm{M_2}$ to estimate $E_{\mathrm{ads}}(\mathrm{AH_x/M_2})$. The second term in Eq. (2.3) can be conceptualized as the product of the number of dangling bonds in the adsorbate and the energy change per dangling bond upon bond formation. Equation (2.3) can be less accurate than Eq. (2.1), as it heavily depends on $E_{\mathrm{ads}}(\mathrm{AH_x/M_1})$, which may deviate somewhat from the overall scaling relation. This shortcoming can be overcome with some additional computational effort [51].

These types of scaling relations have been shown to hold on a wide variety of surfaces, such as transition metal (100) surfaces [52]; nitrides, oxides, and sulfides [53–55]; carbides [56, 57]; transition metal nanoparticles [58, 59]; transition metal surfaces modified with S, Se, As, and P [60]; graphene [61, 62]; and various Ni alloys [63, 64]; We discuss the behavior of scaling relations on different surfaces in Section 2.6.

2.4.2 Scaling Relations for Other Adsorbates

Linear relationships between adsorption energies have been found in many other cases, as shown in Table 2.1. Some studies simply fit a separate scaling relation for every adsorbate they predict. However, in a complex reaction network with complex adsorbates, such as polyol decomposition, this will require a large number of calculations and fitting parameters. Further, some polyol intermediates bond to the surface through multiple C and O atoms. Thus, a general framework for predicting complex adsorbates with few fitting parameters is necessary. Several schemes have been proposed to generalize or extend scaling relations. The simplest generalization [35, 50] of the $\mathrm{AH_x}$ scaling relations to more complex molecules is to simply sum Eq. (2.3) over all the adsorbate atoms that bond to the surface:

$$E_{\mathrm{ads}}(\mathrm{R/M_2}) = E_{\mathrm{ads}}(\mathrm{R/M_1}) + \sum_i \gamma_i [E_{\mathrm{ads}}(\mathrm{A_i/M_2}) - E_{\mathrm{ads}}(\mathrm{A_i/M_1})]. \tag{2.4}$$

Next, γ is redefined as

$$\gamma = \frac{(x_{\max} - x_{\text{intra}})}{x_{\max}}, \tag{2.5}$$

where x_{intra} is the total number of intra-adsorbate bonds attached to A. Hence, all intra-adsorbate covalent bonds are treated the same as A−H bonds, except that an A−B bond will need to be counted as part of γ for both A and B. Terms to account for ring strain and adsorption through alcohol groups can increase the accuracy of predictions for polyols [65], although predicting adsorption of rings on noble metals may present a challenge [66]. C−O bonds may lead to deviations in the values of γ, and a slope taken from fitting may be more accurate than one calculated from Eq. (2.5) [51].

Table 2.1: A summary of the scaling relations that have been observed in the literature.

Scale From	Scale To
C	CH_x [34, 35, 51, 52, 57, 59, 63, 64, 67–73], C_2H_x [74, 75], C_xO [34, 51, 67, 70, 71, 73, 76–78], CHO [51, 67, 70, 73, 76–78], CH_2O [51], CH_xOH [51, 70, 76, 78], CH_2CO [73], CH_3CHO [73], CH_xCH_yOH [73], CN [79], HCN [79], CNH [79], Si [80], H [34, 43, 67, 70, 71, 73, 76, 78]
CH_3	acetylene [81, 82], ethylene [81, 82], H [83], Hydrocarbons that adsorb through a single C atom [83, 84]
CO	CHO [85–87], COOH [85–88], CH_xOH [85, 86], HOCOH [85, 86], CH_2O [87]
CHO	CH_2O [62], CHOH [62], CH_2OH [62], COH [62], CO [62]
O	OH [22, 27, 35, 48, 51, 53, 54, 57, 59, 67, 70, 71, 73, 75], O_2 [22, 89–91], OOH [22, 27, 48], H_2O_2 [27], S [80], CH_3O [70, 73, 75–78], CH_2O [51], ClO_x [91], H [43]
OH	O [60–62, 92, 93], OOH [54, 55, 60, 61, 92, 94, 95], CH_3O [62, 73, 85–87], CHOO [85, 86], CH_2OOH_x [85, 86], CH_2O [62], SO_x,[93] HSO_3[93]
O_2	OH [96], OOH [96]
N	NH_x [35, 53, 56, 58, 59, 68, 75, 97, 98], N_2H_x [58, 97], NO [99], H [43, 58, 97], P [80]
F	Cl [80]
H	OH [100]
S	SH [35, 53, 75], Sulfur-containing molecules [101]
C, O	CH_2O [70, 73, 76–78], CHCO [73], CH_3CO [73], CCHO [73], CHCHO [73], $C_xH_yO_z$ [65, 66, 102–109]
C, N	CH_xNH_y [68]

This scheme has been successfully applied to C_2 hydrocarbons on transition metals [74]. For a generic C_n hydrocarbon, the sum of the γs, which in this case is the slope of the hydrocarbon vs. C scaling relation, is $n - \sum_i (x_{\text{intra},i}/4)$. Surfaces were classified as "noble" if π bonds remain intact upon adsorption and must be counted as part of x_{intra}, but classified as "reactive" if π bonds are broken. This difference was visible in the density of states of the adsorbed molecule. Surfaces that

bind more strongly than Cu were found to be reactive, those that bind more weakly were found to be noble, and Cu's classification depended on the adsorbate and facet. We note that (1) the classification could likely be made more predictive by basing it on the C adsorption energy, though the cutoff would likely depend on the adsorbate and facet, and (2) for some adsorbates and facets, Cu appears to behave like an average of the reactive and noble limiting cases, and a function that smoothly varies between these limiting cases would likely increase accuracy in the region near the transition.

When applying Eq. (2.4) to polyol decomposition intermediates, calculating all the necessary adsorption energies on a single reference metal can be challenging. Therefore, adsorption energies of complex oxygenates on a single metal have been estimated in two ways. In the first scheme, a group additivity framework was developed based on DFT calculations [65, 105, 107, 110]. In the second scheme, estimates were made using the coordinative unsaturation of the adsorbate with both linear and quadratic terms, which is essentially a heuristic generalization of Eqs. (2.1) and (2.2) [103, 106].

Equation (2.4) gave reasonable accuracy for some predictions of polyol intermediates on Rh(111) and Pd(111), with a standard error of $\sim$0.2 eV [108]. With ring strain and alcohol terms, the maximum error was found to be around 0.4 eV for predictions on Ni(111) and a Pt(111) surface covered with 2 ML of Ni [65]. These errors are low enough that predictions are likely to be useful, but detailed, quantitative work on complex adsorbates is better done using a method other than scaling relations [51]. A larger standard error of 0.5 eV on Cu(111) was attributed to differences in adsorption of double bonds [108]. It is likely that a scheme to adjust γ values on noble metals, similar to that discussed above for C_2 hydrocarbons, will be necessary before predictions of complex adsorbates on noble surfaces will be useful.

There are indications that scaling relations may be able to handle some calculations that include van der Waals interactions, and that these interactions essentially introduce a constant shift into the scaling relations [66]. These results were obtained for intermediates that covalently bond to the surface, and it remains to be seen whether scaling relations can be applied to adsorbates that interact with the surface purely through non-covalent interactions, as these kinds of interactions

are not explicitly accounted for in current formulations. For example, it may be possible to scale between water and small alcohols or across alkanes.

An alternative method for efficiently extending scaling relations to more adsorbates involves the use of gas-phase bond energies. This method applies for a class of adsorbates that adsorb through the same type of atom with the same number of dangling bonds. For example, alkyls and adsorbates that are similar to alkyls near the surface are one class, akylidynes (and similar) another, and alkoxides (and similar) another (see Fig. 2.3). It has been shown that changes in adsorption energies within a class are linearly related to changes in the gas-phase bond energies [111]. For example, the difference between the methyl and ethyl adsorption energies in the top site is approximately constant on all surfaces, and this constant is linearly related to the difference in the methane and ethane C−H bond energies. This linear relationship can be traced back to the energy levels of the adsorbate orbitals. Our work on this is presented in Chapters 4-7 This method can be applied to new adsorbates without any additional surface calculations, but thus far has only been applied to adsorbates that bond to the surface through a single C or O atom. It remains to be seen whether it can be generalized to more complex adsorbates.

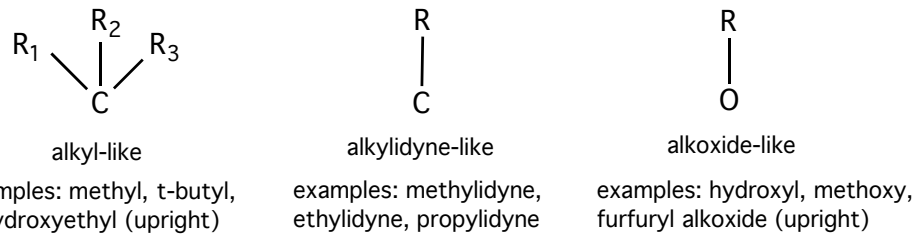

Figure 2.3: Examples of adsorbate classes, where differences in adsorption energy for adsorbates in each class can be predicted based on gas-phase bond energies to H atoms. The R groups can be anything that does not interact with the surface through covalent or lone-pair interactions.

2.5 Why do Scaling Relations Hold?

The original explanation [35] for scaling relations focused on rationalizing Eq. (2.2), and was based on the d-band model [112] and effective medium theory [113]. First, it was assumed that the

change in adsorption energy across transition metals is due to changes in the coupling to the d-electrons; we denote this energy change as ΔE_d. Next, it was assumed that $\Delta E_d(\mathrm{AH_x}) \propto \Delta E_d(\mathrm{A})$, which results in a linear relationship between $E_{\mathrm{ads}}(\mathrm{AH_x})$ and $E_{\mathrm{ads}}(\mathrm{A})$. It was also assumed that, for a particular central atom A on a particular surface, $\Delta E_d \propto V_{ad}^2$, where V_{ad} is the matrix coupling element between the adsorbate and the metal d states; this is supported by the d-band model. According to effective medium theory, there is an optimal electron density, n_0, that results in the lowest energy position for an atom. An adsorbing atom will obtain electron density from all the atoms it is bonded to, including other atoms in the adsorbate as well as surface atoms. Assuming that other adsorbate atoms all contribute $n_0/x_{\max}$ (*e.g.*, H atoms contribute 1/4 of the density required by a C atom), the density contributed by the surface will be $n_{\mathrm{surf}} = n_0(x_{\max} - x)/x_{\max}$. There is some evidence supporting this notion, as $\mathrm{CH_x}$ often prefers to adsorb to 4-x surface atoms on late transition metals, and the C−M distances are fairly constant in these cases. This indicates that each surface atom contributes roughly an equal amount of electron density, even as x changes. Since the coupling should roughly scale with the density ($V_{ad}^2 \propto n_{surf}$), we have $\Delta E_d \propto V_{ad}^2 \propto n_{surf} \propto (x_{\max} - x)/x_{\max}$. Therefore, $E_{\mathrm{ads}}(\mathrm{AH_x})$ is linearly related to $(x_{\max} - x)/x_{\max}$ as well as $E_{\mathrm{ads}}(\mathrm{A})$.

This explanation is fairly simple and intuitive, and it largely rests on well-established theories. However, it does not specify a functional form for how ΔE_d varies across metal surfaces, and why it should be proportional for some adsorbates (*e.g.*, $\mathrm{CH_3}$ and C) but not for others (*e.g.*, C and O). A more general view of explanations for scaling relations was given in a study of atomic adsorption in the top site of near surface alloys of Pt(111) [80]. This study points out that the existence of a scaling relation between two species implies that the species' adsorption energies have a similar functional dependence on surface properties. In this study, the total number of valence electrons in the surface was used as a predictor of the adsorption energy, and the functional dependence on this predictor was similar for period 2 atoms and the period 3 atoms directly below them. In this case, the scaling relations were likely more accurate than the predictions based on the number of valence electrons, as variations between surfaces with the same number of electrons were ignored.

However, this view provides insight into the relationship between scaling relations and electronic structure.

A few other studies have used explicit functions of electronic structure properties to explain scaling relations in particular cases. For example, the number of outer electrons was shown to linearly correlate with adsorption energies on monometallic 3d transition metal surfaces as well as oxides. This relationship was used to justify scaling relations, and to explain trends across a particular transition metal in both metallic and oxide surfaces [54]. However, this relationship is not easily generalizable to alloy surfaces. Scaling relations on carbides have been justified by showing that the adsorption energies of various intermediates can be predicted using the transition-metal derived surface resonance [56, 114]. Our work justifying scaling relations for hydrocarbons on transition metal surfaces is presented in Chapter 6.

Scaling-like relations can be derived from the unity bond index-quadratic exponential potential model (UBI-QEP, formerly called the bond order conservation model) [49], as UBI-QEP can be used to predict adsorption energies of various species based on atomic adsorption energies. For an adsorbate AB (*e.g.*, OH) that is similar to the atomic species A (*e.g.*, O) and thus adsorbs strongly, the adsorption energy can be predicted as

$$E_{\mathrm{ads}}(\mathrm{AB}) = \frac{E_{\mathrm{ads}}(\mathrm{A})^2}{D_{\mathrm{AB}} + E_{\mathrm{ads}}(\mathrm{A})}, \tag{2.6}$$

where D_{AB} is the gas-phase bond energy of AB. This expression was recommended for CH and CH_2. For an adsorbate with strong intramolecular bonding and hence weaker adsorption, the adsorption energy can be predicted as

$$E_{\mathrm{ads}}(\mathrm{AB}) = \frac{E_0(\mathrm{A})^2}{D_{\mathrm{AB}} + E_0(\mathrm{A})/n}, \tag{2.7}$$

where n is the number of surface atoms the adorbate is bonded to and E_0 is the minimum two-center (M−A) bond energy such that $E_{\mathrm{ads}}(\mathrm{A}) = E_0(\mathrm{A})(2 - 1/n)$. Intermediate adsorption strength can be accounted for by averaging these equations; this is recommended for CH_3. Further expressions for polyatomic molecules have also been developed [49].

A Taylor series expansion of Eq. (2.6) about D_{CH} gives $E_{\mathrm{ads}}(\mathrm{CH}) = 0.75E_{\mathrm{ads}}(\mathrm{C}) - 0.25D_{\mathrm{CH}}$,

which is similar to the scaling expression. However, this expression would also be applied to, *e.g.*, NH. Further, the slope and intercept depend on the point that is expanded about as well as which expression (strong binding, weak binding, or intermediate) is chosen. We have not discovered a consistent or logical way to derive scaling relations from UBI-QEP. A comparison between scaling relations and UBI-QEP is shown in Fig. 2.4. The absolute values generally do not show close agreement, although this may depend on the DFT data chosen for fitting the scaling relations. However, the slopes are generally in fair agreement, although there is a significant discrepancy for acetylene. Comparisons between DFT and UBI-QEP are available in previous work [115].

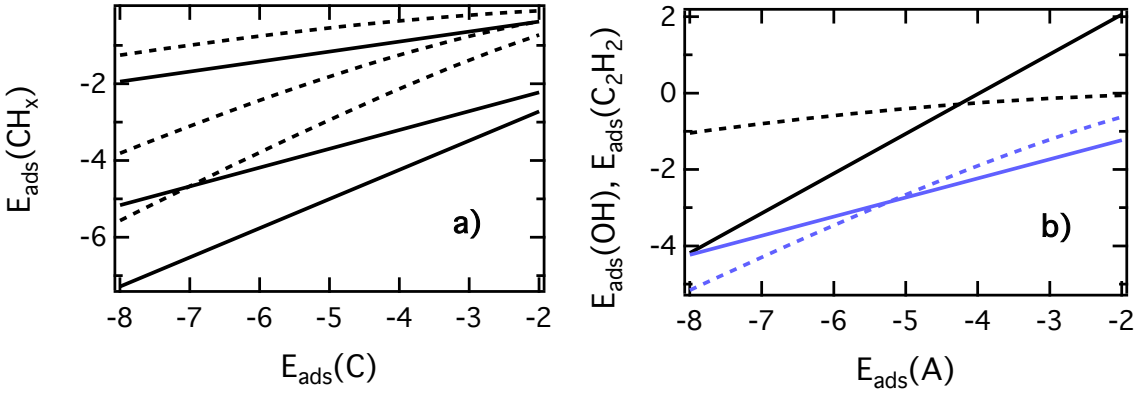

Figure 2.4: Comparison between scaling relations (solid lines) and UBI-QEP (dashed lines) for a) CH_x [35, 49]; b) OH [35, 49] (blue) and acetylene [35, 49, 81] (black). Bond energies used in UBI-QEP were taken from Ref.49, 116.

2.6 Scaling Relations in Different Adsorption Environments

2.6.1 Varying the Surface Structure

Since their inception, it has been clear that changes in the local adsorption environment can affect the parameter values and accuracy of scaling relations. In general, the slope, γ, is fairly insensitive to the type of surface or site (see, for example, Table 2.2 and Figs. 2.2 and 2.5). However, ξ tends to vary more significantly. (Note that different reference states for adsorption energy calculations will change the value of ξ, hindering comparisons across studies that use different

reference states.) The overall picture for scaling relations in different sites or on different surfaces is that a surface will usually bond with an adsorbate commensurate to the adsorbate's unsaturation, no matter the site. Hence, a carbon atom will effectively form a quadruple bond to a single surface atom if placed in a top site, and four single bonds if placed in a hollow site of an fcc(100) surface. The total adsorption energy will be different in these two cases, resulting in a difference in ξ. However, in both cases the variations in $E_{\text{ads}}(\text{C})$ will be approximately four times the variations in $E_{\text{ads}}(\text{CH}_3)$, resulting in a similar γ. Adsorption on different surfaces or in different sites on the same surface are closely related phenomena, and we discuss them in this subsection and the next.

Table 2.2: Average slopes of AH_x scaling relations (γ in Eq. (2.1)) on transition metal (TM) and oxide surfaces, with standard deviations where applicable.

Scale To	Eq. (2.2)	Close-Packed TMs [35, 47, 51, 52, 54]	Stepped TMs [35, 71, 87]	TM Clusters [70]	Oxides [48, 53, 54]
CH	0.75	0.78±0.03	0.77±0.02	0.86	
CH_2	0.50	0.54±0.04	0.46±0.01		
CH_3	0.25	0.32±0.11	0.23±0.03		
OH	0.50	0.47±0.07	0.52±0.03	0.62	0.55±0.06

First, we discuss the behavior of scaling relations on different types of surfaces. When fitting separately on stepped, close-packed, and open transition metal surfaces, γ varies by less than 0.05 eV, while ξ can vary by almost 1 eV [35]. This higher variability of the intercept than the slope for different facets of transition metals has been observed in several cases [74, 90] and even for BEP relations [99]. In some cases, *e.g.* when scaling between OH and OOH on fcc(111) and (100) surfaces, the difference in ξ is small enough that a single scaling relation suffices for both facets, although separate fitting would likely improve the accuracy [94].

Similarly, scaling relations tend to be similar, but not the same, on extended surfaces and nanoparticles, with larger variations in ξ than γ. For example, the same scaling relation can be used between C and CH on both extended surfaces and nanoparticles, but the intercept must be changed for scaling between C and CH_2 or CH_3 [59]. This has been attributed to the differences in local geometry between bridge sites and hollow sites, due to the high curvature of the particle. This

reasoning implies that nanoparticles of different shapes may have different ξ values [59]. A study of NH_x on relaxed and frozen nanoparticles as well as fcc(211) surfaces found that the variations in both γ and ξ were within error, except for ξ for N_2 vs. N [58]. One study found the O_2 vs. O relation to vary moderately between fcc(111) surfaces and nanoparticles [89], while another study found a more significant variation in ξ [90]. On subnanometer clusters, the slopes of scaling relations are higher than those generally found on extended surfaces, which may be due to geometrical changes in the clusters upon adsorption (see Table 2.2) [70].

These moderate variations in scaling relations between different kinds of surfaces even apply when comparing metals to insulating surfaces such as oxides. There is some disagreement about whether the same scaling relations for OOH vs. OH and OH vs. O can be used for both types of surfaces [48, 54]. However, since OH and O are more dissimilar than OH and OOH (which have the same valency and likely the same adsorption geometry), the OH vs. O scaling relations on metals and oxides appear to be more dissimilar as well. Scaling relations are similar, but not quite the same, when comparing transition metals to surfaces modified with S, Se, As, and P [60], or to nitrides, sulfides, and oxides (if the adsorption site is controlled) [53]. The acetylene and ethylene vs. CH_3 scaling relations are similar on Pd with subsurface C as monometallic and bimetallic surfaces, perhaps with a smaller slope and higher intercept on the surfaces with subsurface C [82].

2.6.2 Variations in Adsorption Site

Even on the same surface, different adsorbates often adsorb in different sites, which can introduce inaccuracies into simple scaling relations. It was noted in the original scaling relations paper that putting both C and CH_3 in the top site reduces scatter on stepped surfaces, as compared to adsorbing them both in their most favorable site (which we call min-min scaling relations) [35]. This effect was seen even more strongly in a study of binary nanoparticles [59]. In a study of hydrocarbons on close-packed transition metals [84], it was shown that min-min scaling relations fail in two cases: (1) early transition metals, which have strong agostic C−H−M interactions that stabilize CH_3 and CH_2 but not CH or C, and (2) strongly inhomogeneous alloys (see Fig. 2.5b).

For example, on a Au(111) surface with 1/9 of the surface atoms replaced with Pt, CH_3 adsorbs atop a Pt atom, while C adsorbs in a hollow site where it is bonded to one Pt and two Au atoms. Because bonds to Pt are stronger than bonds to Au, CH_3 is stabilized more than scaling relations predict. While alloys may cause inaccuracies for many types of scaling relations, agostic interactions likely only affect hydrocarbons. In some cases, a straightforward application (as in Fig. 2.5a) of site-specificity can be used to increase the accuracy of scaling relations. For example, in a study of acetylene hydrogenation the ethylene vs. methyl scaling relation was corrected on Rh and Ni by putting methyl in the top site [81].

However, several factors complicate the general application of these more accurate, site-specific scaling relations. First, placing both CH_3 and CH in the top site results in significant scatter when considering a wide range of transition metals [84], and on subnanometer clusters putting two adsorbates in the same site does not decrease the scatter [70]. Second, this scheme requires knowledge of the most favorable adsorption site of the predicted molecule, which generally must be calculated with DFT. Third, it reduces efficiency even if the site preferences are known: if the adsorption energies of both CH_3 and C are required and it is known that C prefers a hollow site while CH_3 prefers a top site, adsorbing C in a hollow site (for its adsorption energy) as well as in the top site (to predict CH_3's adsorption energy) saves little computational time over simply performing the calculations for C and CH_3.

Hence, to take full advantage of the accuracy of site-specific scaling relations, a different scheme has been developed and applied to hydrocarbons on hexagonal transition metal surfaces. In this scheme, scaling is performed across each adsorbate in the site where it completes its tetravalency: CH_3 in the top site, CH_2 in the bridge site, and CH in the hollow site (see Fig. 2.5b). C is also placed in the hollow site. Further details are presented in Chapter 7. Compared to min-min scaling relations, site-specific scaling relations are more accurate, more widely applicable, and have negligible additional computational expense once they are fit. However, they are also more complex and have reduced transparency. Therefore, the choice to use min-min or site-specific scaling relations will depend on the application.

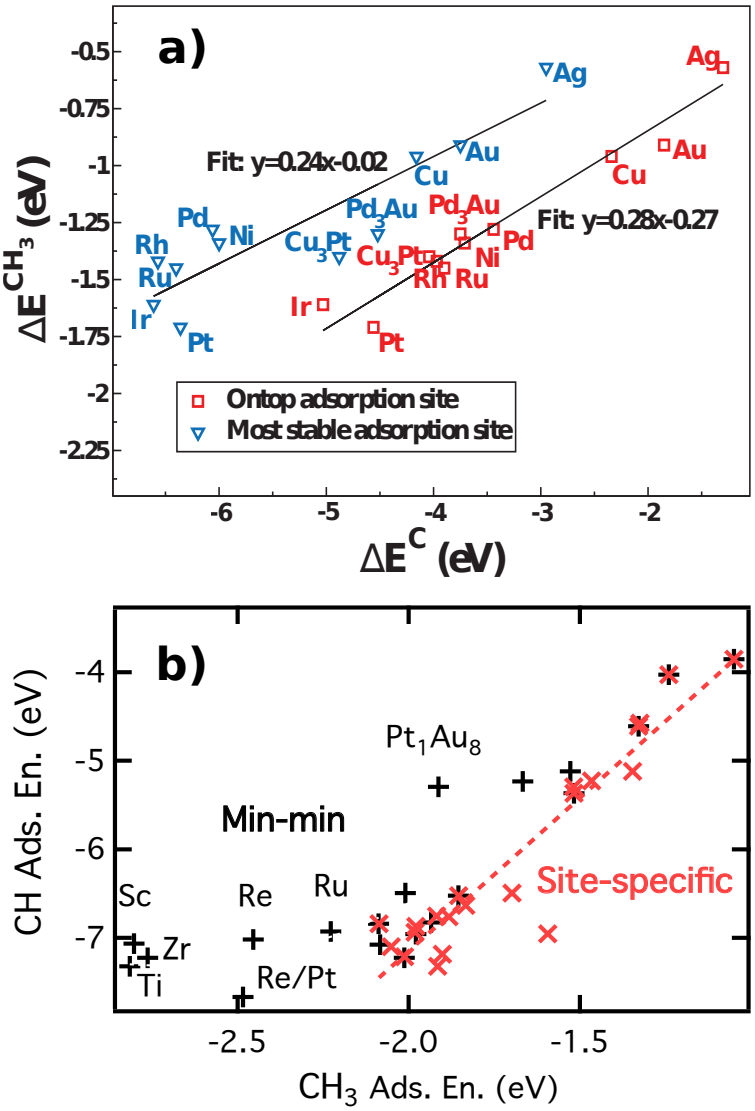

Figure 2.5: a) Comparison between min-min scaling relation and top-top scaling relation for C and CH_3. Reprinted from Ref. 35. b) Comparison between min-min scaling relation and top-fcc scaling relation for CH_3 and CH, replotted using data from Ref. 84

2.6.3 Coverage and Coadsorbates

Most applications of scaling relations ignore the effects of coverage and coadsorbates. However, scaling relations have been observed for CH_x in the presence of O [52]. In fact, the same scaling relation can be applied for OH vs. O for different coverages of O and in the presence of solvent [47]. Scaling relations and BEP relations based on coverage-dependent adsorption energies

have been employed, and there is evidence that BEP relations can be used in this way for small molecules [117]. On the other hand, coadsorbed O has been shown to decrease the accuracy of scaling relations between O and OH as well as O and H_2O [118]. In general, adsorbate-adsorbate interactions may cause scaling relations to fail, and studies generally use coverage models as *a posteriori* corrections to the predictions from scaling relations, rather than including coverage effects in the scaling relations themselves [71, 102, 104, 107, 108]. Therefore, other models of adsorbate-adsorbate interactions may prove useful as corrections to the adsorption energies from scaling relations [49, 119, 120].

2.7 Applications of Scaling Relations

2.7.1 Conversion or Synthesis of Methane

Conversion of methane into hydrogen is a widely used process, and methane synthesis carries possibilities for clean or renewable fuels. Methane conversion has recently gained additional attention due to new techniques in natural gas extraction from underground stores. Since the key intermediates in many reactions involving methane are CH_x, OH_x, and carbon oxides, these reactions are good candidates for applying scaling relations.

One of the most powerful uses of scaling relations is to help simplify the description of catalytic performance, reducing it to a function of a few simple adsorption energies, often called descriptors. For reactions of methane, this generally involves calculating the adsorption energies of C and O on the surfaces of interest, then using scaling relations to predict the adsorption energies of the other intermediates (usually OH, CH_x, CO and H, as shown in Fig. 2.1), giving the reaction energies of all of the elementary steps. For example, the reaction energy of the initial $CH_4(g) + 2 * \longrightarrow CH_3^* + H^*$ step, which is thought to be kinetically important, requires the CH_3 and H adsorption energies. (The asterisk indicates an empty site or an adsorbed species.) If the H atom is assumed to directly form gas phase H_2, only the CH_3 adsorption energy is needed. Transition state energies can then be estimated using BEP relations. Using a microkinetic model, a system of rate equations can then

be developed and solved to give the reaction rate as a function of the atomic adsorption energies. For example, a combined experimental and theoretical study used this method to plot the activity for methane steam reforming as a function of the C and O adsorption energies (see Fig. 2.6a) [34]. The trends predicted by this model matched those from experiment. Similar work on the methane oxidation reaction in electrochemical conditions[67] and methane synthesis from syngas[73] also used the C and O adsorption energies as descriptors. Using scaling relations, the O adsorption energy was identified as a descriptor for activity for the anode reactions in solid-oxide fuel cells on Ni alloys, while C and S were used as proxies for undesirable, strongly bound adsorbates [121]. Reducing catalytic performance to C and O adsorption energies allows fast comparison of new surfaces. For example, calculations indicate that Mo_2C should behave similarly to Ru and Ir in reactions where the C adsorption energy is important [57].

Using scaling relations, CO_2 electroreduction to methane on transition metals can be described by the CO and OH adsorption energies (see Fig. 2.6b for the CO results; the OH adsorption energy is rarely important because the steps it controls are not usually kinetically limiting) [87], while on porphyrin-like materials CHO was used in place of CO since CO didn't bind to all the materials being studied [62]. On Cu, the most selective monometallic catalyst [122], the species containing the carbon atom likely evolves as follows: $CO_2 \longrightarrow COOH \longrightarrow CO \longrightarrow CHO \longrightarrow CH_2O \longrightarrow CH_3O \longrightarrow CH_4$. Regardless of the exact mechanism, the $CO \longrightarrow CHO$ step was found to be kinetically limiting on most transition metals, including Cu and Pt [87]. Since there is a scaling relation between CO and CHO with a slope of about 0.9, the reaction energy of this step is quite insensitive to the surface, impeding the design of more active materials. This step is slightly more favorable on less reactive surfaces, although if the surface is too unreactive CO will desorb instead of continuing to react. Since Cu is near the theoretical maximum, it appears to be impossible to design a surface that is significantly more active than Cu unless the CHO vs. CO scaling relation can be broken. A similar analysis has been made for the electroreduction of CO_2 to CO, where the COOH formation step is limiting [123]. It was noted that the CODH enzyme is an efficient CO_2 electroreduction catalyst because it deviates

slightly from the COOH vs. CO scaling relation.

Scaling relations have been used to study methane reactions in other ways. Since scaling relations for CH_x were found to hold on both clean and O-precovered surfaces, they were used to study the effect of O on CH_4 dissociation. It was found that O has a significant effect and that it changes the reactivity of the metals relative to each other [52]. In a scaling relations study of CO methanation, it was argued that the most active catalysts are Ru, Ni, Co, and Rh because their free energy diagram (generated from scaling relations, similar to Fig. 2.6c) most closely follows a straight line from reactants to products [50]. Scaling relations have been combined with a coverage model to show that coverage effects have a small effect on the location of the peak of the volcano for CO methanation, but may affect selectivity [71].

Alkanes and other hydrocarbons larger than methane have received relatively little attention. Scaling relations have been used to predict some of the energetics of ethane decomposition, but no conclusions about the reaction were drawn other than the suitability of scaling relations for studying it [74]. Using site-specific scaling relations, propane dehydrogenation to propylene was studied on a wide variety of transition metals, as discussed in Chapter 7. Since cracking is a common problem for this reaction, this study used metrics that attempted to account for both activity and selectivity. There has also been some work on Fischer-Tropsch synthesis where, in the spirit of scaling relations, all energies were either assumed to be constant or to scale linearly with the C adsorption energy, resulting in a simple, approximate description of a complex reaction [124]. Another study linked Fischer-Tropsch activity to atomic adsorption energies and qualitatively linked selectivity to adsorption strength [125]. Studies of the thermodynamics of hydrocarbon chain growth have also been conducted using scaling-like relations, as detailed in Chapters 4 and 5.

2.7.2 Conversion or Synthesis of Simple Alcohols

Catalytic reactions involving alcohols have attracted significant research attention, both as proxies for more complex molecules and as useful chemicals in their own right. Using scaling relations in conjunction with other simplifications, the free energies of adsorbed OH and CO have

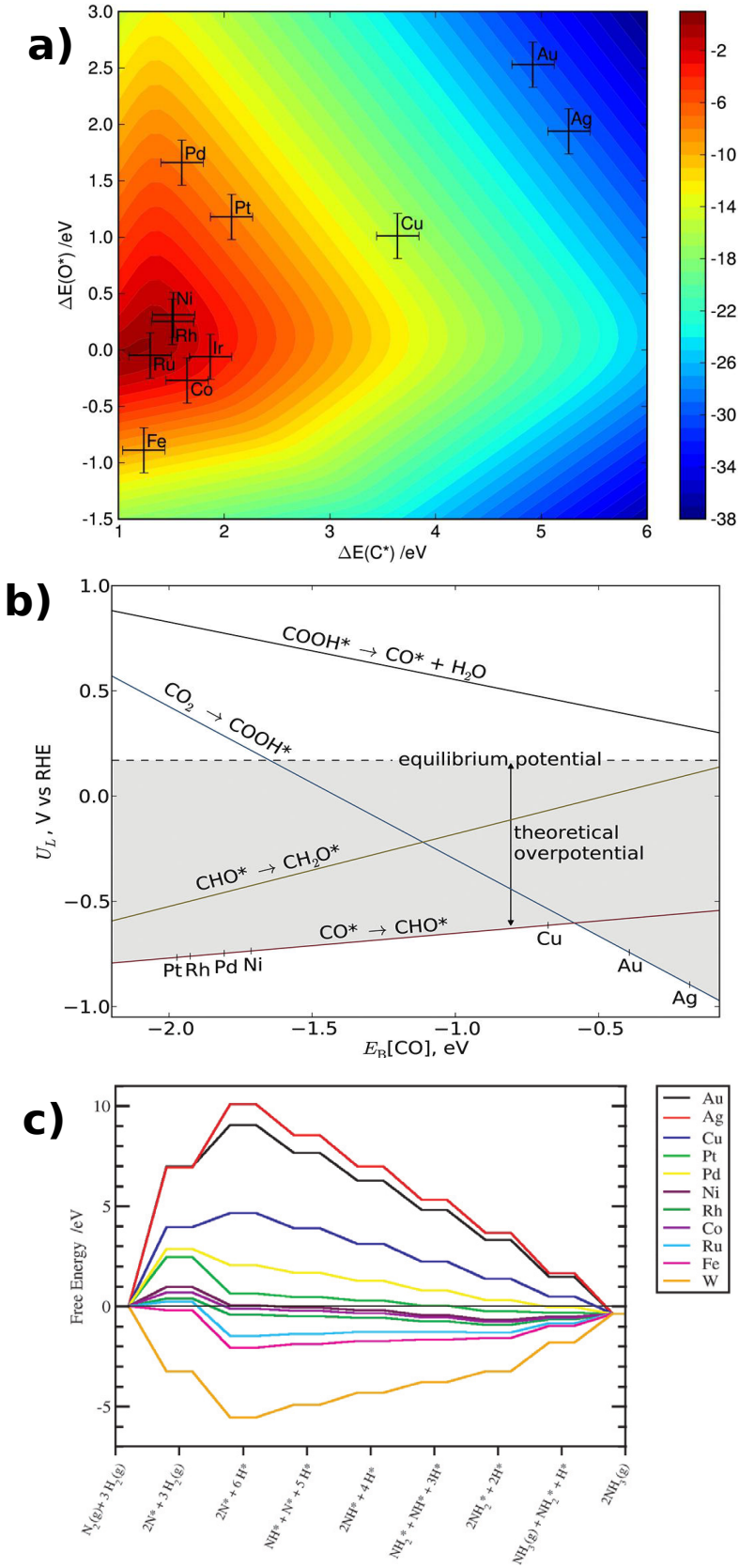

Figure 2.6: Examples of using scaling relations to elucidate trends in catalytic performance. a) A two dimensional volcano plot for methane steam reforming. Reprinted from 34. b) The theoretical overpotential for CO_2 electroreduction as a function of the CO adsorption energy. Reprinted from 87. c) Free energy diagrams for ammonia synthesis. Reprinted from 50.

been identified as descriptors for the activity for methanol electrooxidation on (111) and (100) surfaces of late transition metals [85, 86]. These descriptors were used to design a CuPt(111) alloy catalyst, which was confirmed experimentally to have improved activity over Pt(111) [126]. Similarly, methanol decomposition on four atom clusters has been reduced to C and O adsorption energies[70] or CO and O adsorption energies [21], and methanol dehydrogenation to formaldehyde was reduced to C and O adsorption energies using CatApp [127], a simple application that employs scaling and BEP relations, and a microkinetic model [76, 78]. Further, trends in ethanol decomposition were reproduced using scaling relations and a simple coverage model [102].

Methanol synthesis from syngas was studied using scaling relations and a kinetic model, and the C and O adsorption energies were identified as descriptors [77]. A CuNi alloy was predicted to be an effective catalyst, and this was confirmed experimentally. In a similar but more in-depth study, the activity for production of methane, methanol, and ethanol from syngas was reduced to C and O adsorption energies, allowing elucidation of trends in both activity and selectivity [73].

2.7.3 Conversion of Polyols and Biomass Derivatives

The conversion of biomass derivatives such as multifunctional alcohols is a challenging reaction for catalyst design, but successful catalysts for these reactions could have large impacts on biofuels and biochemicals. Since these reactions involve many complex intermediates, scaling relations can dramatically improve the efficiency of calculations. Scaling relations generally give reasonably good accuracy for these intermediates, which may be partly because only a few, fairly similar surfaces are usually employed. Nevertheless, on these surfaces scaling relations dramatically decrease the computational cost of studying these reactions.

Using group additivity and scaling-like relations based on the coordinative unsaturation of the atoms in the adsorbate, glycerol decomposition has been studied on Pt(111) [103, 106, 110]. These studies found that some dehydrogenation is necessary for C−C bond scission to become competitive with C−O and C−H bond scission. In particular, steps that form CO are generally quite favorable. Other studies have used scaling relations to examine glycerol decomposition on

other late transition metals, confirming these trends [107]. This work has indicated that Pt and Pd have higher selectivity towards C−C bond scission than Rh, Ru, and Ni [107, 108].

In a study reminiscent of the above work on methane and simple alcohols, the C, O, and H adsorption energies were identified as descriptors for ethylene glycol decomposition using scaling relations, BEP relations, a simple coverage model, and a microkinetic model [104]. It is noteworthy that such a complex reaction may be amenable to this kind of analysis; however, it may require a more complex treatment than simpler reactions, as adsorbate-adsorbate interactions were included. This study was able to reproduce kinetic trends on Pt, and found that early dehydrogenation reactions were kinetically important steps. A similar study was performed for ethylene glycol decomposition on Mo carbides [109]. Plots of activity for aqueous phase reforming of acetaldehyde and furfural as a function of the DFT-calculated C and O adsorption energies have been generated from experimental data using triangulation [128]. This study shows an interesting interplay of concepts from theory and experiment.

2.7.4 Oxygen Reduction and Evolution

Improving the activity or materials cost for oxygen reduction reaction (ORR) catalysts is one of the primary prospects for improving the commercial viability of fuel cells. Since ORR intermediates are small molecules that bind exclusively through O atoms, many recent ORR studies employ scaling relations. Scaling for these intermediates has been successful on a wide variety of surfaces, but the exceptions for late transition metal alloys mentioned in Section 2.8.2 should be noted.

An early, successful, widely cited study of the ORR used a kinetic model to generate a two-dimensional volcano plot as a function of the O and OH adsorption energies [129]. Even in this early work, a linear correlation between these adsorption energies was apparent. Since the development of scaling relations, several studies have employed the O adsorption energy [130–135] or the OH adsorption energy [60, 61, 92, 94] as descriptors. These studies conclude that the peak of the volcano occurs at an adsorption energy of OH around 0.10 eV weaker than Pt(111), and this

has significant experimental support [94, 136]. Focusing on the OH adsorption energy is probably preferable to the O adsorption energy because it is likely the most abundant surface intermediate.

Irrespective of the exact mechanism of the ORR, thermodynamic considerations can be used to derive conditions for the optimal catalyst assuming certain intermediates are involved [133]. If OOH and OH are intermediates, the difference in their free energies should be close to 2.46 eV, twice the equilibrium potential of 1.23 V, and the difference in their free energies is approximately the difference in their adsorption energies. However, scaling relations constrain the adsorption energy difference to ≈3.3 eV, imposing a fundamental limit on the maximum efficiency of fuel cells [60, 95, 133]. While some of the strategies mentioned in Section 2.8.2 may ameliorate this problem, the OH vs. OOH scaling relation appears to be particularly hard to break, likely because the two species adsorb similarly. Even in cases where OH and O_2 do not scale, OH and OOH do scale [96]. To overcome this challenge, a tandem cathode scheme has been proposed, in which different elementary steps occur on different catalyst surfaces [92].

The oxygen evolution reaction has been studied using scaling relations on oxides, graphitic materials, and protoporphorins, since under reaction conditions transition metal surfaces will oxidize [47, 48, 55, 61, 133, 137]. These studies come to similar conclusions as those for the ORR: the O adsorption energy, the OH adsorption energy, or their difference can be used as a descriptor for volcano plots, and the scaling relation between OH and OOH limits the maximum efficiency, although it may be possible to overcome this limitation by tuning the proton affinity of certain surface sites [137].

2.7.5 Other Applications

Scaling relations have been applied to a variety of other reactions, often in conjunction with BEP relations and kinetic models. They have been used to generate free energy diagrams for ammonia synthesis as a prediction of the qualitative trends across metals (see Fig. 2.6c) [50], and to discuss the possibility of a low-temperature ammonia synthesis process [98]. Volcano plots have been generated for the electrochemical synthesis of NH_3 from N_2 as a function of the N adsorption

energy, and there was good qualitative agreement on the peak of the volcano and the ordering of the activity of various metals on both extended surfaces and nanoparticles [58, 97]. A two-dimensional volcano plot, with the N and O adsorption energies, has been used to predict trends in NO decomposition [99]. This study found that using scaling and BEP relations introduces no change in the trends of metals, as compared to using energies from DFT. Volcano plots based on the O and CO adsorption energies have been generated for CO oxidation on a variety of metal facets and nanoparticles [89, 90]. The C and N adsorption energies have been found to be good descriptors for HCN synthesis [68, 79], while OH and CO are good descriptors for formic acid decomposition [138]. Scaling relations have been used to predict both surface termination and activity for the electrochemical evolution of chlorine on oxide surfaces [91]. Using a form of scaling relations based on metal-carbon bond energies in carbides, the activity for styrene hydrogenation was found to form a double volcano plot [88]. Assuming that scaling relations hold, fundamental limits on the efficiency of various electrochemical processes have been derived, similar to the above work on the ORR and CO_2 electroreduction [93, 95, 133, 139].

Scaling relations have also been used to design a catalyst for acetylene hydrogenation [81]. The adsorption energies of acetylene and ethylene were used as descriptors for the activity and selectivity, respectively, and these adsorption energies were found to correlate with that of methyl. Stronger adsorption of methyl lead to a more active catalyst, while weaker adsorption lead to a more selective catalyst, indicating the necessity of finding a compromise surface with an intermediate adsorption energy. DFT calculations indicated that NiZn alloys have a promising methyl adsorption energy and are stable, while being significantly cheaper than PdAg alloys. NiZn catalysts were synthesized and found to be quite selective, even more so than PdAg in some cases. Further improvements may be possible by employing some of the strategies for breaking scaling relations (Section 2.8.2) to strengthen acetylene adsorption while weakening ethylene adsorption. Scaling relations were also used to explain the effects of subsurface carbon on acetylene hydrogenation [82].

2.8 Deviations from Scaling Relations

2.8.1 Reported Failures

A few studies have found cases where scaling relations do not appear to hold, which may provide important information about their validity. For example, it has been shown that OOH and OH scale with O_2 but not with O on certain Pt alloys [96, 140]. This is likely due to the repulsive interactions that strongly affect adsorption energies of adsorbates with nearly full electron shells on late transition metals but have a much weaker effect for adsorbates with fairly empty shells. These interactions have been shown to cause O and OH to have different behaviors on these types of alloys [141].

A failure of scaling relations has also been reported for CH_x on AgNi alloys [69]. This is likely due to the fact that C and CH adsorb on the (111) facets of the step sites in some surface models and in the (100) facets in others, while CH_2 and CH_3 always adsorb on the (111) facets. This explanation is borne out by the good correlation between C and CH, and the fact that scaling relations were found to be valid in a similar study of AuNi alloys that included different surface models which only induced small changes in adsorption geometries [64].

Combining scaling relations for CH_x with BEP relations was found to be unreliable for RhNi alloys, while combining BEP relations with energies from DFT was reliable [142]. The unreliability of scaling relations in this case may be due to one or more of a variety of factors, including: the presence of co-adsorbed S in some cases; a lack of site-specificity; the small number of surfaces; the use of Eq. (2.2) instead of fitting γ; or the demand for high accuracy when considering such similar surfaces. The authors conclude that scaling relations are more useful for screening a range of transition metals than for performing further screening on a smaller subset, and that caution should be exercised when combining them with BEP relations [142].

2.8.2 Strategies for Inducing Deviations

As noted in Section 2.7, it is sometimes desirable to design materials that deviate from scaling relations, as they may impose limitations on catalytic performance by fixing the reaction energy of a particular elementary step. We now summarize some possible strategies, based in part on a previous discussion [87]. First, the above discussion of scaling relations in different environments suggests some possibilities. For example, the shape and size of nanoparticles [59], the geometry and frequency of step sites [35, 69], the presence and geometry of site blockers [69], adsorbate-induced relaxations [63], and alloying [69] may all affect different adsorbates differently. Differences in the effect of electronic structure on similar adsorbates can also lead to deviations from scaling relations. Examples include differences in OH and O on Pt alloys [96] and agostic interactions for hydrocarbons, as shown in Chapter 7. Even if scaling relations were perfectly accurate across all surfaces, they could still be broken using non-surface mediated interactions. These interactions could come from other intermediates [143], promoters [143], solvent [95, 143–145], or ligands [14, 146]. Additionally, nanostructures, zeolites, homogeneous catalysts, or enzymes may be used to affect intermediates based on their size or shape.

2.9 Summary, Conclusions, and Outlook

Scaling relations are linear relationships between adsorption energies of similar adsorbates. They may vary moderately on different facets, extended surfaces vs. nanoparticles, or metal surfaces vs. oxides/sulfides/nitrides, and the variation in the intercept is usually larger than the variation in the slope. Scaling relations occur when two adsorbates have a similar dependence on surface attributes. Changes in the surface structure, adsorbate geometry, non-surface mediated interactions, and occasionally electronic effects may cause deviations from scaling relations.

Scaling relations have been applied in a wide variety of cases. They can be used to simplify descriptions and to aid in high-throughput screening, often by reducing catalytic performance to a function of a few simple adsorption energies. Volcano plots have been generated for many

reactions based on the adsorption energy of atoms or other small adsorbates, and usually the number of dimensions of the volcano plot is equal to the number of different elements through which intermediates adsorb. This scheme allows simple rationalization of trends and more efficient screening of surfaces. Scaling relations can also constrain the optimal catalyst that can be achieved by fixing the reaction energy for a particular elementary step.

The summary of the application of scaling relations above implies the following:

- Scaling relations should not be assumed to apply for systems that may have significant structural or electronic differences from the training set.
- A combination of semi-empirical techniques (*e.g.*, scaling relations and BEP relations) has been successfully used in many cases, but errors may compound and high accuracy should not be assumed.
- Scaling relations are less likely to be useful when considering a small number of similar surfaces, where one is seeking to understand small energy differences.
- When studying different types of surfaces (*e.g.*, different facets or metals and oxides), it may be necessary to develop separate scaling relations on each type of surface, depending on the specific systems and the desired accuracy.
- If a particular intermediate is known to be particularly important, accuracy can be improved by scaling from that intermediate or from a very similar intermediate.
- A low mean error does not imply a low maximum error. In most cases, some individual surfaces deviate from scaling relations enough to affect the reactivity.

There are many possibilities for future work on scaling relations. For example, it may be possible to add complexity to scaling relations for increased accuracy or generality with little or no increase in computational effort. In particular, including more adsorbates and more types of surfaces or sites in a single framework may be useful. For example, it would be useful to predict when double

bonds should be counted as intra-adsorbate bonds and when they should be counted as bonds to the surface. Adapting scaling relations to account for non-covalent interactions may increase their applicability, and combining them with other models (e.g., for adsorbate-adsorbate interactions) may allow increasingly accurate predictions of catalytic performance. Exploring deviations from scaling relations will aid in deciding when they can safely be used and in finding better catalysts than those constrained by the relations. One possibility for this is to use electronic structure to explicitly explain the validity of scaling relations, which may provide insight into when they will hold and when they will fail. There may also be methods for further increasing the efficiency gains from scaling relations, such as finding scaling relations between adsorption through different atoms. Since scaling relations often allow the description of surface reactivity in terms of a few simple adsorption energies, a database of adsorption energies on multimetallic surfaces may allow screening of catalysts for many reactions at once.

Chapter 3

Literature Review: Predicting Adsorption From Surface Properties

3.1 Abstract

Predicting adsorption energies from surface properties is vitally important in surface science and catalysis. The Newns-Anderson model, which was based on a Green's function solution to a model Hamiltonian, elucidates how adsorption energies depend on the metal bands' interactions with the adsorbate orbitals. Effective medium theory identifies three separate contributions to the adsorption energy, most importantly the effect of the surface's electron density and the change in the energy of the one-particle states. Concepts from both of these theories were combined to form the d-band model, a simpler theory of adsorption that has been widely employed. Several other approaches have also been used, and many surface properties have been employed to predict adsorption energies.

3.2 Introduction

Understanding the relationship between adsorption energies and surface properties is an important goal in surface science. Not only is this relationship of scientific interest, but it has important technological ramifications, as adsorption is critical in a variety of technologies.

Scaling relations allow predictions of adsorption energies of a set of adsorbates given that of a particular adsorbate. These relations can significantly reduce the time needed to calculate a set of adsorption energies, and can also be used in analytical treatments of surface chemistry. However, they offer little insight into which surface properties affect adsorption energies. Gaining

this insight could lead to the rational design of catalytic surfaces as well as the development of models for quickly predicting adsorption energies.

Surface systems are difficult to treat theoretically because they do not have the full periodicity of a solid-state system, but they have a much larger number of atoms than most gas-phase or liquid-phase systems. This makes both analytical and computational approaches more difficult. Nevertheless, by combining concepts from solid-state systems as well as gas-phase systems, significant progress has been made in understanding adsorption.

Some early theories of adsorption were designed to allow predictions to be made with reasonable computational effort. However, with the advent of powerful computers and density functional theory (DFT), full computations of adsorption systems have become possible. Hence, the focus on adsorption theories has shifted. The goals of more recent theories are to improve our understanding of adsorption, to enable rational design of catalytic surfaces, and to significantly improve the efficiency of predictions, enabling high-throughput screening. DFT has also allowed researchers to check their predictions much more quickly and accurately than previously.

We begin with an overview of two early approaches to predicting adsorption energies, the Newns-Anderson model and effective medium theory. These models are rarely used for explicit prediction of adsorption energies, but they provide qualitative insight into adsorption. These two models lead to the development of the d-band model, which is widely used to explain trends in adsorption energies. We also mention other approaches, including various studies that empirically identify surface properties that correlate with adsorption energies.

3.3 The Newns-Anderson Model

In the 1960s and 70s, several researchers studied adsorption using model Hamiltonians [147]. The most important of this work resulted in the so-called Newns-Anderson or Newns-Anderson-Grimley model. Anderson originally developed a Green's function method for studying defects in metals [148]. This formalism was applied by Newns and coworkers to chemisorption [149, 150], and a similar formalism was developed independently by Grimley [151, 152].

The Newns-Anderson model applies the model, second-quantized Hamiltonian:

$$H = \epsilon_a \sum_{\sigma} n_{a\sigma} + \sum_{k,\sigma} \epsilon_k n_{k,\sigma} + \sum_{k,\sigma} (V_{ak} c^{+}_{a\sigma} c_{k\sigma} + V_{ka} c^{+}_{k\sigma} c_{a\sigma}), \tag{3.1}$$

where $n = c^{+}c$ is the number operator, c^{+} and c are the creation and annihilation operators, V_{ak} is the matrix coupling element between the adsorbate state ϕ_a (with energy ϵ_a) and the surface state ϕ_k (with energy ϵ_k), and σ is an index over the spin states. To focus on the states that are involved in chemisorption, the density of states projected on the adsorbate orbital is examined:

$$\rho_a := \sum_i |\langle \phi_i | \phi_a \rangle|^2 \delta(\epsilon - \epsilon_i) \tag{3.2}$$

Using a Green's function method, the final density of states on the adsorbed species can be calculated:

$$\rho_a(\epsilon) = \frac{1}{\pi} \frac{\Delta}{(\epsilon - \epsilon_a - \Lambda)^2 + \Delta^2}, \tag{3.3}$$

where

$$\Delta(\epsilon) = \pi \sum_k |V_{ak}|^2 \delta(\epsilon - \epsilon_k) \tag{3.4}$$

and Λ is the Hilbert transform of Δ:

$$\Lambda(\epsilon) = \frac{\Pr}{\pi} \int_{-\infty}^{+\infty} \frac{\Delta(\epsilon')}{\epsilon - \epsilon'} d\epsilon', \tag{3.5}$$

where Pr is the principal value. Finally, the change in the one-electron energies due to adsorption can be calculated by integration:

$$E_{\text{ads}} = 2 \left(\frac{1}{\pi} \int_{-\infty}^{\epsilon_f} \tan^{-1}\left(\frac{\Delta(\epsilon)}{\epsilon - \epsilon_a - \Lambda(\epsilon)}\right) d\epsilon - \epsilon_a \right), \tag{3.6}$$

where ϵ_f is the Fermi level.

This formalism is often applied to a model band in order to understand how varying the properties of the band affects the adsorption energy. The Newns-Anderson model has also been directly applied to some simple surface systems, including hydrogen interconversion [153], hydrogen adsorbed on jellium [154–156], hydrogen adsorbed on Pt group metals [149, 157], and alkalis adsorbed on free-electron like and transition metals [158]. However, the most important legacy of the Newns-Anderson model has been its effect on subsequent theories of adsorption.

3.4 Effective Medium Theory

Effective medium theory is another simple model of adsorption that can be derived from DFT [159–162]. In its simplest form, it assumes that the adsorption energy of a particular atom depends only on the electron density at the position where the atom is located. The adsorption energy as a function of the electron density for any type of atom can be calculated using the local density approximation of DFT, which gives the energy of the atom in a homogeneous electron gas (see Fig. 3.1). (A slightly more realistic picture is given by using an average density near the atom, determined by a sampling function.) By using a simple superposition of atomic electron densities of the atoms in the surface as input to this model, calculations can be made very efficiently. However, this form implies that a particular type of atom will have the same adsorption energy on every surface, as it will move around until it is located at the optimal density. Hence, even from its start, effective medium theory has included electrostatic corrections to the adsorption energy [113].

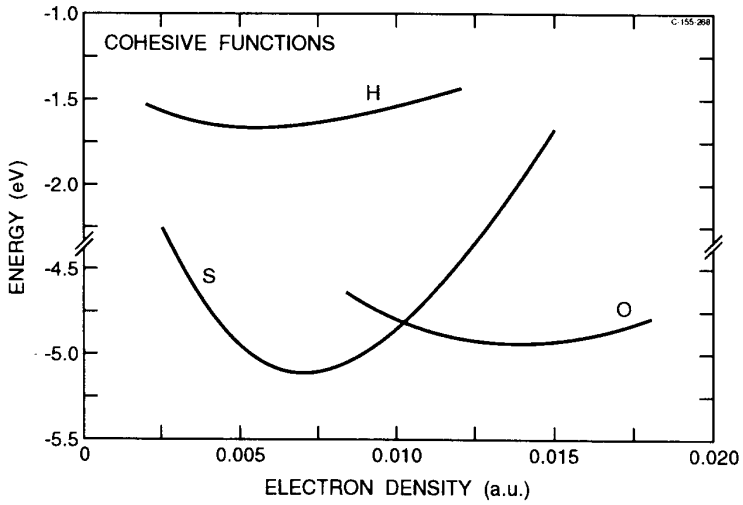

Figure 3.1: Cohesive functions for C, H, and S, showing the energy of embedding them into a homogeneous electron gas as a function of the density of the gas. From Ref. 163.

To increase the accuracy of effective medium theory, covalent interactions can be accounted for as a change in the one-particle states [164]. This can be calculated using an integral over the actual density of states if it is known, or can be approximated using an expression using perturbation

theory.

Including all the effects mentioned above, the full form of effective medium theory is [163]

$$E_{\text{tot}} = \sum_i E_{c,i}(n_i) + E_{AS} + E_{1el}, \tag{3.7}$$

where i is an index over the atoms of the system, E_c is the cohesive energy (i.e., Fig. 3.1), E_{AS} is an electrostatic energy term, and E_{1el} is the change in the one-electron energies between the homogeneous gas and the real system. The first two terms generally do not change much between different metals. On transition metals, the third term is dominated by interactions with the d-band, and its importance lead to the development of the d-band model, as described in the next section. Therefore, effective medium theory and d-band theory often end up with a similar picture when considering what factors control differences in adsorption energy between surfaces (see the next section). Indeed, calculations using effective medium theory show that the filling of the d-band is a primary factor in determining the adsorption energy [159, 165, 166].

Effective medium theory has been used in several studies to calculate adsorption energies of atoms on metal surfaces. This includes H on transition metals [160, 165]; H and O on jellium [113]; O on Ag, Cu, and Ni [163]; and O on 3d transition metals [163]. In general, these results capture the trends but do not give good absolute accuracy. For example, the errors for O on 3d transition metals were on the order of 1 eV. However, the accuracy for H on transition metals is much higher [162]. Effective medium theory has also been used to calculate heats of solution of H and He in metals [164], hydrogen-induced relaxations in Cu(111) [167], the effect of promoters [159, 168], the potential energy surface of H_2 on Cu and Ni [169], the structure of nanoparticles [170, 171], and various properties of metal surfaces [172]. Importantly, it has been used to provide support for a model of d-band shifts [173], to explain scaling relations [35], and to explain differences between early and late transition metals, as early transition metals cannot provide as much electron density [174]. There are also indications that the ideas behind effective medium theory can be applied to a wide variety of systems, and can explain some universal features of bonding [175].

3.5 The d-band Model

Currently, the d-band model is the dominant model for explaining and predicting trends in adsorption energies on transition metal surfaces. The heart of the d-band model is the assumption that variations in adsorption energies are due to changes in the interaction of the adsorbate electronic states with the d-band of the metal. Therefore, the adsorption energy is often broken into two pieces:

$$E_{\text{ads}} = \Delta E_{sp} + \Delta E_d, \tag{3.8}$$

where ΔE_{sp} is the contribution of the s and p bands to the adsorption energy, while ΔE_d is the contribution of the d band. This separation has been justified using effective medium theory, where ΔE_{sp} was associated with the embedding energy and ΔE_d was associated with the covalent interaction [161, 163, 164, 166]. The value of ΔE_{sp} is assumed to be approximately constant, although it is known to contribute significantly to the absolute value of the bonding. It is usually determined through fitting to adsorption energies. The value of ΔE_d has been estimated in a variety of ways.

The most complex treatment of the d-band model involves the application of the Newns-Anderson model to the interaction between the adsorbate and the sp-band, and a separate application to the interaction with the d-band [161, 166]. In other words, ΔE_{sp} and ΔE_d are estimated by appling Eq. (3.6) just to the sp states and then just to the d states. This is rarely done using a realistic density of states for the metal; instead, this approach is generally applied to a semi-elliptical model band [176]. Although ΔE_{sp} is assumed to be constant, the Newns-Anderson model still provides insight, as it shows that an adsorbate state interacting with a broad band will shift and broaden into a resonance state (see Fig. 3.2.) ΔE_d can then be calculated by considering how this resonance state interacts with the d band. The Newns-Anderson model shows that this results in a splitting of the d-band into bonding and antibonding states. As the band center increases, the adsorption bond becomes stronger due to decreased occupation of antibonding states. Increasing the coupling results in increased splitting, but also increases the orthogonalization

energy [112, 173, 177]. These qualitative arguments have been used to explain why Au is the noblest metal in many contexts [178].

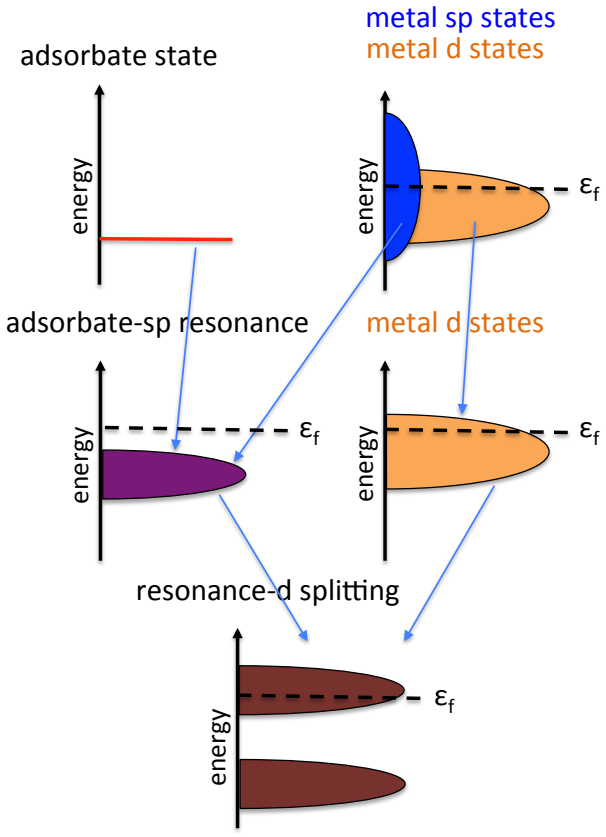

Figure 3.2: A schematic of the d-band model. An adsorbate state first broadens and shifts when interacting with the wide *sp*-bands. This resonance then interacts with the narrow d-band, forming bonding and antibonding states. A higher d-band center results in more unfilled antibonding states and stronger adsorption.

A much simpler treatment involves the use of the perturbation theory expression for the interaction of two orbitals [163, 173, 179–181]:

$$E = -2(1 - f_d) \sum_k \frac{|V_{ak}|^2}{(\epsilon_d - \epsilon_a)} \tag{3.9}$$

For example, some studies on CO adsorption have used this expression to account for the interactions between the d-band and both the filled 5σ and empty $2\pi^*$ orbitals [177]:

$$E_{\text{ads}}(\text{CO}) = -4\left[f\frac{V_\pi^2}{\epsilon_{2\pi} - \epsilon_d} + fS_\pi V_\pi\right] - 2\left[(1-f)\frac{V_\sigma^2}{\epsilon_d - \epsilon_{5\sigma}} + (1+f)S_\pi V_\pi\right], \tag{3.10}$$

where S is the overlap, which is assumed to scale roughly with V. The perturbation theory expression has been shown to capture trends in adsorption energy, but has never been shown to give quantitative accuracy for a wide variety of metal surfaces.

The simplest and most common treatment is to assume that the adsorption energy is proportional to the d-band center. This has been shown to work well in many cases, such as CO on various Pt surfaces [182], simple molecules on a particular late transition metal (including monometallic, alloy, and strained surfaces) [183], O on 3d metals [112], CO and H_2 on a few late transition metals [184], H and O on Pt skin alloys [185], dissociation of CO, N_2, and O_2 on a few late transition metals [186], O on Pt alloys [187], and CO on strained surfaces [174, 188]. However, these cases generally involve similar metals. It is known that the d-band center alone does not generally provide good accuracy when a range of metals are considered [189, 190]. Even when only considering a set of similar surfaces, the d-band center does not always give good accuracy [96]. Because adsorption energies are often related to catalytic performance, the d-band center has been used to rationalize trends for the oxygen reduction reaction on Pt alloys [30, 191]. However, it has been shown that this scheme fails when applied to a wider variety of metals [32].

A few studies have considered exceptions to the usual trends in the relationship between the d-band center and adsorption energies [141, 192]. Since these exceptions can be rectified by considering the effect of V_{ad}, these systems are well captured by the d-band model in its usual formulation. Other studies have considered which other factors may affect the adsorption energy, including the studies in this thesis. For example, some studies show improved accuracy if only the metal orbitals that interact significantly with the adsorbate are considered [188, 193]. The shape of the d band has also been shown to affect adsorption energies in some cases, as opposed to just the center [194]. The work function and melting temperature of the metal have also been shown to increase the accuracy of predictions, although these properties may be difficult to extend to alloy systems [195].

3.6 Other Approaches

Most other approaches to predicting adsorption energies from electronic structure have involved simple descriptors without complex theoretical backing. Since adsorption is often difficult to treat theoretically, these approaches have the advantage that they focus on predictive accuracy, which is generally the single most important factor. However, these approaches are less likely to be valid for predictions of systems that are fairly different from the training set.

For example, a previous study developed a model for predicting adsorption energies from very simple metal and adsorbate attributes [196]. The final model included the metal surface's surface energy, number of d electrons, first ionization potential, and atomic radius, as well as the adsorbate's HOMO-LUMO gap, molecular volume, and mass. A careful fitting procedure ensured the accuracy of this model for simple molecules on monometallic late transition metals, but it is unclear whether this would apply to other systems, and extension to alloy surfaces may prove difficult.

Other studies have found other surface attributes to be correlated with the adsorption energy. For example, the density of states at the Fermi level has been found to be correlated with the ethylene [197, 198] and OH_x [96] adsorption energies. It has been claimed that this may be due to a correlation between the DOS at the Fermi level and the d-band center [185], although one of these studies finds that using both properties significantly improves the predictive power over just using the d-band center [96]. Another study uses the attributes of the Slater orbitals associated with the metal atoms in the surfaces to predict adsorption energies [199]. The total number of valence electrons in the adsorbate and surface [80] and the number of "outer" electrons [54] have also been shown to correlate with adsorption energies in some cases. For transition metal carbides, the transition-metal derived surface resonance has been shown to correlate with adsorption energies [56].

A variety of other techniques have been used to study adsorption, including linear combinations of atomic orbitals [200–205], molecular orbital techniques such as extended Hückel theory [206–210], and the interstitial electron model [211, 212]. However, these techniques have

largely fallen out of favor, likely due to the availability of DFT for higher accuracy and the d-band model for increased simplicity.

3.7 Conclusion

The Newns-Anderson model, the most influential theory of adsorption from the 1960s and 70s, has had lasting effects on our understanding of interactions between adsorbate states and the metal bands. Because it uses a model Hamiltonion, the Newns-Anderson model is essentially a "top-down" approach, beginning with a complex description and applying approximations to gain insight. Effective medium theory takes the opposite approach, beginning with a very simple description and adding in effects. These two theories culminated in the development of the d-band model. Effective medium theory was used to justify the separation of the adsorption energy into a contribution from the s and p electrons as well as a contribution from the d electrons, and the Newns-Anderson model was used to study how different band parameters affect the interaction between the d band and the adsorbate orbital. This leads to our current understanding, that the location of the d-band center relative to the Fermi level is the single most important factor in determining adsorption energies, although other factors are also important, notably the d-band filling and the surface-adsorbate coupling.

Chapter 4

Adsorption of Alkyls on Cu(111)

4.1 Abstract

To better understand the nature of alkyl intermediates often invoked in reactions involving hydrocarbon reactants and products, the adsorption of linear and branched C_1-C_4 alkyls on Cu(111) at 1/4 ML and 1/9 ML coverages was studied using density functional theory. The adsorption energy and site preference are found to be coverage-dependent, and both direct alkyl−alkyl interactions and changes in the Cu electronic structure play a role in these trends. It was found that methyl strongly prefers the hollow sites, the branched alkyls strongly prefer the top site, and the linear C_2-C_4 alkyls have weak site preferences that change with coverage. To explain these differences, rationalize alkyl adsorption trends, and predict the binding energy of other alkyls, a simple model was developed in which the binding energy is fit as a linear function of the number of C−Cu and C−H−Cu interactions as well as the C−H bond energy in the corresponding alkane. Site preference can be understood as a compromise between C−Cu interactions and C−H−Cu interactions. Density of states analysis was used to gain a molecular-orbital understanding of the bonding of alkyls to Cu(111).

4.2 Introduction

Alkyl chemistry on transition metals has received significant attention due to its importance in several industrially significant processes, such as the steam reforming of methane to hydrogen, the reforming of methane to syngas, olefin hydrogenation, dehydrogenation of alkanes to olefins,

and Fischer-Tropsch synthesis [125, 213–220]. Additionally, alkyl groups have been invoked in the electrocatalytic reduction of carbon dioxide to hydrocarbons on copper electrodes [87, 122, 221]. This reaction has recently attracted considerable interest due to its potential as a source for environmentally-benign fuels [222–224]. A deep understanding of alkyl adsorption on copper could be valuable for understanding this reaction; in particular, it could help explain the observation that the reaction produces mostly short-chained hydrocarbons [225], the reasons for which are poorly understood. This poor understanding of long-chain production may stem from the fact that few systematic studies have probed how and why alkyl chain length and branching affects binding energy and site preference. In this chapter, we use density functional theory (DFT) to examine linear and branched C_1 to C_4 alkyls adsorbed in various sites, orientations, and coverages on Cu(111) in an attempt to understand their relative stability, site preferences, and adsorption mechanisms. These results represent a starting point toward developing a mechanism for long-chain alkane production under electrochemical conditions, and for obtaining a generalized understanding of alkyl adsorption trends with chain length and branching.

Methyl adsorption on transition metals has received considerable attention, partly due to its relative simplicity. DFT calculations [217, 220, 226–233] have indicated that the hollow sites are the most favorable for Ni(111), Rh(111), Cu(111), and Fe(100), while the top site is the most favorable for Pt(111), Pd(111), Au(111), and Ag(111). We note that the calculated preferred site on Rh(111) appears to depend on the exchange-correlation functional and the number of Rh layers, but that experiment indicates that the hollow sites are favored [217, 232]. Where available, experimental work is generally in agreement with the computational findings [234–236]. An early model for hydrocarbon adsorption proposed that CH_x would obey the tetravalency principle [206, 208]. While this is true on some surfaces (e.g., Pt(111) [237]), this is not the case for those where CH_3 adsorbs in a hollow site. The difference in site preference between Cu(111) and Pd(111) [227] as well as Ni(111) and Pt(111) [207] has been attributed to the size of the metal's d-orbitals. In Pd and Pt, the relatively large d-orbitals dominate the bonding; this type of bonding favors the top site. Since the d-orbitals are smaller in Cu and Ni, the s orbitals dominate the bonding, which favors

the hollow sites.

Methyl's structure on Cu(111) has been characterized using both theoretical and experimental techniques. Based on vibrational spectroscopy, Lin and Bent [238] argued that methyl adsorbs in a threefold hollow site on Cu(111). Chuang et al. [239] used pyrolosis of azomethane to generate methyl groups on Cu(111) and found that some of these groups decomposed to CH_2 and H. Pascal et al. [234] performed photoelectron diffraction for methyl on Cu(111) and found that at half saturation coverage, about 70% of methyl species were in fcc hollows and 30% were in hcp hollows. At saturation coverage, all methyl species were found to be in fcc hollows. DFT studies [226, 228] have confirmed that the fcc hollow is the most stable site, while the hcp hollow is nearly as stable.

Alkyls can be deposited on metal surfaces by dosing alkyl bromides or alkyl iodides, which readily dissociate to produce alkyls. This technique has been widely used to study alkyls on various surfaces [240]. However, alkyls longer than C_1 have not received a significant amount of theoretical treatment; they are generally expected to behave similarly to methyl. DFT studies have indicated that ethyl prefers the top site on Pt(111) [237, 241, 242], Cu(111) [243], Rh(111) [244], and Pd(111) [245]. Hence, on Cu(111) and Rh(111), DFT predicts that methyl and ethyl prefer different sites. To our knowledge, the reasons for this difference have not been discussed previously.

Adsorption of branched alkyls on transition metal surfaces has received relatively little attention. Weaver et al. [246] found that branched alkyls are more reactive than linear alkyls on Pt(111). Jenks et al. [247] characterized methyl, ethyl, propyl, and isopropyl on Cu(110) using reflection-absorption infrared spectroscopy, and found that the terminal methyl groups in isopropyl have a similar orientation to those in ethyl. A recent DFT study [215] considered C_1 to C_3 branched and linear alkyls on Pt(111), and found that isopropyl is bound less strongly than propyl.

Softened vibrational modes in methyl have been observed using experimental and/or theoretical techniques in Rh(111) [232, 248], Ni(111) [235, 249], and Cu(111) [229, 233, 238, 250], but not in Pt(111) [207, 236], or Ru(0001) [236]. Various explanations for mode softening have been proposed. Lin and Bent [238], using selectively deuterated iodoalkanes, found that mode softening occurred in C_1 to C_3 linear alkyls on Cu(111) for α C−H bonds, but not for other C−H bonds.

They proposed that this occurred due to charge donation from the metal to antibonding orbitals in the alkyls. Schüle et al. [251] performed a configuration interaction study of methyl adsorption on Ni(111) and also attributed mode softening to charge transfer from the surface to methyl. However, more recent DFT calculations of methyl on Ni(111) [252] and Pt(111) [207] have indicated that mode softening is caused by agostic interactions, in which charge density from the C−H bonding orbital is attracted to the metal. Michaelides and Hu [229] found a relationship between the extent to which a metal can soften modes and the activation energy to dehydrogenate methyl. They also proposed that mode softening occurs in the hollow sites but not the top site.

In this manuscript, we describe the results of calculations of alkyl adsorption for a variety of linear and branched alkyls on Cu(111). To our knowledge, this is the first such systematic study of such a series of alkyl species on a metal surface. We then examine the effects of coverage on alkyl adsorption and some potential explanations for these effects. Next, we develop a simple, accurate model that allow us to conceptualize the site preference of the various alkyls and predict the adsorption energy of any alkyl in any site. Finally, we examine the nature of alkyl−Cu(111) bonding using density of states (DOS) calculations. Results from this work are compared to observations from experiment where available.

4.3 Methods

The Vienna ab initio Simulation Package (VASP) [253, 254] was used for periodic DFT calculations. The plane-wave basis set was cut off at 396 eV, and the projector-augmented wave method [255] was used. The PW91 [256] exchange-correlation functional was used; a previous study of methyl on Rh(111) [217] found that PW91 predicted that the hollow sites are more favorable, in agreement with experiment, while RPBE predicted that the top site is more favorable. Additionally, a study of methyl on Cu(111) [233] found that RPBE incorrectly predicted the hcp hollow as the most favorable, while we found that PW91 correctly predicted the fcc hollow site as the most favorable. To model the copper substrate, four layers were used, with the bottom two fixed at the theoretical lattice constant of 3.65 Å (the experimental lattice constant is 3.61 Å). For the 3×3

surface cell calculations, a 7×7×1 Monkhorst-Pack k-point mesh with Methfessel-Paxton smearing was used for geometric relaxation; an 11×11×1 mesh was used for calculations with a 2×2 surface cell. The forces were converged to 0.01 eV/Å. The only exceptions were for methyl in the bridge sites at 1/4 ML; these were converged to 0.02 eV/Å since they relaxed into hollow sites at 0.01 eV/Å. The relaxed geometry was then fixed and single-point energy calculations were performed with the tetrahedron smearing scheme and an 11×11×1 k-point mesh for the 3×3 supercell and a 15×15×1 mesh for the 2×2 supercell. The final energies and charge densities were taken from these latter calculations. This change to more accurate k-point density and smearing scheme was necessary to ensure absolute convergence of adsorption energies, which allowed comparison across different coverages. Test calculations demonstrated that spin polarization had a negligible effect; hence, spin polarization was not employed. DOS calculations were performed by fixing the charge density and performing non-self consistent DFT at 19×19×1 k-points for the 3×3 supercell and 29×29×1 k-points for the 2×2 supercell.

Two methods were used to assign atomic charges: the Bader charge [257] and density derived electrostatic and chemical charges (DDEC) [258]. The Bader charge is widely used in periodic DFT calculations; it uses minima in the charge density to partition space and assign charge density to particular atoms. The DDEC is a newer technique that chooses atomic charges to reproduce the electrostatic potential and to be chemically meaningful. The atoms in a given system are referenced to isolated ions of the same element. The DDEC gave results that are more chemically intuitive; however, the arguments related to atomic charges made in this paper are supported by both methods. Atomic graphics were created with QuteMol [259].

4.4 Results and Discussion

4.4.1 Adsorption Geometries

Geometry optimizations were performed with each alkyl adsorbed in each of the four high-symmetry sites on Cu(111) at two distinct orientations (rotated about an axis perpendicular to

the surface) at coverages of 1/9 ML and 1/4 ML. Since all the previously-cited theoretical and experimental studies have agreed that alkyls adsorb in an upright configuration, we did not explore the stability of non-upright orientations. Side views of each alkyl adsorbed in the top site are given in Fig. 4.1; the essential profile of each alkyl is preserved upon translation to other sites. Top views are shown of the stable configurations of methyl (Fig. 4.2), propyl (Fig. 4.3), and the branched alkyls (Fig. 4.4); these figures also define the site terms we will employ throughout this work. The "30" or "60" on the end of a site designation indicates a rotation of 30° or 60°. For example, the top30 site is obtained by rotating the adsorbate 30° about an axis perpendicular to the surface. The sites for propyl are the same as those for ethyl and butyl. The potential energy surface of alkyls on Cu(111) appears to be quite complex; there are often multiple minima in or near a high-symmetry site with different energies. These differences are generally small but are sometimes non-negligible. To simplify the data, we report the energies and geometrical parameters for the lowest energy minimum near each site. If two minima have the same energy (within 0.005 eV), we report the one closer to the high-symmetry site.

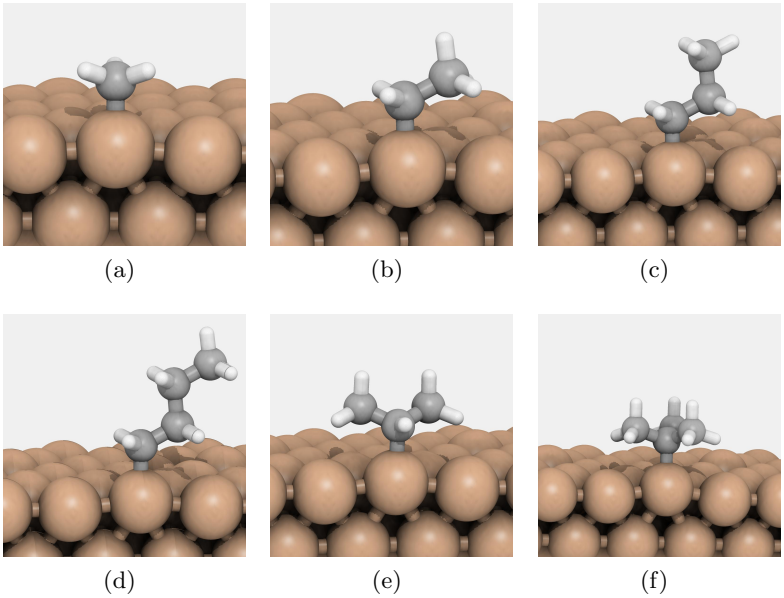

Figure 4.1: Side views of alkyls in the top site: (a) methyl, (b) ethyl, (c) propyl, (d) butyl, (e) isopropyl, (f) tert-butyl.

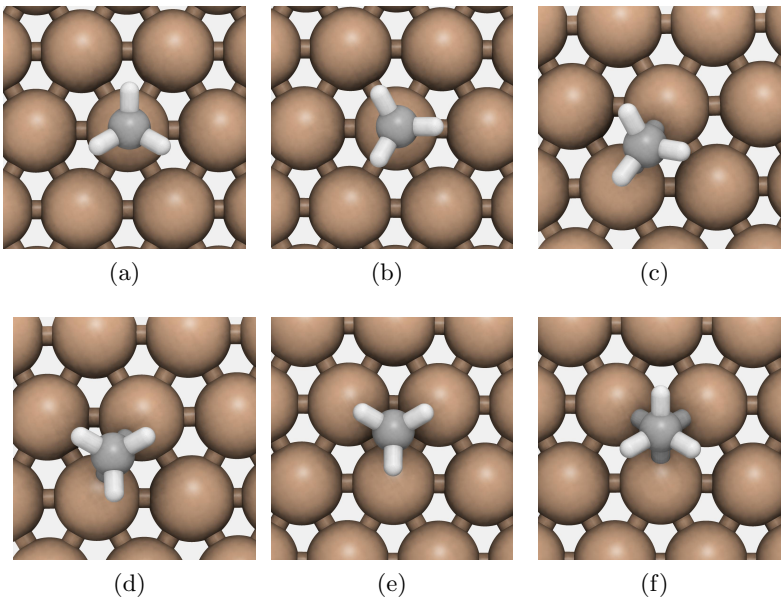

Figure 4.2: Top view of methyl in various sites: (a) top, (b) top30, (c) bridge, (d) bridge30, (e) fcc/hcp, (f) fcc60/hcp60.

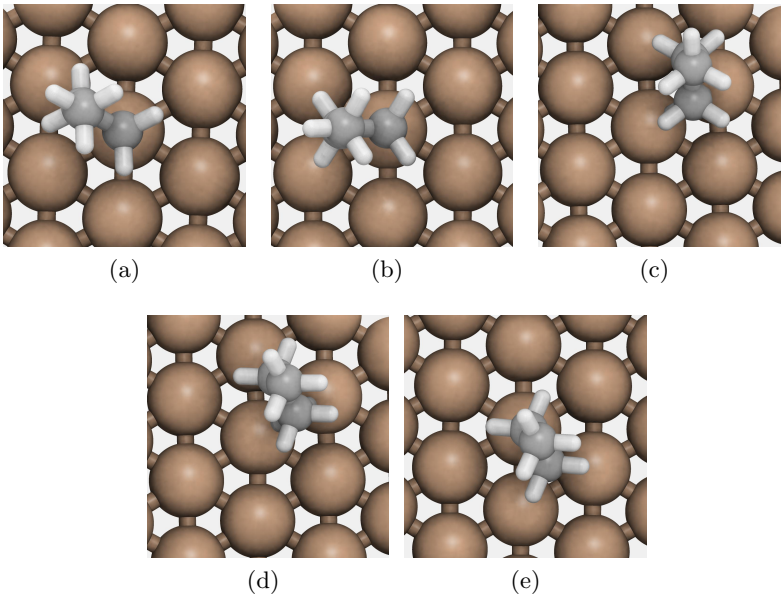

Figure 4.3: Top view of propyl in various sites: (a) top, (b) top30, (c) bridge, (d) bridge30, (e) fcc/hcp. This also defines the sites for ethyl and butyl.

Selected C−Cu and H−Cu distances are given in Tables 4.1 and 4.2. Pascal et al. [234] found that methyl lies 1.66 ± 0.02 Å above the Cu(111) surface with a C−Cu bond length of 2.22

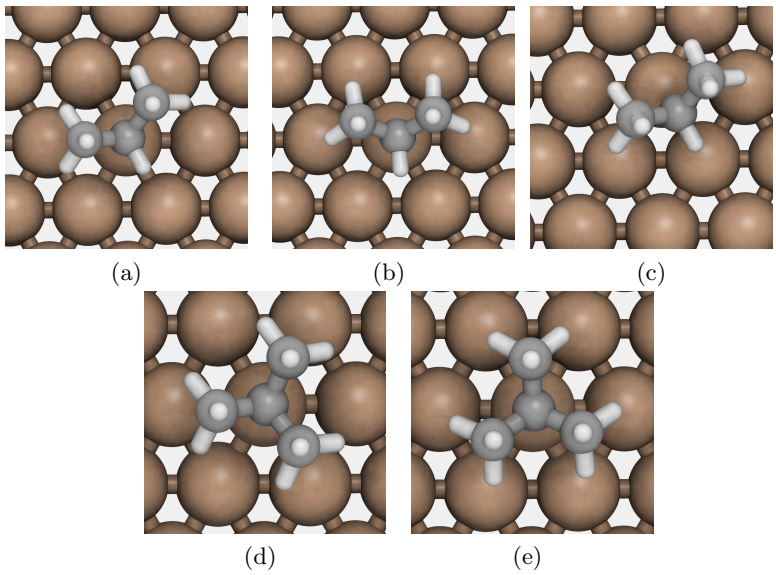

Figure 4.4: Top view of branched alkyls in various sites: (a) top, (b) top30, (c) bridge, (d) top, (e) top30.

$\pm$ 0.02 Å, which compares well with our calculated values of 1.68 Å and 2.24 Å. At 1/9 ML, the parameters for ethyl, propyl, and butyl are generally quite similar, while those for methyl, isopropyl, and tert-butyl vary from the linear C_2-C_4 alkyls and from each other. In the fcc hollow, there is a trend for ethyl, propyl, and butyl: as the carbon chain lengthens, the C−Cu distance decreases and the H−Cu distance increases. The alkyls generally were close to the center of the hollow in the fcc hollow, while they were off-center in the hcp hollow. This may be due to a small amount of repulsion between the alkyl and the Cu atom in the second layer in the hcp hollow. In nearly all cases, the H−Cu distances are significantly longer in the bridge30 site than in any other site.

The alkyls induced relaxation in the copper lattice, particularly for adsorption in the top site. For example, at 1/9 ML coverage, tert-butyl in the top site stretches the Cu−Cu bond length to 2.81 Å, compared to 2.56 Å in the relaxed, bare lattice. Roughly, the smaller the C−Cu distance in the top site (which correlates with stronger adsorption), the less the lattice is distorted, with methyl in the top site resulting in a Cu−Cu bond length of 2.67 Å. A previous study [207] of methyl and H on Pt(111) found that in the top site, H interacted more strongly with the surface than methyl, which pushed more Pt d states above the Fermi level and strengthened Pt−Pt bonds. This same

Table 4.1: C−Cu and H−Cu distances in Å at 1/9 ML in the sites and orientations defined in the Figures in the main text. Only α carbon and hydrogen atoms are included.

	top	top30	bridge	bridge30	fcc	fcc60	hcp	hcp60
Methyl C−Cu	2.00	2.00	2.13	2.17(×2)	2.24(×3)	2.31(×3)	2.24(×3)	2.31(×3)
			2.22					
Methyl H−Cu	–	–	2.12	2.22(×2)	2.16(×3)	–	2.16(×3)	–
Ethyl C−Cu	2.03	2.03	2.12	2.20	2.18	NS[a]	2.23	NS
			2.33	2.21	2.38(×2)		2.33(×2)	
Ethyl H−Cu	–	–	2.05	2.18	2.09(×2)	NS	2.06	NS
				2.19			2.07	
Propyl C−Cu	2.02	2.02	2.12	2.19	2.16	NS	2.18	NS
			2.33	2.22	2.42(×2)		2.33	
							2.44	
Propyl H−Cu	–	–	2.07	2.19	2.12	NS	2.08	NS
				2.21	2.13		2.13	
Butyl C−Cu	2.03	2.03	2.12	2.19	2.13	NS	2.28(×2)	NS
			2.33	2.21	2.48		2.35	
					2.49			
Butyl H−Cu	–	–	2.07	2.18	2.18	NS	2.08	NS
				2.21	2.17		2.10	
i-Propyl C−Cu	2.06	2.06	2.12	NS	NS	NS	NS	NS
			2.55					
i-Propyl H−Cu	–	–	2.07	NS	NS	NS	NS	NS
t-Butyl C−Cu	2.10	2.10	NS	NS	NS	NS	NS	NS

[a]Not Stable.

logic—that stronger adsorbate-metal interaction leads to stronger metal-metal bonds—may explain why those alkyls that adsorb more strongly cause less lattice distortion.

The internal geometry of the alkyls differs little between sites. The most important change is that the C−H distance lengthens from 1.10 Å to 1.11 Å when the H atom is interacting with a Cu atom. While this is only a change of 0.01 Å, it is significant due to the steep potential well of the C−H bond. This lengthening has been associated with softened vibrational modes [229]. Additionally, the C_α−C_β bond length tends to increase in higher-coordinated sites. For example, the C_α−C_β bond in ethyl is 1.52 Å in the top sites, 1.53 Å in the bridge sites, and 1.54 Å in the

Table 4.2: C−Cu and C−H bond distances in Å at 1/4 ML in the sites and orientations defined in the Figures in the main text. Only α carbon and hydrogen atoms are included.

	top	top30	bridge	bridge30	fcc	fcc60	hcp	hcp60
Methyl C−Cu	2.00	2.00	2.12	2.18(×2)	2.24(×2)	2.31	2.26(×3)	2.30
			2.25		2.25	2.32(×2)		2.33(×2)
Methyl H−Cu	–	–	2.10	2.21(×2)	2.17(×2)	–	2.19(×2)	–
Ethyl C−Cu	2.02	2.02	2.11	2.21(×2)	2.18	NS[a]	2.15	NS
			2.37		2.39(×2)		2.43(×2)	
Ethyl H−Cu	–	–	2.06	2.18	2.08(×2)	NS	2.10(×2)	NS
				2.19				
Propyl C−Cu	2.02	2.02	2.10	2.21	2.13	NS	2.11	NS
			2.41	2.22	2.48(×2)		2.48	
							2.63	
Propyl H−Cu	–	–	2.06	2.18	2.15	NS	2.13	NS
				2.20	2.16		2.28	
Butyl C−Cu	2.02	2.02	2.09	NS	2.11	NS	2.12	NS
			2.44		2.52		2.44	
					2.55		2.66	
Butyl H−Cu	–	–	2.12	NS	2.18	NS	2.09	NS
					2.21		2.33	
i-Propyl C−Cu	2.06	NS	2.12	NS	NS	NS	NS	NS
			2.48					
i-Propyl H−Cu	–	–	1.96	NS	NS	NS	NS	NS
t-Butyl C−Cu	2.10	NS	NS	NS	NS	NS	NS	NS

[a]Not Stable.

hollow sites.

4.4.2 Binding Energy Trends

The binding energies of the linear alkyls at 1/4 and 1/9 ML are given in Table 4.3, referenced to the alkyl in the gas phase:

$$E_{\text{ads}} = E_{\text{Alkyl/Cu(111)}} - E_{\text{Cu(111)}} - E_{\text{Alkyl}}. \tag{4.1}$$

As demonstrated in Table 4.3, methyl diverges from the trends of the other linear alkyls in two ways. First, methyl is significantly more stable, whereas the adsorption energy for ethyl, propyl,

and butyl are quite similar. Second, methyl's site preference is different, particularly at 1/4 ML where it prefers the fcc hollow, while the longer alkyls prefer the top or bridge site. We attempt to explain this surprising observation in the next section. Lin and Bent's finding [238] that α C−H bonds for C_1-C_3 have softened vibrational modes indicates that the hollow sites were likely the adsorption sites in their experiments. Since they used a 4 L dose, this seems to contradict our calculations, which predict that at higher coverage ethyl and propyl have a small preference for top and bridge sites. However, Lin and Bent dissociated alkyl iodides and alkyl bromines to produce alkyl groups, and the presence of iodine or bromine may effectively lower the coverage of alkyls. In any case, C_2-C_4 linear alkyls appear to adsorb with approximately equal energies in several types of sites. In contrast, methyl clearly favors the hollow sites. Note that for methyl, the fcc and hcp hollow are essentially isoenergetic at 1/9 ML coverage, while the fcc hollow is favored at 1/4 ML. This agrees with Pascal et al.'s [234] finding that there is a mix of fcc and hcp sites at low coverages, and only fcc sites at high coverages. Butyl and propyl display very similar behaviors, particularly at low coverage: at 1/9 ML, butyl is 0.01 eV less stable than propyl, on average. Hence, we expect alkyls longer than butyl to display essentially the same behavior, aside from changes in alkyl−alkyl repulsions.

The branched alkyls are only stable at low-coordinated sites and bind much less strongly than their linear counterparts, in agreement with Yang et al.'s finding that isopropyl is less strongly bound than propyl on Pt(111) [215]. In fact, at 1/4 ML tert-butyl's binding energy is positive, indicating that repulsive alkyl−alkyl interactions are stronger than the alkyl−Cu interaction. Additionally, branched alkyls are overall less stable; i.e., the isomerization reaction from linear alkyls to branched alkyls is endothermic (at 1/9 ML, by 0.11 eV for propyl/isopropyl, 0.17 eV for butyl/tert-butyl; at 1/4 ML, by 0.42 eV for propyl/isopropyl, 1.04 eV for butyl/tert-butyl).

4.4.3 Coverage Effects

The binding energy data allow us to gain an idea of the magnitude of alkyl−alkyl interactions on the surface. We can measure the difference in alkyl−alkyl interactions at 1/9 and 1/4 ML by

Table 4.3: Binding energies in eV of linear alkyls at 1/4 and 1/9 ML in the sites and orientations defined in Figs. 4.2 to 4.4.

1/9 ML								
	top	top30	bridge	bridge30	fcc	fcc60	hcp	hcp60
Methyl	−1.33	−1.33	−1.41	−1.42	**−1.49**[a]	−1.30	**−1.49**	−1.31
Ethyl	−1.04	−1.04	**−1.06**	−1.05	**−1.06**	NS[1]	**−1.06**	NS
Propyl	−1.09	−1.10	**−1.12**	−1.10	−1.10	NS	−1.11	NS
Butyl	−1.08	−1.09	**−1.11**	−1.09	−1.09	NS	−1.09	NS
Isopropyl	−0.78	**−0.79**	−0.76	NS	NS	NS	NS	NS
Tert-butyl	**−0.55**	−0.54	NS	NS	NS	NS	NS	NS
1/4 ML								
	top	top30	bridge	bridge30	fcc	fcc60	hcp	hcp60
Methyl	−1.33	−1.32	−1.37	−1.38	**−1.44**	−1.26	-1.43	−1.25
Ethyl	**−1.04**	−1.02	−1.03	−1.00	−1.00	NS	−1.00	NS
Propyl	**−1.10**	−1.08	−1.09	−1.06	−1.06	NS	−1.06	NS
Butyl	**−1.08**	−1.05	**−1.08**	NS	−1.05	NS	−1.05	NS
Isopropyl	**−0.48**	NS	−0.45	NS	NS	NS	NS	NS
Tert-butyl	**0.34**	NS	NS	NS	NS	NS	NS	NS

[a]The most stable site(s) for each alkyl at each coverage is in bold

Table 4.4: The difference in binding energy (ΔBE) and total energy (ΔE) between a linear alkyl and the corresponding branched alkyl (in eV).

1/9 ML		
	ΔBE	ΔE
Propyl/Isopropyl	0.31	0.11
Butyl/Tert-butyl	0.54	0.17
1/4 ML		
	ΔBE	ΔE
Propyl/Isopropyl	0.62	0.42
Butyl/Tert-butyl	1.41	1.04

subtracting the binding energies; this is shown in Fig. 4.5a. We can gain an idea of the magnitude of direct alkyl−alkyl interactions, as opposed to those mediated by the surface, by examining the binding energies in the top site. At 1/9 ML, all the alkyls display essentially the same binding energies in the top and top30 sites. Further, both charge calculations and the relaxed geometries indicate that each alkyl has the same effect on the lattice in the top and top30 sites. However, at 1/4 ML the top30 site becomes relatively less stable for the linear alkyls as the chain length increases. This orientation reduces the shortest distance between an alkyl and its periodic images,

which increases their interaction. Therefore, the differences between the values in Fig. 4.5a for the top and top30 sites give an idea of the magnitude of direct alkyl−alkyl interactions in the top30 site. This value ranges from ∼0.00 eV for methyl to ∼0.04 eV for butyl. These interactions appear to be much stronger for the branched alkyls, such that the top30 site is no longer stable at 1/4 ML. We attribute the small negative value for propyl in the top site to a small error in the calculations. The PW91 functional does not include van der Waals interactions, and this will have an effect on direct interactions. Based on previous work on alkylthiolate adsorbates on Au(111), we estimate that the difference in van der Waals interactions between 1/9 ML and 1/4 ML would be roughly ∼0.1 eV for methyl and ∼0.2 eV for butyl [260]; i.e., it would shift the curves in Fig. 4.5a down by these amounts. However, site preference is not likely to be affected significantly, since alkyl−alkyl distances do not change upon translation between sites.

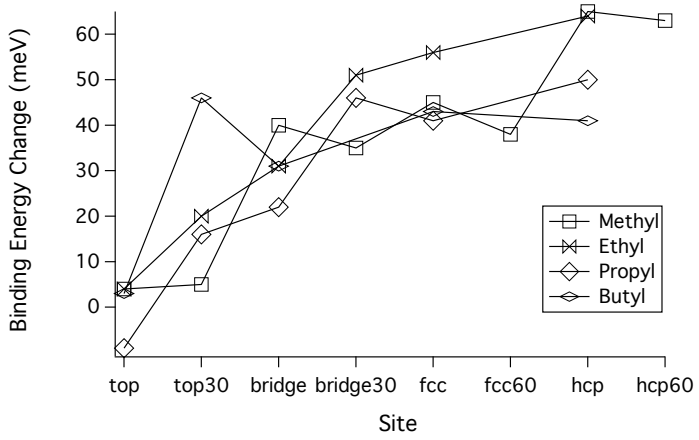

Figure 4.5: The change in binding energy upon a change in coverage from 1/9 ML to 1/4 ML; positive values indicate that the alkyl binds more strongly at 1/9 ML

Although there is little or no methyl−methyl interaction at these coverages in the top site, the binding energy in the hollow sites changes by about 0.05 eV when the coverage is reduced. The other linear alkyls behave similarly: the effect of coverage is higher at higher-coordinated sites. This trend holds regardless of orientation, so direct alkyl−alkyl interactions are unlikely to be the cause. We attribute these differences to variations in both dipole-dipole interactions and the influence of

the alkyls on Cu's electronic structure.

The shorter alkyls are more useful for studying these non-direct interactions due to the lack of direct interactions; hence, we focus on methyl. Using the DDEC, we calculated the dipole moment on the C atom at 1/9 ML. Figure 4.6a shows the effect of coverage on binding energy (the quantity in Fig. 4.5) versus the dipole moment on the C atom for methyl in all eight sites we considered. There is a correlation between the two, and we conclude that dipole-dipole interactions are one cause of the changes in the effect of coverage across different sites. However, the dipole moment is nearly the same in the fcc and hcp sites, yet the effect of coverage is different. We attribute this to changes in the d-band center.

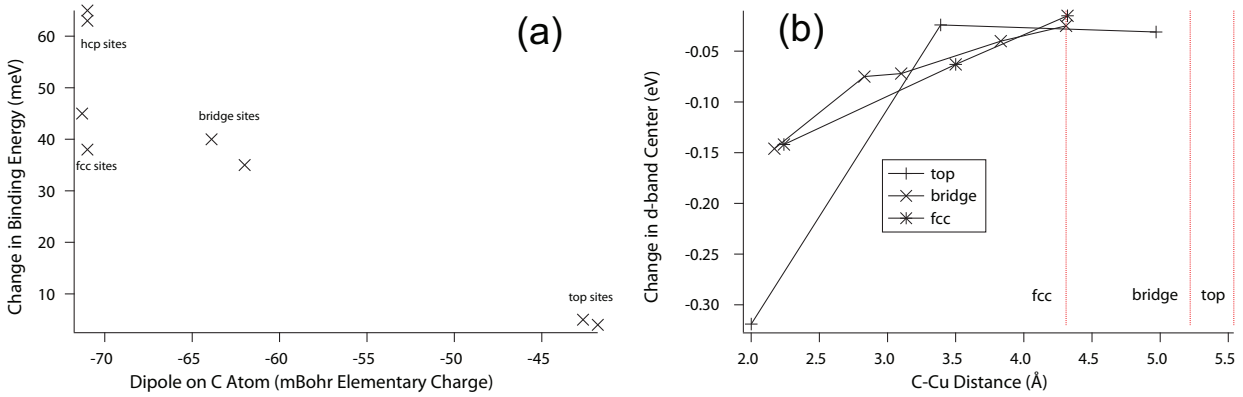

Figure 4.6: (a) The difference between the binding energy at 1/9 ML and 1/4 ML versus the dipole moment (perpendicular to the surface) of the C atom in methyl for various sites. (b) The change in d-band center of each surface Cu atom as a function of the distance between that Cu atom and the C atom in methyl at 1/9 ML. The change is relative to the bare Cu surface. The distance between the C atom and the closest Cu atom that is bonded to a neighboring methyl group in each site is given by the vertical, dotted lines.

Adsorbed methyl lowers the d-band center of nearby Cu atoms; the magnitude of this shift is shown in Fig. 4.6b for each surface Cu atom as a function of the C−Cu distance for methyl in the top, bridge, and fcc sites. According to d-band theory, a downward shift in the d-band center should result in more antibonding filling and weaker bonding, so this shift may be responsible for the lattice-mediated interactions. Figure 4.6b also shows the distance between a C atom and the Cu atom bonded to a neighboring methyl group. The d-band shift appears to persist to further

distances in higher-coordinated sites, whereas most of the effect for top-adsorbed methyl is confined to the atom onto which methyl is adsorbed. Furthermore the d-band shift does not need to persist as far in higher-coordinated sites to have an effect on adsorption, as the distance between methyl and a neighbor-bonded Cu atom is smaller.

There is significant difference in the effect of coverage between the fcc and hcp sites, even though the alkyls have nearly identical effects on the lattice in these two sites and the distance from the C atom to a neighbor-bonded Cu atom is essentially the same. We attribute this to the fact that there is an additional atom near the alkyl (in the subsurface layer) in the hcp site. When this atom's d-band center is shifted, it destabilizes alkyl adsorption; in the fcc hollow this effect does not occur. This reasoning would also explain the differences between the fcc60 and hcp60 sites.

4.4.4 Linear Site-Preference Model

The trends in the binding energies show some striking features, particularly the differences between methyl and the other alkyls. A likely source of the difference in site preference is that methyl has three hydrogen atoms near the surface, which allows three agostic interactions in the hollow sites. To elucidate the energetic importance of these interactions, we develop a simple model for the binding energy of an alkyl in a given site as a function of the number of C−Cu and H−Cu interactions. The number of C−Cu and H−Cu interactions for each case is the number of C−Cu and H−Cu distances shown in Tables 4.1 and 4.2. However, it is generally clear from Figs. 4.2 to 4.4 how many C−Cu and H−Cu interactions there are for a given alkyl and site. Since the bridge30 site has H−Cu interactions that are significantly longer than in other sites, we give these interactions their own parameter. Hence, we propose that the binding energy can be approximated as follows:

$$E_{\text{ads}} = E_{\text{C-Cu}} + \Delta E_{\text{C-Cu}}(n_{\text{C-Cu}} - 1) + E_{\text{H-Cu}} n_{\text{H-Cu}} + E'_{\text{H-Cu}} n'_{\text{H-Cu}}, \tag{4.2}$$

where $n_{\text{C-Cu}}$ is the number of C−Cu interactions, $n_{\text{H-Cu}}$ is the number of H−Cu interactions, and $n'_{\text{H-Cu}}$ is the number of "long" H−Cu interactions, which only occur in the bridge30 site. The other parameters in Eq. (4.2) have simple physical interpretations: $E_{\text{C-Cu}}$ corresponds to the energy of

one C−Cu interaction (i.e., the binding energy in the top site), $\Delta E_{\text{C-Cu}}$ corresponds to the change in energy of the C−Cu interaction as the number of C−Cu interactions increases by one, $E_{\text{H-Cu}}$ corresponds to the energy of one H−Cu interaction, and $E'_{\text{H-Cu}}$ corresponds to the energy of one "long" H−Cu interaction. Hence, the first two terms on the right side of Eq. (4.2) give the energy of the C−Cu interactions, while the last two terms give the energy of the H−Cu interactions.

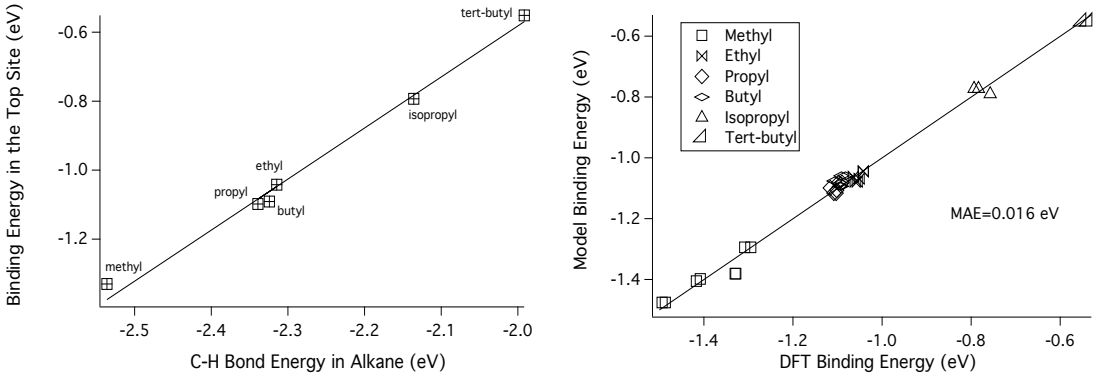

(a) (b)

Figure 4.7: (a) The binding energy in the top site at 1/9 ML v. the C−H bond strength in the corresponding alkane, calculated from $C_nH_{2n+1} + \frac{1}{2}H_2 \longrightarrow C_nH_{2n+2}$. (b) The binding energy from the linear site-preference model as a function of the binding energy from DFT.

Previous work [261] on organometallics and bismuth suggests that the C−Cu bond strength of an alkyl (i.e., $E_{\text{C-Cu}}$) should linearly correlate with the bond strength of the corresponding C−H bond in the corresponding alkane, with a slope on the order of one. This concept has been applied to surfaces previously [261, 262]. Figure 4.7a shows that the calculated C−Cu bond energies do indeed correlate linearly with the C−H bond energies, which were calculated with plane-wave DFT as the reaction energy of $C_nH_{2n+1} + \frac{1}{2}H_2 \longrightarrow C_nH_{2n+2}$. The linear fit has an R^2-value of 0.994 and a slope of 1.48. Apparently, the factors that determine the C−H bond energy have a similar, but larger, effect on the C−Cu bond strength, resulting in a slope steeper than 1. Using experimental bond strengths [263] also gives a linear fit, with a steeper slope of 1.98.

Based on the correlation between the C−Cu bond energy and the corresponding C−H bond strength, we will write $E_{\text{C-Cu}}$ as a linear function of the C−H bond energy in the corresponding

alkane and assume that $\Delta E_{\text{C-Cu}}$, $E_{\text{H-Cu}}$, and $E'_{\text{H-Cu}}$ are approximately constant:

$$E_{\text{C-Cu}} = a_{\text{C-Cu}} + b_{\text{C-Cu}} E_{\text{C-H}}. \tag{4.3}$$

We then fit the model to the DFT binding energies, with $a_{\text{C-Cu}}$, $b_{\text{C-Cu}}$, $\Delta E_{\text{C-Cu}}$, $E_{\text{H-Cu}}$, and $E'_{\text{H-Cu}}$ as fitting parameters. Therefore, this simple model has five fitting parameters and can be used to predict the binding energy of any alkyl at any site on Cu(111). We only apply it at 1/9 ML because the model ignores coverage effects, which are non-negligible at 1/4 ML. Figure 4.7b displays the accuracy of the linear site-preference model, which has a mean absolute error (MAE) of 0.016 eV. The values of the parameters are $a_{\text{C-Cu}} = 2.471$, $a_{\text{C-Cu}} = -1.519$, $E_{\Delta\text{C-Cu}} = 0.043$, $E_{\text{H-Cu}} = -0.060$, and $E_{\text{H-Cu}'} = -0.033$.

The C−Cu terms behave as expected by the tetravalency principle: as the number of C−Cu interactions increases, the binding energy increases, if all else is equal. We expect the H−Cu terms to be negative (stabilizing), which they are. Further, the "long" H−Cu interactions are also stabilizing, but less so. Hence, the site preference of an alkyl is a compromise between C−Cu interactions, which are more stable in low-coordinated sites, and H−Cu interactions, which are more stable in high-coordinated sites. It appears that the difference in site preference between methyl and the other alkyls is due to the fact that methyl can form three H−Cu interactions in the hollow sites, while the other linear alkyls can only form two. Similarly, the branched alkyls prefer the top site because they can form only one or zero H−Cu interactions.

The current work suggests that linear site-preference models may be an effective way to extend and improve linear scaling relations [35, 53, 74]. However, it remains to be seen whether linear site-preference models apply to other systems and whether all of the parameters in the model obey simple trends between metals.

4.4.5 Density of States Analysis

To understand the C−Cu bond, we will examine the projected density of states (PDOS) of various alkyls adsorbed in the top site. Methyl's molecular orbitals (MOs), from lowest energy

to highest, consist of an occupied 2a1 orbital, an occupied pair of degenerate 1e MOs, and a 3a1 singly-occupied molecular orbital (SOMO). As shown in Fig. 4.8, the DOS of methyl in the top site displays many of the same features noted by Michaelides and Hu [252] for methyl on Ni(111): the 2a1 and 1e MOs become stabilized upon adsorption and the 3a1 MO mixes strongly. In our case, the 2a1 MO does not broaden, but the 1e MOs do. The states derived from the 3a1 orbital appear to split into bonding and antibonding states, as expected from studies of radical adsorption [186]. This splitting is due to the orbital's interaction with the Cu d-band. For the other alkyls, we see essentially the same behavior for orbitals in similar energy ranges. As Fig. 4.8b and c show, the states derived from the filled MOs may shift or broaden. The SOMOs, which lie between -5 and -2 eV, mix strongly and split into bonding and antibonding states. Unoccupied orbitals near 0 eV mix, but they appear to be too high in energy to play a significant role.

The most important determining factor for the strength of the C$-$Cu bond appears to be the energy of the alkyl's SOMO. This is demonstrated by Fig. 4.9, which shows that when the energy of this orbital is higher, the binding energy in the top site is less negative (weaker). We can justify this by noting that as the energy of the SOMO moves away from the d-band center (which is at about -7.1 eV, referenced to vacuum energy), its interaction with the d-band is expected to decrease. This will result in decreased splitting between the bonding and antibonding states. In general, this decreased splitting will allow more antibonding states to fall below the Fermi level and become occupied, decreasing the strength of the bond. The differences in splitting are supported by Fig. 4.8: in the case of methyl, there appear to be bonding states from about -3.6 to -2 eV and antibonding states from about -1.4 to 3 eV; for ethyl, bonding states from about -3.7 to -2 eV and antibonding states from about -1.2 to 2.9 eV; and for isopropyl, bonding states from about -3.1 to -1.5 eV and antibonding states from about -1 to 1 eV. For isopropyl, the high SOMO leads to little interaction and little splitting; hence, many antibonding states are filled. Ethyl and methyl appear to have similar antibonding filling. For the same splitting, methyl's lower SOMO would result in more filled antibonding states. However, the increased splitting for methyl pushes the antibonding states up, with the end result that methyl and ethyl have similar antibonding

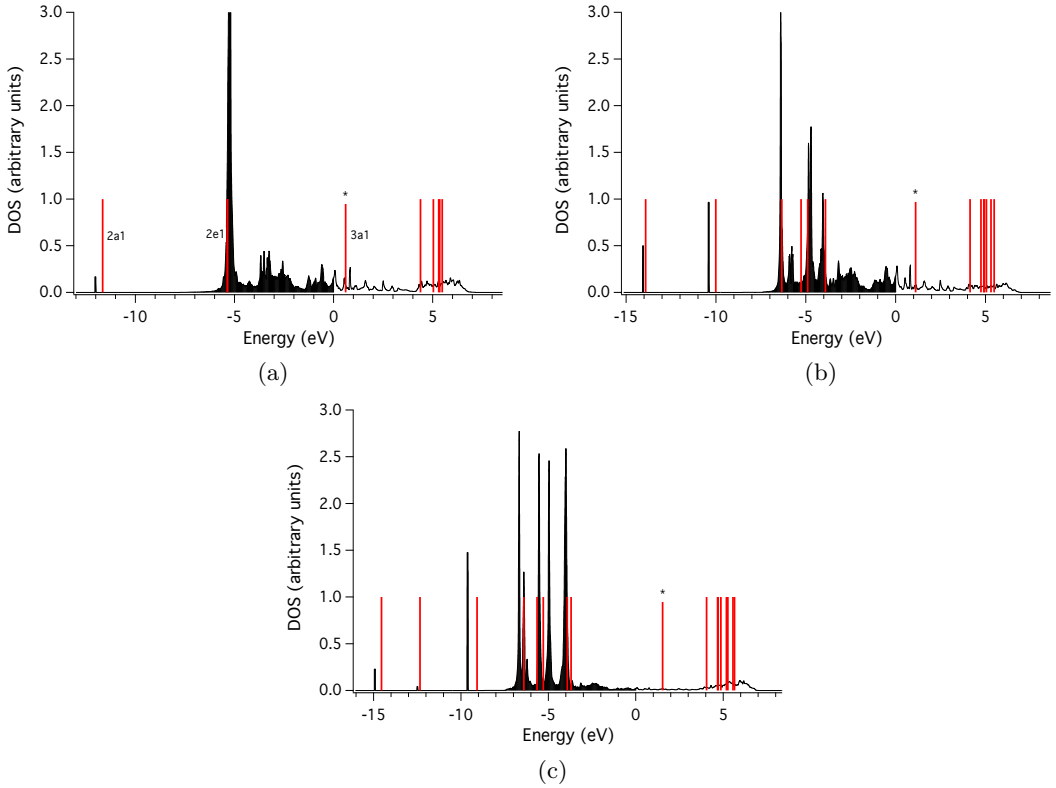

Figure 4.8: PDOS on the C atom in (a) methyl, (b) ethyl, and (c) isopropyl adsorbed in the top site, relative to the Fermi energy. Occupied states are filled in black. The energies of the gas phase orbitals are shown as short, vertical, red lines (orbitals with very small projections on the α C are not shown), and the SOMO is indicated with an asterisk.

filling. Methyl's increased splitting increases the stabilization of bonding states as well as the destabilization of antibonding states. More bonding states are filled than antibonding, analogous to a gas phase bond where the bonding orbital is filled and the antibonding orbital is only half filled. Therefore, the stabilization of bonding states contributes more to the energy, causing methyl to form a stronger bond than ethyl.

The importance of the energy of the SOMO explains why propyl's properties are often not intermediate to those of ethyl and butyl. According to our calculations, propyl's SOMO is lower than butyl's, which is about the same as ethyl's (see Fig. 4.9). Previous photoelectron studies [264, 265] agree that butyl and ethyl have similar energy levels that differ from propyl's. These studies also support the overall trend that methyl has the lowest SOMO, followed by the

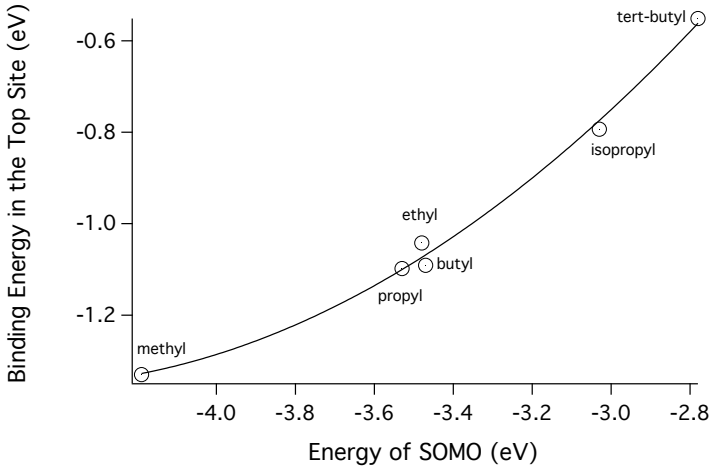

Figure 4.9: The binding energy in the top site as a function of the energy of the SOMO in the gas phase (calculated with plane-wave DFT).

linear alkyls, followed by the branched alkyls. However, these studies indicate that propyl's SOMO is ∼0.1 eV higher than ethyl and butyl's, in contrast to our finding that propyl's is ∼0.1 eV lower. This difference is likely within the error in the relationship between the Kohn-Sham orbitals and ionization potentials [266].

The C−H−M interaction in adsorbed methyl has been shown to be an agostic, three-center interaction on Ni(111) [252] and Pt(111) [207] consisting of delocalization of C−H bonding orbitals toward metal atoms. Our calculations indicate that all alkyls on Cu(111) experience this same agostic interaction when the H−Cu distance is short enough. Figure 4.11 shows the PDOS of the 1e-derived states on the d-orbitals of the α C of methyl in the fcc and fcc60 sites. As methyl rotates from the fcc60 site to the fcc site, the agostic interactions are "turned on", with little change in other respects. The agostic interactions shift the 1a- and 1e-derived states to lower energies. Additionally, the shape of the 1e-derived peaks is significantly different: there is increased splitting, and there are fewer states in the upper peak and more in the lower peak. For energies higher than the 1e orbitals, there appears to be little or no change in the PDOS. Plots of the full PDOS are available in Fig. 4.10. In the bridge30 site, which has two "long" H−Cu interactions, we see these same changes to a lesser degree. Hence, we conclude that while the 1a MO may play a role in agostic

interactions, the 1e MOs are the most important. There is little change in the PDOS above the 1e MOs, which indicates that the antibonding orbitals likely do not play a significant role. However, it is difficult to completely rule this out using these methods. The additivity of C−Cu and H−Cu interactions demonstrated by the accuracy of the linear site-preference model may be due to the fact that these interactions involve different orbitals and energy ranges. Charge calculations indicate

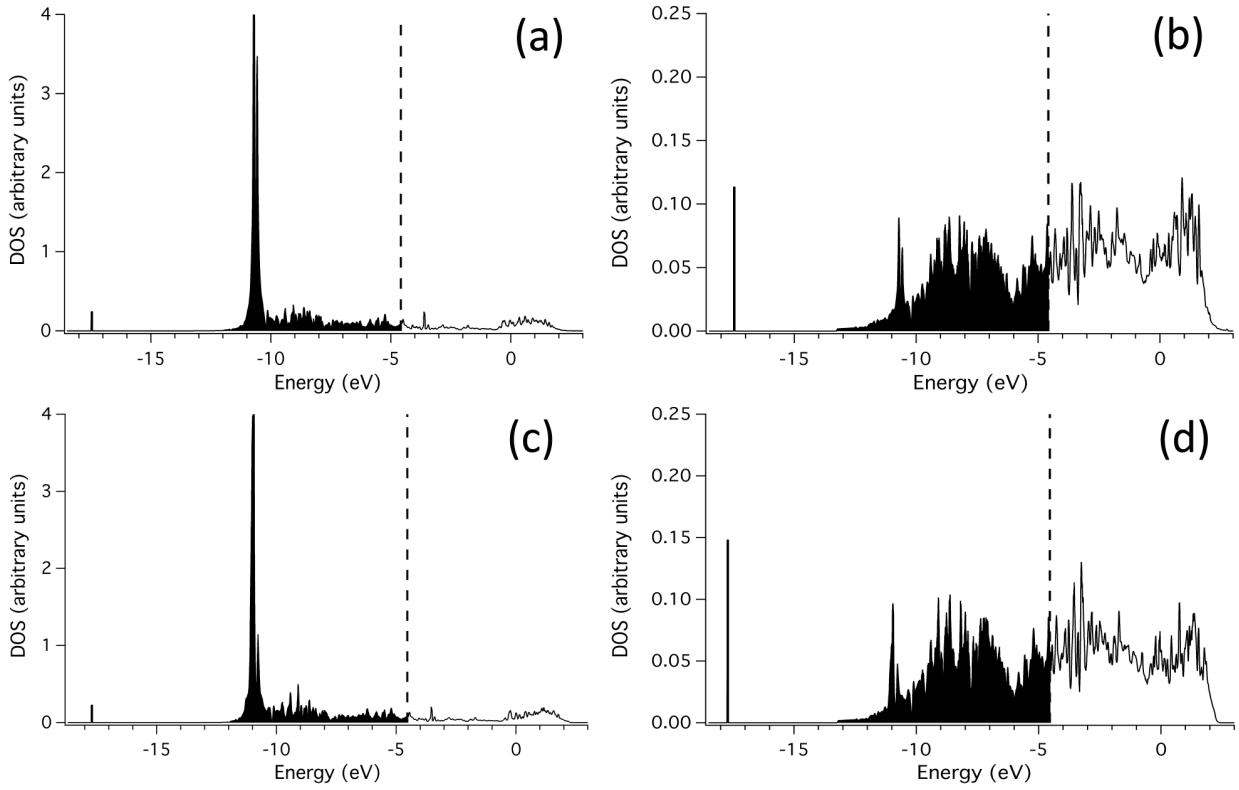

Figure 4.10: Projected DOS for adsorbed methyl: (a) carbon p states, fcc60; (b) copper p states, fcc60; (c) carbon p states, fcc; and (d) copper p states, fcc; relative to vacuum energy, with the Fermi energy indicated by the dashed line. Occupied states are filled with black.

that little charge transfer is involved in agostic interactions; however, careful examination of the charge density indicates that there is greater charge delocalization towards the Cu atoms in the fcc site than in the fcc60 site. Isosurfaces of the difference in charge density between methyl in the fcc and fcc60 sites are shown in Fig. 4.12, with the pink surface indicating higher charge in the fcc site and the purple surface indicating higher charge in the fcc60 site. The charge density

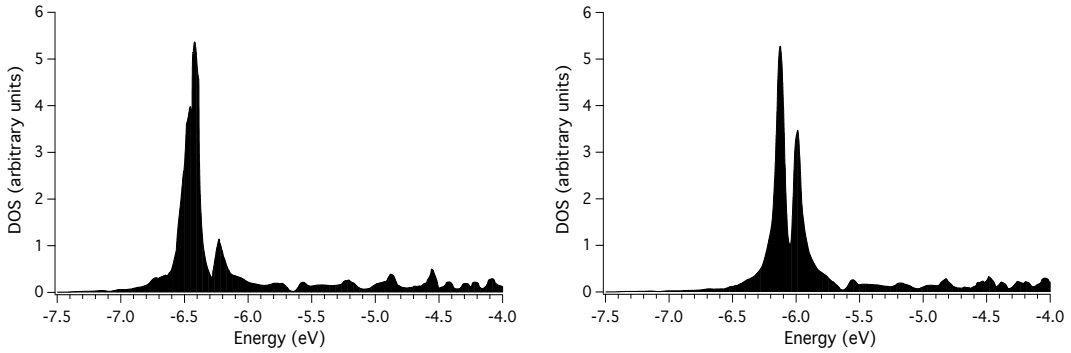

Figure 4.11: Projected DOS on carbon p states showing the 1e-derived states for adsorbed methyl in the (a) fcc60 site and (b) fcc site, relative to the Fermi energy. Occupied states are filled with black.

in the fcc site is nearer to the surface and more delocalized towards Cu atoms. Therefore, we conclude that the agostic mechanism proposed by Michaelides and Hu—that C−H bonding density is delocalized towards Cu atoms—is likely at work in our system. This weakens and lengthens C−H bonds, softening their vibrational modes. For the longer alkyls, there are not two stable sites

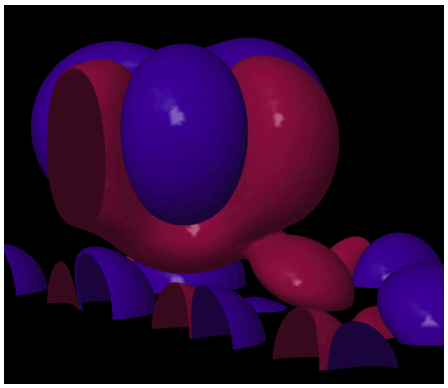

Figure 4.12: Isosurfaces of charge density difference between methyl in the fcc and fcc60 sites. The pink surface indicates more electron density in the fcc site, while the purple surface indicates more electron density in the fcc60 site.

whose primary difference is the presence of agostic interactions, as is the case for methyl. This makes it more difficult to pinpoint changes due solely to agostic interactions. However, the PDOS of longer alkyls in the hollow sites show the same change in shape of the states derived from the

C−H bonding orbitals as was observed in methyl; hence, we conclude that the C−H−M interaction likely has the same mechanism in all alkyls in which it occurs.

Full PDOS plots for methyl in the fcc and fcc60 sites are given in Fig. 4.10. Upon rotation between the two sites, there appear to be very few changes besides the 1a- and 1e-derived states.

4.5 Conclusion

As a first step to understanding hydrocarbon chain growth during reactions such as the electroreduction of CO_2, we have studied the adsorption of linear and branched C_1 to C_4 alkyls on Cu(111) using plane-wave DFT. The adsorption energy and site preference were found to depend on the coverage, with both direct alkyl−alkyl interactions and induced d-band shifts playing a role. We created a simple model to rationalize site preferences based on the number of C−Cu and H−Cu interactions in a given site, as well as predict the adsorption energy of any alkyl in any site. Using this model, we propose that alkyl site preference can be understood by considering the balance between favorable H−Cu interactions and unfavorable C−Cu interactions. Methyl prefers the hollow sites because it can form three favorable H−Cu interactions, while the branched alkyls prefer lower coordinated sites because they have fewer repulsive C−Cu interactions. These factors are more balanced for C_2 to C_4 linear alkyls, which have weak site preferences that change with coverage. A strong linear correlation between an alkyl's adsorption energy in the top site and the C−H bond strength in the corresponding alkane was observed. The top site adsorption energy was similarly shown to be correlated with the energy of the unpaired electron in the gas-phase alkyl, which explains the large difference in adsorption energy between methyl and the other linear alkyls.

Chapter 5

A Simple, Accurate Model for Alkyl Adsorption on Late Transition Metals

5.1 Abstract

A simple model that predicts the adsorption energy of an arbitrary alkyl in the high-symmetry sites of late transition metal fcc(111) and related surfaces is presented. The model makes predictions based on a few simple attributes of the adsorbate and surface—including the d-shell filling and the matrix coupling element—as well as the adsorption energy of methyl in the top sites. We use the model to screen surfaces for alkyl chain-growth properties and to explain trends in alkyl adsorption strength, site preference, and vibrational softening.

5.2 Introduction

Alkyl groups are important in many surface reactions, such as the steam reforming of methane to syngas, the dehydrogenation of alkanes to olefins, Fischer-Tropsch synthesis, and the electroreduction of CO_2. Hence, understanding and predicting alkyl adsorption on transition metals could lead to improved design of catalysts for many processes, including those involving hydrocarbon chain growth. While methyl adsorption on particular surfaces has been well studied [207, 217, 226, 267], the overall trends for alkyl adsorption on different sites and surfaces have not been elucidated.

Simple models can facilitate the design of catalytic surfaces. Adsorption energies have been shown to be good predictors of catalytic activity, specifically through the Sabatier principle [20, 22] and Brønsted-Evans-Polanyi (BEP) relations [42, 44]. Several models have been developed to

quickly estimate the adsorption energy of molecules on various surfaces. Some are based on the d-band model [112, 173], which is in turn based on the Newns-Anderson model [148, 150, 153]. The Newns-Anderson model uses a model Hamiltonian to calculate the change in the density of states (DOS) upon adsorption. The d-band model, using the frozen potential approximation, assumes that the adsorption energy is approximately equal the change in energy of the one-particle states, which it calculates using the Newns-Anderson model [268]. Further, it assumes that only the d-states contribute to variations in adsorption across metals. The resulting expression for the adsorption energy is fairly complex; thus, in practice most researchers use simple linear or perturbation theory expressions to account for the dependence of the adsorption energy on the d-band center [173, 181, 183, 269]. The d-band model has previously been used to interpret trends in methyl adsorption [217, 226].

Linear scaling relations allow the prediction of the adsorption energy of a particular species based on that of another species [35, 53]. These relations have mostly been applied to small, simple adsorbates with varying numbers of H atoms, although they have also been extended to larger oxygenates [65, 102], larger hydrocarbons [35, 74], and other atomic species [80].

The d-band model and scaling relations both focus on differences between metals, but ignore differences between sites. This can reduce accuracy, as a given adsorbate may prefer different sites on different metals [35]. Additionally, it is useful to have a general model that can predict variations in adsorption energy across a broad class of adsorbates, which is beyond most previous models.

In this manuscript, we develop a model that can accurately predict the adsorption energy of any alkyl in the high-symmetry sites of late transition metal (M) fcc(111) and related surfaces, given the adsorption energy of methyl in the top sites and a few simple attributes of the metal. In addition to being useful for screening catalytic surfaces, the model provides physical insight into the mechanism for alkyl binding (including agostic C−H−M interactions) to metal surfaces. While we previously demonstrated scaling relations for alkyls on Cu(111) [267], in the current contribution we demonstrate that these relations can be extended in a simple way to other late transition metals. We also show that adsorbate translations between sites can be written in terms of metallic and

adsorbate parameters to allow predictions of site preferences for arbitrary alkyls on late transition metals.

We begin by showing that the top site adsorption energy of an alkyl is linearly related to the C−H bond strength in the corresponding alkane and to the adsorption energy of methyl in the top site. We then show how terms can be added to account for additional C−M and C−H−M interactions, and how these can be used to predict the adsorption energy of an alkyl in the hollow and bridge sites. Finally, we use the model to explain trends in alkyl adsorption and to study alkyl chain growth.

5.3 Methods

Plane-wave density functional theory (DFT) calculations were performed with the Vienna ab-initio Simulation Package (VASP) [253, 254] and the PW91 exchange-correlation functional [256]. PW91 has been shown to predict the site preference of methyl more accurately than the RPBE functional on Rh(111) [217] and Cu(111) [267]. Four layers of each surface were included, and the bottom two were fixed at the optimized bulk distance. (For the (211) surface, we count the number of (111) layers.) A 3×3 surface cell was used, resulting in an alkyl coverage of 1/9 ML for all calculations. The plane-wave basis was expanded up to 396 eV, a k-point mesh of $7\times7\times1$ was used, and the projector augmented-wave method [255] was used for core electrons. QuteMol was used for all atomic graphics [259].

A total of 219 adsorption energies were calculated for methyl, ethyl, propyl, butyl, isopropyl, and tert-butyl on many monometallic and bimetallic surfaces. Tables 5.1 and 5.2 show the full data set used for training and testing the model. "A on B" means a layer of metal A on surface B, and "1 A in B" means that one atom on the surface of B was replaced by one atom of A (i.e., a A_1B_8 surface composition). For Cu(211), we denote the sites closest to the step edge as step sites, and other sites as plane sites. For 1 Pd in Cu(111), Pd sites are those that include a Pd atom, Cu sites 1 are those that consist only of Cu atoms but near a Pd atom, and the Cu sites 2 are those furthest from the Pd atom. For the calculations of alkyls coardsorbed with K on Cu(111),

the distance between K and the alkyls was maximized as the model does not account for changes in direct adsorbate-adsorbate interactions. Images of the various sites are available in the previous chapter, but we briefly note that the bridge site has one C−H−M interaction, the bridge30 site has two C−H−M interactions, the fcc (hcp) site is the eclipsed configuration and the fcc60 (hcp60) site is the staggered configuration.

5.4 The Model

5.4.1 Scaling in the Top Site

In the top site, an alkyl bonds directly to a single metal atom. Our DFT calculations indicate that alkyls may rotate around this bond with energy changes generally less than 0.01 eV. Previous work has shown that adsorption in the top site is largely governed by the interaction of the alkyl's singly occupied molecular orbital (SOMO) with the metal states [226, 267]. Based on our current and previous [267] results, as well as work on other adsorbates [261, 262], we propose that the top site adsorption energy of an alkyl is linearly related to the C−H bond strength in the corresponding alkane. We will derive a theoretical justification for this relationship using the perturbation theory expression for the interaction of a two-level system [270]. We apply this expression to the interaction of the SOMO with both the H 1s orbital (to calculate the C−H bond energy, $E_{\text{C-H}}$) and the d-band of a metal (to calculate the adsorption energy in the top site, $E_{\text{C-M}}$). Therefore, we write the C−H bond energy as

$$E_{\text{C-H}} = \frac{a_1}{\epsilon_a - \epsilon_{\text{H}}} + a_2\epsilon_a + a_3, \tag{5.1}$$

where ϵ_{H} is the H 1s energy and ϵ_a is the energy of the SOMO. Similarly, we write the adsorption energy in the top site as

$$E_{\text{C-M}} = \frac{b_1}{\epsilon_a - \epsilon_d} + b_2\epsilon_a + b_3, \tag{5.2}$$

where ϵ_d is the d-band center. The $\{a_i\}$ and $\{b_i\}$ are constants that are independent of the alkyl, but the $\{b_i\}$ depend on the metal. Hence, we employ the central paradigm of the d-band model, which is that changes in adsorption energy are due to the interaction of adsorbate states with the metal

Table 5.1: The adsorption energies of C_1−C_4 linear alkyls (in eV) in various sites on various surfaces. See the text for definitions.

Methyl								
	top	top30	bridge	bridge30	fcc	fcc60	hcp	hcp60
Ag(111)	−1.050	—	—	—	−0.968	−0.905	−0.977	—
Au(111	−1.329	−1.328	−0.810	−0.811	−0.648	−0.613	−0.661	−0.634
Cu(111)	−1.346	−1.345	−1.432	−1.511	−1.524	−1.330	−1.528	−1.343
Cu(211), Step	−1.576	−1.575	−1.829	—	−1.496	—	—	—
Cu(211), Plane	−1.338	—	—	—	—	—	—	—
Cu(100)	−1.432	−1.432	—	—	—	—	—	—
Ni(111)	−1.699	−1.698	−1.812	—	−2.011	−1.634	−1.976	−1.610
Pd(111	−1.854	−1.855	−1.623	−1.629	−1.673	−1.509	−1.589	−1.433
Pt(111)	−2.087	−2.089	−1.460	−1.460	−1.381	−1.195	−1.256	−1.108
Rh(111)	−1.883	−1.881	−1.851	−1.824	−1.935	−1.526	−1.897	−1.500
Ir(111)	−1.980	—	—	—	−1.660	−1.232	—	—
Cu on Pd(111)	−1.466	−1.465	−1.577	−1.589	−1.667	−1.408	−1.658	−1.415
Pd on Cu (111)	−1.518	−1.510	—	−1.284	−1.243	−1.155	−1.260	−1.178
Pt on Ag(111)	−2.013	−2.013	−1.644	−1.597	−1.499	—	−1.459	—
Au on Pd(111)	−1.241	—	—	—	−0.630	−0.607	−0.611	—
1 Pd in Cu(111), Pd	−1.512	—	—	−1.455	−1.467	—	−1.484	—
1 Pd in Cu(111), Cu 1	−1.314	—	—	−1.391	−1.453	—	−1.501	—
1 Pd in Cu(111), Cu 2	−1.338	—	—	—	—	—	—	—
K coads. on Cu(111)	−1.617	—	—	—	—	—	—	—
Ethyl								
	top	top30	bridge	bridge30	fcc	fcc60	hcp	hcp60
Ag(111)	−0.793	−0.797	—	—	−0.576	—	−0.593	—
Au(111	−1.129	−1.132	−0.504	−0.487	−0.328	—	−0.432	—
Cu(111)	−1.066	−1.068	−1.101	−1.091	−1.099	—	−1.103	—
Cu(211), Step	−1.328	−1.319	—	—	—	—	—	—
Cu(211), Plane	−1.020	—	—	—	—	—	—	—
Cu(100)	−1.167	−1.170	—	—	—	—	—	—
Ni(111)	−1.455	−1.457	−1.492	—	−1.551	—	−1.526	—
Pd(111	−1.695	−1.701	−1.319	−1.354	−1.244	—	—	—
Pt(111)	−1.929	−1.937	−1.163	−1.187	−0.945	—	—	—
Rh(111)	−1.691	—	—	−1.489	−1.563	—	—	—
Cu on Pd(111)	−1.201	−1.212	−1.254	−1.236	−1.247	—	−1.220	—
Pd on Cu(111)	−1.351	−1.340	—	—	−0.958	—	—	—
Pt on Ag(111)	−1.895	−1.901	—	—	—	—	—	—
Au on Pd(111)	−1.050	−1.031	—	—	—	—	—	—
1 Pd in Cu(111), Pd	−1.281	—	—	—	−1.031	—	—	—
1 Pd in Cu(111), Cu 1	−1.038	−1.030	—	—	−1.049	—	—	—
1 Pd in Cu(111), Cu 2	−1.057	—	—	—	—	—	—	—
K coads. on Cu(111)	−1.312	−1.358	—	—	—	—	—	—
Propyl								
	top	top30	bridge	bridge30	fcc	fcc60	hcp	hcp60
Ag(111)	−0.8367	−0.8406	—	—	—	—	—	—
Au(111	−1.1569	−1.1681	−0.5380	−0.5800	−0.3647	—	−0.4749	—
Cu(111)	−1.1134	−1.1218	−1.1554	−1.1441	−1.1475	—	−1.1526	—
Pd(111	−1.7237	−1.6758	−1.3683	−1.3978	−1.2748	—	−1.2509	—
Pt(111)	−1.9542	−1.9684	−1.2089	−1.2184	−0.9826	—	—	—
Cu on Pd(111)	−1.2473	−1.2603	−1.3082	−1.2869	−1.2970	—	−1.2686	—
Butyl								
	top	top30	bridge	bridge30	fcc	fcc60	hcp	hcp60
Cu(111)	−1.110	−1.119	−1.150	−1.139	−1.139	—	−1.146	—

Table 5.2: The adsorption energies of C_3−C_4 branched alkyls (in eV) in various sites on various surfaces. See the text for definitions.

Isopropyl								
	top	top30	bridge	bridge30	fcc	fcc60	hcp	hcp60
Ag(111)	−0.573	−0.575	—	—	—	—	—	—
Au(111	−0.922	−0.927	—	—	—	—	—	—
Cu(111)	−0.813	−0.822	−0.796	—	—	—	—	—
Cu(211), Step	−1.123	−1.128	—	—	—	—	—	—
Cu(100)	−0.936	−0.958	—	—	—	—	—	—
Pt(111)	−1.734	−1.753	—	—	—	—	—	—
Cu on Pd(111)	−0.964	−0.980	—	—	—	—	—	—
1 Pd in Cu(111), Pd	−1.054	—	—	—	—	—	—	—
1 Pd in Cu(111), Cu 1	−0.768	—	—	—	—	—	—	—
1 Pd in Cu(111), Cu 2	−0.805	—	—	—	—	—	—	—
Tert-butyl								
	top	top30	bridge	bridge30	fcc	fcc60	hcp	hcp60
Au(111	−0.702	−0.713	—	—	—	—	—	—
Cu(111)	−0.569	−0.582	—	—	—	—	—	—
Pt(111)	−1.493	−1.519	—	—	—	—	—	—
Cu on Pd(111)	−0.753	−0.777	—	—	—	—	—	—

d-band. A similar expression is often quoted in relation to d-band theory [173], usually without the linear term. The linear term is important in the case of an initially half-filled orbital interacting with a filled orbital [271]. This form of interaction accurately fits both the alkane bond data and the adsorption data, as shown in Fig. 5.1. While data are only shown for Cu(111) and Pt(111), Eq. (5.2) also fits the data well on other surfaces. The Kohn-Sham orbital energies from DFT are used; they have been shown to be linearly related to the orbital energies from the mean-field approximation [266].

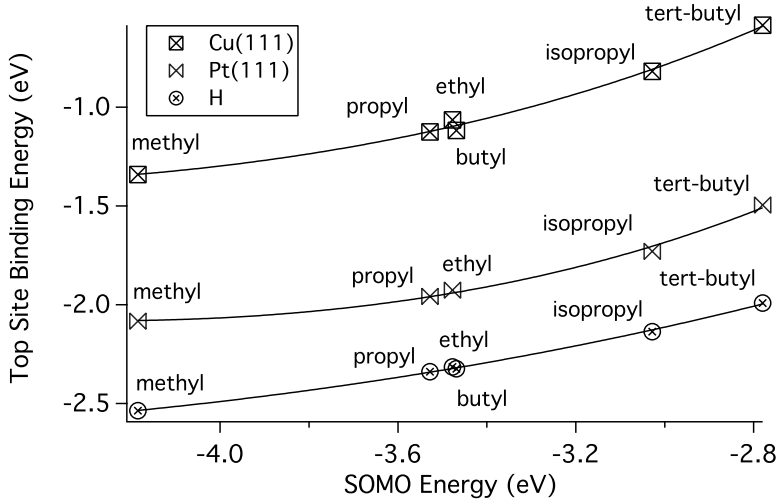

Figure 5.1: The binding energy of an alkyl bonding to a hydrogen atom, the top site of Cu(111), and the top site of Pt(111) as a function of the energy of the SOMO, as well as fits based on Eqs. (5.1) and (5.2).

To show that $E_{\text{C-M}}$ is linearly related to $E_{\text{C-H}}$, we would like to find the necessary conditions for the existence of constants c_1 and c_2 such that $c_1 E_{\text{C-H}} + c_2 \simeq E_{\text{C-M}}$. Using Eq. (5.1) and some algebraic manipulation, we can write $c_1 E_{\text{C-H}} + c_2$ as

$$c_1 E_{\text{C-H}} + c_2 = (c_1 a_3 + c_2) + \frac{c_1 a_1}{\epsilon_a - \epsilon_d} + \frac{c_1 a_1 (\epsilon_{\text{H}} - \epsilon_d)}{(\epsilon_a - \epsilon_d)(\epsilon_a - \epsilon_{\text{H}})} + c_1 a_2 \epsilon_a. \tag{5.3}$$

Setting $b_1 = c_1 a_1$, $b_2 = c_1 a_2$, and $b_3 = c_1 a_3 + c_2$, we recover the form of Eq. (5.2) with an extra term. This term will go to zero if $\epsilon_H = \epsilon_d$, and setting these orbital energies to be equal still results in a good fit to the adsorption energy and alkane bond strength data. The linear relationship will

likely break down if the d-band center ϵ_d is very different from the H $1s$ energy ϵ_H, such that making them equal results in Eqs. (5.1) and (5.2) fitting the data poorly. Hence, we expect the approximation to fail if ϵ_H and ϵ_d have very different values.

The above argues that $E_{\text{C-M}}$ on a particular metal surface is linearly related to $E_{\text{C-H}}$ for an arbitrary alkyl. We would now like to demonstrate that the same slope can be used for different metals. This is supported by Fig. 5.1, which shows that the curvature of the $E_{\text{C-M}}(\epsilon_a)$ plot is approximately the same for both Cu and Pt. Indeed, our DFT calculations generally indicate that changing the metal has a similar effect on the adsorption energy of all alkyls. In our final model, we will use E_{MeTop}, the adsorption energy of methyl in the top site, to scale alkyl adsorption energies across metals. Therefore, we would like to show that across metals there is a linear relationship between $E_{\text{C-M}}$ and E_{MeTop}, i.e. that $\delta E_{\text{C-M}} \approx \delta E_{\text{MeTop}}$. We will calculate the adsorption energy of two different alkyls (with SOMOs at ϵ_{a1}, ϵ_{a2}) on two different metals (with d-band centers ϵ_{d1}, ϵ_{d2}, matrix coupling elements V_{ad1} and V_{ad2}, and d-band fillings f_1 and f_2) using the perturbation theory result. For example, the adsorption energy of alkyl 1 on metal 2 is written as

$$E_{\text{ads}} = \alpha_1 + \frac{\alpha_2 V_{ad2}^2 (1 - f_2)}{(\epsilon_{a1} - \epsilon_{d2})} + \alpha_3(\epsilon_{a1} - \epsilon_{d2}) + \alpha_4 V_{ad2}^2 f_2, \tag{5.4}$$

where the $\{\alpha_i\}$ are constants that we assume to be the same across alkyls and metals. After fitting to the data, this equation predicts our database of 100 adsorption energies of alkyls on the top sites of late transition metal surfaces with a mean absolute error (MAE) of 0.11 eV. (43 of these data points are for rotations of other top site data points, resulting in 57 unique alkyl-metal combinations.) We will show that changing the metal has approximately the same effect on the adsorption energy of both alkyls, i.e. that

$$E_{\text{dif}} := (E_{\text{A1,M2}} - E_{\text{A1,M1}}) - (E_{\text{A2,M2}} - E_{\text{A2,M1}}) \simeq 0, \tag{5.5}$$

where $E_{\text{Ai,Mj}}$ is the adsorption energy of alkyl i on metal j. Since E_{dif} measures how the adsorption energy of two alkyls changes across two metals, when it is small one alkyl can be used to scale the

other. After canceling the linear and constant terms, E_{dif} can be written as

$$E_{\text{dif}} = \alpha_2 \left((1-f_2) \frac{V_{ad2}^2(\epsilon_{a2} - \epsilon_{a1})}{(\epsilon_{a1} - \epsilon_{d2})(\epsilon_{a2} - \epsilon_{d2})} - (1-f_1) \frac{V_{ad1}^2(\epsilon_{a2} - \epsilon_{a1})}{(\epsilon_{a1} - \epsilon_{d1})(\epsilon_{a2} - \epsilon_{d1})} \right). \tag{5.6}$$

For late transition metals, $(1-f)$ is small, so E_{dif} will be small. Therefore, the change in $E_{\text{C-M}}$ is likely to be approximately equal to the change in E_{MeTop}. This relation should also hold when E_{dif} is small for other reasons, e.g. when the change in the SOMO energy is less than the difference between the SOMOs and the d-band centers. The linear relationship between $E_{\text{C-M}}$ and E_{MeTop} is more accurate than the perturbative expression used in this derivation. Therefore, while Eq. (5.6) is likely to give some idea of when this approximation will break down, it is not likely to be useful for determining the absolute size of the error in the linear relationship. A more general argument for the validity of this type of scaling relation between similar adsorbates is available in previous work [80].

Motivated by our DFT calculations and the above derivations, we write the adsorption energy in the top site as

$$E_{\text{C-M}} = K_1 + K_2 E_{\text{C-H}} + E_{\text{MeTop}}. \tag{5.7}$$

The value of K_1 is a constant offset, and K_2 (which, after fitting, we find to be slightly greater than 1) is necessary since the adsorption energy vs. SOMO curve is steeper than the C−H bond energy vs. SOMO curve, as can be seen in Fig. 5.1. We fit this model to the results of our DFT calculations of linear and branched C_1-C_4 alkyl adsorption energies in the top site of various surfaces with the $\{K_i\}$ as fitting parameters, resulting in an MAE of 0.035 eV. The values of E_{MeTop} and $E_{\text{C-H}}$ were calculated with DFT as shown in Tables 5.1 and 5.2.

Both of the above derivations assume that V_{ad} is approximately constant across alkyls. According to our Hartree-Fock calculations of overlap in alkanes, the variation is less than 2%, so this is a fairly good assumption. However, we can account for the variation across alkyls by including a term proportional to the product of the relative value of V_{ad} for the metal and the value of V_{aH} in the corresponding alkane. We estimated V_{aH}, the overlap between the α C and the H atom, by using Hartree-Fock calculations in GAMESS [272]. We can add these two terms to our

expression for $E_{\text{C-M}}$:

$$E_{\text{C-M}} = K_1 + K_2 E_{\text{C-H}} + E_{\text{MeTop}} + K_1' V_{\text{ad}}^2 + K_2' V_{\text{aH}}^2 V_{\text{ad}}^2, \tag{5.8}$$

thereby reducing the MAE of the top-site predictions from 0.034 to 0.025 eV. However, for simplicity's sake we will use Eq. (5.7) in the final model.

5.4.2 Adding C−M Interactions

Upon translation of an alkyl from a top site to a hollow site, the number of C−M interactions increases from one to three, and the number of C−H−M interactions may increase as well. Since these two kinds of interactions involve different orbitals in the alkyls, we will treat them as separate, additive terms. First we examine how the adsorption energy changes as only the number of C−M interactions increases, as when methyl moves from the top site to the staggered hollow site (see Fig. 5.2). The tetravalency principle suggests that this will be destabilizing [206].

Our calculations indicate that $\Delta E_{\text{C-M}}$, the energy change upon adding C−M interactions, is approximately constant across alkyls. Based on our DFT calculations, we use

$$\Delta E_{\text{C-M}} = K_3 V_{ad}^8 f^4, \tag{5.9}$$

where f is the d-shell filling of the metal in its atomic state and V_{ad} is the matrix coupling element between the adsorbate and d states. Values for V_{ad}^2 were taken from previous calculations of pure metals using linearized muffin-tin orbital theory [112]. After fitting, K_3 turns out to be positive, which means that adding C−M interactions is destabilizing. This relation is empirical, and it may not be valid (for example) for earlier transition metals. However, we demonstrate below that Eq. (5.9) is strongly correlated with a derived expression for $\Delta E_{\text{C-M}}$. Equation (5.9) is more useful than the derived expression for scaling relations because it has a simple dependence on surface properties. We also note that $\Delta E_{\text{C-M}}$ for all alkyls can be easily calculated by subtracting methyl's top site adsorption energy from its staggered hollow site adsorption energy, both calculated with DFT.

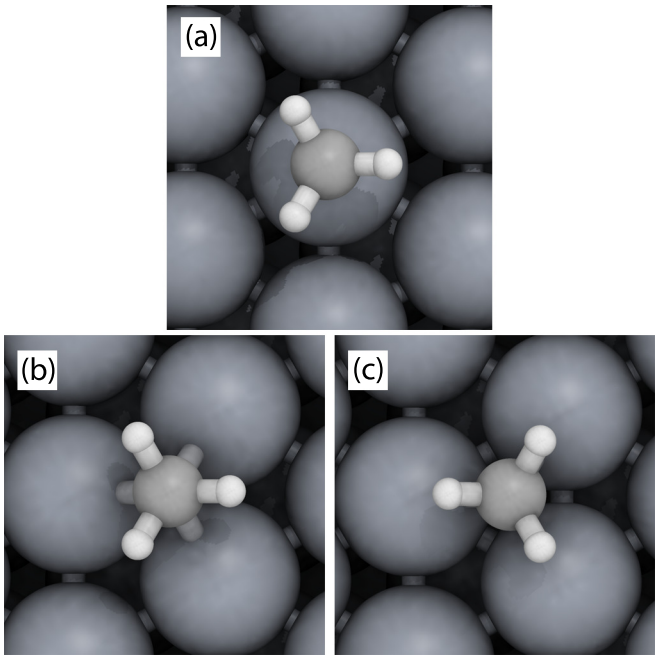

Figure 5.2: a) Methyl in the top site, with one C−M interaction and zero C−H−M interactions. b) Methyl in the staggered hollow site, with three C−M interactions and zero C−H−M interactions. c) Methyl in the eclipsed hollow site, with three C−M interactions and three C−H−M interactions.

To elucidate the physics involved in adding C−M interactions, we again use the perturbative expression for the SOMO−d interaction. We will apply this expression to methyl in the top and staggered hollow sites. In these two sites on the same metal, only the value of V_{ad} differs. The relationship between V_{ad} and d, the adsorbate-metal distance, is $V_{ad} \propto r_d^{3/2} d^{-7/2}$, where r_d is the size of the d orbitals [192, 273]. This relation can be used in conjunction with the perturbative expression for the adsorption energy to predict the adsorption energy in both the top and staggered hollow sites for methyl with an MAE of 0.11 eV. Subtracting the top adsorption energy from the staggered hollow adsorption energy, we find

$$\begin{aligned} \Delta E_{\text{C-M}} \propto & \quad E_{\text{hol}} - E_{\text{top}} \\ = & \quad r_d^3 \left(\frac{\beta_2}{d_{\text{hol}}^7} - \frac{\beta_1}{d_{\text{top}}^7} \right) \left(\frac{\alpha_2 (1-f)}{(\epsilon_a - \epsilon_d)} + \alpha_4 f \right), \end{aligned} \tag{5.10}$$

where β_1, β_2, α_2, and α_4 are constants. Since f is near 1 for late transition metals, the $(1-f)$ term can be set to 0 and the $\alpha_4 f$ term can be set to 1, with α_4 being absorbed into the overall

proportionality constant. The DFT results confirm that these are good approximations. This leaves

$$\Delta E_{\text{C-M}} \propto r_d^3 \left(\frac{\beta_2}{\beta_1 d_{\text{hol}}^7} - \frac{1}{d_{\text{top}}^7} \right). \tag{5.11}$$

The quantity β_2/β_1 accounts for the angular dependence of V_{ad}. In other words, at the same C−M distance, V_{ad} will have a different value in the top and hollow sites. To estimate its value, we assume that the SOMO has the $\cos(\theta)$ angular dependence of a 2p orbital, where θ is measured relative to an axis perpendicular to the surface. We also assume that the collection of d orbitals is spherically symmetric about the metal atom. Hence, at a given C−M distance,

$$\frac{\beta_2}{\beta_1} = 3\frac{r_d^3 d^{-7}}{r_d^3 d^{-7} cos(\theta_{\text{hol}})} = 3\left(\frac{d_{\text{hol}}^2 - l^{2/3}}{d_{\text{hol}}^2} \right), \tag{5.12}$$

where d_{hol} is the C−M distance in the staggered hollow site, θ_{hol} is the C−M angle in the staggered hollow site, and l is the M−M distance. The 3 in Eq. (5.12) comes from the number of atoms the adsorbate is coupling to in the hollow site, and the cosine has been evaluated using simple geometry. Assuming that $d_{\text{hol}} \simeq l$, this reduces to

$$\frac{\beta_2}{\beta_1} \simeq 2. \tag{5.13}$$

Using either Eq. (5.12) or Eq. (5.13) results in $\Delta E_{\text{C-M}}$ from Eq. (5.11) having a strong linear correlation with $\Delta E_{\text{C-M}}$ from the DFT results, with an R^2 value of 0.95 (see Fig. 5.3a). Eq. (5.11) also correlates very well with $V_{ad}^8 f^4$ from Eq. (5.9), with an R^2 value of 0.96 (see Fig. 5.3b). Hence, we conclude that the destabilization of the staggered hollow site as compared to the top site is due to a decrease in the coupling, which is due to an increase in the C−M distance.

5.4.3 Adding C−H−M interactions

C−H−M interactions have been observed on many metals, as evidenced by vibrational softening [236]. In fact, site preference of alkyls can be discovered experimentally by noting the presence or absence of vibrational softening, which does not occur in the top site [217, 236]. C−H−M interactions are thought to consist of donation from C−H bonding orbitals to the surface [207, 229]. They are stabilizing, as demonstrated by the decrease in energy when methyl

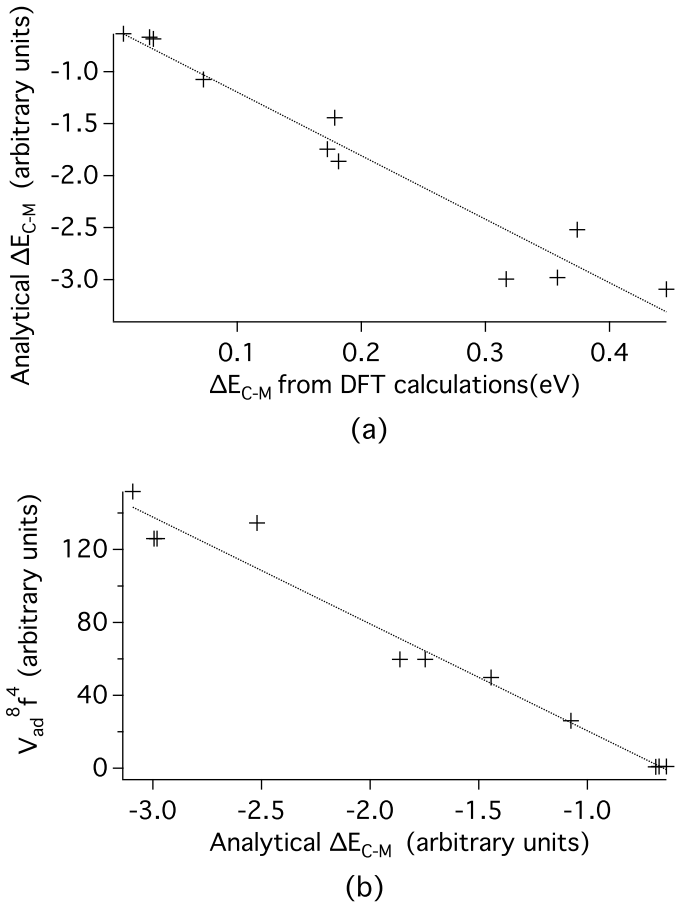

Figure 5.3: a) The correlation between $\Delta E_{\text{C-M}}$ from DFT calculations and $\Delta E_{\text{C-M}}$ from Eq. (5.11). b) The correlation between $\Delta E_{\text{C-M}}$ from Eq. (5.11) and $\Delta E_{\text{C-M}}$ from Eq. (5.9). In both cases, β_2/β_1 is set to 2. Some units are arbitrary because the tabulated values for V_{ad} are relative to Cu, and due to the presence of arbitrary proportionalities.

is rotated from the staggered hollow conformation to the eclipsed conformation (see Fig. 5.2). We assume that this stabilization is proportional to the number of C−H−M interactions. We found that

$$E_{\text{H-M}} = K_4 + K_5 E_{\text{C-H}} + K_6 \epsilon_d (1 - f) \tag{5.14}$$

gave accurate results for fitting to our database of adsorption energies. This equation has a simple physical interpretation. Across alkyls, the energy of the C−H−M interaction should scale with the C−H bond energy, since this bond is donating electrons. This is accounted for by the $E_{\text{C-H}}$ term. After fitting, we found K_5 to be positive, meaning a stronger C−H bond leads to a stronger

C−H−M interaction. Across metals, the energy of the C−H−M interaction should depend on the available states in the d-band, $(1-f)$, and the level of those states, ϵ_d, since these states are accepting electrons. We found K_6 to be positive, meaning a lower d-band center or more available states leads to a stronger C−H−M interaction. Since this term has a $(1-f)$ factor, it is 0 for many late transition metal surfaces. However, it can have a significant effect on surfaces with $f < 1$, and we include it to improve accuracy on these surfaces. To avoid having to calculate the d-band center for each new surface, we note that is possible to use $(1-f)^2$ instead of $\epsilon_d(1-f)$. This substitution results in no loss of accuracy, which may be partially because $(1-f)$ is 0 for many late transition metals.

5.4.4 The Bridge Site Correction

As we discuss later, the adsorption energy in the bridge sites can be predicted with reasonable accuracy using the relations given above. However, the accuracy of these predictions can be significantly improved by adding another term, denoted E_{bridge}. This term accounts for the fact that the adsorption energy is not really linear in the number of C−M interactions, as the hollow and bridge sites are different chemical environments. Accurate results were achieved by adding a term proportional to the Pauli repulsion, which depends on V_{ad}^2 and the d-band filling [112, 274]. Hence, we set E_{bridge} to 0 outside of the bridge sites, and in the bridge sites we set it to

$$E_{\text{bridge}} = K_7 + K_8 V_{ad}^2 f. \tag{5.15}$$

After fitting, we found K_8 to be positive, indicating that higher Pauli repulsion means more destabilization in the bridge sites. Other differences in the bridge sites, such as asymmetric C−M distances (as in Fig. 4a) and longer C−H−M interactions (as in Fig. 4b), are either accounted for by K_7 or are generally small.

The model ignores the difference between the fcc and hcp hollows. We found that the difference between the two types of hollows correlates roughly with V_{ad}^2. Taking this into account improves the qualitative accuracy of the model, but it has a negligible effect on the MAE.

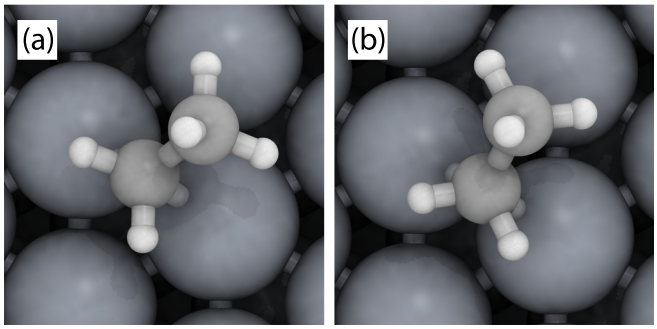

Figure 5.4: a) Ethyl in a bridge site with one C−H−M interaction. b) Ethyl in a bridge site with two C−H−M interactions.

5.5 Results and Discussion

5.5.1 Predicting Hollow and Top Site Adsorption Energies

Using Eqs. (5.7), (5.9) and (5.14) to predict $E_{\text{C-M}}$, $\Delta E_{\text{C-M}}$, and $E_{\text{H-M}}$, we can create a model that accurately predicts adsorption in the top and hollow sites:

$$E_{\text{ads}} = E_{\text{C-M}} + \Delta E_{\text{C-M}}(n_{\text{C-M}} - 1) + E_{\text{H-M}} n_{\text{H-M}}, \tag{5.16}$$

where $n_{\text{C-M}}$ is the number of C−M interactions and $n_{\text{H-M}}$ is the number of C−H−M interactions. We assume that the adsorption energy is the same in the fcc and hcp hollows, which is a good approximation in most cases (the average difference is less than 0.02 eV). For inhomogeneous surfaces, quantities such as V_{ad} are averaged over the atoms surrounding the site. After fitting to the data, Eqs. (5.7), (5.9), (5.14) and (5.16) predict adsorption energies of several alkyls in the top and hollow sites of all the previously mentioned surfaces except Cu(100) with an MAE of 0.041 eV. The parity plot is shown in Fig. 5.5. Alternatively, calculating $\Delta E_{\text{C-M}}$ from a DFT calculation of methyl in the staggered hollow site on each surface instead of using Eq. (5.7) results in an MAE of 0.038 eV. Since alkyls prefer the top or hollow sites on all the fcc(111) surfaces we have tested, this model will be sufficient for many applications. As shown in Table 5.3, the model accurately reproduces the site preferences of alkyls on many surfaces.

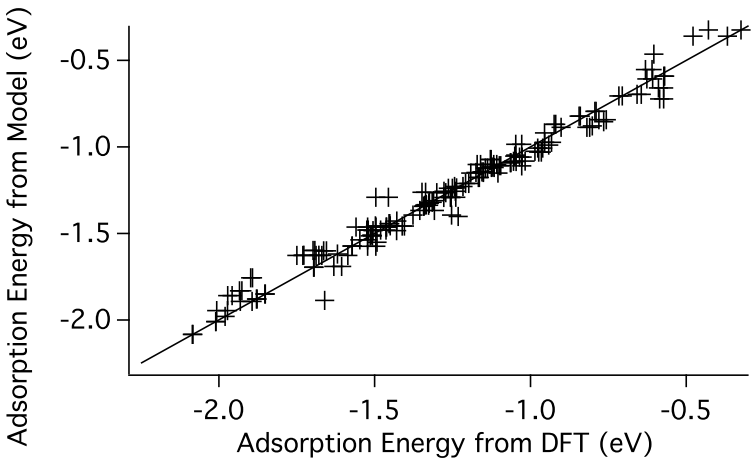

Figure 5.5: The adsorption energy in the top and hollow sites predicted by Eqs. (5.7), (5.9), (5.14) and (5.16) as a function of the adsorption energy in these sites from DFT.

Table 5.3: The site preference predicted by the model (Eq. (5.16)) in comparison with selected previous work.

System	Model	Experiment	DFT
Methyl, Ethyl, Propyl, Butyl on Cu[a]	hol[b]	hol [275]	hol [233, 267]
Methyl, Ethyl on Pt	top	top [276]	top [215]
Propyl, Isopropyl on Pt	top	–	top [215]
Methyl on Ni	hollow	hollow [235]	hol [226]
Methyl on Pd, Ag, Au	top	–	top [226]
Methyl on Rh	hollow	hollow [277, 278]	hol [217]

[a] All surfaces are (111)

5.5.2 Predicting All High-Symmetry Sites

Equations (5.7), (5.9) and (5.14) can be used to predict adsorption energies in the top, hollow, and bridge sites by using the appropriate number of C−M and C−H−M interactions in Eq. (5.16). This results in an MAE of 0.055 eV (see Fig. 5.6a for the parity plot). However, we can improve the accuracy by including the bridge correction term, Eq. (5.15):

$$E_{\text{ads}} = E_{\text{C-M}} + \Delta E_{\text{C-M}}(n_{\text{C-M}} - 1) + E_{\text{H-M}} n_{\text{H-M}} + E_{\text{bridge}}. \tag{5.17}$$

This model predicts the adsorption energy of several alkyls in top, hollow, and bridge sites on all the previously mentioned surfaces except Cu(100) with an MAE of 0.041 eV; the parity plot is shown

in Fig. 5.6b. The values of the parameters are given in Table 5.4, as well as confidence intervals at the 90% confidence level. We also conducted some basic sensitivity analyses to determine the importance of each parameter. Table 5.4 gives the MAE of the model if each parameter is eliminated and the other parameters are optimized without it. It also gives the MAE if each parameter's value is increased or decreased by 2% and the value of the other parameters is held constant. Based on the sensitivity analyses, we conclude that K_1, K_2, and K_3 are the most critical parameters, while K_1 and K_2 are the most sensitive to small perturbations in value. This is likely because the C−M bond strength is a larger energetic contribution to the adsorption energy than the C−H−M interactions or the bridge site correction. Hence, the parameters determining the C−M bond strength in the top and hollow sites are the most critical for determining the adsorption energy.

Table 5.4: The parameters for the model based on Eq. (5.17), their values, confidence intervals at the 90% confidence level, the MAE if each parameter is eliminated, and the MAE if the value of each parameter is increased or decreased by 2%.

K_i	Value	Confidence Interval	MAE (elim)	MAE (+2%)	MAE (-2%)
K_1	3.028	(2.900, 3.157)	0.126	0.068	0.073
K_2	1.204	(1.149, 1.258)	0.120	0.071	0.066
K_3	0.0031	(0.0030, 0.0031)	0.157	0.042	0.043
K_4	0.444	(0.313, 0.574)	0.047	0.043	0.044
K_5	0.194	(0.141, 0.248)	0.048	0.044	0.043
K_6	0.128	(0.094, 0.162)	0.046	0.042	0.042
K_7	−0.123	(−0.160, −0.086)	0.048	0.042	0.042
K_8	0.091	(0.076, 0.105)	0.054	0.042	0.042

Our model is more accurate than previous scaling relations and provides physical insight into site preference which is lacking in previous scaling relations. Further, once it is parameterized, our model may require fewer DFT calculations as input since it is not necessary to find the most favorable site for the adsorbate used for scaling (methyl in our case). However, it is more complex and requires more fitting parameters.

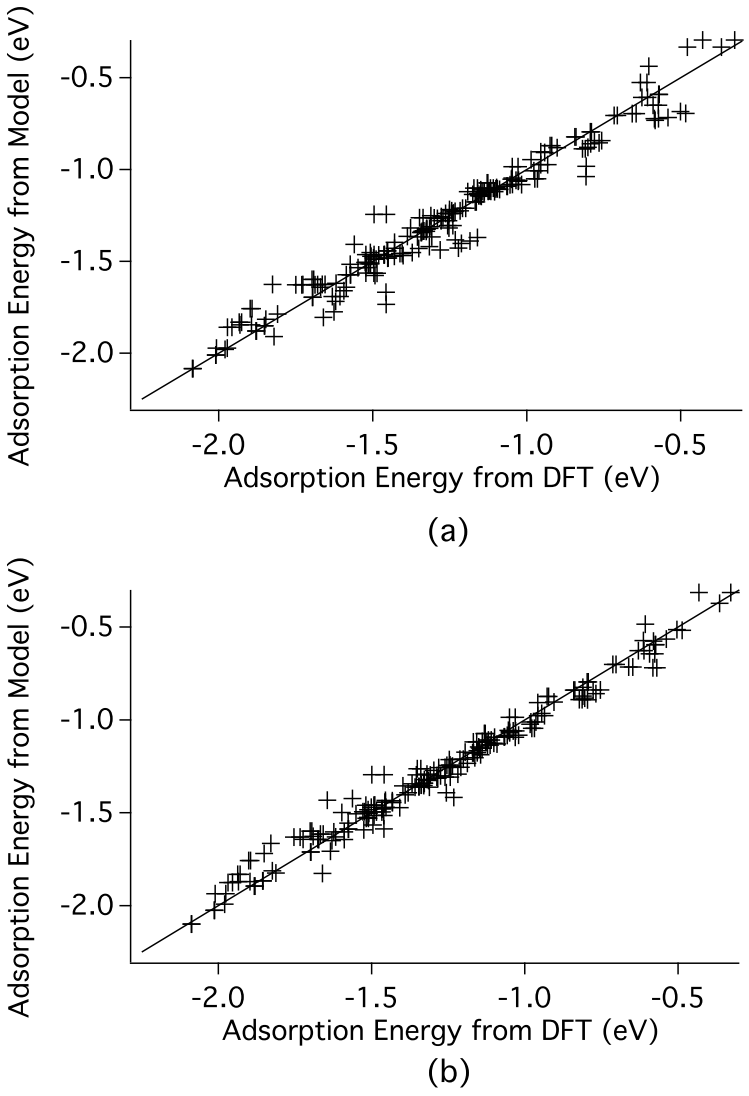

Figure 5.6: a) Parity plot of the model predictions of the top, hollow and bridge sites without E_{Bridge} (Eq. (5.16)). b) Parity plot of the model predictions of the top, hollow and bridge sites with E_{Bridge} (Eq. (5.17)).

5.5.3 Alkyl Adsorption Trends

The model presented above has eight fitting parameters, but the number of parameters can be reduced if a lower accuracy is acceptable, as implied by the results of the sensitivity analyses in Table 5.4. Eliminating parameters also distills the physics underlying alkyl adsorption. By setting K_2 to 1 (i.e., assuming the relation between $E_{\text{C-M}}$ and $E_{\text{C-H}}$ has a slope of 1) and K_4, K_7, and K_8

to 0, we are left with a four-parameter model with an MAE of 0.066 eV. This is a simple, intuitive model for alkyl adsorption in which the adsorption energy in the top site is the sum of $E_{\text{C-H}}$, E_{MeTop}, and a constant offset (K_1). Adding C−M interactions increases the energy by $|K_3 V_{\text{ad}}^8 f^4|$, and adding C−H−M interactions decreases the energy by $|K_5 E_{\text{C-H}} + K_6 \epsilon_d (1-f)|$. Again, $\Delta E_{\text{C-M}}$ can also be calculated with a DFT calculation of methyl in the staggered hollow site in lieu of employing Eq. (5.7), increasing computational expense but reducing the number of parameters.

The model gives a clear explanation of the trends in alkyl adsorption. Variations across alkyls are due to changes in the C−H bond strength of the corresponding alkane (which is in turn due to changes in the SOMO of the alkyl) and changes in the number of hydrogen atoms bonded to the carbon atom nearest the surface. The site preference of an alkyl is a compromise between stabilizing C−H−M interactions and destabilizing C−M interactions. The balance between these two is primarily controlled by the values of V_{ad} and f for the particular metal surface: alkyls strongly prefer the top site on metals with nearly full d-bands where V_{ad} is large, but may prefer hollow sites on metals where V_{ad} is small or the d-band is only partly filled. Hence, on the periodic table, metals further up (i.e., those with smaller d orbitals) and those further to the left (i.e., those with lower d-band filling) are more likely to bind alkyls in the hollow site. These trends are evident in Table 5.3.

The model can also be used to explain trends in the magnitude of vibrational mode softening by predicting the strength of the C−H−M interaction. Metals with fuller d-bands or lower d-band centers have weaker C−H−M interactions, which we found to correlate with shorter C−H bonds. Hence, a fuller d-band or lower d-band center should result in less mode softening, in agreement with the available experimental evidence for surfaces where the hollow site is preferred [236]. This explains, for example, why there is more C−H mode softening on Ni(111) than Cu(111).

5.5.4 Application to Chain Growth

Simple scaling relations like those described here are useful in identifying catalytic surfaces with unique and desirable properties. By combining our model with scaling relations developed

by other groups [35] to predict the adsorption energy of methylene from the adsorption energy of methyl, we can quickly calculate the reaction energy of alkyl chain growth on different surfaces. We define the chain growth energy as the reaction energy of $C_nH^*_{2n+2} + CH^*_2 \longrightarrow C_{n+1}H^*_{2n+4} + *$, where the $*$ indicates an adsorbed molecule or a bare surface. As shown in Table 5.5, this reaction was found to be exothermic on all the surfaces we tested. Of these surfaces, it is most favorable on Ag(111) and least favorable on Ni(111). It is always more favorable to form linear alkyls than branched alkyls. Rh(111), which is the most similar to the Fischer-Tropsch metals, is less favorable for chain growth than most other surfaces. The rate-determining step (which is contested in the literature [125, 279]) is a critical factor in Fischer-Tropsch catalysis, but our model may provide insight into how to tune the chain-growth energy. Chain growth is more favorable on Cu, which is used for CO_2 electroreduction. It is more favorable on Cu(111) than Cu(211), and the first step can be promoted further by replacing 1/9 of the Cu(111) surface atoms with Pd atoms.

Table 5.5: The energy of alkyl chain growth in eV on various surfaces.

Surface	Me $\longrightarrow$ Et	Et $\longrightarrow$ Pr	Pr $\longrightarrow$ Bu	Et $\longrightarrow$ i-Pr	i-Pr $\longrightarrow$ t-Bu
Ag(111)	−2.10	−2.19	−2.19	−2.00	−2.04
Au(111)	−1.60	−1.69	−1.69	−1.50	−1.54
Cu(111)	−1.13	−1.35	−1.33	−1.10	−1.19
Ir(111)	−0.44	−0.53	−0.52	−0.33	−0.37
Ni(111)	−0.24	−0.49	−0.47	−0.21	−0.29
Pd(111)	−0.66	−0.75	−0.75	−0.56	−0.60
Pt(111)	−0.25	−0.34	−0.33	−0.15	−0.19
Rh(111)	−0.51	−0.61	−0.61	−0.42	−0.46
Cu on Pd(111)[a]	−0.88	−1.10	−1.08	−0.86	−0.94
Pd on Cu(111)	−1.27	−1.36	−1.35	−1.17	−1.20
Pt on Ag(111)	−0.38	−0.47	−0.47	−0.28	−0.32
Au on Pd(111)	−1.76	−1.85	−1.85	−1.66	−1.70
1 Pd in Cu(111)[b]	−1.28	−1.37	−1.36	−1.18	−1.21
Cu(211)	−0.62	−0.81	−0.79	−0.57	−0.65

[a] "A on B" means a layer of metal A on surface B;
[b] "1 Pd in Cu(111)" means that one atom on the surface of Cu(111) was replaced by one atom of Pd (i.e., a Pd_1Cu_8 surface composition)

One advantage of having a simple, analytic expression for the adsorption energy is that simple expressions can be derived for alkyl chain growth. For example, if it is assumed that all alkyls prefer

the top site, the chain growth energy is

$$E_{\text{Chain, Top}} = -\gamma E_{\text{MeTop}} + F, \tag{5.18}$$

where γ is the proportionality constant between the methyl adsorption energy and the methylene adsorption energy, and F depends only on the alkyls, not on the metal. Therefore, if alkyls prefer the top site, stronger methyl adsorption leads to less favorable chain growth. This can be seen in the data for Ag, Au, Pd, and Pt. The expression becomes considerably more complicated for other sites, but the derivations are straightforward.

5.5.5 Extending the Model

The model above is quite accurate for alkyls on late transition metal fcc(111) surfaces. When considering how to extend the model to other cases, it is instructive to consider which systems the model predicts poorly. Table 5.6 lists the nine systems with the highest prediction errors (see also Fig. 5.7). Two of these are on Ir(111), out of the total of three data points on this surface. These errors may indicate that the model is less accurate for earlier transition metals. To explore this possibility, we performed some test calculations on Ru(0001), and found that model had even higher prediction errors on this surface, up to 0.31 eV. To test whether the hcp structure was responsible, we also ran test calculations on an artificial "Pd(0001)" surface, and found that the model had nearly the same accuracy there as on Pd(111). Hence, we conclude that the model is potentially accurate on hcp(0001) surfaces, but will need to be further generalized to accurately predict adsorption on transition metals with a d-shell filling of 0.7 or less. In its current form, it can give semi-quantitative results for group 8 and group 9 metal surfaces. The large error on Cu(211) may indicate that the model is less accurate on (211) surfaces, and that for high accuracy they should be treated separately. However, since most of the ten data points on Cu(211) were predicted accurately, this particular data point may simply be an outlier. The large errors for some of the eight tert-butyl adsorption energies are perhaps not surprising, as the tertiary carbon in tert-butyl is in a fairly different chemical environment than the carbon atom in methyl. Accounting for

changes in V_{ad} across alkyls, as discussed above, helps correct this error. The large errors for Pt on Ag(111) are difficult to explain, particularly since the other bimetallic surfaces were predicted quite accurately. It is possible that Ag modifies the matrix coupling element dramatically, which causes error in the predictions. It has been shown previously [141, 192] that Pt skin alloys have modified matrix coupling elements as compared to pure Pt, and that Pt/Ag/Pt(111) has a particularly large change in adsorption energy compared to other alloys [192].

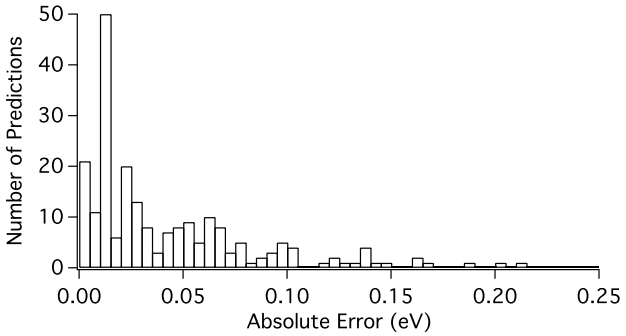

Figure 5.7: Histogram of the number of predictions of Eq. (5.17) with a given absolute error.

Table 5.6: The nine systems with the greatest prediction errors, calculated with Eq. (5.17).

Error (eV)	Surface	Alkyl	Site
−0.211	Pt on Ag(111)	methyl	bridge
−0.204	Pt on Ag(111)	methyl	fcc
0.186	Ir(111)	methyl	staggered fcc
0.167	Ir(111)	methyl	fcc
−0.164	Pt on Ag(111)	methyl	hcp
−0.163	Cu(211)	methyl	bridge
0.150	Cu(111)	tert-butyl	top
−0.144	Pt on Ag(111)	ethyl	top
−0.140	Rh(111)	ethyl	fcc

Our preliminary calculations indicate that the model can readily accommodate other adsorbates that are similar to alkyls. We calculated the adsorption energy of 2-hydroxyethyl in an upright configuration on Pt(111) and Rh(111), and found that the model predicted these with an accuracy similar to the alkyls. Hence, we suggest that the model may be applicable to any adsorbate that bonds through an sp^3 hybridized carbon.

5.6 Conclusion

We have constructed a simple model that accurately predicts alkyl adsorption energies on fcc(111) and related surfaces, extending our model of alkyl adsorption on Cu(111) [267]. Given the adsorption energy of methyl in the top site, the model predicts the adsorption energy of any alkyl in any high-symmetry site. To predict the adsorption energy in the top site, we scale across metals with the methyl adsorption energy and across alkyls with the C−H bond energy of the corresponding alkane. The energy changes upon translating the alkyl to other sites are written in terms of simple attributes of the alkyl and metal. This model can be used to quickly screen metals for adsorption properties or to conceptualize variations across alkyls, sites, and surfaces. This represents a proof-of-concept that the scope and accuracy of scaling relations can be increased by scaling in sites with simple bonding modalities and adding terms to account for translations. The same general framework may be useful for other chemistries.

Chapter 6

Site-Specific Scaling Relations for Hydrocarbons on Transition Metals

6.1 Abstract

Screening a large number of surfaces for their catalytic performance remains a challenge, leading to the need for simple models to predict adsorption properties. To facilitate rapid prediction of hydrocarbon adsorption energies, scaling relations that allow for calculation of the adsorption energy of any intermediate attached to any symmetric site on any hexagonal metal surface through a carbon atom were developed. For input these relations require only simple electronic properties of the surface and of the gas-phase reactant molecules. Determining adsorption energies consists of up to four steps: (i) calculating the adsorption energy of methyl in the top site using density functional theory or by simple relations based on the electronic structure of the surface; (ii) using modified versions of classical scaling relations to scale between methyl in the top site and C_1 species with more metal-surface bonds (i.e. C, CH, CH_2) in sites that complete adsorbate tetravalency; (iii) using gas-phase bond energies to predict adsorption energies of longer hydrocarbons (i.e. CR, CR_2, CR_3); and (iv) expressing energetic changes upon translation of hydrocarbons to various sites in terms of the number of agostic interactions and the change in the number of carbon-metal bonds. Combining all of these relations allows accurate scaling over a wide range of adsorbates and surfaces, resulting in efficient screening of catalytic surfaces and a clear elucidation of adsorption trends. The relations are used to explain trends in methane reforming, hydrocarbon chain growth, and propane dehydrogenation.

6.2 Introduction

Much research has been devoted to the adsorption of hydrocarbons on transition metals, due to its importance in surface science and catalysis. Alkyls [63, 125, 207, 208, 219, 229, 239, 249, 280–291], alkylidenes [63, 125, 208, 219, 239, 249, 285–295], alkylidynes [63, 125, 208, 244, 249, 286–293], atomic carbon [63, 125, 287–291], and atomic H [63, 125, 181, 189, 189, 207, 219, 244, 249, 287–291] have all been implicated in a wide variety of catalytic transformations as well as graphene deposition. Perhaps the most important quantity associated with adsorption is the adsorption energy, as adsorption energies have been widely used to predict the activity and selectivity of catalytic surfaces. For example, the Sabatier principle states that the most active catalyst often binds the relevant chemical species with an intermediate bond strength [20–24]. Additionally, Brønsted-Evans-Polanyi (BEP) relations can be used to predict activation energies from adsorption energies, thereby allowing predictions about the relative rates of a reaction pathway on different surfaces [21, 24, 31, 36–39, 44]. Hence, to a good approximation, designing a catalyst with high activity or selectivity consists of designing a surface with the proper adsorption properties. Therefore, understanding and predicting adsorption energies are important, fundamental goals in catalysis and surface science, and predicting hydrocarbon adsorption energies could aid in catalyst design for many processes.

Due largely to surface science and theoretical work, much progress has been made in understanding and predicting adsorption trends [296, 297]. In particular, the d-band model has been widely used to explain adsorption trends, primarily in terms of the d-band center [112, 149, 156, 173, 179, 191, 269, 298], and has been used to screen alloy surfaces for their adsorption energies [192]. However, the d-band model generally does not give quantitatively accurate predictions unless the set of metals being screened is restricted, e.g. to a single metal in fairly similar environments [96, 183]. Indeed, recent work [32] has shown that catalytic activity does not always have a simple dependence on the d-band center, and a study of CH_3 adsorption on Au nanoparticles has shown that other factors, such as adsorbate-s coupling and the charge on the nanoparticle, can be used to predict

the adsorption energy in some cases [299]. One goal of the present work is to elucidate what factors other than the d-band center contribute to variations in hydrocarbon adsorption energies.

Several models have been created in order to efficiently screen surfaces for their adsorption properties. The unity bond-index quadratic exponential potential method (UBI-QEP, formerly known as the bond-order conservation model [300]), effective medium theory [164], and the Newns-Anderson model [153] (on which the d-band model is based) are older models that are mainly used to rationalize trends or when many adsorption energies are needed, for example as inputs to microkinetic models [301]. Advances in density functional theory (DFT) have allowed relatively accurate calculations of adsorption energies in individual cases. However, DFT is still too computationally expensive to allow the calculation of reaction networks on a large number of surfaces. This problem can be partially resolved through the use of scaling relations, which have been identified for flat surfaces [35, 50, 53, 65, 74, 80, 102, 104], steps and kinks [35, 74, 90], and nanoparticles [59, 90]. Scaling relations use the adsorption energy of one chemical species to predict the adsorption energy of others, allowing surfaces to be screened based on just a few calculations. These relations are often simple and accurate, combining near-DFT accuracy with reasonable computational expense.

It has been noted previously [35] that the accuracy of scaling relations can be improved by scaling to specific sites. However, this leaves the problem of predicting which site an adsorbate prefers on a particular surface. In our previous work [83], we developed a model that predicts the site preference of alkyls on late transition metals. We now extend this model to all transition metals, as well as to all hydrocarbons that bind to the surface through a single carbon atom. This allows us to take advantage of the accuracy of site-specific scaling relations.

The primary goal of this work is to develop relations that allow the prediction of a variety of hydrocarbons in a variety of sites based primarily on the adsorption energy of methyl in the top site(s), as depicted in Fig. 6.1. We begin by developing an expression to accurately predict adsorption energies in particular sites from electronic structure parameters. This expression will be used to provide intuitive insight and a rationale for the validity of scaling relations. We

then demonstrate the accuracy of C_1 site-specific scaling relations, which allow predictions for hydrocarbons with a variable number of pendant groups (see (1) in Fig. 6.1). Next, we demonstrate the accuracy of using gas-phase C−H bond energies to scale across different adsorbates with the same number of pendant groups, allowing predictions for how variations in the identity of these pendant groups affect adsorption energies (see (2) in Fig. 6.1). We then develop relations for predicting translations of adsorbates between different sites on hexagonal transition metal surfaces (see (3) in Fig. 6.1). All of these relations are combined into a single model, and the model is applied to methane reforming, C−C coupling, chain termination, and propane dehydrogenation.

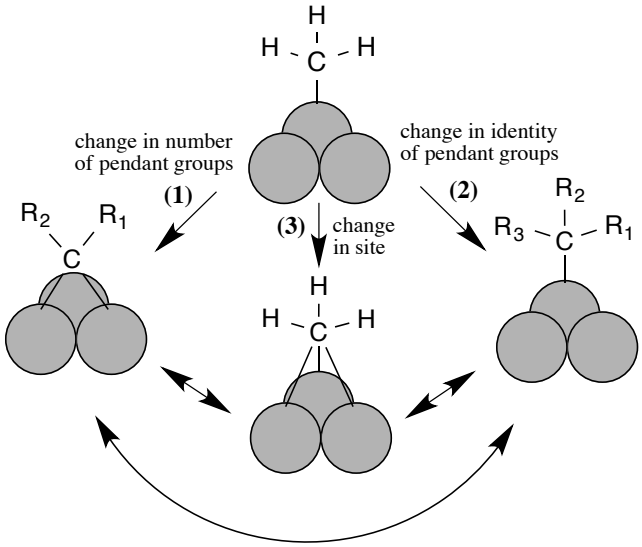

Figure 6.1: Using the adsorption energy of methyl in the top site, predictions can be made of the adsorption energy of hydrocarbons with (1) a varying number of alkyl groups attached to the adsorbing carbon atom, (2) a varying identity of those alkyl groups, and (3) a varying adsorption site.

6.3 Methods

Using plane-wave DFT, a large database (more than 500 data points) of hydrocarbon adsorption energies on twenty-seven hexagonal (fcc(111) and hcp(0001)) transition metal surfaces from groups 3 to 5 and 7 to 11 (shown in Table 6.1) was created. All surfaces were used in the studies of the effect of electronic structure parameters on adsorption energies and in the final model, while

a smaller set was used for developing site-specific scaling relations and expressions for adsorbate translation (Sections 6.4.3 to 6.4.5). Two models of an SnPt alloy were used to model the effect of Sn promoters on Pt surfaces: a Pt surface with dispersed Sn atoms, Sn_3Pt_6(d), and a Pt surface with lines of Sn atoms, Sn_3Pt_6(c). The dispersed model was used for all other bimetallics, and their electronic structure parameters are in Table 6.2.

The DFT calculations were performed with the Vienna ab-initio Simulation Package (VASP) [253, 254]. The PW91 exchange-correlation functional [256] was used, as it has been shown to correctly predict alkyl site preferences in several cases [217, 267] and to give an accurate adsorption energy for methyl on Pt(111) [302]. The projector augmented-wave method [255, 303] was used for the core electrons. The k-point mesh was a 7×7×1 Monkhorst-Pack [304] grid, and the plane-wave basis was cut off at 396 eV. Spin polarization was employed only for Ni and Co. Four layers were used to model the substrates, with the bottom two fixed at their bulk positions. A 3×3 surface cell was used, resulting in a coverage of 1/9 ML. Density of states (DOS) calculations were performed by fixing the charge density with tetrahedral smearing, increasing the k-point mesh to 19×19×1, and performing a non-self-consistent calculation. The DOS was sampled over intervals on the order of 10^{-4} eV. Band centers were calculated by projecting the wavefunction on atom-centered spherical harmonics within a cutoff radius and taking the first moment of the entire band for a given atom. Atomic graphics were created in QuteMol [259].

In a few cases—methyl in the top site and CH in the bridge site of Ti(0001) and ethyl in the top site of Re(0001), Sc(0001), and Zr(0001)—adsorbates had to be constrained to prevent them from relaxing out of site. The lowest carbon atom was fixed in the directions parallel to the surface but allowed to relax perpendicularly to the surface.

Table 6.1: The surfaces used in this chapter, along with their d-and p-band centers (in eV) and their matrix coupling elements relative to Cu.

surface	scaling?[a]	ϵ_d	ϵ_p	V_{ad}	E_{ads}(Methyl, Top)
Cu	y	−2.21	0.85	1.00	−1.34
Cu/Pd[b]	y	−1.66	0.93	1.08	−1.47
Pd_1Cu_8 (Pd)[c]	n	−1.90	0.97	1.88	−1.51
Pd_1Cu_8 (Cu 1)	n	−2.20	0.82	0.99	−1.31
Pd_1Cu_8 (Cu 2)	n	−2.24	0.86	0.98	−1.34
Ag	y	−3.79	1.07	1.23	−1.05
Au	y	−3.08	0.68	2.22	−1.33
Pt_1Au_8 (Pt)[d]	y	−1.49	0.51	2.81	−1.91
Pt_1Au_8 (Au 1)	y	−3.02	0.73	2.23	−1.32
Pt_1Au_8 (Au 2)	y	−3.05	0.75	2.23	−1.33
Au/Pd	y	−3.19	0.08	2.12	−1.24
Ni	y	−1.13	1.10	1.46	−1.70
Pd	y	−1.50	0.91	2.30	−1.85
Pd/Cu	y	−2.03	0.87	2.31	−1.52
Au_1Pd_8 (Au)	n	−2.84	0.86	2.42	−1.50
Au_1Pd_8 (Pd 1)	n	−1.49	0.78	2.35	−1.81
Au_1Pd_8 (Pd 2)	n	−1.52	0.88	2.28	−1.84
Pt	y	−2.00	−0.71	2.86	−2.09
Pt/Ag	y	−1.42	0.73	3.00	−2.01
Co	n	−1.32	−0.60	1.44	−1.87
Rh	y	−1.79	−1.50	2.38	−1.88
Ir	y	−2.32	−2.64	2.72	−1.98
Ru	y	−1.94	−2.11	2.30	−1.83
Ru/Pd	n	−1.30	−0.69	2.66	−2.05
Os	y	−2.29	−2.58	2.70	−1.92
Re	y	−1.75	−1.75	2.98	−1.59
Re/Pt	y	−1.37	−2.02	3.20	−2.05
Ti	y	−0.73	−1.04	2.85	−1.92
Ti/Pd	n	−0.07	−0.77	2.91	−2.26
Zr	y	−0.85	−0.80	3.93	−1.90
Hf	n	−0.96	−0.98	4.71	−1.83
Sc	y	−0.32	−0.61	2.80	−1.98
Hf_1Sc_8 (Hf)	n	−0.60	−0.65	4.19	−2.03
Hf_1Sc_8 (Sc 1)	n	−0.30	−0.64	2.89	−1.94
Hf_1Sc_8 (Sc 2)	n	−0.36	−0.67	2.85	−2.00

[a] The "scaling?" column indicates whether the surface was used in Sections 3.2-3.5.

[b] A/B means a pseudomorphic overlayer of A on B(111) or B(0001).

[c] A_1B_8 means a single A atom in the surface of B(111) or B(0001).

Table 6.2: The electronic structure parameters of the surfaces used in the propane dehydrogenation study.

surface	ϵ_d	ϵ_p	V_{ad}	E_{ads}(Methyl, Top)
Sn_3Pt_6(c) (Pt)	−2.12	−0.91	2.79	−1.91
Sn_3Pt_6(d) (Pt)	−2.21	−1.07	2.82	−1.85
Sn_3Pt_6(d) (Sn)	–	–	–	−1.39
Cu_3Pt_6 (Cu)	−1.68	−0.36	1.04	−1.20
Cu_3Pt_6 (Pt)	−1.86	−0.18	2.85	−2.18
Ag_3Pt_6 (Ag)	−3.07	−0.34	1.43	−0.99
Ag_3Pt_6 (Pt)	−1.93	−0.63	2.79	−2.07
Au_3Pt_6 (Au)	−3.26	0.05	2.37	−1.46
Au_3Pt_6 (Pt)	−1.89	−0.28	2.79	−2.03

6.4 Results and Discussion

6.4.1 Using Metallic Parameters to Predict Methyl Adsorption in the Top Site

We first examine the factors that control adsorption for what is perhaps the simplest case, methyl bonded to a single atom in the top site; this will aid in developing scaling relations below. Using a linear fit to the d-band center, ϵ_d, gives a mediocre accuracy for predicting the adsorption energy, with a mean absolute error (MAE) of 0.15 eV. Adding terms to account for the idealized d-band filling, f, and matrix coupling element, V_{ad}, similar to previous work [83], only provides moderate improvement (MAE of 0.11 eV). In particular, none of these terms can explain why Pt binds methyl more strongly than Pd. However, adding a dependence on the p-band center significantly increases the accuracy:

$$E_{\mathrm{ads}} = \beta_1\epsilon_d + \beta_2 V_{\mathrm{ad}}^2 f + \beta_3\epsilon_p + \beta_4\epsilon_a, \tag{6.1}$$

where ϵ_a is the energy of methyl's singly occupied molecular orbital (SOMO). Equation (6.1) predicts our database of methyl top-site adsorption energies with an MAE of 0.06 eV, with parameter values as shown in Table 6.3.

The final term in Eq. (6.1) accounts for the Pauli repulsion and the amount of adsorbate-metal coupling [112, 274]. As shown in Table 6.3, β_4 turns out to be negative, and the coupling appears to be a stronger effect than the Pauli repulsion. Since β_3 is positive, a lower p-band is stabilizing,

Table 6.3: The values of the parameters in Eq. (6.1), the standard error, and the MAE if they are eliminated.

	Value	Standard Error	MAE [a] if eliminated
β_1	−0.31	0.02	0.21
β_2	−0.22	0.03	0.12
β_3	0.09	0.02	0.11
β_4	0.45	0.01	0.53

[a] With all the parameters, the MAE is 0.06 eV.

while a lower d-band is destabilizing. The p-band center term likely accounts for differences in the adsorbate-p resonance; this will be explored more thoroughly in the next chapter. Values of V_{ad} were calculated using the C−M distance for methyl in the top site [273]:

$$V_{ad}^2 \propto r_d^3/d^7, \tag{6.2}$$

where r_d is the size of the d orbitals in the appropriate metal atom (previously tabulated [273, 305]) and d is the C−M distance. Thus, using Eq. (6.1) with appropriate electronic structure parameters, one can predict the adsorption energy of methyl in the top site of any hexagonal surface.

6.4.2 Scaling Across Similar Hydrocarbons

We now examine how to predict adsorption energies of longer hydrocarbons in their tetravalent sites, shown as (2) in Fig. 6.1. These relations are useful for studying the reactions of longer hydrocarbons as well as C−C coupling.

Using the energy of the SOMOs of different alkyls, Eq. (6.1) can be used to predict our database of 85 top-site alkyl adsorption energies with an MAE of 0.10 eV. (The parameter values are similar to when Eq. (6.1) is applied just to methyl.) We previously demonstrated that for alkyls the SOMO controls both top-site adsorption energies and gas-phase bond energies, allowing predictions of changes in adsorption energies based on gas-phase bond energies [83, 267]:

$$E_{\mathrm{ads}}(\text{-yl,Top}) = a_1 + a_2 E_{\text{C-H}} + E_{\mathrm{MeTop}}, \tag{6.3}$$

where E_{ads}(-yl,Top) is the adsorption energy of an alkyl in the top site, $E_{\text{C-H}}$ is the C−H bond

energy of the corresponding alkane, and E_{MeTop} is the adsorption energy of methyl in the top site.

An analogous relation can be applied to other types of hydrocarbons. In each case, the adsorption energy of a C_n adsorbate in its tetravalent site is predicted using the adsorption energy of the corresponding C_1 adsorbate in the same site and the total energy of the C−H bonds broken to produce the C_n adsorbate from an alkane. For example, to predict the adsorption energy of ethylidyne in the fcc hollow, we use the adsorption energy of methylidyne in the fcc hollow and the energy necessary to dehydrogenate gas-phase ethane to gas-phase ethylidyne and $3/2H_2$. Applying this to alkyls gives an MAE of 0.04 eV, applying it to alkylidenes gives an MAE of 0.03 eV, and applying it to alkylidynes gives an MAE of 0.03 eV.

6.4.3 Site-Specific C_1 Scaling Relations

We now use Eq. (6.1) to rationalize site-specific C_1 scaling relations, which are depicted schematically as (1) in Fig. 6.1. The first column of Table 6.4 shows that Eq. (6.1) accurately predicts the adsorption energies of C_1 hydrocarbons in their "tetravalent sites", i.e. those sites that fulfill the tetravalency principle. As noted in previous work [80, 306], if there is a function $f(w_i)$ of the metallic parameters w_i that determines, within a multiplicative and an additive constant, the adsorption energy of different chemical species, then there will be a scaling relation between those species. We therefore apply Eq. (6.1) to each pair of methyl and another C_1 adsorbate in their tetravalent sites, with a single set of fitting parameters but with a multiplicative and an additive offset. For example, to explain the scaling between methyl and methylidyne, we set

$$E_{\mathrm{ads}}(\mathrm{CH_3}) = \beta_1\epsilon_d + \beta_2\epsilon_a + \beta_3\epsilon_p + \beta_4 V_{\mathrm{ad}}^2 f, \tag{6.4}$$

$$E_{\mathrm{ads}}(\mathrm{CH}) = \eta_1 + \eta_2(\beta_1\epsilon_d + \beta_2\epsilon_a + \beta_3\epsilon_p + \beta_4 V_{\mathrm{ad}}^2 f). \tag{6.5}$$

The $\{\beta_i\}$ and $\{\eta_i\}$ were fit to the data, and the MAEs for each adsorbate when paired with methyl are given in the second column of Table 6.4. For each pair, methyl's adsorption energies were predicted with an MAE of less than 0.09 eV. Hence, it is clear that each pair of adsorbates can be accurately predicted from metallic parameters using a single set of fitting parameters, which implies

that scaling across the tetravalent sites should allow accurate predictions. This is indeed the case, and the MAEs of this type of site-specific scaling are given in the third column of Table 6.4. The similarities in the MAEs in all three columns of Table 6.4 give further support to the idea that scaling relations stem from the applicability of Eq. (6.1) to all C_1 hydrocarbons.

Table 6.4: MAEs in eV of various predictions of adsorption energies in tetravalent sites.

Adsorbate	MAE, ES[a]	MAE, ESSR with CH_3[b]	MAE, SR from CH_3[c]
CH_3	0.07	–	–
CH_2	0.17	0.17	0.18
CH	0.24	0.25	0.26
C	0.29	0.29	0.32
H	0.13	0.13	0.11

[a] Electronic structure (ES): Equation (6.1) is applied to each adsorbate individually, each with its own set of fitting parameters.
[b] Electronic structure scaling relations (ESSR): Equation (6.1) is applied to each pairing of CH_3 and another adsorbate with a single set of fitting parameters as well as an additive and multiplicative offset, as in Eqs. (6.4) and (6.5).
[c] Scaling relations (SR).

In contrast, scaling between hydrocarbons in their most favorable site (which can change across surfaces) is inaccurate when applied to a wide variety of transition metals, as shown in Fig. 6.2. Scaling from methyl in its most favorable site to methylidyne in its most favorable site results in a large MAE of 0.49 eV. We will refer to this type of scaling as min-min scaling. Min-min scaling relations have been shown to be accurate for C_1 hydrocarbons on various metals from groups 8-10 [35], but fail when applied to a wider variety of metals. Figure 6.2 demonstrates that min-min scaling relations fail in two cases: strongly inhomogeneous surfaces such as Pt_1Au_8, and surfaces with strong C−H−M interactions, such as Ti and Ru. On Pt_1Au_8, methyl prefers to bind directly atop the Pt atom, while methylidyne prefers the fcc hollow site, where it interacts with both Pt and Au atoms. Thus, the Au atoms directly destabilize methylidyne but not methyl. On Ti and Ru, methyl's adsorption geometry in the hollow site causes its C−H bonds to interact with metal atoms, while methylidyne does not experience these C−H−M interactions. This stabilizes methyl without affecting methylidyne.

Adding site-specificity can resolve these issues. The basic scheme is as follows: scaling

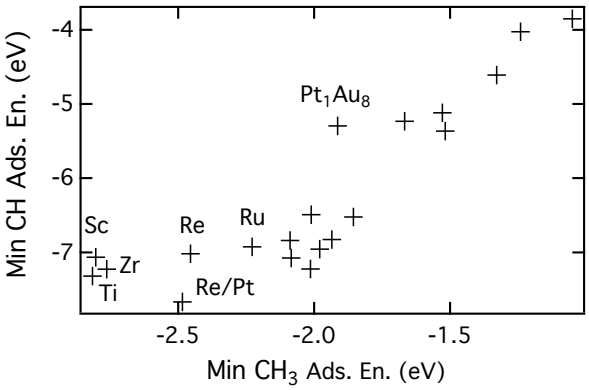

Figure 6.2: Methylidyne adsorption energies as a function of methyl adsorption energies.

relations between different types of C_1 adsorbates (methyl, methylidene, methylidyne, and carbon) are used only to scale energies between tetravalent sites. Thus, methyl in the top site can be used for scaling to all other C_1 adsorbates, even if methyl is actually more stable in another site. As discussed in Section 6.4.5 below, other relations will be employed to determine whether adsorbates translated to other types of sites are more stable. Inhomogeneities can be accounted for by averaging the methyl adsorption energies over the three top sites around the hollow site, and scaling from methyl in the top site avoids the effect of C−H−M interactions. For example, to predict CH in the hollow site of Pt_1Au_8, we scale from the average of the methyl adsorption energies in the Pt and Au top sites around the hollow site. To ensure that scaling across the tetravalent sites is the most accurate form of site-specific scaling, the adsorption energies of methylidyne in all four high-symmetry sites were calculated on the surfaces used for scaling. We then scaled from methyl in the top site to methylidyne in each site (see Fig. 6.3). Scaling to methylidyne in the top site was the least accurate, resulting in an MAE of 0.70 eV, while scaling to the bridge resulted in an MAE of 0.40 eV. Scaling to the fcc hollow was the most accurate, with an MAE of 0.26 eV, followed by the hcp hollow with an MAE of 0.30 eV.

The accuracy of scaling across the tetravalent sites is intuitively sensible, since each case involves the formation of bonds analogous to gas-phase single bonds. We note that tetravalency has a long history in the literature of both hydrocarbon adsorption [206] and scaling relations [35],

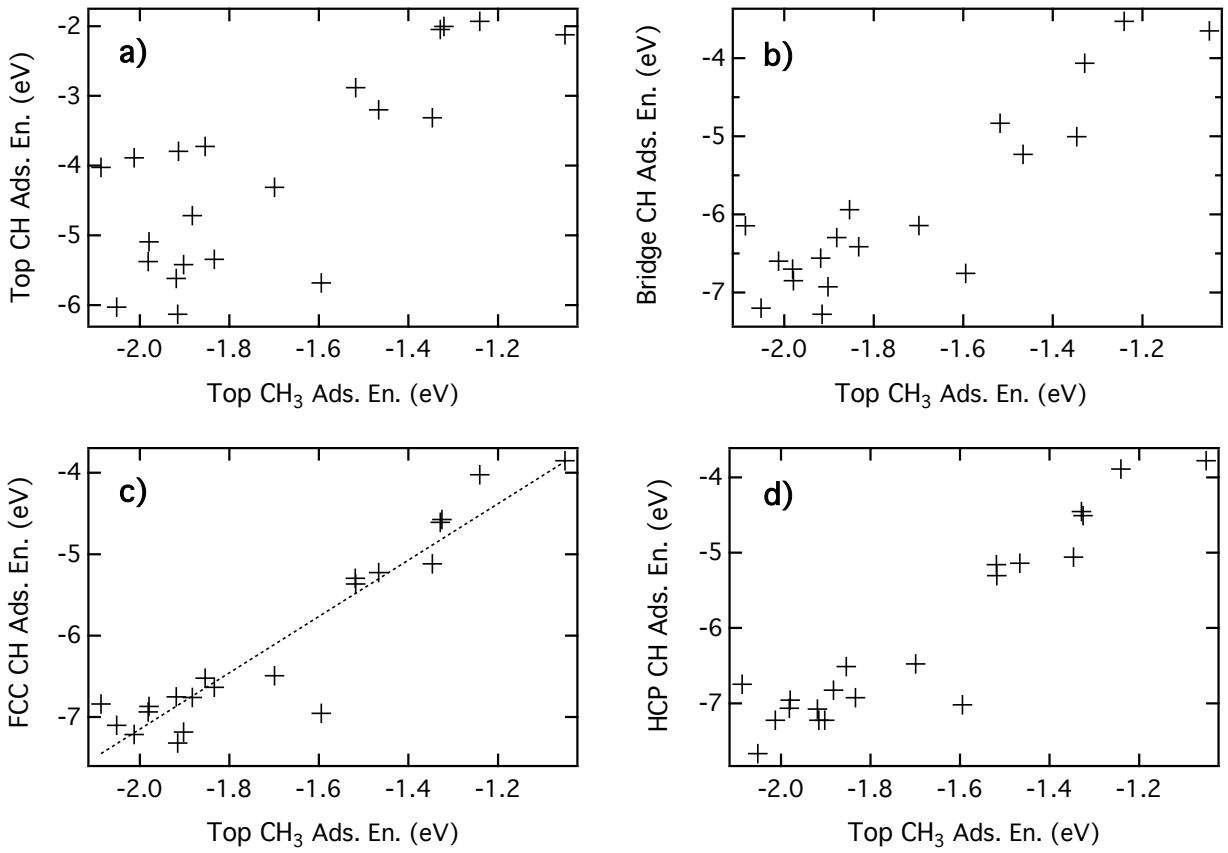

Figure 6.3: Methylidyne adsorption energies as a function of methyl adsorption energies: a) Top-top scaling relation, b) top-bridge scaling relation, c) top-fcc scaling relation (which we use in our model), and d) top-hcp scaling relation.

and that tetravalency was assumed in a previous study employing group additivity for adsorbed hydrocarbons [45]. Therefore, we scale from methyl in the top site to methylene in the bridge site and to methylidyne in the fcc hollow site (see Table 6.4 for the MAEs and Fig. 6.4 for a plot). Since it is not possible for the C atom to complete its tetravalency on a surface with hexagonal symmetry, we scale to it in the fcc hollow site.

It has been noted previously [207] that atomic hydrogen and alkyls are isolobal and thus should have similar bonding properties; however, there are notable discrepancies in the adsorption behavior of methyl and hydrogen. It turns out that the methyl top site adsorption energy scales with the hydrogen top site adsorption energy (see Table 6.4), and the differences in adsorption

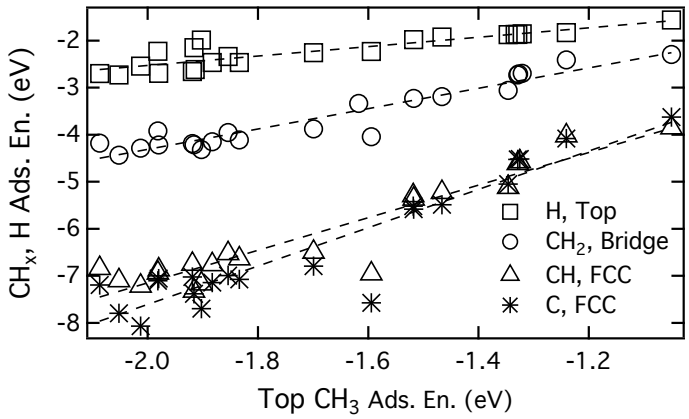

Figure 6.4: Site-specific scaling relations, with each C_1 adsorbate in its tetravalent site and H in its divalent site.

behavior between hydrogen and methyl are primarily due to the differences in their behavior in more highly coordinated sites.

6.4.4 Modifying C_1 Scaling Relations

In principle, one could choose any hydrocarbon (alkyl, alylidene, alkylidyne, or carbon) as a basis from which to scale all other adsorbates. To aid in deciding on the most useful form of site-specific scaling relations for a particular case, we have calculated MAEs for using each adsorbate to predict every other adsorbate, as shown in Table 6.5. This table can be used to decide which form of scaling is most useful in a particular application. However, it is necessary to scale from methyl for most inhomogeneous surfaces, since there are generally more unique top sites than unique bridge and hollow sites. In this case, there is no way to decouple the effects from individual metal atoms surrounding a hollow site to make predictions for the top site. Therefore, the values in Table 6.5 are calculated by excluding Pt_1Au_8, resulting in slightly different values than in Table 6.4. For these homogeneous surfaces, more accurate scaling is achieved for adsorbates with a similar number of adsorbate-metal bonds. Hence, if only homogenous surfaces are considered, choosing an adsorbate that is similar to the most important intermediate(s) would likely increase the accuracy of predictions of catalytic performance.

Table 6.5: MAEs in eV for scaling relations (SR) and modified scaling relations (MSR)[a].

	CH_3	CH_2	CH	C	H
CH_3 SR	–	0.15 (3.7%)[b]	0.27 (4.0%)	0.33 (4.6%)	0.12 (4.3%)
CH_3 MSR	–	0.11 (2.5%)	0.19 (2.8%)	0.23 (3.2%)	0.06 (2.1%)
CH_2 SR	0.07 (3.6%)	–	0.11 (1.7%)	0.17 (2.4%)	0.14 (5.1%)
CH_2 MSR	0.07 (3.5%)	–	0.09 (1.4%)	0.14 (1.9%)	0.10 (3.8%)
CH SR	0.07 (3.3%)	0.07 (1.6%)	–	0.19 (2.6%)	0.16 (5.7%)
CH MSR	0.06 (3.0%)	0.06 (1.4%)	–	0.18 (2.5%)	0.12 (4.3%)
C SR	0.08 (3.7%)	0.09 (2.1%)	0.17 (2.5%)	–	0.16 (5.8%)
C MSR	0.08 (3.7%)	0.08 (1.8%)	0.16 (2.3%)	–	0.12 (4.3%)
H SR	0.11 (5.2%)	0.26 (6.2%)	0.52 (7.6%)	0.68 (9.5%)	–
H MSR	0.05 (1.9%)	0.14 (3.3%)	0.22 (3.2%)	0.23 (3.2%)	–

[a] Scaling is done from the adsorbate in the left-most column to the adsorbate in top row, both in their tetravalent site. [b] The MAE as a percentage of the adsorption energy on Pt(111) is given in parentheses.

In order to increase the utility of scaling relations for catalyst screening, it is useful to know under what conditions scaling relations produce significant errors and how to increase their accuracy. For example, different adsorbates have slightly different dependencies on the d-band center. Therefore, the accuracy can be improved by adding a term proportional to the d-band center. Additionally, the energy change due to deformation of the lattice will be higher for adsorbates that bind more strongly, so we also can add a term proportional to the deformation energy. It has previously been shown [63] that this energy can affect the accuracy of scaling relations. We estimate this energy by moving an atom out of the surface by 5% of the lattice constant, and subtracting the energy of this deformed surface from the energy of the bare, relaxed surface. This quantity, E_{def}, has a moderate correlation with both the melting temperature of the metal and the s-band center. We denote this more accurate form of scaling relations which includes E_{def} and ϵ_d terms as modified scaling relations. For example, the adsorption energy of CH can be predicted as $E_{\mathrm{ads}}(\mathrm{CH}) = b_1 + b_2 E_{\mathrm{ads}}(\mathrm{CH_3}) + b_3 \epsilon_d + b_4 E_{\mathrm{def}}$, with the $\{b_i\}$ as fitting parameters. As shown in Table 6.5, adding these two terms results in moderate decreases in the MAE, particularly for adsorbates that are fairly different. Adding these two terms to min-min scaling relations has very little effect on their accuracy.

6.4.5 Translating Adsorbates to Different Sites

Scaling across the tetravalent sites is accurate, but it is not very useful if adsorption energies in the most favorable sites cannot be predicted. In the spirit of our previous work [83], we will write the energy changes upon translation of adsorbates to different sites in terms of metallic and adsorbate parameters. These expressions are shown schematically as (3) in Fig. 6.1.

In this work we only predict those sites that are the most favorable for a reasonable number of hexagonal transition metal surfaces. Table 6.6 shows the frequency with which CH_x prefers different sites. It is clear that hydrocarbons very rarely prefer sites with lower coordination than their tetravalent sites. The exception is CH on the pseudomorphic overlayer Cu/Pd, which prefers the bridge site by 0.01 eV, likely because Cu is too small (relative to Pd) for its electron density to reach far into the hollow site. We predict the top site and hollow sites for alkyls and H, the bridge and hollow sites for alkylidenes, and the hollow sites for alkylidynes and C.

Table 6.6: Number of surfaces on which a given site is preferred for a given adsorbate.[a]

Adsorbate(s)	Top	Bridge	Hollow
CH_3	9	0	11
CH_2	0	4	11
CH	0	1	19

[a] All data are for those surfaces on which enough calculations were performed to make a reasonable determination of site preference.

We extend our previous model of alkyl adsorption on late transition metal surfaces to all hexagonal transition metal surfaces and apply it to both alkyls and alkylidenes. We retain the overall scheme for calculating the energy of translations across sites, which involves adding contributions for each C−H−M interaction and each additional C−M interaction beyond the tetravalent site. We treat these as separate, additive terms since they involve different orbitals in the hydrocarbons.

To determine the energetics of adding C−M interactions, we examine methyl in the top and staggered hollow sites. This translation primarily involves a change in the matrix coupling element [83]. The matrix coupling element between surface metal atoms (V_{dd}) will also be included

as a measure of how far the d-orbitals extend into the hollow site as compared to the top site. There is also a change in electron-electron repulsion between the adsorbate state and the filled metal states. Since the p electrons are more delocalized, they have a stronger effect in the hollow site than the d states. Hence, the center of the occupied p states (ϵ_p(occ)) will also be included. Therefore, this energetic change can be written as

$$\Delta E_{\text{C-M}} = c_1 + c_2 V_{\text{ad}}^2 f + c_3 \epsilon_p(\text{occ}) + c_4 V_{\text{dd}}^2. \tag{6.6}$$

V_{dd} is proportional to r_d^3/d_{M}^5, where d_{M} is the M-M distance; it is calculated relative to Cu. When applied to methyl, this equation gives an MAE of 0.07 eV. Equation (6.6) can also be used to predict the change in energy upon translating CH from the fcc hollow to the bridge site with an MAE of 0.10 eV and to the top site with an MAE of 0.13 eV, suggesting broad applicability. On late transition metals, the second term in Eq. (6.6) is proportional to $V_{ad}^8 f^4$ if V_{ad} is taken from previous linearized muffin-tin orbital calculations [112] and f is the atomic filling, which explains the previous finding that $V_{ad}^8 f^4$ calculated in this way can predict $\Delta E_{\text{C-M}}$ on late transition metals [83]. For H, the V_{ad}^2 and V_{dd}^2 terms are less important because the H 1s orbital is less directional than the SOMO of an alkyl. This difference between H and alkyls has been previously discussed [207]. For inhomogeneous surfaces, simple averages of metallic parameters over the atoms surrounding a particular site are used as the effective parameters for that site, although weighting the average using V_{ad} has been suggested as a better approximation for the d-band center [297].

To predict the energetics of hydrocarbon translations, we must also predict the energetics of adding C−H−M interactions. The number of empty d-states correlates with the strength of C−H−M interactions, consistent with the idea that agostic interactions consist of donation from C−H bonds to metal states [229]. The lattice constant is also a good predictor of the strength of C−H−M interactions, which may be because a smaller lattice will involve closer—and hence stronger—C−H−M interactions. The H−M distance has previously been shown to affect the strength of C−H−M interactions [307], and the linear form chosen may be a linear approximation

to a more complex form. Therefore, we write the strength of C−H−M interactions as

$$E_{\text{C-H-M}} = d_1 + d_2(1 - f) + d_3 a, \tag{6.7}$$

where a is the lattice constant of the bonding metal atoms (scaled by $\sqrt{2}$ for hcp metals). Combining these relations with the scaling relations across alkyls, the adsorption energy of alkyls in the top and hollow sites can be predicted based on that of methyl in the top site with an MAE of 0.07 eV. For alkyls, the hollow sites have two additional C−M interactions and up to three C−H−M interactions. These relations also allow predictions of the adsorption energy of alkylidenes in the bridge and hollow sites based on methylene in the bridge site with an MAE of 0.07 eV. Alkylidenes have one additional C−M interaction in the hollow site, and up to two C−H−M interactions depending on the adsorbate and its orientation. For now, the difference between the fcc and hcp hollows will be ignored. Below, we demonstrate that including this difference for C and alkylidynes can improve the accuracy of the predictions.

6.4.6 Combining Site-Specific Scaling Relations and Translation Expressions

Combining all of the previous relations allows accurate predictions of the adsorption energy in multiple sites of any hydrocarbon that bonds through a single carbon atom to a hexagonal transition metal surface, using only the adsorption energies of methyl in the top sites and a few simple metallic and adsorbate parameters. Several simplifications and unifications can be made to reduce the number of fitting parameters. The following equations will be used to predict C in the hollow sites, alkylidynes in the hollow sites, alkylidenes in the bridge and hollow sites, and alkyls

in the top and hollow sites:

$$E_{\text{ads}}(\text{C, hol}) = \quad \text{A}_1 + 4\text{A}_2 E_{\text{MeTop}} + \text{A}_3\epsilon_d + 3\text{A}_4 E_{\text{def}} + (\text{A}_5 + 4\text{A}_6)E_{\text{C-H}} \tag{6.8}$$

$$E_{\text{ads}}(\text{-yne, hol}) = \quad \text{A}_1 + 3\text{A}_2 E_{\text{MeTop}} + \text{A}_3\epsilon_d + 3\text{A}_4 E_{\text{def}} + (\text{A}_5 + 3\text{A}_6)E_{\text{C-H}} \tag{6.9}$$

$$E_{\text{ads}}(\text{-ene, bridge}) = \quad \text{A}_1 + 2\text{A}_2 E_{\text{MeTop}} + \text{A}_3\epsilon_d + 2\text{A}_4 E_{\text{def}} + (\text{A}_5 + 2\text{A}_6)E_{\text{C-H}} \tag{6.10}$$

$$E_{\text{ads}}(\text{-yl, top}) = \quad \text{A}_1 + E_{\text{MeTop}} + (\text{A}_5 + 1\text{A}_6)E_{\text{C-H}} \tag{6.11}$$

$$\Delta E_{\text{C-M}} = \quad \text{B}_1 + \text{B}_2 V_{\text{ad}}^2 f + \text{B}_3\epsilon_p(\text{occ}) + \text{B}_4 V_{\text{dd}}^2 \tag{6.12}$$

$$E_{\text{C-H-M}} = \quad \text{C}_1 + \text{C}_2(1-f) + \text{C}_3 a. \tag{6.13}$$

Capitalized Roman letters are fitting parameters. Equations (6.8) to (6.11) are used to predict the adsorption energy of hydrocarbons in their tetravalent sites, and Eqs. (6.12) and (6.13) are used to predict changes in energy upon translation of alkyls or alkylidenes to hollow sites. The numeric coefficients in front of the E_{MeTop} terms are derived from the original formulation of scaling relations [35], those in the E_{def} terms are the number of C−M bonds, and those in the $E_{\text{C-H}}$ term are the number of C−H bonds broken to produce the adsorbate from an alkane. The adsorption energy of hydrogen in the top and hollow sites can also be predicted:

$$E_{\text{ads}}(\text{H, top}) = \quad \text{D}_1 + \text{D}_2 E_{\text{MeTop}} \tag{6.14}$$

$$\Delta E_{\text{H-M}} = \quad \text{B}_1 + \text{B}_3\epsilon_p(\text{occ}), \tag{6.15}$$

where Eq. (6.15) is used to predict the energy change upon translation from a top to a hollow site. Hence, using only a few simple DFT calculations (methyl in the top site(s), a DOS calculation, and a calculation of E_{def}), the adsorption energies of a large collection of hydrocarbons, as well as atomic hydrogen, can be predicted for various sites. This is useful for quickly predicting the energetics of reaction networks. A schematic of how the model relates various adsorption energies is given in Fig. 6.5.

This model has 15 fitting parameters (see Table 6.7) and an MAE of 0.13 eV (0.07 eV for alkyls, 0.17 eV for alkylidenes, 0.20 eV for alkylidynes, 0.23 eV for C, and 0.11 eV for H) when applied to our 527 point dataset (see Fig. 6.6 for the parity plot). This MAE is roughly the size

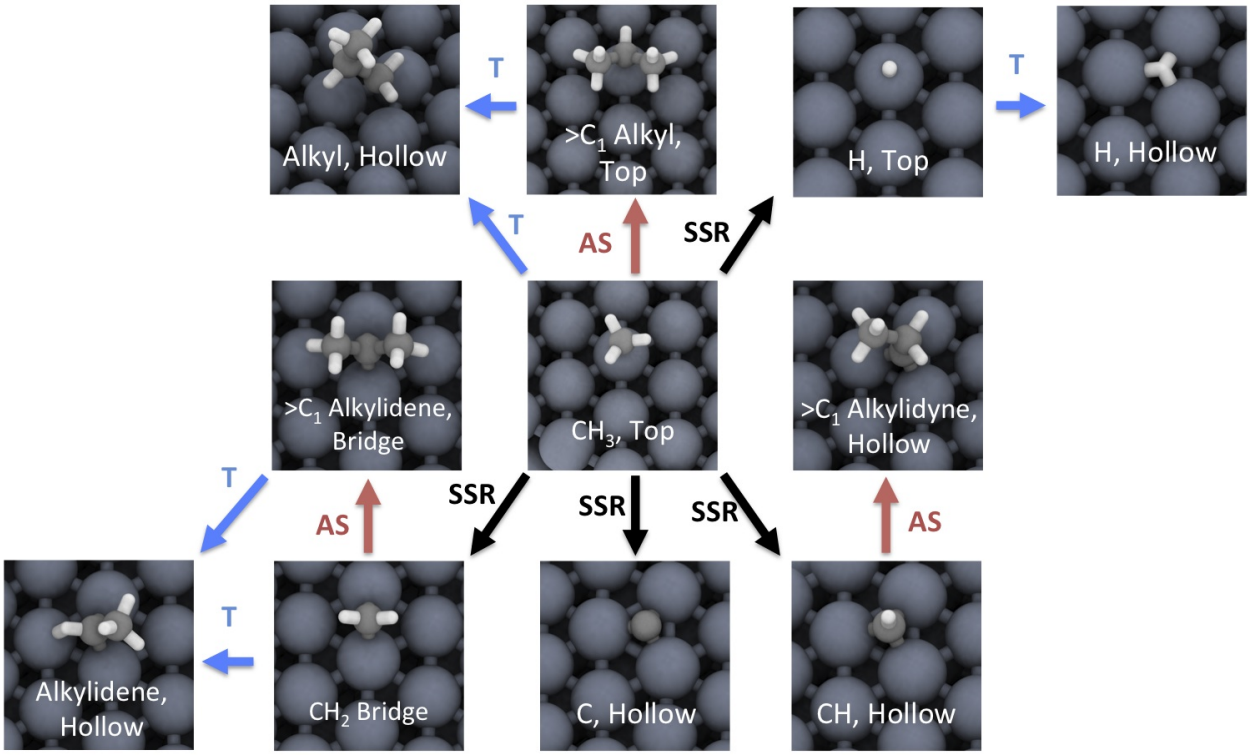

Figure 6.5: Given the adsorption energy of methyl in the top site(s), predictions can be made of the adsorption energy of any hydrocarbon that bonds to the surface through a single cabon atom. Site-specific scaling relations (SSRs) scale across the sites where single bonds are formed between the adsorbate and surface, adsorbate scaling relations (ASRs) use gas-phase bond energies, and translations (Ts) account for changes in C−M and C−H−M interactions.

of typical errors in DFT, which are expected to be on the order of 0.1 eV [306]. Table 6.7 shows that the standard errors are small compared to the parameter values, indicating that the values are well defined. Using predictions from Eq. (6.1) as input to the model gives an MAE of 0.17 eV. In this case, the adsorption energy of alkyl, aklylidene, alkylidyne, and carbon intermediates in all high-symmetry sites can be predicted without DFT calculations of adsorption energies. Further, previous work indicates that it may be possible to predict the electronic structure parameters without DFT calculations of the DOS [305, 308], which would allow extremely efficient screening.

The model, like min-min scaling relations, is useful for screening surfaces for their catalytic properties. It is more accurate than previous scaling relations, particularly across a wide range of metals. However, this increase in accuracy is accompanied by an increase in complexity and a

Table 6.7: The values of the parameters and the standard error.

Parameter	Value	Standard Error
A_1	2.92	0.07
A_2	0.65	0.02
A_3	−0.45	0.02
A_4	−1.79	0.09
A_5	1.33	0.03
A_6	−0.19	0.005
B_1	−0.59	0.05
B_2	0.29	0.02
B_3	−0.13	0.02
B_4	−0.022	0.003
C_1	−0.67	0.15
C_2	−0.21	0.07
D_1	−0.74	0.15
D_2	0.89	0.09

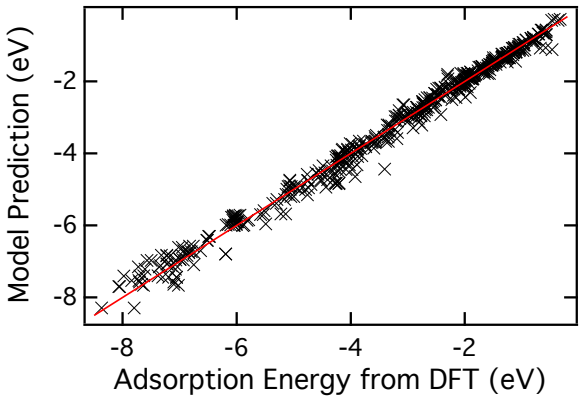

Figure 6.6: Parity plot for Eqs. (6.8) to (6.15) applied to the 527 point dataset.

loss of immediate applicability to other surface facets. Therefore, while this model will be useful in many cases, we do not expect it to supplant min-min scaling relations in all cases. Yet, even in cases where min-min scaling relations are used, our model may give insight into the approximations made and hence when these relations may fail. Essentially, min-min scaling relations will fail when scaling from or to alkyls or alkylidenes on strongly inhomogeneous surfaces, on those with a very negative $\Delta E_{\text{C-M}}$, and on those with strong C−H−M interactions (see below).

6.4.7 Achieving Higher Accuracy

Sometimes a high accuracy is desired for adsorption energy predictions, for example when using them to predict reaction rates, which can be sensitive to barrier heights. We first note that higher accuracy is achieved if only the most stable data point for each adsorbate on each surface is included (MAE of 0.12 eV). This indicates that predicting only the most stable site improves the accuracy, and often this is the only quantity of interest. Additionally, including more parameters in the model can increase the accuracy. The following equations have improved accuracy and only a modest increase in the number of parameters:

$$E_{\text{ads}}(\text{C, hol}) = \quad \text{A}_1 + 4\text{A}_2 E_{\text{MeTop}} + \text{A}_3{}'\epsilon_d + 3\text{A}_2 E_{\text{def}} + (\text{A}_5 + 4\text{A}_6)E_{\text{C-H}} \tag{6.16}$$

$$E_{\text{ads}}(\text{-yne, hol}) = \quad \text{A}_1 + 3\text{A}_2 E_{\text{MeTop}} + \text{A}_3{}'\epsilon_d + 3\text{A}_4 E_{\text{def}} + (\text{A}_5 + 3\text{A}_6)E_{\text{C-H}} \tag{6.17}$$

$$E_{\text{ads}}(\text{-ene, bridge}) = \quad \text{A}_1{}' + 2\text{A}_2 E_{\text{MeTop}} + \text{A}_3\epsilon_d + 2\text{A}_4 E_{\text{def}} + (\text{A}_5 + 2\text{A}_6)E_{\text{C-H}} \tag{6.18}$$

$$E_{\text{ads}}(\text{-yl, top}) = \quad \text{A}_1 + E_{\text{MeTop}} + (\text{A}_5 + 1\text{A}_6)E_{\text{C-H}} \tag{6.19}$$

$$\Delta E_{\text{C-M}}(\text{-ene}) = \quad \text{B}_1 + \text{B}_2 V_{\text{ad}}^2 f + \text{B}_3\epsilon_p(\text{occ}) + \text{B}_4 V_{\text{dd}}^2 \tag{6.20}$$

$$\Delta E_{\text{C-M}}(\text{-yl}) = \quad \text{B}_1 + \text{B}_2 V_{\text{ad}}^2 f + \text{B}_3{}'\epsilon_p(\text{occ}) + \text{B}_4 V_{\text{dd}}^2 \tag{6.21}$$

$$E_{\text{C-H-M}} = \quad \text{C}_2(1-f) + \text{C}_3 a + \text{C}_4{}'(1-f)^4. \tag{6.22}$$

$$\Delta E_{\text{HCP}}(\text{C, -yne}) = \quad \text{F}_1 + \text{F}_2 E_{\text{def}} \tag{6.23}$$

$$E_{\text{ads}}(\text{H, top}) = \quad \text{D}_1 + \text{D}_2 E_{\text{MeTop}} + \text{D}_3 E_{\text{def}} \tag{6.24}$$

$$\Delta E_{\text{H-M}} = \quad \text{B}_1 + \text{D}_4 V_{\text{ad}}^2 f + \text{B}_3\epsilon_p(\text{occ}) + \text{D}_5\epsilon_p. \tag{6.25}$$

For predicting hydrocarbons in their tetravalent sites, the terms are exactly the same as in the previous section, but some of the fitting parameters are uncoupled to give more flexibility in the values between different adsorbates. The same is true for $\Delta E_{\text{C-M}}$. For $E_{\text{C-H-M}}$, a $(1-f)^4$ term is added. A ΔE_{HCP} term is added for C and alkylidynes, and a few terms are added for H.

The MAE of this model is 0.11 eV: 0.06 eV for alkyls, 0.12 eV for alkylidenes, 0.18 eV for alkylidynes, 0.21 eV for C, and 0.07 eV for H. The values of the parameters and the standard errors

are in Table 6.8.

Table 6.8: The values of the parameters and the standard errors, for the more accurate model.

Parameter	Value	Standard Error
A_1	2.99	0.06
A_1'	3.61	0.10
A_2	0.70	0.02
A_3	−0.26	0.02
A_4	−1.45	0.10
A_5	1.39	0.03
A_6	−0.21	0.005
B_1	−0.82	0.05
B_2	0.34	0.02
B_3	−0.20	0.02
B_3'	−0.12	0.02
B_4	−0.016	0.004
C_2	−0.56	0.10
C_3	−0.024	0.007
C_4	1.42	0.19
D_1	−0.81	0.15
D_2	0.71	0.09
D_3	−2.21	0.47
D_4	0.024	0.021
D_5	−0.03	0.01
F_1	0.12	0.05
F_2	−1.78	0.41

6.4.8 Efficacy of min-min scaling relations

To elucidate the differences between min-min scaling relations and site-specific scaling relations, the model was used to predict where min-min scaling relations should be valid and where they should fail. Some representative examples are given in Fig. 6.7. The relationship between alkylidynes and C essentially reduces to min-min scaling relations because they prefer the same site and cannot experience C-H-M interactions. However, for alkylidenes and particularly for alkyls, site-specific scaling relations and min-min scaling relations can be significantly different. This is most noticeable for methyl, which can experience strong C-H-M interactions, but it is also true for tert-butyl, which can prefer the hollow site on early transition metals. Hence, on strongly inhomogeneous surfaces, on those with a very negative $\Delta E_{\text{C-M}}$, and on those with strong C-H-M

interactions, min-min scaling relations are likely to fail for alkyls and alkylidenes.

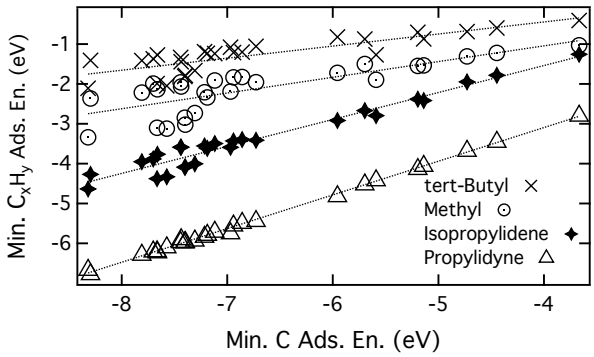

Figure 6.7: Predicted adsorption energies of various hydrocarbons as a function of the predicted carbon adsorption energies.

6.4.9 Applications

The model's predictions are consistent with several previously discovered trends, such as those for mode softening and site preference. Mode softening does not occur for methyl adsorbed in the top site, meaning that softened modes can be used to discover site preference. In agreement with experimental work, the model indicates that metals further to the left and closer to the top of the periodic table tend to bind hydrocarbons in more highly coordinated sites [236]. For those metals where methyl binds in the hollow site, the model's predictions of $E_{\text{C-H-M}}$ are consistent with previously discovered trends in the strength of mode softening (Ni>Rh>Cu) [236, 248].

Insight can also be gained into hydrocarbon chain growth, as the reaction energy of methyl coupling with the other C_1 hydrocarbons can be quickly calculated, as shown in Fig. 6.8a. The C + CH pathway, which has been previously identified as a possible mechanism on Fe and Co [309], is the most favorable on all of the tested surfaces except Au, although the difference is small on Ag and Pd_1Cu_8. We have also calculated the reaction energy of chain termination as a function of branching (see Fig. 6.8b). In general, chain termination is more favorable for more highly branched alkyls. There is essentially no change in chain termination energy between ethyl, propyl, and butyl, in agreement with previous work (data not shown) [288].

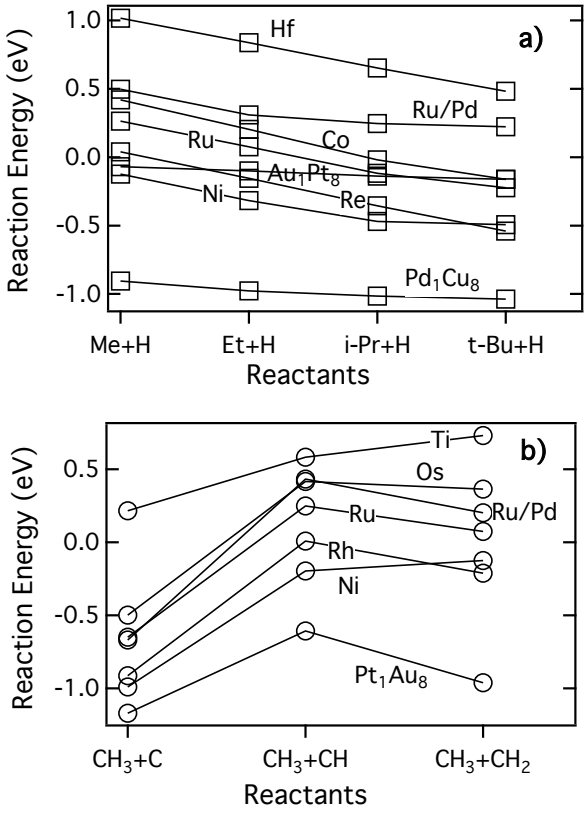

Figure 6.8: The reaction energy of a) methyl coupling with the other C_1 adsorbates and b) chain termination for alkyls with different branching structures.

Further, the model can be used to rationalize some previously determined trends in methane reforming. Since the oxygen adsorption energy may play a role in determining reactivity, we only consider metals that have previously been shown to have oxygen adsorption energies near the optimum [34]; these are shown in Fig. 6.9a. Based on the first dehydrogenation step of methane, which is thought to be important for determining activity [34, 310], it appears that Ru and Rh should be more active than Ir and Ni. Indeed, Rh and Ru have generally been found to have the highest activity for methane reforming [34, 311].

We conclude this section with a more extended discussion of an example system that illustrates the versatility of the model. The model is particularly useful for calculating potential energy diagrams for reactions involving longer hydrocarbons, allowing investigation of, for example,

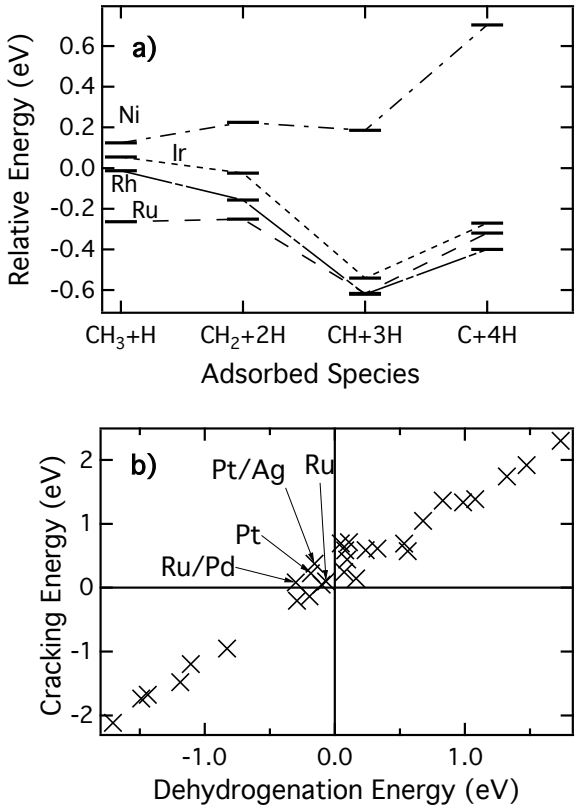

Figure 6.9: a) Potential energy surfaces for methane dehydrogenation, relative to the bare surface and methane in the gas phase; b) energy of propane cracking to methyl and ethyl as a function of the energy of propane dehydrogenation to propyl and H.

the dehydrogenation or oxidative dehydrogenation of propane to propylene. As a basis for comparison, we have compiled a rough ordering of catalytic performance from several experimental studies [312–314] on propane and ethane dehydrogenation:

$$\mathrm{SnPt} > \mathrm{CuPt} > \mathrm{Ag} \sim \mathrm{AuPt} \sim \mathrm{Pt} > \mathrm{Ni} \sim \mathrm{Rh} > \mathrm{Pd}. \tag{6.26}$$

Propane (oxidative) dehydrogenation involves competition between dehydrogenation and cracking [315]. One feature of the model is that it allows one to quickly calculate adsorption energies for hydrocarbon adsorbates having different length. Hence, we have plotted the energy of propane cracking into methyl and ethyl as a function of propane dehydrogenation to propyl and

H (see Fig. 6.9b). (Dehydrogenation to isopropyl and H is also possible, but the model indicates it is less favorable on all surfaces.) An ideal surface would be favorable for dehydrogenation and unfavorable for cracking, and using this simple measure Pt is found to be the best pure metal of those tested. This may partially explain why Pt has generally been observed to be the best pure metal for oxidative dehydrogenation [315].

An additional feature of the model is that it considers intermediates that involve multiple bonds to the metal surface. This can be useful for analyzing propane dehydrogenation because previous work has proposed that "deep dehydrogenation" of C_3 hydrocarbons leads to cracking [316]. A likely cracking mechanism identified previously is α-dehydrogenation of propyl to propylidene, followed by further bond-breaking steps to form CH and CH_3C. This allows the development of a slightly more sophisticated metric for the efficacy of catalysts for propane dehydrogenation. We first compute the energy of propyl α-dehydrogenation as well as the energy of cracking propylidene to CH and CH_3C, and then add the maximum of these to the energy of dehydrogenating propane to propyl. This metric is highest for surfaces that are favorable for the initial step of propane dehydrogenation but are unfavorable for cracking, either because propylidene formation is unfavorable or because propylidene cracking is unfavorable. Applying this metric to the relevant surfaces, we find the following order, which compares fairly well with the experimental one:

$$\mathrm{Ag} > \mathrm{Ag_3Pt_6} > \mathrm{Au_3Pt_6} > \mathrm{Sn_3Pt_6(d)} > \mathrm{Cu_3Pt_6} \sim \mathrm{Sn_3Pt_6(c)} > \mathrm{Pt} > \mathrm{Ni} > \mathrm{Pd} \sim \mathrm{Rh}. \qquad (6.27)$$

The predicted ordering is nearly identical when using predictions of the methyl adsorption energy based on Eq. (6.1) and values of V_{ad} from pure metal calculations, meaning that this ordering can be predicted from a single DOS calculation for each surface (or some other method for determining the band centers). The only exception is the Sn atoms in Sn_3Pt_8(d), which require a DFT calculation of methyl adsorption since Sn is not a transition metal.

The model is physically transparent and allows us to trace changes in reaction energies to features of the adsorbate and surface. For example, Cu_3Pt_6 has a copper atom neighboring every hollow site, which destabilizes alkylidynes but has little effect on alkyls. This destabilizes cracking

more than dehydrogenation. In fact, this may explain why promoters such as Sn, Pb, As, and Ge are often added to Pt to improve performance for propane dehydrogenation [315]. Simple min-min scaling relations would likely not capture this effect adequately, as the destabilization of an adsorbed carbon atom would be indiscriminately applied to both alkylidynes and alkyls. We have performed further calculations on Au_3Pt_6 and Ag_3Pt_6, and found that Ag and Au should have a similar effect as Cu. Ag in particular is predicted to make propylidene cracking much less favorable, while Sn has the greatest effect on the α dehydrogenation of propyl.

There are, of course, many further complexities to consider. For example, Au generally cannot dissociate O_2, which would likely make it a poor catalyst for oxidative dehydrogenation, even though it scores well according to our metric. However, using the model to calculate this metric is an efficient way to make a first screening of a large number of surfaces.

These applications demonstrate the broad utility of site-specific scaling relations, and the possibility of using them to employ design paradigms more sophisticated than tuning one or two adsorption energies. While more detailed studies involving DFT calculations of the reaction energies and barriers would allow further insight into these systems, our model allows fast, accurate screening of a variety of surfaces. Further, the framework proposed here allows these reaction energies to be directly traced back to surface properties, which is potentially a powerful route to catalyst design.

6.5 Conclusions

Since predicting hydrocarbon adsorption energies would allow efficient catalyst screening, we have studied how adsorption energies vary across metals and across adsorbates. For predictions from a metal's electronic structure, adding a dependence on the p-band center to the usual dependencies on the d-band center, the matrix coupling element, and the d-band filling can significantly improve the accuracy. Since this expression accurately gives the adsorption energies of all C_1 hydrocarbons in their tetravalent sites, it can be used to justify site-specific scaling relations, which in turn offer insight into the validity of min-min scaling relations. Site-specific scaling relations offer improved accuracy over min-min scaling relations, particularly for inhomogeneous surfaces and

earlier transition metals. In addition to the C_1 site-specific scaling relations, we have developed expressions for scaling to longer hydrocarbons and for adsorbate translations to different sites, which allow accurate predictions of adsorption energies in various sites. Combining all of these relations together allows efficient screening of transition metal surfaces for their catalytic properties for reactions involving hydrocarbons.

Chapter 7

Predicting O−M and C−M Adsorption Energies from Surface Attributes

7.1 Abstract

Understanding which surface properties control adsorption on metal surfaces has long been a primary goal in surface science and catalysis, for both fundamental and technological reasons. Moreover, for the purposes of designing catalysts for enhanced selectivity, it can be desirable to understand surface properties that lead to significant differences in adsorption energies of hydrocarbons and oxygenates. In this work, expressions for predicting adsorption energies of CH_3 and OH are developed, based in part on screening a large number of possible predictors. These expressions include the d-band center, d-band filling, and matrix coupling element, which are well known in the literature, as well as the relatively unstudied p-band center. These expressions are also applied to other adsorbates, including alkyls, alkoxides, C, O, and H, allowing elucidation of how the adsorbate structure affects the adsorption energy. While all alkyls behave similarly and all alkoxides behave similarly, there are significant differences between alkyls and alkoxides. In particular, adsorbate-surface coupling is net attractive for hydrocarbons but net repulsive for oxygenates, likely due to the deeper valence states on O atoms. As demonstrated within the context of the partial oxidation of ethylene, this difference can potentially be used to rapidly screen catalysts for improved selectivity based on the values of simple electronic structure parameters. We then design and experimentally test a novel TiAg catalyst with improved selectivity over pure Ag.

7.2 Introduction

Adsorption energies of molecules on transition metal surfaces have proven to be useful predictors of the catalytic performance of these surfaces for a wide variety of processes, such as renewable fuel production, petrochemical production, and electrochemistry. In particular, adsorption energies of simple hydrocarbons and oxygenates have been shown to correlate strongly with the activity and/or selectivity of a number of different reactions [25, 29, 33]. Hence, accurate prediction of adsorption energies could allow rational design of catalysts for a wide variety of important processes.

As an example, it is useful to consider the selective epoxidation of olefins such as ethylene, which is one of the most important and most studied reactions in heterogeneous catalysis. The key driver for catalyst improvement is achieving higher selectivity to the desired product, ethylene oxide, rather than the undesired combustion products. While the exact mechanism is still a matter of debate, there is evidence that the selectivity-determining step is reaction of a surface oxametallacycle ($-OCH_2CH_2-$) intermediate (see Fig. 7.1) [317–320]. Oxametallacycle ring-closure produces the epoxide, whereas H transfer leads to combustion. Prior work has indicated that the desired process can be promoted relative to the undesired process by increasing the oxygen-metal (O−M) bond strength relative to the carbon-metal (C−M) bond strength [317, 318, 321]. If so, more selective catalyst compositions could be identified based on an understanding of the fundamental surface properties associated with relatively strong O−M bonds and weak C−M bonds. While this scheme may not apply to all olefins, there is evidence that ethylene and several other olefins behave similarly [322, 323].

Identifying these descriptors requires a detailed model for how hydrocarbon and oxygenate adsorption varies across metal surfaces with different properties. Previous chapters have shown that, given the adsorption energy of methyl in the top site, the adsorption energy of any alkyl in any site can be accurately predicted. There has also been recent work successfully predicting electronic structure parameters from alloy structures, with no quantum chemical calculations other

Figure 7.1: Pathways for Ethylene Epoxidation (Desirable, Upper Pathway) and Combustion (Undesirable, Lower Pathway).

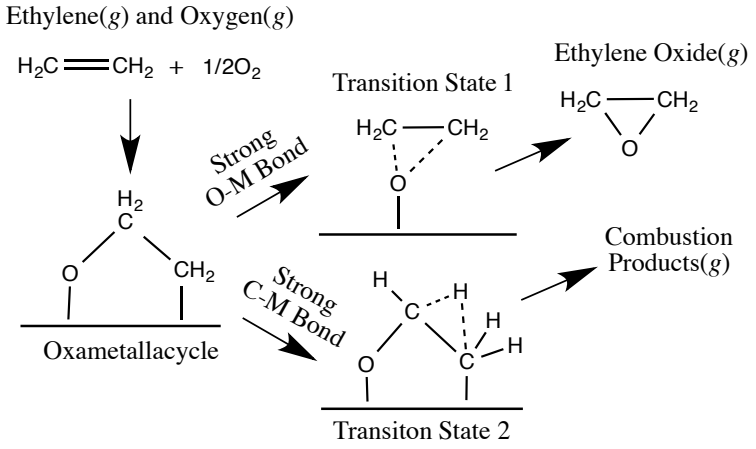

than those used in the initial fitting [305, 308]. The goal of this chapter is to bridge the gap between these previous studies by developing accurate expressions that predict adsorption energies of simple adsorbates that are bound to the surface through C−M and O−M bonds in particular sites based on surface properties.

Accurate prediction of adsorption energies from electronic structure parameters on a wide range of surfaces is difficult, in part because adsorbate site preference can change across metals. Further, most previous studies only consider a small number of surface properties. In the present work, we systematically examine a large number of properties for their predictive power for adsorption energies on a wide range of surfaces. The simple adsorbates CH_3 and OH are used to measure the reactivity of an individual metal atom by adsorbing them in the top site. The surface properties are tested for their predictive power alone as well as in multi-term expressions. We use our findings to develop simple, accurate, physically transparent expressions for CH_3 and OH adsorption energies. We then generalize these expressions to predict the adsorption strength of other adsorbates that bond through a C or O atom, with a focus on metrics that can rapidly predict differences between those adsorption energies. To demonstrate their utility, we apply these expressions to ethylene epoxidation and methane oxidation. Further, we experimentally test a novel

catalyst for ethylene epoxidation, and show it has improved selectivity over Ag.

7.3 Methods

7.3.1 Computational

Plane-wave DFT calculations were performed with the Vienna ab-initio Simulation Package (VASP) [253, 254]. The PW91 exchange-correlation functional [256] and the projector augmented-wave method [255, 303] were used, along with an energy cut-off of 396 eV and a 7×7×1 Monkhorst-Pack [304] k-point grid. One adsorbate was placed in each 3×3 surface cell with four layers of metal. The bottom two layers were fixed at their bulk positions, and all other atoms were allowed to relax. Spin polarization was employed only for Ni and Co. The density of states (DOS) was calculated by performing a single-point calculation with tetrahedral smearing and a smearing width of 0.01 eV. The charge density from this calculation was fixed, the k-point mesh was increased to 19×19×1, and a non-self-consistent calculation was performed. The DOS was sampled over intervals on the order of 10^{-4} eV. Band centers were calculated by projecting the wavefunction on atom-centered spherical harmonics within a cutoff radius and taking the first moment of the entire band for a given atom. The default number of bands was used in all calculations; test calculations indicate that increasing the number of bands has a negligible effect on adsorption energies.

Further details on the surfaces employed in most of this work are available in the previous chapter. The exceptions are those surfaces which were only employed in the ethylene epoxidation studies. The MAg alloys (M=Cu, Pd, Au) consisted of 1/3 monolayers of M dispersed throughout the Ag surface cell, such that each Ag surface atom was bonded to three M atoms. The $K_{ads}Ag$ surface consisted of 1/9 monolayers of K adsorbed on Ag in the top site in order to maximize the $K-CH_3$ and K−OH distances.

7.3.2 Experimental

Bimetallic catalysts were synthesized by taking Ag 1-3 μm powder (99.9% from Strem Chemicals) and performing TiO_2 atomic layer deposition. The process and reactor have been described previously [324].

Ethylene epoxidation was performed in a differential reactor composed of a 6.35 mm quartz tube. A mass spectrometer (SRS-RGA200) was used to analyze the product stream. After reduction in H_2 for 1.5 h at 325°, the system was allowed to cool to 280°, and then ethylene and oxygen were introduced (11 sccm of 10% C_2H_4 in He, 4 sccm Ar, and 3 sccm O_2). The temperature was slowly raised to 330°, and selectivities were measured at these conditions.

7.4 Theory and Model Development

7.4.1 Applying Simplified Versions of the d-Band Model

First, as a basis of comparison, we apply some expressions that have been previously employed in the literature. The d-band model [112] has been widely applied, most often under the assumption that the adsorption energy has a linear dependence on ϵ_d, the d-band center. As is evident in Fig. 7.2, a higher ϵ_d correlates with stronger adsorption for both CH_3 and OH. However, a linear fit to the data gives poor accuracy, with a mean absolute error (MAE) of 0.15 eV for CH_3 and 0.48 eV for OH. It is clear that ϵ_d alone cannot provide quantitative predictions across a range of metals, even when restricted to a single row of the periodic table.

To increase the accuracy of the predictions, the effects of the matrix coupling element, V_{ad}, and the idealized d-band filling, f, are often included [173, 181, 269]. In previous work,[83] we have written the adsorption energy of alkyls on late transition metals as

$$E_{\text{ads}} = \alpha_1 + \frac{\alpha_2 V_{ad}^2 (1-f)}{(\epsilon_d - \epsilon_a)} + \alpha_3(\epsilon_d - \epsilon_a) + \alpha_4 V_{ad}^2 f, \tag{7.1}$$

where ϵ_a is the energy of an alkyl's (e.g., CH_3's) singly occupied molecular orbital (SOMO). Values of V_{ad} are tabulated [112], but more accurate results are achieved if V_{ad} is calculated using

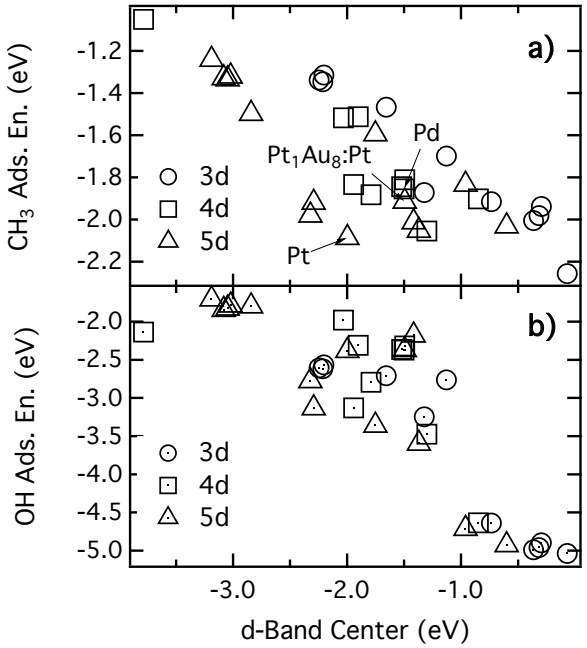

Figure 7.2: Adsorption energy of a) CH_3 and b) OH in the top site as a function of the d-band center. Comparing Pt to Pd or to the Pt atom in Pt_1Au_8 shows that the d-band center cannot always account for variations, even between similar metals or the same metal.

the C−M distance for CH_3 in the top site as $V_{ad}^2 \propto r_d^3/d^7$, where r_d is the size of the d orbitals in the appropriate metal atom (previously tabulated) and d is the C−M distance [273, 305]. The value of α_4 is negative for CH_3 and positive for OH, indicating that the two species have a different dependence on the adsorbate-metal coupling. When fit to our database, Eq. (7.1) gives an MAE of 0.11 eV for CH_3 and 0.15 eV for OH. These MAEs are still fairly high compared to typical variations in adsorption energies for these species; therefore, we conclude that there are other important factors determining the variations in adsorption energy across metals. In particular, traditional application of the concepts from d-band theory predicts that Pd should bind adsorbates more strongly than Pt, since Pd has a higher d-band center and a similar matrix coupling element. However, CH_3 binds more strongly to Pt by roughly 0.2 eV. This trend has been seen in several previous theoretical studies [35, 226], as well as in experimental adsorption energies of CO [177, 325, 326], which generally correlate with those of CH_3 [34]. Further, the Pt atom in Pt_1Au_8 has a higher d-band

center than the Pt atoms in pure Pt, yet it binds CH_3 less strongly. There are similar problems for OH; for example, Eq. (7.1) incorrectly predicts that adsorption will be stronger on Au than Ag.

Hence, the d-band model in its usual formulation can be both quantitatively and qualitatively inaccurate, and it is clear that other factors affect the adsorption energy. Since changes in adsorption energies of 0.1 to 0.2 eV can result in significant differences in selectivity [317, 318], high accuracy is often desirable. To aid in developing a model capable of identifying relatively subtle differences in adsorption energies, we systematically tested which other surface properties are good predictors for hydrocarbon and oxygenate adsorption.

7.4.2 Developing New Expressions for Predicting CH_3 and OH Adsorption Energies

The MAEs from using a variety of surface properties to predict adsorption energies of CH_3 and OH in the top site are shown in Table 7.1. (A table containing all of the properties is in Appendix A.) For CH_3, the best predictors are related to the d-band (ϵ_d^2, w_d, etc.). Most of these properties are fairly good predictors for OH as well, but χ (the electronegativity) and r_{cov} (the metal atom's covalent radius) are also excellent predictors. Hence, it is already clear that oxygenate and hydrocarbon adsorption energies do not necessarily follow the same trends.

Every combination of properties was tested for its accuracy for predicting adsorption energies in multi-term expressions up to 5 terms (in addition to a constant term). The properties that performed poorly in these expressions were then eliminated, and all combinations of the remaining properties were checked for expressions with 6 terms. The most accurate expressions in each case are available in Appendix A, and the MAEs of these expressions are given in Table 7.2. Using more than one attribute dramatically increases the accuracy; however, after approximately 3 to 4 terms only small improvements in the accuracy are achieved.

Based on our findings, the accuracy, complexity, and physical transparency of various expressions for the adsorption energy can be evaluated. We propose that good compromises between

Table 7.1: Accuracy of using linear fits of surface properties to predict adsorption energies.

Variable	Description	MAE for CH_3 (eV)	MAE for OH (eV)
c	Constant	0.27	0.91
ϵ_d	d-Band center	0.15	0.48
ϵ_d^2	–	0.14	0.62
f_d	Idealized filling of d band	0.20	0.22
f_d(DFT)	Filling of d band from DFT	0.16	0.42
w_d	d-Band width about Fermi level	0.19	0.46
$\rho_d(1)$	Number of d states within 1 eV of Fermi level	0.17	0.75
ϵ_p	p-Band center	0.21	0.74
$\rho_p(1)$	Number of p states within 1 eV of Fermi level	0.22	0.43
ϵ_s	s-Band center	0.22	0.79
V_{ad}^2	Matrix coupling element	0.20	0.74
r_{cov}	Covalent radius	0.22	0.42
χ	Electronegativity	0.23	0.35
$V_{ad}^2 f$	–	0.26	0.78

Table 7.2: MAE of the most accurate expression with a given number of non-constant terms.

Number of Terms	0	1	2	3	4	5	6
MAE for CH_3 (eV)	0.27	0.14	0.08	0.06	0.06	0.05	0.04
MAE for OH (eV)	0.91	0.22	0.14	0.10	0.08	0.07	0.06

these attributes are given by:

$$E_{\text{ads}}(\text{CH}_3) = \beta_1 + \beta_2\epsilon_d + \beta_3\epsilon_p + \beta_4 V_{ad}^2 f, \tag{7.2}$$

$$E_{\text{ads}}(\text{OH}) = \gamma_1 + \gamma_2\epsilon_d + \gamma_3\epsilon_p + \gamma_4 V_{ad}^2 f + \gamma_5 V_{ad}^2. \tag{7.3}$$

Equation (7.2) is the most accurate three-term expression for CH_3, with an MAE of 0.06 eV. Equation (7.3) is not the most accurate four-term expression for OH, but it is quite accurate (MAE of 0.10 eV) and allows the prediction of both CH_3 and OH adsorption energies from a single set of electronic structure parameters. The parameter values are given in Table 7.3, and examples demonstrating the use of these equations are below. To provide a visual confirmation of the accuracy of the proposed expressions, we show a parity plot in Fig. 7.3.

Equations (7.2) and (7.3) mostly consist of terms that are well-known in the literature; the exception is ϵ_p. However, this term fits easily into the paradigm of the d-band model, which treats

Table 7.3: Values of the parameters in Eqs. (7.2) and (7.3).[a]

Adsorbate	β_1,γ_1	β_2,γ_2	β_3,γ_3	β_4,γ_4	γ_5
CH_3	−1.99	−0.34	0.11	−0.20	
OH	−4.00	−0.32	0.16	1.07	−0.55

[a] Units are such that the energies are in eV.

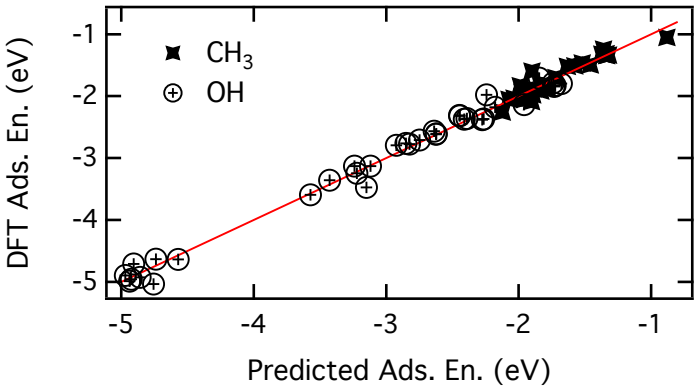

Figure 7.3: Parity plot showing the accuracy of the proposed expressions (Eqs. (2) and (3)) for predicting CH_3 and OH adsorption energies in the top site.

chemisorption on transition metals in two steps [112]. The ϵ_p term accounts for the first step, the renormalization of adsorbate states by the broad s and p bands of the metal surface. The second step, interaction of the renormalized adsorbate states with the narrow d-band to form bonding and antibonding states, is accounted for by the other terms.

A higher ϵ_d generally leads to more unoccupied antibonding states and stronger adsorption. However, a lower ϵ_p correlates with stronger adsorption. For example, Pt has a much lower ϵ_p than Pd, which may explain the exception to the ϵ_d trend noted above. Hence, the relationship between ϵ_p and the adsorption energy is the opposite trend as that usually found for ϵ_d. This is because the p-induced resonance is completely filled and does not split into well-defined bonding and antibonding states [112]. A lower p-band should interact more strongly with adsorbate states and result in a lower resonance state, as confirmed by our calculations using the Newns-Anderson model on a model chemisorption function (see Fig. 7.4). A lower resonance state will be more energetically favorable relative to the initially half-filled adsorbate state. Hence, we conclude that

a lower ϵ_p results in a lower-energy renormalized state, which results in stronger adsorption.

More concretely, Fig. 7.4 shows the adsorbate-projected density of states that results from the interaction of an adsorbate state with a metal band, which is given by the Newns-Anderson model as [150]

$$\rho_a(\epsilon) = \frac{1}{\pi}\frac{\Delta}{(\epsilon - \epsilon_a - \Lambda)^2 + \Delta^2}, \tag{7.4}$$

where

$$\Delta(\epsilon) = \pi \sum_k |V_{ak}|^2 \delta(\epsilon - \epsilon_k) \tag{7.5}$$

and Λ is the Hilbert transform of Δ. We will apply Eq. (7.4) to the interaction of an adsorbate state with the p band. Based on previous work [156], we use simple model functions for Δ and Λ:

$$\Delta = \quad c(1-\epsilon)^2 \tag{7.6}$$

$$\Lambda = \quad c[\frac{1}{2}\epsilon(3-2\epsilon^2) + (\Theta(\epsilon-1) - \Theta(-1-\epsilon))(\epsilon^2-1)^{\frac{3}{2}}], \tag{7.7}$$

where Θ is the step function. Because of Eq. (3.3), a shift in the band by δ_p is equivalent to replacing ϵ with $\epsilon - \delta_p$ in Eqs. (7.6) and (7.7). Hence, we can calculate how shifting the band affects the resonance induced by the interaction of the p-band and the adsorbate state. Taking $c = 1$ and $\epsilon_a = -4$, we calculated this resonance for various values of δ_p. As shown in Fig. 7.4, a lower p-band center results in a lower resonance (i.e., a resonance at lower energies). Additionally, the resonance is stronger for lower p-band centers due to increased interaction.

7.4.3 Differences Between C−M and O−M Bonds

The primary difference between adsorption through O atoms and adsorption through C atoms is the dependence on V_{ad}. After fitting, the $V_{ad}^2 f$ term is negative (attractive) for CH_3, but positive (repulsive) for OH. The V_{ad}^2 term, which is only in the expression for OH, is negative but smaller in magnitude than the $V_{ad}^2 f$ term. Therefore, increasing the coupling results in stronger adsorption of CH_3 but weaker adsorption of OH. These differences explain, for example, why OH adsorbs more strongly on Ag than Au, but CH_3 adsorbs more strongly on Au than Ag: Au has a larger V_{ad}, which is net attractive for CH_3 but net repulsive for OH.

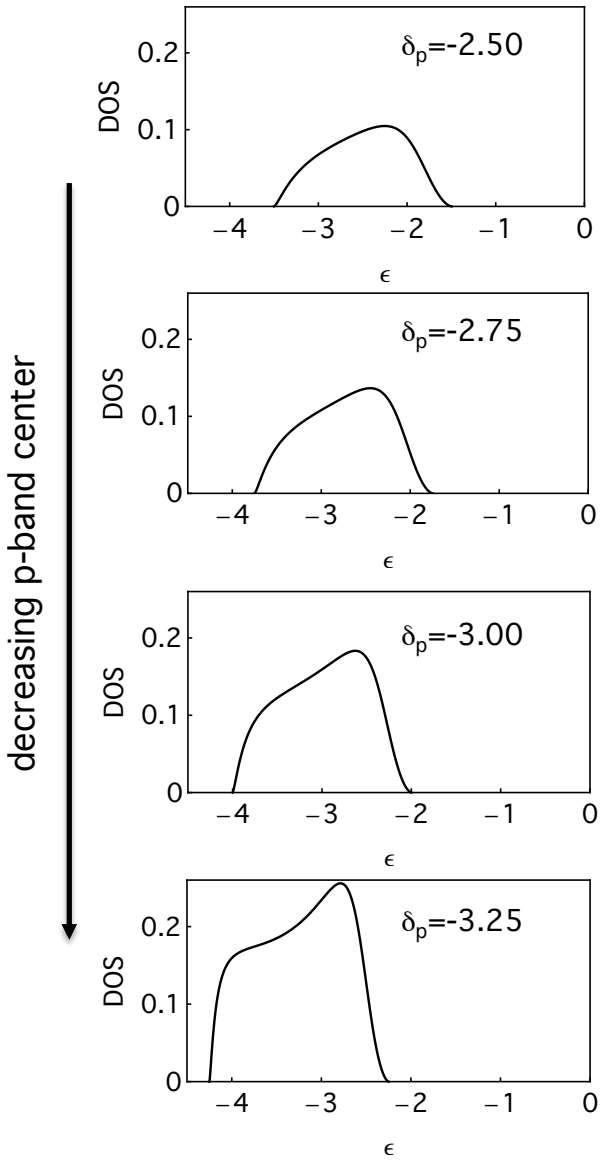

Figure 7.4: The adsorbate-induced resonance for various values of the d-band center, calculated using the Newns-Anderson Model.

To help explain the differences between CH_3 and OH adsorption, Bader charge calculations [327] were performed for CH_3 and OH adsorbed on a subset of 8 metals. For OH, a larger $V_{ad}^2 f$ results in less charge transfer to OH (see Fig. 7.5) because of increased repulsion between the O states and the metal states. As O is quite electronegative, less charge transfer results in weaker bonding. However, once $V_{ad}^2 f$ is controlled for, a larger V_{ad}^2 apparently results in stronger bonding,

as implied by perturbation theory. CH_3 has higher valence states that can couple and split more easily. Therefore, a larger $V_{ad}^2 f$ results in a stronger interaction and stronger bonding [112], and $V_{ad}^2 f$ does not correlate well with charge transfer.

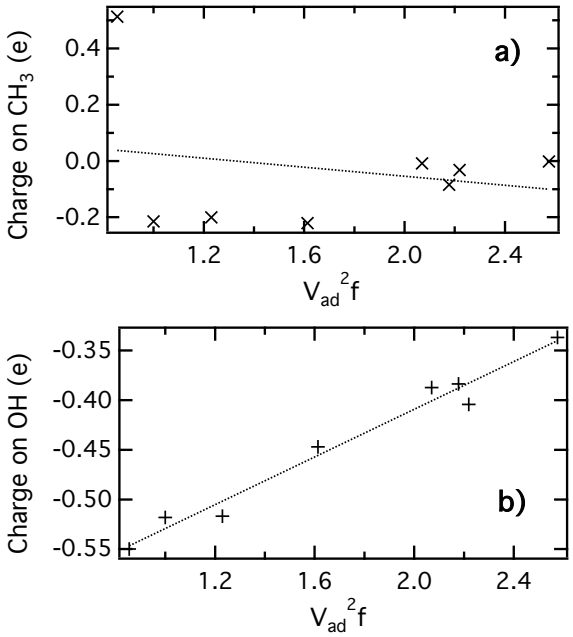

Figure 7.5: The net charge on the adsorbed a) CH_3 group and b) OH group as a function of $V_{ad}^2 f$. Linear fits are included to show that the correlation is much stronger for OH than CH_3.

7.4.4 Other Adsorbates with C−M and O−M Bonds

To confirm the generality of these expressions, they were applied to other adsorbates that have the same valence as CH_3 or OH but have different structures: alkyls, 2-hydroxyethyl, simple alkoxides, and furfuryl alkoxide. Since we are currently interested only in how these structures affect the single adsorbate-metal bond, these adsorbates were placed in the top site and in orientations where the only interaction was through a single C or O atom. This may not be the most stable configuration, particularly for multifunctional adsorbates at low coverage [328].

For a particular metal, variations in alkyl adsorption energies in the top site are controlled by the energy of the singly occupied molecular orbital (SOMO) [83, 267]. However, hydroxyethyl

does not quite follow this trend. Instead, the gap between the SOMO and the lowest unoccupied molecular orbital (LUMO) controls the variation in the binding energy for any radical that forms single bonds between C and a metal atom. The SOMO-LUMO gap also controls the strength of the analogous gas-phase C−H bonds. Figure 7.6a shows that this applies generally for both C−M and O−M bonds. Hence, by including the effect of the SOMO-LUMO gap (ϵ_{gap}), adsorption energies of a variety of adsorbates in the top site can be predicted from electronic structure parameters:

$$E_{\text{ads}}(\text{C}-\text{M}) = \beta'_1\epsilon_{\text{gap}} + \beta'_2\epsilon_d + \beta'_3\epsilon_p + \beta'_4 V_{ad}^2 f, \tag{7.8}$$

$$E_{\text{ads}}(\text{O}-\text{M}) = \gamma'_1\epsilon_{\text{gap}} + \gamma'_2\epsilon_d + \gamma'_3\epsilon_p + \gamma'_4 V_{ad}^2 f + \gamma'_5 V_{ad}^2. \tag{7.9}$$

These equations give MAEs of 0.06 eV for C−M bonds and 0.09 eV for O−M bonds when applied to the adsorption energies shown in Fig. 7.6a (the parity plot is in Fig. 7.6b), indicating that these electronic structure parameters can be used to predict the adsorption energies of a variety of adsorbates. Adding a constant term to these expressions has little effect on the MAE (≈0.01 eV).

Previous work has indicated that gas-phase bond energies can be used to predict changes in adsorption energy for similar adsorbates [83, 262]. As shown in Fig. 7.7, this is an accurate and general principle, likely because the SOMO-LUMO gap controls changes in adsorption energies in the top site as well as gas-phase bond energies. For hydrocarbons, more highly branched alkyls such as isopropyl and *tert*-butyl have higher steric effects as well as weaker gas-phase bonds, leading to an effective slope slightly greater than one. We show in the next section that the more significant deviations from parity in Fig. 7.7 are likely due to steric effects.

Further, Equations (7.2) and (7.3) can also be used to predict the adsorption energies of C and O. Because the same expressions apply for similar adsorbates, they can be used to rationalize so-called scaling relations, which are linear relationships between adsorption energies of similar adsorbates [80], as shown in the previous chapter. H in the fcc hollow site can also be predicted with good accuracy (MAE of 0.08 eV) using Eq. (7.2).

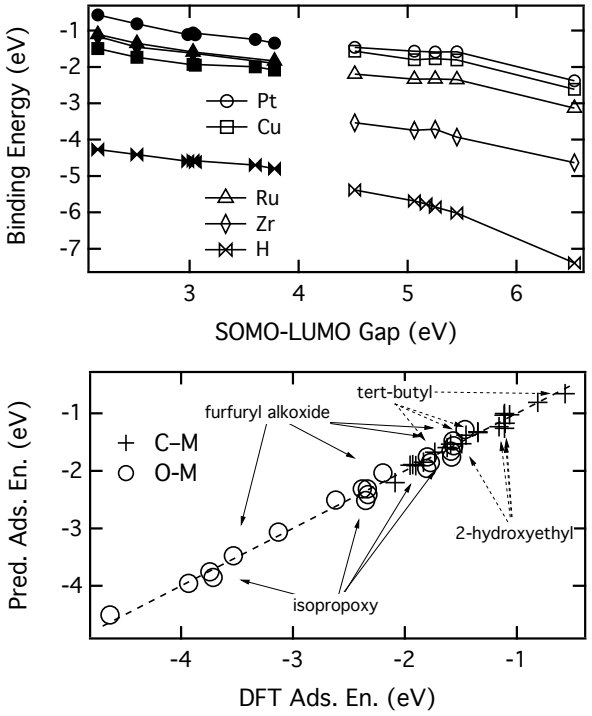

Figure 7.6: a) Top-site adsorption energies and gas-phase bond energies as a function of the SOMO-LUMO gap. Each set of connected points represents different radicals binding to a particular metal surface atom or an H atom. Filled symbols are C−M bonding adsorbates and open symbols are O−M bonding adsorbates. b) Parity plot showing the application of Eqs. (7.8) and (7.9) to a variety of adsorbates. A few adsorbates are labelled for concreteness.

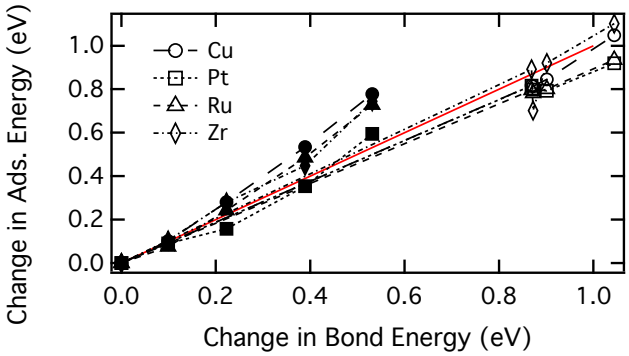

Figure 7.7: Changes in adsorption energies as a function of changes in gas-phase bond energies.

7.4.5 Steric Effects

As shown above, gas phase bond energies can be used to predict certain adsorption energy changes. The most significant errors for these predictions occur for isopropyl and tert-butyl, and

eliminating these adsorbates increases the accuracy of these predictions (see Fig. 7.8). Based on their adsorption geometries, these are also the adsorbates that likely have the highest steric effects. To gain a rough idea of the extent of steric effects, the geometry of each adsorbate on each surface was frozen, and the surface was replaced with a hydrogen atom that was allowed to relax. The energy of this partially frozen molecule was calculated and compared to the energy of the relaxed molecule, which gives an idea of how much distortion was induced in the adsorbate. The distortion energy of methyl for a particular surface (which was a little less than 0.01 eV in each case) was subtracted from the distortion energy of each other molecule. The mean of this for each adsorbate is shown in the fourth column of Table 7.4, demonstrating that isopropyl and tert-butyl experienced stronger steric effects than the other adsorbates. The distortion energy for each adsorbate on each surface was added to its adsorption energy to "correct" the adsorption energy for distortion effects. The mean of this is shown for each adsorbate in the fifth column of Table 7.4. This shows that correcting for the distortion energy brings the adsorption energy difference closer to the gas phase energy difference for isopropyl and tert-butyl, and has a small effect on other adsorbates. Since this method accounts for adsorbate distortion but not the steric repulsion that remains in the adsorption geometry, we do not expect perfect accordance. However, this argument demonstrates that steric effects are likely the reason that isopropyl and tert-butyl deviate from the predictions based on the gas phase bond energies.

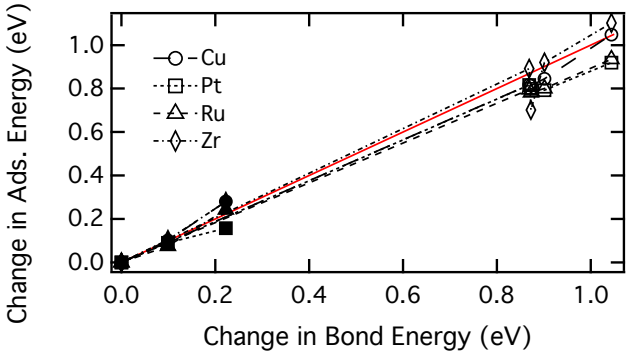

Figure 7.8: The change in adsorption energy as a function of the change in the gas-phase bond energy, with isopropyl and tert-butyl eliminated.

Table 7.4: Steric Effects for Adsorbates that Bind through a Carbon Atom.

Adsorbate	Gas-Phase Energy Difference[a]	Mean Adsorption Energy Difference	Mean Distortion Energy Difference	Mean Corrected Adsorption Energy Difference
methyl	0[b]	0	0	0
2-hydroxyethyl	0.10	0.09	0.00	0.07
ethyl	0.22	0.24	0.01	0.23
isopropyl	0.39	0.44	0.02	0.39
tert-butyl	0.53	0.68	0.03	0.61

[a] All differences are relative to methyl.
[b] All energies are in eV.

7.4.6 Translations To Other Sites

Although the above developments relate primarily to adsorption in the top site, displacements to other sites can be predicted based on approaches from previous chapters, which we briefly summarize here. We have previously developed expressions for predicting changes in adsorption energy upon translation of alkyls from the top site to other sites. For translation of CH_3 from a top site to a staggered hollow site, the change in adsorption energy can be predicted as:

$$\Delta E_{\text{trans}} = c_1 + c_2 V_{\text{ad}}^2 f + c_3 \epsilon_p(\text{occ}) + c_4 V_{\text{dd}}^2. \tag{7.10}$$

The change in coupling upon translation, accounted for by the $V_{\text{ad}}^2 f$ term, is the primary source of the adsorption energy change [83], while the $\epsilon_p(\text{occ})$ term accounts for electron-electron repulsion [84]. The V_{dd}^2 term accounts for how far the d orbitals extend into the hollow site [84]. As shown in Fig. 7.9, this expression can also be used to predict energetic changes upon translation of OH from the top to the fcc hollow. Hence, CH_3 and OH translations appear to follow similar physical models. (Agostic C−H−M interactions can be accounted for separately [84].) However, OH is much more likely to prefer the hollow site than CH_3. This is likely because OH−d interactions are more repulsive than CH_3−d interactions, as noted above. The d-orbitals are quite localized, leading to stronger d interactions in the top site than the hollow site. Since the s and p electrons are more delocalized and contribute significantly to the bonding [112], the hollow site tends to be more stable for OH. In any case, because adsorption in the hollow site roughly scales with adsorption in the top site, trends in binding energy to the top site can be used to capture trends for adsorption in the hollow site.

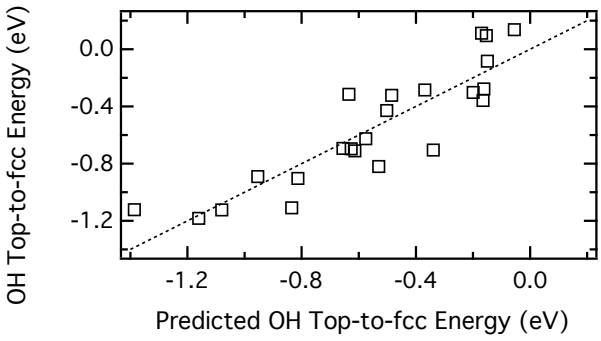

Figure 7.9: Adsorption energy changes upon translation of OH from a top site to an fcc hollow calculated from DFT as a function of predictions based on Eq. (7.10).

7.4.7 Examples and Comparison to Previous Work

To concretely demonstrate the use of the equations in this chapter, we calculate a few adsorption energies explicitly. We begin with the adsorption energies of isopropyl and propoxy in the top site of Pt(111).

Pt(111) has the following values for its surface properties: $\epsilon_d = -2.00$ eV, $\epsilon_p = -0.71$ eV, $V_{ad}^2 = 2.86$, $f = 0.9$, and the SOMO-LUMO gap is 2.52 eV for isopropyl and 5.25 eV for propoxy. Combining these with the values in Table 7.5, the adsorption energies are found to be -1.68 eV (DFT: -1.73) for isopropyl and -1.63 eV (DFT: -1.59) for propoxy.

Table 7.5: Values of the Parameters in Eqs. (7.8) and (7.9).[a]

Bond Type	β_1',γ_1'	β_2',γ_2'	β_3',γ_3'	β_4',γ_4'	γ_5'
C−M	−0.42	−0.30	0.05	−0.46	
O−M	−0.51	−0.17	0.11	0.97	−0.60

[a] Units are such that the energies are in eV.

We also demonstrate top and fcc hollow site calculations for methyl and hydroxyl on Ru(0001). In addition to Eqs. (7.8) and (7.9), we need Eq. (7.10).

Based on Ru's, methyl's, and hydroxyl's electronic structure parameters, the predicted top site energies are -1.85 eV for methyl (DFT: -1.83) and -3.07 eV for hydroxyl (DFT: -3.13). Using Eq. (7.10) and the appropriate values of the fitting parameters ($c_1 = -1.51$ eV, $c_2 = 0.52$,

$c_3 = -0.37$, and $c_4 = -0.024$ for methyl while $c_1 = -2.10$ eV, $c_2 = 0.21$, $c_3 = -0.42$, and $c_4 = 0.017$ for hydroxyl) as well as the electronic structure parameters ($V_{\mathrm{ad}}^2 = 2.30$, $f = 0.7$, $\epsilon_p(\mathrm{occ}) = -2.62$, and $V_{\mathrm{dd}}^2 = 8.90$ for Ru), the predicted changes in energy upon translation from the top to the fcc hollow are -0.09 eV for methyl (DFT: -0.12) and -0.43 eV for hydroxyl (DFT: -0.50). This results in predicted fcc hollow adsorption energies of -1.94 eV for methyl (DFT: -2.02) and -3.50 eV for hydroxyl (DFT:-3.56).

There are several cases in the literature where catalytic performance has been essentially reduced to the strength of C$-$M and/or O$-$M bonds, including CO methanation [29], acetylene hydrogenation [81], methane steam reforming [34], and methane oxidation [67]. These cases demonstrate the wide utility of simple models to predict C and O adsorption energies, and how Eqs. (7.2) and (7.3) can be used in catalyst design. For example, previous work [67] has shown that trends in activity for methane oxidation in solid oxide fuel cells can be predicted based on the C and O adsorption energies. Our model, though fit to data calculated using different adsorbates, a different functional, and a different DFT code, generally reproduces the qualitative trends in adsorption through C atoms and O atoms (see Fig. 7.10). This demonstrates that the model qualitatively agrees with previous work and may be useful in catalyst design.

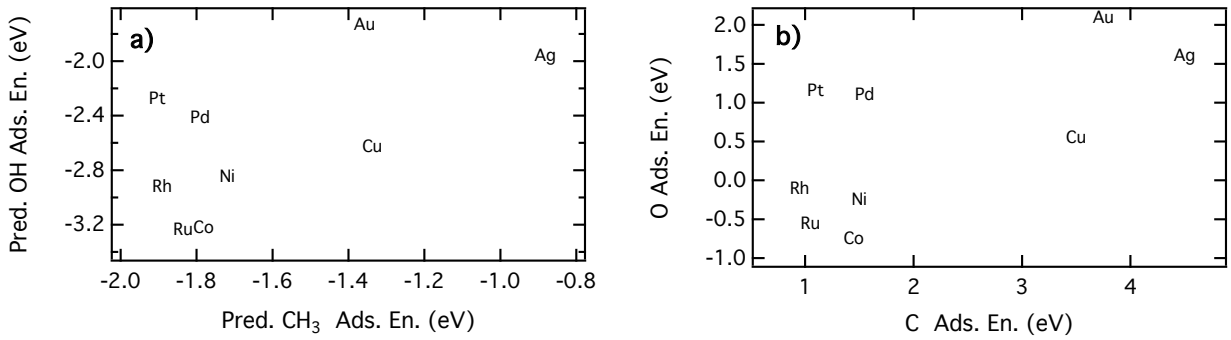

Figure 7.10: a) The adsorption energy of OH as a function of CH_3, as predicted by our model. b) The adsorption energies of C and O, as calculated by DFT in previous work [67].

7.5 Design and Experimental Testing of an Ethylene Epoxidation Catalyst

7.5.1 Design

As an example of the utility of Eqs. (7.2) and (7.3), we examine structures proposed to be important for ethylene epoxidation on various surfaces. In previous work, an expression containing the adsorption energy difference between CH_3 and CH_3O as well as other terms was found to quantitatively predict differences in activation energies between the selective and non-selective pathways [318, 319]. We instead use a simple difference between OH and CH_3 adsorption energies, which is likely to be useful as a qualitative metric. Since the primary difference between O−M and C−M bonds is their dependence on the V_{ad} terms, these terms can be used to predict the difference in their bond strengths. (The values of β_2 and γ_2 are quite similar, as are those of β_3 and γ_3.)

Figure 7.11a shows the strong correlation between the coupling terms and the difference in the OH and CH_3 adsorption energies. Fig. 7.11b focuses on those surfaces that are potentially relevant for ethylene epoxidation. For simplicity, it does not include surfaces that bind OH very strongly (since surfaces that bind O strongly are likely to oxidize) or inhomogeneous surfaces. Ag is well-known as a selective catalyst for ethylene epoxidation, and its selectivity can be increased by alkali promotion [7]. In its metallic state, Cu has been found to be even more selective than Ag for epoxidation of non-allylic olefins [323, 329–331]. As can be seen in Fig. 7.11, these trends are all present in the adsorption energy differences. Since these differences can be predicted from V_{ad} and f, the selectivity can potentially be tuned by tuning the electronic structure of the surface. To explain why $K_{ads}Ag$ is above the curve, we compared the K−OH and K−CH_3 interactions in vacuum at their adsorption distance (≈ 5 Å) and at a much larger distance (≈ 11 Å). K stabilizes OH through direct interactions by about 0.1 eV more than CH_3. This indicates that K may stabilize the O−M interaction more than the C−M interaction through both surface-mediated and direct interactions.

We also examined CuAg, PdAg, and AuAg alloy surfaces. If the C atom in the oxametallacycle binds to Ag and the O atom binds to the other metal, we find a predicted selectivity

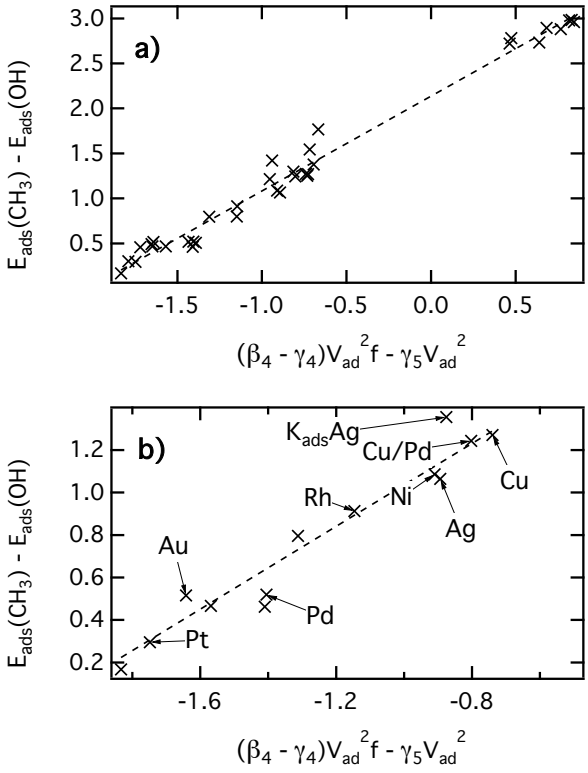

Figure 7.11: The difference between the CH_3 and OH adsorption energies as a function of $(\beta_4 - \gamma_4)V_{ad}^2 f - \gamma_5 V_{ad}^2$. a) All of the data points used in this work. The slope of the best fit line is 1.05. b) Late transition metals, with selected surfaces labelled. (The $K_{ads}Ag$ surface, which has 1/9 ML of K adsorbed on Ag(111), was not used in the rest of this work.)

trend of CuAg(1.73) > PdAg(1.37) > AuAg(1.16) > Ag(1.09), where the adsorption energy differences are given in eV. This agrees well with previous findings based on the oxametallacycle: CuAg > PdAg > Ag > AuAg, where AuAg and Ag were found to be very similar [317]. CuAg is more selective than Ag because the Cu stabilizes the O−M interaction significantly, while the C−M interaction is nearly unaffected. Therefore, our metric agrees with a number of known trends in experimental selectivities, and we now apply it to the design of a novel catalyst.

Figure 7.12 shows why Ag is the most selective monometallic catalyst: it adsorbs O strongly relative to C, but not so strongly that the surface completely oxidizes. In particular, it has a strong adsorption energy difference compared to other metals that adsorb OH with a similar strength. However, other metals, like Cu and Ti, should be more selective if they can be kept close to their

metallic form. By placing Cu in the surface of Ag particles, it can be kept from fully oxidizing, loosening the restriction that the surface must not adsorb O too strongly [319, 332]. This may also be the mechanism for the increased selectivity observed when Re is added to Ag [333]. Therefore, we propose that placing Ti in the surface of Ag particles may be highly selective, as Ti should be more selective than Cu, Ag, or Re if it can be kept fairly metallic.

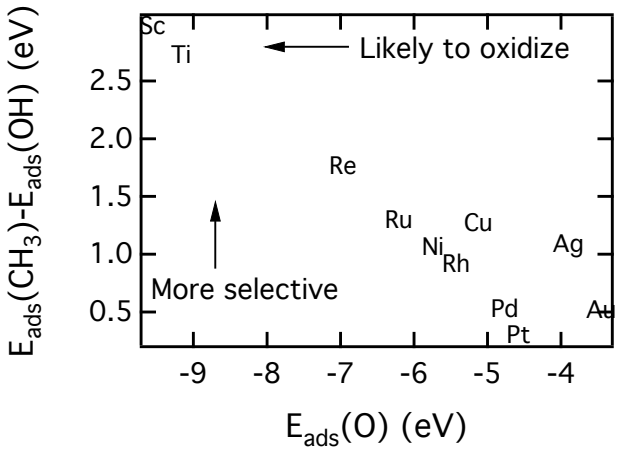

Figure 7.12: Adsorption energy difference for CH_3 and OH, a measure of selectivity, as a function of the adsorption energy of O, a measure of how likely the surface is to oxidize.

7.5.2 Reactor Studies

Ag powder with 0, 1, 5, and 8 cycles of TiO_2 deposited using ALD were tested for their selectivity in ethylene epoxidation, as described in the methods section. The selectivity of the AgTi catalysts as compared to Ag is shown in Fig. 7.13. It is clear that the addition of TiO_2 significantly increases the selectivity, and the effect is larger for increased amounts of TiO_2.

The effect of TiO_2 on the activity is much more subtle, but it appears that 1 cycle of TiO_2 decreases the rate, while larger amounts of TiO_2 increase the rate over pure Ag. This may indicate that the overall surface does not behave simply as a weighted average of Ag and TiO_2/Ag.

Further studies on Ag with more cycles of TiO_2 are needed to discern the optimal material, and further characterization of the material is necessary. As the amount of TiO_2 increases, the

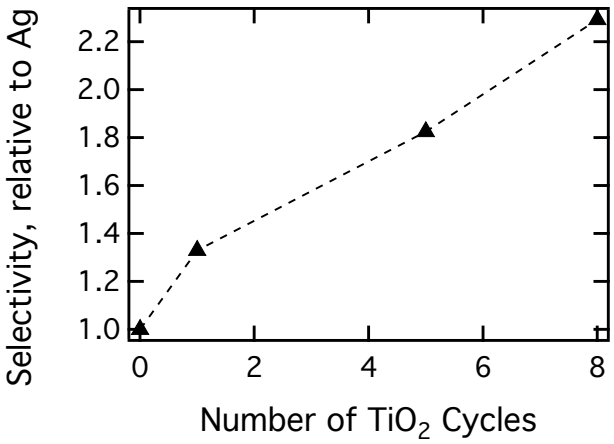

Figure 7.13: The selectivity of Ag catalysts coated with varying quantities of TiO_2 (deposited using ALD), relative to pure Ag.

material will likely behave more like bulk TiO_2 and its performance will decrease. Additionally, testing the effect of TiO_2 ALD on supported Ag nanoparticles would give a stronger indication of whether this concept may find practical application.

7.6 Conclusions

We have tested a large number of surface properties for their utility in predicting adsorption energies for hydrocarbons and oxygenates. Based on this work, we have developed simple, physically transparent, accurate expressions for predicting adsorption energies on a variety of transition metal surfaces. Using a single set of electronic structure parameters, the adsorption energies of CH_3, OH and other similar adsorbates in the top site as well as C, O, and H in the fcc hollow can be predicted. Energies for alkyls and alkoxides in other sites can then be determined using previously developed techniques. While the d-band center, d-band filling, and matrix coupling element are important predictors that are widely used in the literature, adding a dependence on the p-band center can significantly improve the accuracy of predictions. There are significant differences between hydrocarbon adsorption and oxygenate adsorption; in particular, the matrix coupling element is net attractive for hydrocarbons and net repulsive for oxygenates. These techniques were

used to design an AgTi catalyst with increased selectivity over pure Ag.

Chapter 8

A Unified Picture of Adsorption on Transition Metal Surfaces Through Different Atoms

8.1 Abstract

A key issue in catalyst design is understanding of how adsorption energies of surface intermediates vary across both different surfaces and various types of adsorbing atoms. In this work, we examine the trends in adsorption energies of a wide variety of adsorbates that attach to transition metal surfaces through different atoms (H, C, N, O, F, S, etc.). All adsorption energies, as calculated by density functional theory, have nearly identical dependence on the metal bands and the adsorbates' highest occupied molecular orbital (HOMO) energies. However, the dependence on the adsorbate-surface coupling and the d-band filling varies with the energy of the HOMO. Adsorbates with deep HOMOs experience a higher level of Pauli repulsion than those with higher HOMOs. Hence, adsorbates with similar HOMO energies (i.e., those that are nearby on the periodic table) have correlated adsorption energies, while those with very different HOMO energies do not. This leads to a classification of adsorbates into two groups, where adsorption energies in each group correlate.

8.2 Introduction

Adsorption is a critical process in many areas of research, particularly heterogeneous catalysis. As transition metals form an important class of catalysts, understanding and predicting adsorption energies on transition metal surfaces may have an impact on a variety of chemical and energy

applications. In fact, surface activity [29, 44, 73, 125] and selectivity [44, 73, 125, 318] can often be expressed in terms of a few simple adsorption energies.

Variations across adsorbates that bond through a particular type of atom can be understood based on gas-phase bond energies [83, 84, 111, 267] or using so-called scaling relations [35, 84]. For example, the adsorption energy of C-bound adsorbates can be predicted using the adsorption energy of C or CH_3 [35, 84]. Therefore, these relations provide a general framework for understanding adsorption through any single type of atom (e.g., carbon or oxygen). It is also important, however, to understand what drives differences in surface binding between these different types of atoms. Such differences are of crucial importance because many catalytic processes can be optimized by tailoring the adsorption of one type of atom relative to another. For example, to maximize activity and selectivity for synthesis gas conversion, the C and O adsorption energies must be tuned against one another [73]. Further, the selectivity for ethylene epoxidation depends on the relative affinity of the surface for adsorption through C and O atoms [318, 319, 334]. However, despite the importance of the differences between different atoms, in practice most theories of adsorption do not distinguish between different types of atoms, and the differences are poorly understood.

In this chapter, we provide a unified treatment of adsorption through a variety of atoms, allowing an elucidation of the chemistry underlying the adsorption process. To ensure the generality of our framework, we include most of the period 2 atoms (C, N, O, F) as well as H and S. Hence, the atoms we study will be involved in the vast majority of catalytic systems.

8.3 Methods

To develop and test our framework, adsorption energies and electronic structure parameters were calculated on 49 transition metal surfaces (from all groups except 5 and 6) using density functional theory (DFT). Because our goal is to identify descriptors that show the difference between different atoms, we initially performed calculations on hexagonal surfaces at low (1/9 monolayer) coverage. These calculations were performed with the Vienna ab-initio Simulation Package (VASP), [253, 254] the PW91 [256] exchange-correlation functional and the projector

augmented-wave method. [255, 303] A 7×7×1 k-point mesh was used, and the basis set was cutoff at 396 eV. A 3×3 surface cell and four metal layers were used, with the bottom two layers fixed at their bulk positions. Only calculations with Ni or Co employed spin polarization, and the default number of bands was employed in all cases except for K on Sc. Test calculations on other systems indicate that the default number of bands is usually sufficient. The density of states was calculated by performing a single-point calculation on the relaxed geometry to generate a charge density, which was then fixed and used in a non-self-consistent calculation with 19×19×1 k-points with 324 bands (the default for Cu, Ag, and Au). Adsorption energies are referenced to the adsorbates in the gas-phase and bare, relaxed slabs.

The d-band center is not uniquely defined, as an integration range must be specified. The d-band center was calculated by integrating up to 0.3 eV above the Fermi energy, as this was found to give the most accurate results. However, the conclusions of this work, and indeed the values of the d-band center, are insensitive to the integration range. The matrix coupling element was calculated relative to Cu using C−M distances from methyl adsorption calculations, d, in the formula $V_{ad}^2 \propto r_d^3/d^7$, where r_d is the size of the d orbitals. This has been described in previous chapters. Electronic structure parameters for hollow sites were calculated as averages of the values for the atoms surrounding the site. HOMO energies were calculated by performing a spin-polarized calculation of the adsorbate, and averaging the spin-up and spin-down electrons in each band. In previous work we have used gaps between the highest occupied and lowest unoccupied states in place of HOMO energies [334]. The gaps correlate well with the HOMO energies in all cases except for BH_2, perhaps because it has such a different number of valence electrons. Because of this difference, the HOMO energies are better predictors of correlation than the gaps.

The close-packed surfaces of the following metals were used, along with alloys of them, for a total of 49 surfaces and 78 unique top sites: Sc, Ti, Zr, Hf, Re, Ru, Os, Rh, Ir, Ni, Pd, Pt, Cu, Ag, Au. Not every adsorbate was calculated on every surface. For the work on all 12 adsorbates, a subset of 15 surfaces was used.

8.4 Correlations Between Different Adsorbates

To understand trends in adsorption through different types of atoms, we considered two simple classes of adsorbates: monovalent hydride species such as H, CH_3, NH_2, OH, SH, and F, as well as atoms including H, C, N, O, S, and F. (In the case of H and F, the monovalent hydrides are single atoms.) Both types of adsorbates are important in surface reactions of small molecules; conceptually, monovalent hydrides are formed by abstraction of a single hydrogen atom from a stable molecule, while the atoms are formed by complete dehydrogenation.

By investigating the extent to which the adsorption energies of these various species are correlated with each other, we found that adsorption through different atoms can be divided into two groups: C and H are in one group, while O, N, S, and F are in the other. When the monovalent hydrides are adsorbed in the top site (i.e., to a single surface atom), the adsorption energies within each group correlate, as shown in Fig. 8.1a. However, species from different groups generally do not correlate (see Fig. 8.2). The same is true for the atoms in the fcc hollow (i.e., adsorbed to three surface atoms), as shown in Fig. 8.1b. There is a generally higher level of correlation among all the atoms as compared to the hydrides, perhaps due to increased uniformity in orbital shape.

The correlations in Fig. 8.1 have immediate, practical value: by performing a DFT calculation of one atom from each group (e.g., C and O), the adsorption energies of all the other atoms can be quickly estimated. By subsequently applying scaling relations, this allows the prediction of the adsorption energy of nearly all adsorbates of practical interest. Further, these correlations suggest strategies and limitations for catalyst design. For example, NO oxidation rates depend on the N and O adsorption energies [99]. As a first approximation, only one of these adsorption energies is independent, which simplifies catalyst design but makes design of the optimal catalyst difficult to achieve on conventional surfaces.

Although adsorption energies correlate with bond energies to H when comparing bonding through a single type of atom [84, 111], this correlation does not hold when comparing across different types of atoms. Similar behavior has been seen in bonding to metal centers in

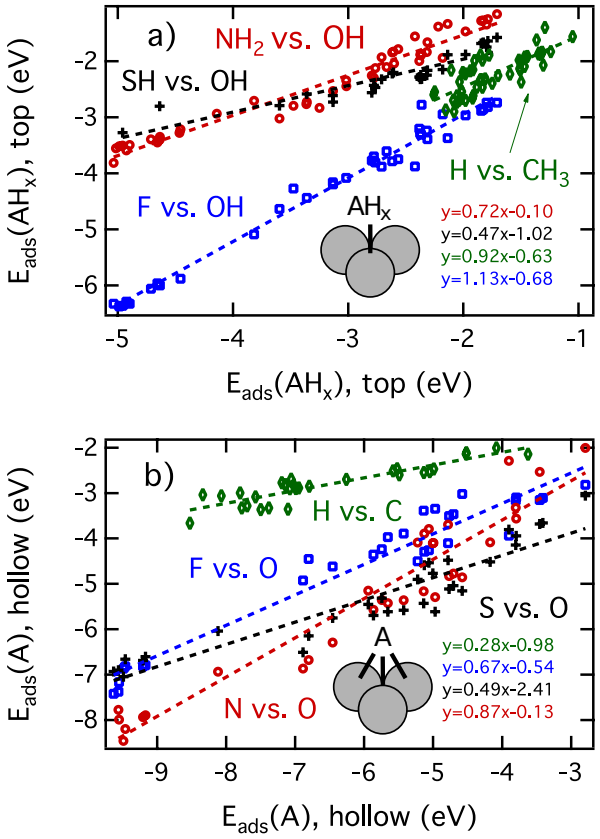

Figure 8.1: Correlations between the adsorption energies of a) OH, NH_2, SH and F in the top site; CH_3 and H in the top site; b) O, N, S, and F in the fcc hollow; C and H in the fcc hollow. Equations of fits are inset.

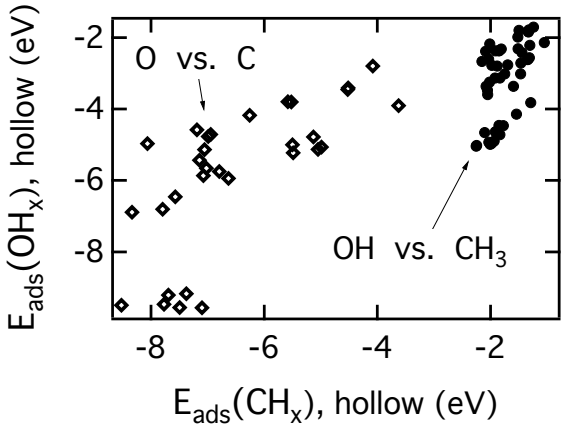

Figure 8.2: Relationship between adsorption energies of OH and CH_3, as well as O and C, demonstrating the lack of correlation between adsorbates from different groups.

organometallic complexes [335]. Nevertheless, gas-phase bond energies can give insight into adsorption energies even if the adsorbing atom changes: for the monovalent adsorbates, the slopes of the fits correlate with their gas-phase bond energies to H, such that a stronger bond leads to a steeper slope. In particular, the slopes of the NH_2, SH, F, and OH vs. OH fits linearly correlate with the NH_3, H_2S, HF, and H_2O bond energies ($R^2 = 0.98$); see Fig. 8.3. This implies that that adsorbates that bond more strongly are more sensitive to variations in the surface.

Figure 8.3 shows that adsorbates that bond to H more strongly are also more sensitive to variations in the surface; i.e., their adsorption energies change more, which leads to a higher slope in correlations.

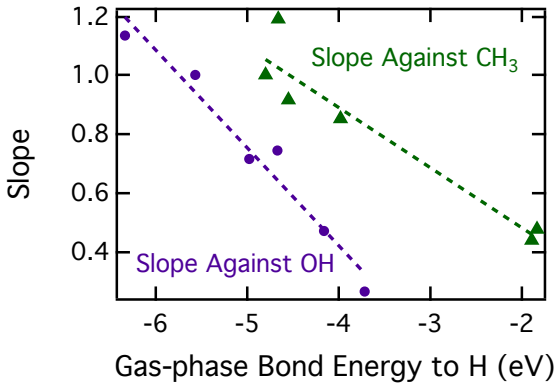

Figure 8.3: The slope of the correlation between OH and the adsorbates it correlates with (F, OH, NH_2, Cl, SH, and PH_2) and the slope of the correlation between CH_3 and the adsorbates it correlates with (CH_3, SiH_3, BH_2, H, Na, K) are given as a function of gas-phase bond energies to H.

8.5 CH_3, OH, H, SH, NH2, and F in the Top Site

We will now rationalize the grouping of the adsorbates based on electronic structure, in the framework of the d-band model [112]. We begin our analysis with the monovalent adsorbates in the top site, as this ensures that changes in adsorption energy are due to the properties of a particular surface atom. Upon adsorption, adsorbate states interact with the metal bands, splitting into bonding and antibonding states. The formation and occupation of these states has a large effect

on the adsorption energy. The hybridization and orthogonalization (Pauli repulsion) of adsorbate and metal states also play a significant role. The metal band centers and the surface-adsorbate coupling are often used to predict these effects [83, 84, 177, 181, 183, 193, 269, 334]. Based on this previous work, we predict the adsorption energy as

$$E_{\text{ads}} = E_{\text{elec}} + a_1 V_{ad}^2 f + a_2 V_{ad}^2 \tag{8.1}$$

where V_{ad} is the matrix coupling element between the adsorbate states and the metal d states, and f is the d-band filling. E_{elec} accounts for changes in the metal bands and the adsorbate's highest occupied molecular orbital (HOMO):

$$E_{\text{elec}} = b_1 \epsilon_a + b_2 \epsilon_d + b_3 n_p \tag{8.2}$$

where ϵ_a is the energy of the HOMO, ϵ_d is the d-band center (the average energy of the metal d states relative to the Fermi energy), and n_p is the number of p electrons, determined by integration over the occupied states. (The p-band center ϵ_p can be used in place of n_p, but n_p strongly (and inversely) correlates with ϵ_p and is more uniquely defined.)

However, the full formulation of d-band theory, as derived from the Newns-Anderson model, involves an integral over all states and puts no particular emphasis on the band center [176]. The reason for the accuracy of using the band center is likely as follows. Any metal atom in its monometallic surface will have roughly the same overlap with its neighboring atoms, since the lattice constant roughly scales with the size of the atom's orbitals. Further, its neighbors' bands will be at a very similar energy to its own bands. This leads to roughly the same shape for bands for all monometallic surfaces, with only its position changing significantly. The same is true for alloys where all the metal atoms are fairly similar. When the band shape is roughly the same, the d-band center gives a good approximation for the changes in the contributions from the d-band, and the number of p electrons can account for changes in the contributions from the p (and possibly s) band [334].

However, for alloys with dissimilar metal atoms, the band shape can be dramatically different. While most alloys in the literature contain similar components, some dissimilar alloys, such as MoPt

or PtTi, may have important catalytic applications. In these cases, we find that more terms than just the d-band center are often necessary. For example, Fig. 8.4 shows the density of states (DOS) for the Ti atoms in Ti and a TiPd alloy. Just considering the band centers (Eqs. (8.1) and (8.2), fit to the whole set of data), the error in predicting CH_3's adsorption energy is 0.16 eV for Ti and 0.40 eV for TiPd. The error for Ti is acceptable, but the error for TiPd is rather large. By considering the shape of the d band, these errors become 0.15 eV and 0.20 eV. Specifically, we add two terms to account for the band shape. The first is the d-band's second moment, or variance (v_d), as a wider band leads to stronger adsorption. This is likely because a wider band will have more states near ϵ_a that will interact strongly with the adsorbate. The second term accounts for sharp peaks at the top or bottom of the band, as in Fig. 8.4b. Sharp peaks at the top of the band result in unoccupied bonding states, significantly weakening adsorption. This behavior can be captured by multiplying the skewness, s_d, by the kurtosis, k_d, which is a standard statistical measure of peakedness. Thus, in the general case,

$$E_{\text{elec}} = c_1\epsilon_a + c_2\epsilon_d + c_3 n_p + c_4 v_d + c_5 s_d k_d. \tag{8.3}$$

Importantly, all of the adsorbates have approximately the same dependence on the metal bands and on ϵ_a, no matter which form of E_{elec} is used, and we therefore constrain the fitting parameters in E_{elec} to be the same in all cases (see Table 8.1). Hence, variations in E_{elec} across different surfaces will be the same for all adsorbates. For simplicity, we use Eq. (8.2) in the rest of this chapter.

Table 8.1: Adsorbate-specific fitting parameters and HOMO energies (in eV)

	H	CH_3	NH_2	SH	OH	F
a_1	-0.48	-0.10	0.60	0.34	1.03	1.21
a_2	0	0	$-0.67a_1$	$-0.67a_1$	$-0.67a_1$	$-0.67a_1$
ϵ_a	-3.81	-4.19	-6.05	-6.21	-7.39	-10.49

Therefore, the V_{ad} terms determine to which group the adsorbates belong. For C and H, a_1 is negative and a_2 is approximately zero, leading to a net stabilization when V_{ad}^2 is increased. For O, N, S, and F, a_1 is positive and the relationship $a_2 = -0.67a_1$ fits the data well. This leads to a net destabilization when V_{ad}^2 is increased for surfaces with mostly full d bands, but a stabilization

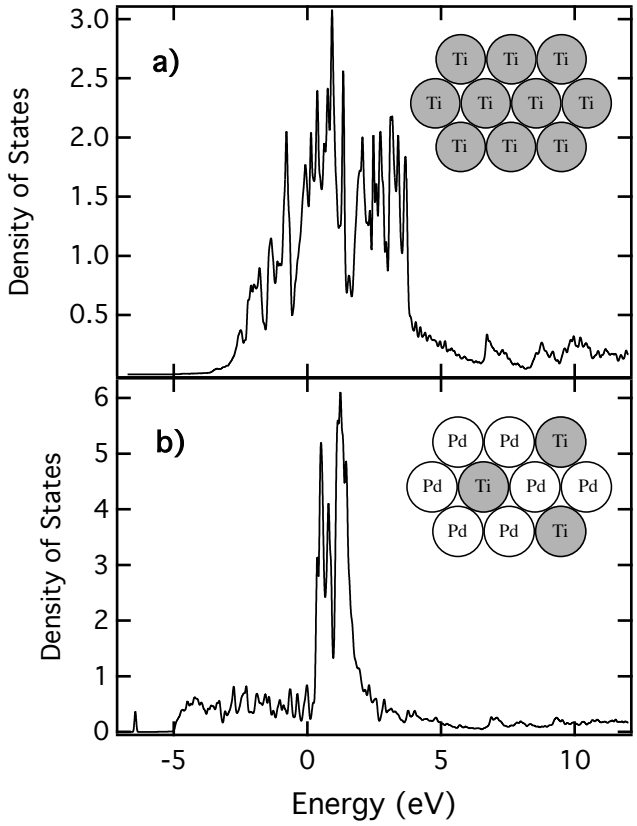

Figure 8.4: DOS plots for Ti atoms in a)Ti(0001), b) 1/3 ML of Ti in Pd(111) (structures inset).

for surfaces with fairly empty—and hence more reactive—d bands. This difference is due to the energies of the adsorbate electronic states [112]: CH_3 and H have much higher ϵ_a values than OH, NH_2, SH, and F, as shown in Table 8.1. Increasing V_{ad}^2 increases both the covalent interaction and the Pauli repulsion [177]. Since it is easy for higher-energy adsorbate states in CH_2 and H to induce splitting, greater coupling to the d band leads to stronger adsorption. For the deeper states of the other adsorbates, there are two regimes: on surfaces with mostly full d bands, the Pauli repulsion dominates and greater coupling leads to weaker adsorption, while on surfaces with fairly empty d bands, the covalent interaction dominates and greater coupling leads to stronger adsorption. (Even if the adsorbate-d interactions become unfavorable, the adsorbate-sp interactions will be favorable and adsorption will still be exothermic for radical species [112].)

Equations (8.1) and (8.2), along with the relations among the fitting parameters given above,

give accurate results for most surfaces, with a mean absolute error (MAE) of 0.20 eV (see Fig. 8.5). This analysis also allows predictions of differences in adsorption energy between adsorbates from the two groups based on the V_{ad} terms, as shown in Fig. 8.6.

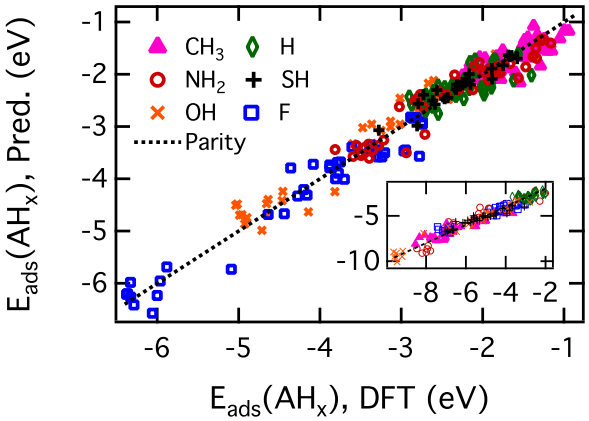

Figure 8.5: Parity plot for using Eqs. (8.1) and (8.2) to predict adsorption energies of the monovalent adsorbates as compared to the values from DFT. A single set of fitting parameters was used in Eq. (8.2), and parameters for Eq. (8.1) are in Table 8.1. Inset: Parity plot of using scaled values of the fitting parameters to predict atomic adsorption energies.

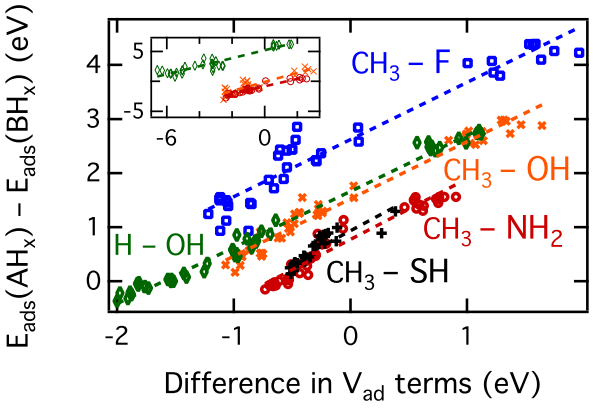

Figure 8.6: Adsorption energy differences for the monovalent adsorbates in the top site as a function of the differences in the V_{ad} terms in Eq. (8.1), e.g. $E_{\text{ads}}(\text{CH}_3) - E_{\text{ads}}(\text{OH})$ as a function of $[a_1(\text{CH}_3) - a_1(\text{OH})]V_{ad}^2 f - a_2(\text{OH})V_{ad}^2$. Inset: Adsorption energy differences for the atoms in the fcc hollow as a function of the scaled V_{ad} terms, e.g. $E_{\text{ads}}(\text{C}) - E_{\text{ads}}(\text{O})$ as a function of $[4a_1(\text{CH}_3) - 2a_1(\text{OH})]V_{ad}^2 f - 2a_2(\text{OH})V_{ad}^2$. Values for $a_i(\text{AH}_x)$ are in Table 8.1.

8.6 C, O, H, S, N, and F in the FCC Hollow

We now apply Eqs. (8.1) and (8.2) to the atomic species in the fcc hollow, in order to demonstrate that the trends that hold for the hydrides also hold for the atoms. Rather than refitting the parameters, we employ previously developed scaling relations [35], which imply that the adsorption energies of the monovalent adsorbates can be scaled by the number of dangling bonds in the atom:

$$E_{\mathrm{ads}}(\mathrm{A}) = \gamma E_{\mathrm{ads}}(\mathrm{AH_x}) + \xi, \tag{8.4}$$

where γ is the valency of A (4 for C, 3 for N, 2 for O and S, 1 for F and H). This approach has been explicitly validated for C, N, O and S [35]. Using Eq. (8.4), the parameters in Eqs. (8.1) and (8.2) can be scaled to derive expressions for atomic adsorption energies, fitting the single parameter ξ for each atom. For example, since C has the ability to form 4 single bonds while CH_3 can only form 1, all of CH_3's parameters can be multiplied by 4 to give estimates for C. This will be simpler, though less accurate, than refitting the parameters to the atomic adsorption energies. This gives reasonable accuracy (MAE of 0.4 eV; see the inset of Fig. 8.5), and the inset of Fig. 8.6 shows that this scheme allows the prediction of the differences in the atomic adsorption energies with no additional fitting. Hence, the V_{ad} terms display the same qualitative behavior for the atoms as for the monovalent hydrides: C and H are always stabilized by increased coupling, while the other atoms' behavior depends on the filling of the d band. This is likely because the HOMO energies of the atomic species are not dramatically different from those of the hydrides.

While we used Eq. (8.4) to derive these expressions, it may be more appropriate to consider the accuracy of these expressions as a partial explanation for scaling relations. In other words, these results suggest that a similarity in adsorbate HOMO energies is necessary in order for a scaling relation to hold, as is the case for these atoms and their hydrides, since a large change in HOMO energy would result in different adsorption behavior.

8.7 Relationship Between Electronic Structure and Correlations

Equation (8.1) does not rigorously demonstrate that there will be a linear relationship among the adsorption energies for the adsorbates in a particular group. However, adsorbates that have a similar dependence on surface properties should have correlated adsorption energies [80]. Further, the nature of the transition between the two groups of adsorbates is unclear as of yet—i.e., how do adsorbates with moderate HOMO energies behave? To explore these subjects, the adsorption energies of K, Na, BH_2, SiH_3, PH_2, F, and Cl were calculated in the top sites of 15 surfaces. These calculations confirm that Eqs. (8.1) and (8.2) can predict adsorption energies for a variety of adsorbates with a single set of fitting parameters in Eq. (8.2) (MAE of 0.17 eV; see Fig. S2 for the parity plot). They also confirm that adsorbates with a high HOMO energy are stabilized by an increase in V_{ad}^2, while those with a low HOMO energy are destabilized on late transition metals but stabilized on early transition metals. In particular, adsorbates with high HOMO energies are modeled well by a negative a_1 value and an a_2 value of 0, while adsorbates with low HOMO energies are accurately modeled by a positive a_1 value and an a_2 value of $-0.67a_1$, which is the same behavior as that seen in Table 8.1. Interestingly, PH_2, which has an intermediate HOMO energy, has almost 0 (slightly positive) dependence on V_{ad}, indicating that it is near the transition between the adsorbate groups.

Since the value of a_1 determines an adsorbate's behavior, the difference in a_1 is a good predictor of whether two adsorbates will correlate. Further, ϵ_a correlates with a_1, while being much easier to calculate and conceptualize. This implies that adsorbates with similar HOMO energies should correlate, while those with very different HOMO energies should not correlate. As shown in Fig. 8.7, this is indeed the case. (The adsorbate electronegativity correlates with the HOMO, and hence it can also be used to predict whether adsorption energies will correlate, as suggested previously in studies of organometallics [335].) Additionally, Fig. 8.7 shows that the adsorbates basically form two groups, and the cutoff lies between CH_3 and PH_2, which is exactly where a_1 goes from negative to positive. Therefore, we conclude that adsorbates with similar a_1 (or ϵ_a) values are

likely to correlate, and they are even more likely to correlate if a_1 has the same sign for both.

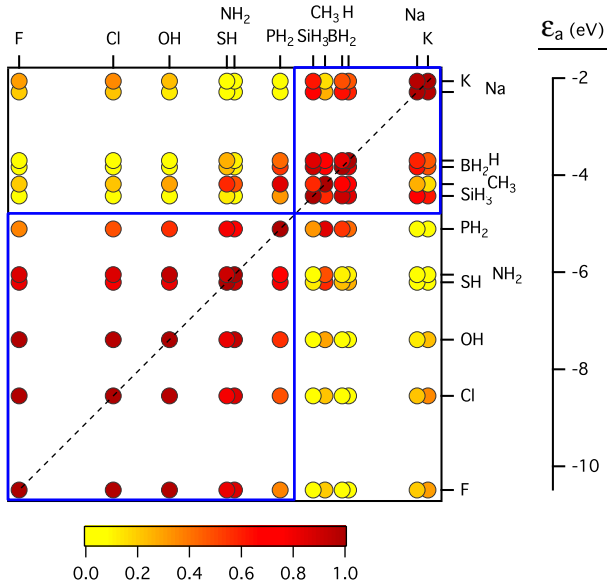

Figure 8.7: R^2 values for linear correlations between various adsorbates, arranged by their HOMO energies. The upper box contains adsorbates with $a_1 < 0$, while the lower box contains adsorbates with $a_1 > 0$. H's ϵ_a value has been increased slightly for display purposes only.

Figure 8.8 shows the R^2 values for correlations between different atoms. A different scale is used than in the main text so that differences are more visible. In general, atomic species correlate more strongly than monovalent hydrides.

8.8 Other Sites and Surfaces

Thus far, this paper only gives methods that apply to particular adsorption sites (namely top and fcc hollow sites) on close-packed surfaces, and we now briefly discuss other sites and surfaces. We focus on the bridge site for atoms, as it is important in diffusion [336], and the hollow site for the monovalent adsorbates, as it is often the preferred site. (The exception is NH_2, where we instead use the bridge site as the hollow site is often unstable.) The same correlations as in Fig. 8.1 apply within and across these sites as well. For example, O in the fcc hollow can predict S, F, and N in the bridge sites (see Fig. 8.9a). This is likely because the hollow and bridge sites for

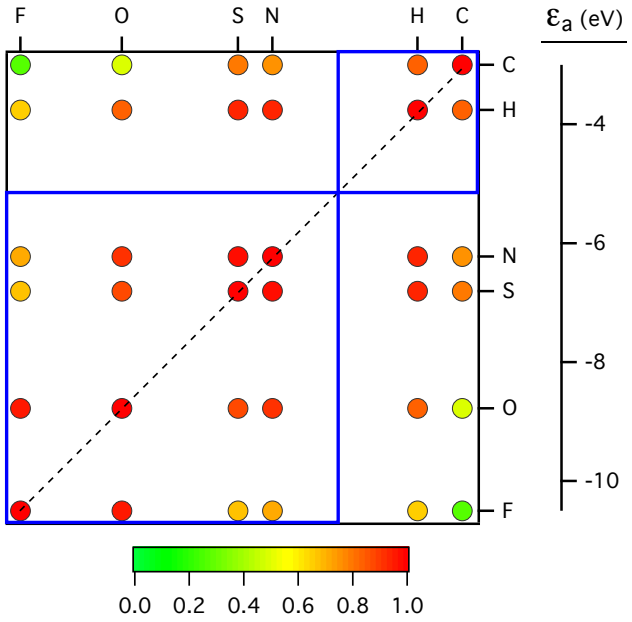

Figure 8.8: a) R^2 values for linear correlations between various atomic species.

a particular atom correlate [337], as predicted by bond-order conservation [49]. The same holds true for the monovalent adsorbates in the top and hollow sites, although the scatter is increased somewhat (see Fig. 8.9b).

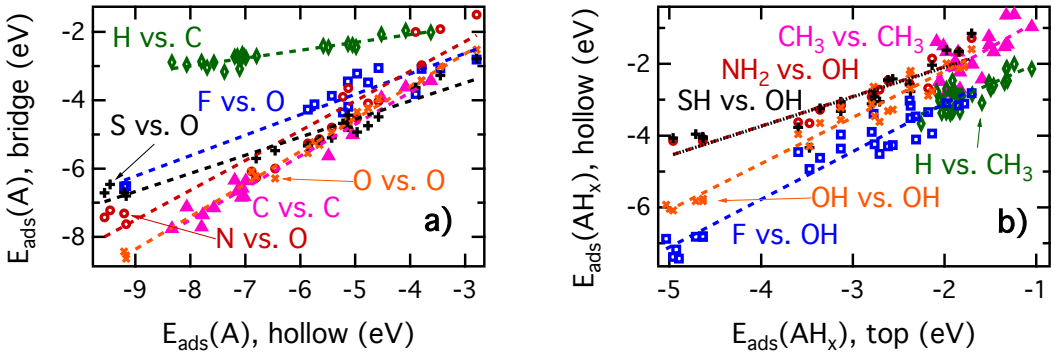

Figure 8.9: a) Atomic adsorption energies in the bridge site as a function of their adsorption energies in the fcc hollow. b) Adsorption energies of monovalent hydrides in the fcc hollow as a function of their adsorption energies in the top site.

The same correlations also appear to hold for monovalent adsorbates in the top sites of

stepped surfaces. For example, OH and NH_2 have correlated adsorption energies, but OH and CH_3 do not. In fact, the correlations fall on the same lines as those for the close-packed surfaces, as shown in Fig. 8.10. Therefore, our conclusions appear to be independent of the specific site and surface.

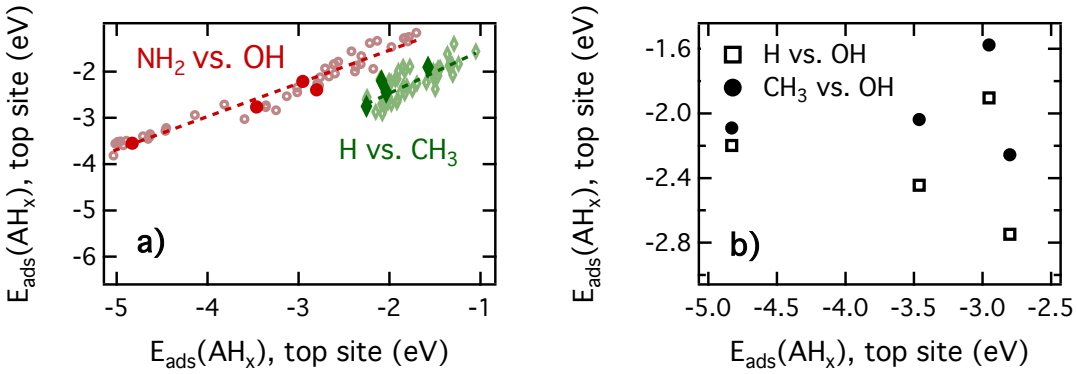

Figure 8.10: a) Adsorption energy correlations on close-packed and stepped surfaces. The faded data points and fits are the same as in Fig. 1, while the darker data points are from stepped surfaces. b) The relationship between OH's adsorption energy and that of H and CH_3 on stepped surfaces. For fcc metals, steps were modeled using the (211) surface, while for hcp metals steps were modeled by removing a row of surface atoms. The adsorbates were placed in the top site at the top of the step.

Using these correlations does not give reliable results for which site a particular adsorbate will prefer on a particular surface, as these energy differences are often relatively small. However, these small differences may be important in some cases. In previous chapters, we developed expressions for predicting adsorption energy changes upon translation between sites:

$$\Delta E_{\text{trans}} = c_1 + c_2 V_{\text{ad}}^2 f + c_3 \epsilon_p(\text{occ}) + c_4 V_{\text{dd}}^2. \tag{8.5}$$

The V_{ad} term approximates the change in coupling, the ϵ_p term accounts for the change in electron-electron repulsion, and the V_{dd} term accounts for how far the d orbitals extend into the bridge and hollow sites. This equation must be fit separately for each adsorbate, but it results in reasonably accurate predictions for both the hollow-to-bridge (for atoms) and top-to-hollow (for monovalent adsorbates) translations, with MAEs of 0.07 eV and 0.12 eV, respectively (the parity plots are

in Fig. 8.11). For CH_3, agostic interactions were accounted for by adding terms proportional to the d-band filling and the lattice constant, based on the work in previous chapters. These terms significantly improve predictions for CH_3 but have little effect on the accuracy for other adsorbates.

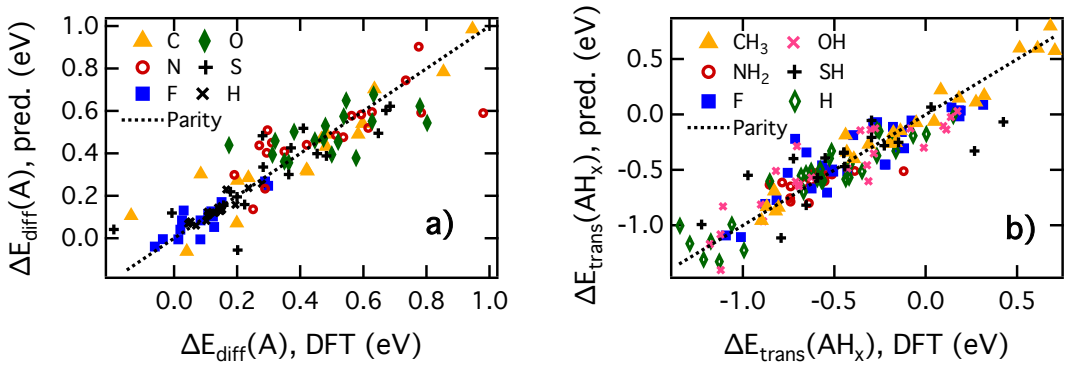

Figure 8.11: Parity plots for using Eq. (8.5) to predict a) diffusion barriers for atoms (the difference between the bridge and fcc hollow adsorption energies) and b) the change in energy upon translating the monovalent adsorbates from the top site to an fcc hollow.

8.9 Predictions from Alloy Structure

Further unification in our understanding of adsorption can be achieved by elucidating the relationship between the surface's electronic structure parameters (ϵ_d, n_p, V_{ad}, and f) and its alloy structure. As a first approximation, V_{ad} and f can be assumed to be constant for a particular transition metal. Previous work has shown that, on late transition metals, the width of the d-band about the Fermi level $W_d(\epsilon_f)$ can be predicted from V_{dd}, the coupling of the metal d-orbitals to each other, which can in turn be predicted based on the geometric properties of a surface alloy [308, 338]. The d-band center is correlated with this width.

However, as implied by molecular orbital theory or tight-binding, V_{dd} actually correlates with the total band width W_d, not with $W_d(\epsilon_f)$. For late transition metals, $W_d(\epsilon_f)$ and W_d correlate, but this is not true in general. Therefore, we have developed a similar but more general scheme to predict the d-band center.

First, V_{dd} for a particular atom i is predicted as

$$V_{dd} = \sum_j \frac{(r_{di} r_{dj})^{3/2}}{d_{ij}^5}, \tag{8.6}$$

where r_d is the size of the d-orbitals (which is constant for a particular element), d_{ij} is the distance between atoms i and j, and the sum is taken over all the nearest neighbors of atom i. W_d is calculated as $V_{dd} + c$, where the constant c and the values of r_d are calculated by fitting to our DFT data of W_d for atoms in various surfaces. The values of d are calculated using simple geometry, based on the lattice constant of the system. The lattice constant can be estimated using a weighted average of the pure metals' lattice constants.

To calculate ϵ_d from W_d, equations derived from the rectangular band model are employed. These derivations assume that the d-band filling is constant. For atoms with a full d-band, a simple linear relationship between W_d and ϵ_d is assumed.

We assumed that the coupling between the p states and the d states V_{pd} determines n_p. This can be calculated as

$$V_{pd} = \sum_j \frac{(r_i r_j)^{3/2}}{d_{ij}^{7/2}}, \tag{8.7}$$

and this quantity was assumed to correlate with n_p, since the p band does not change its shape or filling dramatically.

As shown in Fig. 8.12, these schemes give reasonable results (MAE of 0.25 eV for ϵ_d, MAE of 0.02 electrons for n_p, and MAE of 0.04 eV for predictions of adsorption energies of CH_3 in the top site). They allow extremely fast screening of surfaces for their adsorption properties, as demonstrated in previous work [338]. They also allow an understanding of how alloy structure affects adsorption energies. For example, increasing V_{dd} will result in a wider d band. The effect of an increased width on ϵ_d depends on the filling of the d-band, as noted previously [174]. For late transition metals, a wider band will generally lead to a lower center, but for early transition metals a wider band may lead to a higher center.

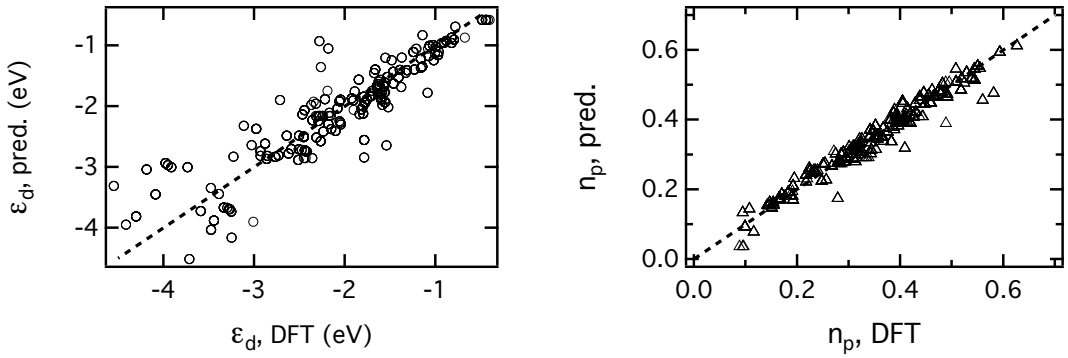

Figure 8.12: Parity plots for predicting a) the d-band center and b) the number of p electrons from the alloy structure of a surface.

8.10 Conclusions

In summary, the adsorption energies of adsorbates that bind to metal surfaces through O, N, S, and F atoms are linearly correlated, and the same is true for C and H. This applies to both the atomic species and their monovalent hydrides. This grouping can be rationalized by considering how adsorption energies depend on electronic structure. The monovalent adsorbates all have the same dependence on the HOMO energies and the metal bands, but their dependence on V_{ad} and f varies. Increased coupling stabilizes adsorbates with high HOMO energies, such as CH_3 and H. However, adsorbates with low HOMO energies, such as OH, NH_2, SH, and F are stabilized by increased coupling on early transition metals but destabilized on late transition metals. Based on our studies of more adsorbates, we have found that in general (1) adsorption energies correlate if the adsorbates have the same type of dependence on the coupling (i.e., always stabilizing vs. sometimes destabilizing), and (2) adsorbates within and across groups correlate if their HOMO energies are similar. Using V_{ad} and f, adsorption energies in one group can be predicted using an adsorption energy from the other group, allowing adsorption energies for all of the adsorbates to be estimated from a single calculation. By elucidating how the electronic structure parameters depend on alloy structure, high-throughput screening and rational design of catalysts can be performed.

Chapter 9

Conclusions and Future Work

9.1 Conclusions

Much of this thesis consists of taking previously developed models and improving their accuracy and/or applicability, as well as combining them. For example, the accuracy and applicability of both the d-band model and scaling relations have been improved, and the relationship between them has been clarified. The work presented here results in the following picture of radical adsorption on transition metals.

A radical adsorbate can be approximated as a set of radical orbitals. Both the geometry and energy of these orbitals are important, but in a fixed geometry only the energy of the orbitals matters. Their energies determine the strength of the repulsion between the surface and the adsorbate, but do not affect how the adsorption energies depend on the metal bands. A surface can be approximated as a p band (the number of p electrons suffices to characterize it) and a d band (its average energy and filling are most important, but the shape of the band can also affect the adsorption energy) which interacts with the adsorbate with a strength determined by V_{ad} and f. Both hybridization and orthogonalization effects can be accounted for using these factors.

Because orbital energies do not change dramatically for different radicals that adsorb through the same atom, these radicals will share certain similarities in their behavior. Most critically, this results in scaling relations among these radicals. However, since the geometry of the orbitals can change between these radicals, scaling relations may require consideration of the adsorption site to maintain their validity. Adsorption energies of radicals that bond through different atoms will also

correlate if their radical orbitals have similar energies.

Some aspects of adsorption on surfaces can be understood by thinking about bonding in the gas phase, although the differences between surface systems and the gas phase can sometimes be important. For example, a molecule's radical orbitals and unsaturation can give significant insight into gas-phase bonding (e.g., the maximum number of H atoms the radical will bond to and the geometry of the saturated molecule) as well as adsorption (e.g., the geometry in a certain site, and the part of the surface the molecule is interacting with when it is in a particular geometry). As a more concrete example, when CH_3 adsorbs it mostly interacts with whatever is directly below it, because of the shape of its radical orbital. This determines which site it will prefer on a particular surface. Further, the differences in adsorption energies for similar radicals often closely tracks the difference in their bond energies to H.

Many previous models of adsorption do not account for the adsorption site. While this may work in some cases, our work shows that this often causes these models to fail when applied to a wide variety of surfaces. This applies to both predictions from electronic structure and to scaling relations. The importance of accounting for the site is sensible: different sites are different chemical environments, and may affect adsorbates differently.

9.2 Extensions to the Models

While the models developed here present generalizations to previous work, further generalization is likely possible. Given the huge variety of surfaces found in technology and nature and the importance of adsorption on many of these surfaces, these generalizations may prove useful.

The most important and obvious generalization is to include other types of surfaces. Including different facets of transition metals (including open surfaces, steps, kinks, and defects) would likely improve the applicability of this work to real catalysts. Similarly, applying these methods to adsorption on nanoparticles may improve their utility. While the close-packed surfaces that are the focus of this thesis are important in many cases, and trends across metals often hold on any facet, occasionally the effect of the facet is critical. In this work, a few other facets are briefly studied,

and it seems likely that most of our models can be readily extended to these other types of surfaces.

A more difficult generalization would be to include materials other than transition metals, such as simple metals or metal compounds like oxides. These types of surfaces are also used in many technological processes, and their popularity in the computational literature has been steadily increasing. While we have not performed any calculations on these surfaces, the validity of scaling relations on them indicates that some of the concepts we have developed may apply to them. These surfaces consist of more localized electrons, and the "dangling bond" concept is more applicable to them. Hence, adsorption on these surfaces may share even more similarities to gas-phase bonding.

Including more adsorbates in the framework would also increase the applicability of our models. Most important are adsorbates that bond to the surface through more than one atom. As a first approximation, contributions from each adsorbing atom can be added separately, but this may not be sufficiently accurate for some applications. Less importantly, our work focuses on adsorbates that form covalent bonds with the surface, and mostly ignores steric repulsion and van der Waals interactions between the adsorbate and surface. These interactions will likely require a different approach than that given here. A group additivity scheme may be the most effective.

Little of the work presented here is performed at high coverage. It is possible that surface-mediated interactions can be accounted for by studying the effect of adsorbates on the surface's electronic properties. However, direct adsorbate-adsorbate interactions will likely need to be accounted for in a different way. The simplest method may be to fit a pair-potential curve for adsorbates in the gas phase.

9.3 Applications

Due to the general and fundamental nature of some of the work in this thesis, it is potentially applicable to many technologies.

The easiest applications will be those where surface reactivity has already been connected to adsorption energies, and there are known to be transition metals that have properties near the optimal catalyst. In these cases, the models from this work can be applied for rational design

or high-throughput screening in a search for catalysts with lower cost, higher performance, etc. Further, the "optimal" catalyst identified in previous studies may actually be the optimal catalyst that obeys simple scaling relations, and the methods developed here may allow the design of a catalyst that has better performance than what was previously described as optimal.

More challenging applications include those where the reaction is known to correlate with adsorption energies, but the optimal catalyst is unachievable on surfaces that obey simple scaling relations. Because the models developed here account for more subtleties—for example, how alloys affect different adsorbates and different sites in different ways—they may be useful for identifying surfaces that break conventional scaling relations in desirable ways.

Even more challenging are applications where the reaction is not well understood on a mechanistic level. Our models may provide insight into mechanisms, as reaction networks can be quickly generated. However, experimental work or detailed DFT studies may be required to gain a firm understanding.

Implicit in the above is the idea that coupling our models with kinetic approaches to predict catalytic performance may be necessary in some cases, instead of relying on previously developed correlations or qualitative metrics. Combining our models with BEP relations and simple mean-field microkinetic models would require only a trivial increase in computational expense. However, applying a more accurate Monte Carlo scheme would require significantly more resources for each surface tested.

Our models may find applications in fields other than catalysis, such as graphene deposition and surface functionalization. Because of the difficulty of synthesizing high-quality graphene, designing a surface for graphene synthesis is a particularly promising application.

Bibliography

[1] U. S. Climate Change Technology Program – Technology Options for the Near and Long Term; 2006; p 1.4.7.

[2] Smil, V. Nature **1999**, 400, 415.

[3] Stephens, I. E. L.; Bondarenko, A. S.; Grønbjerg, U.; Rossmeisl, J.; Chorkendorff, I. Energy Env. Sci. **2012**, 5, 6744–6762.

[4] Gattrell, M.; Gupta, N.; Co, A. J. Electroanal. Chem. **2006**, 594, 1–19.

[5] Henrici-Olivé, G.; Olivé, S. Angew. Chem. Int. Ed. **1976**, 15, 136–141.

[6] van der Laan, G. P.; Beenackers, A. A. C. M. Catal. Rev.-Sci. Eng. **1999**, 41, 255–318.

[7] Serafin, J.; Liu, A.; Seyedmonir, S. J. Mol. Catal. A: Chem. **1998**, 131, 157–168.

[8] Davis, J.; Barteau, M. Surf. Sci. **1987**, 187, 387–406.

[9] Williams, R.; Pang, S.; Medlin, J. Surf. Sci. **2014**, 619, 114–118.

[10] Su, X.; Shen, Y.; Somorjai, G. A. J. Am. Chem. Soc. **1996**,

[11] Wang, H.; Krier, J. M.; Zhu, Z.; Melaet, G.; Wang, Y.; Kennedy, G.; Alayoglu, S.; An, K.; Somorjai, G. A. ACS Catal. **2013**, 3, 2371–2375.

[12] Robinson, A. M.; Montemore, M. M.; Tenney, S. A.; Sutter, P.; Medlin, J. W. J. Phys. Chem. C **2013**, 117, 26716–26724.

[13] Nørskov, J. K.; Abild-Pedersen, F.; Studt, F.; Bligaard, T. Proc. Natl. Acad. Sci. USA **2011**, 108, 937–943.

[14] Pang, S. H.; Schoenbaum, C.; Schwartz, D. K.; Medlin, J. W. Nat. Comm. **2013**, 4, 2448.

[15] Potyrailo, R.; Rajan, K.; Stoewe, K.; Takeuchi, I.; Chisholm, B.; Lam, H. ACS Comb. Sci. **2011**, 13, 579–633.

[16] Priyadarshini, D.; Kondratyuk, P.; Picard, Y. N.; Morreale, B. D.; Gellman, A. J.; Miller, J. B. J. Phys. Chem. C **2011**, 115, 10155–10163.

[17] Duzenli, D.; Seker, E.; Senkan, S.; Onal, I. Catal. Lett. **2012**, 142, 1234–1243.

[18] Senkan, S. M. Nature **1998**, 394, 350.

[19] Salciccioli, M.; Stamatakis, M.; Caratzoulas, S.; Vlachos, D. G. Chem. Eng. Sci. **2011**, 66, 4319–4355.

[20] Sabatier, P. Ber. Dtsch. Chem. Ges. **1911**, 44, 1984–2001.

[21] Ferguson, G.; Mehmood, F.; Rankin, R.; Greeley, J. P.; Vajda, S.; Curtiss, L. A. Top. Catal. **2012**, 55, 353–365.

[22] Okamoto, Y.; Sugino, O. J. Phys. Chem. C **2010**, 114, 4473–4478.

[23] Cheng, J.; Hu, P. J. Am. Chem. Soc. **2008**, 130, 10868–10869.

[24] Cheng, J.; Hu, P.; Ellis, P.; French, S.; Kelly, G.; Lok, C. M. J. Phys. Chem. **2008**, 112, 1308–1311.

[25] Nørskov, J. K.; Bligaard, T.; Logadottir, A.; Bahn, S.; Hansen, L.; Bollinger, M.; Bengaard, H.; Hammer, B.; Sljivancanin, Z.; Mavrikakis, M.; Xu, Y.; Dahl, S.; Jacobsen, C. J. Catal. **2002**, 209, 275–278.

[26] Damjanovic, A.; Brusic, V. Electrochim. Acta **1967**, 12, 1171–1184.

[27] Rankin, R. B.; Greeley, J. ACS Catal. **2012**, 2, 2664–2672.

[28] Hansgen, D.; Vlachos, D. G.; Chen, J. G. Nat. Chem. **2010**, 2, 484–489.

[29] Bligaard, T.; Nørskov, J. K.; Dahl, S.; Matthiesen, J.; Christensen, C. H.; Sehested, J. J. Catal. **2004**, 224, 206–217.

[30] Stamenkovic, V.; Mun, B.; Arenz, M.; Mayrhofer, K.; Lucas, C.; Wang, G.; Ross, P.; Markovic, N. Nat. Mat. **2007**, 6, 241–247.

[31] Wang, S.; Temel, B.; Shen, J.; Jones, G.; Grabow, L.; Studt, F.; Bligaard, T.; Abild-Pedersen, F.; Christensen, C.; Nørskov, J. K. Catal. Lett. **2011**, 141, 370–373.

[32] Hofmann, T.; Yu, T. H.; Folse, M.; Weinhardt, L.; Bär, M.; Zhang, Y.; Merinov, B. V.; Myers, D. J.; Goddard III, W. A.; Heske, C. J. Phys. Chem. **2012**, 116, 24016–24026.

[33] Cheng, J.; Hu, P. Angew. Chem. **2011**, 123, 7792–7796.

[34] Jones, G.; Jakobsen, J. G.; Shim, S. S.; Kleis, J.; Andersson, M. P.; Rossmeisl, J.; Abild-Pedersen, F.; Bligaard, T.; Helveg, S.; Hinnemann, B.; Rostrup-Nielsen, J. R.; Chorkendorff, I.; Sehested, J.; Nørskov, J. K. J. Catal. **2008**, 259, 147–160.

[35] Abild-Pedersen, F.; Greeley, J.; Studt, F.; Rossmeisl, J.; Munter, T. R.; Moses, P. G.; Skúlason, E.; Bligaard, T.; Nørskov, J. K. Phys. Rev. Lett. **2007**, 99, 016105.

[36] Brønsted, J. N. Chem. Rev. **1928**, 5, 231–338.

[37] Evans, M.; Polanyi, M. Trans. Faraday Soc. **1938**, 34, 11–24.

[38] Michaelides, A.; Liu, Z.-P.; Zhang, C. J.; Alavi, A.; King, D. A.; Hu, P. J. Am. Chem. Soc. **2003**, 125, 3704–3705.

[39] Liu, Z.-P.; Hu, P. J. Chem. Phys. **2001**, 115, 4977–4980.

[40] Liu, Z.-P.; Hu, P. J. Chem. Phys. **2001**, 114, 8244–8247.

[41] Logadottir, A.; Rod, T.; Nørskov, J. K.; Hammer, B.; Dahl, S.; Jacobsen, C. J. Catal. **2001**, 197, 229–231.

[42] Sutton, J. E.; Vlachos, D. G. ACS Catal. **2012**, 2, 1624–1634.

[43] Wang, S. et al. Phys. Chem. Chem. Phys. **2011**, 13, 20760–20765.

[44] van Santen, R. A.; Neurock, M.; Shetty, S. G. Chem. Rev. **2010**, 110, 2005–2048.

[45] Kua, J.; Faglioni, F.; Goddard III, W. A. J. Am. Chem. Soc. **2000**, 122, 2309–2321.

[46] Toulhoat, H.; Raybaud, P. J. Catal. **2003**, 216, 63–72.

[47] Rossmeisl, J.; Logadottir, A.; Nørskov, J. Chem. Phys. **2005**, 319, 178–184.

[48] Rossmeisl, J.; Qu, Z.-W.; Zhu, H.; Kroes, G.-J.; Nørskov, J. K. J. Electroanal. Chem. **2007**, 607, 83–89.

[49] Shustorovich, E. M.; Zeigarnik, A. V. Russ. J. Phys. Chem. **2006**, 80, 4–30.

[50] Jones, G.; Bligaard, T.; Abild-Pedersen, F.; Nørskov, J. K. J. Phys.: Condens. Matter **2008**, 20, 064239.

[51] Sutton, J.; Vlachos, D. J. Catal. **2012**, 297, 202–216.

[52] Xing, B.; Pang, X.; Wang, G. J. Catal. **2011**, 282, 74–82.

[53] Fernández, E.; Moses, P.; Toftelund, A.; Hansen, H. A.; Martínez, J. I.; Abild-Pedersen, F.; Kleis, J.; Hinnemann, B.; Rossmeisl, J.; Bligaard, T.; Nørskov, J. K. Angew. Chem. Int. Ed. **2008**, 47, 4683–4686.

[54] Calle-Vallejo, F.; Inoglu, N. G.; Su, H.-Y.; Martínez, J. I.; Man, I. C.; Koper, M. T. M.; Kitchin, J. R.; Rossmeisl, J. Chem. Sci. **2013**, 4, 1245–1249.

[55] Man, I. C.; Su, H.-Y.; Calle-Vallejo, F.; Hansen, H. A.; Martínez, J. I.; Inoglu, N. G.; Kitchin, J.; Jaramillo, T. F.; Nørskov, J. K.; Rossmeisl, J. ChemCatChem **2011**, 3, 1159–1165.

[56] Vojvodic, A.; Hellman, A.; Ruberto, C.; Lundqvist, B. I. Phys. Rev. Lett. **2009**, 103, 146103.

[57] Medford, A.; Vojvodic, A.; Studt, F.; Abild-Pedersen, F.; Nørskov, J. K. J. Catal. **2012**, 290, 108–117.

[58] Howalt, J. G.; Bligaard, T.; Rossmeisl, J.; Vegge, T. Phys. Chem. Chem. Phys. **2013**, 15, 7785–7795.

[59] Fu, Q.; Cao, X.; Luo, Y. J. Phys. Chem. C **2013**, 117, 2849–2854.

[60] Tritsaris, G.; Nørskov, J.; Rossmeisl, J. Electrochim. Acta **2011**, 56, 9783–9788.

[61] Calle-Vallejo, F.; Martínez, J.; García-Lastra, J.; Abad, E.; Koper, M. T. M. Surf. Sci. **2013**, 607, 47–53.

[62] Tripkovic, V.; Vanin, M.; Karamad, M.; Björketun, M. E.; Jacobsen, K. W.; Thygesen, K. S.; Rossmeisl, J. J. Phys. Chem. C **2013**, 117, 9187–9195.

[63] Fan, C.; Zhu, Y.; Xu, Y.; Zhou, Y.; Zhou, X.-G.; Chen, D. J. Chem. Phys. **2012**, 137, 014703.

[64] Huang, Y.; Du, J.; Ling, C.; Zhou, T.; Wang, S. Catal. Sci. Technol. **2013**, 3, 1343–1354.

[65] Salciccioli, M.; Chen, Y.; Vlachos, D. G. J. Phys. Chem. C **2010**, 114, 20155–20166.

[66] Liu, B.; Cheng, L.; Curtiss, L.; Greeley, J. Surf. Sci. **2014**, 622, 51–59.

[67] Kleis, J.; Jones, G.; Abild-Pedersen, F.; Tripkovic, V.; Bligaard, T.; Rossmeisl, J. J. Electrochem. Soc. **2009**, 156, B1447–B1456.

[68] Grabow, L.; Studt, F.; Abild-Pedersen, F.; Petzold, V.; Kleis, J.; Bligaard, T.; Nørskov, J. K. Angew. Chem. Int. Ed. **2011**, 50, 4601–4605.

[69] Xu, Y.; Fan, C.; Zhu, Y.; Li, P.; Zhou, X.; Chen, D.; Yuan, W. Catal. Today **2012**, 186, 54–62.

[70] Mehmood, F.; Rankin, R. B.; Greeley, J.; Curtiss, L. A. Phys. Chem. Chem. Phys. **2012**, 14, 8644–8652.

[71] Lausche, A.; Medford, A.; Khan, T.; Xu, Y.; Bligaard, T.; Abild-Pedersen, F.; Nørskov, J. K.; Studt, F. J. Catal. **2013**, 307, 275–282.

[72] Liu, H.; Wang, B.; Fan, M.; Henson, N.; Zhang, Y.; Towler, B.; Harris, H. G. Fuel **2013**, 113, 712–718.

[73] Medford, A. J.; Lausche, A. C.; Abild-Pedersen, F.; Temel, B.; Schjødt, N. C.; Nørskov, J. K.; Studt, F. Top. Catal. **2013**, 57, 135–142.

[74] Jones, G.; Studt, F.; Abild-Pedersen, F.; Nørskov, J. K.; Bligaard, T. Chem. Eng. Sci. **2011**, 66, 6318–6323.

[75] Xing, B.; Wang, G.-C. Phys. Chem. Chem. Phys. **2014**, 16, 2621–2629.

[76] Lausche, A.; Hummelshøj, J.; Abild-Pedersen, F.; Studt, F.; Nørskov, J. K. J. Catal. **2012**, 291, 133–137.

[77] Studt, F.; Abild-Pedersen, F.; Wu, Q.; Jensen, A.; Temel, B.; Grunwaldt, J.-D.; Nørskov, J. K. J. Catal. **2012**, 293, 51–60.

[78] Lausche, A.; Abild-Pedersen, F.; Madix, R.; Nørskov, J. K.; Studt, F. Surf. Sci. **2013**, 613, 58–62.

[79] Gómez-Díaz, J.; Vargas-Fuentes, C.; López, N. J. Chem. Phys. **2011**, 135, 124707.

[80] Calle-Vallejo, F.; Martínez, J. I.; García-Lastra, J. M.; Rossmeisl, J.; Koper, M. T. M. Phys. Rev. Lett. **2012**, 108, 116103.

[81] Studt, F.; Abild-Pedersen, F.; Bligaard, T.; Sorensen, R.; Christensen, C. H.; Nørskov, J. K. Science **2008**, 320, 1320–1322.

[82] Studt, F.; Abild-Pedersen, F.; Bligaard, T.; Sørensen, R.; Christensen, C.; Nørskov, J. Angew. Chem. Int. Ed. **2008**, 47, 9299–9302.

[83] Montemore, M. M.; Medlin, J. W. J. Phys. Chem. C **2013**, 117, 2835–2843.

[84] Montemore, M. M.; Medlin, J. W. J. Phys. Chem. C **2013**, 117, 20078–20088.

[85] Ferrin, P.; Nilekar, A.; Greeley, J.; Mavrikakis, M.; Rossmeisl, J. Surf. Sci. **2008**, 602, 3424–3431.

[86] Ferrin, P.; Mavrikakis, M. J. Am. Chem. Soc. **2009**, 131, 14381–14389.

[87] Peterson, A. A.; Nørskov, J. K. J. Phys. Chem. Lett. **2012**, 3, 251–258.

[88] Corvaisier, F.; Schuurman, Y.; Fecant, A.; Thomazeau, C.; Raybau, P.; Toulhoat, H.; Farrusseng, D. J. Catal. **2013**, 307, 352–361.

[89] Falsig, H.; Hvolbæk, B.; Kristensen, I. S.; Jiang, T.; Bligaard, T.; Christensen, C. H.; Nørskov, J. K. Angew. Chem. Int. Ed. **2008**, 120, 4913–4917.

[90] Jiang, T.; Mowbray, D. J.; Dobrin, S.; Falsig, H.; Hvolbæk, B.; Bligaard, T.; Nørskov, J. K. J. Phys. Chem. **2009**, 113, 10548–10553.

[91] Hansen, H. A.; Man, I. C.; Studt, F.; Abild-Pedersen, F.; Bligaard, T.; Rossmeisl, J. Phys. Chem. Chem. Phys. **2010**, 12, 283–290.

[92] Siahrostami, S.; Björketun, M. E.; Strasser, P.; Greeley, J.; Rossmeisl, J. Phys. Chem. Chem. Phys. **2013**, 15, 9326–9334.

[93] Kriek, R. J.; Rossmeisl, J.; Siahrostami, S.; Björketun, M. E. Phys. Chem. Chem. Phys. **2014**, 16, 9572–9579.

[94] Viswanathan, V.; Hansen, H.; Rossmeisl, J.; Nørskov, J. ACS Catal. **2012**, 2, 1654–1660.

[95] Viswanathan, V.; Hansen, H. Top. Catal. **2013**, 57, 215–221.

[96] Hyman, M.; Medlin, J. J. Phys. Chem. C **2007**, 111, 17052–17060.

[97] Skúlason, E.; Bligaard, T.; Gudmundsdóttir, S.; Studt, F.; Rossmeisl, J.; Abild-Pedersen, F.; Vegge, T.; Jónsson, H.; Nørskov, J. K. Phys. Chem. Chem. Phys. **2012**, 14, 1235–1245.

[98] Vojvodic, A.; Medford, A.; Studt, F.; Abild-Pedersen, F.; Khan, T. S.; Bligaard, T.; Nørskov, J. K. Chem. Phys. Lett. **2014**, 598, 108–112.

[99] Falsig, H.; Shen, J.; Khan, T. S.; Guo, W.; Jones, G.; Dahl, S.; Bligaard, T. Top. Catal. **2013**, 57, 80–88.

[100] Michalsky, R.; Zhang, Y.-J.; Peterson, A. A. ACS Catal. **2014**, 4, 1274–1278.

[101] Joshi, Y. V.; Ghosh, P.; Venkataraman, P. S.; Delgass, W. N.; Thomson, K. T. J. Phys. Chem. C **2009**, 113, 9698–9709.

[102] Ferrin, P.; Simonetti, D.; Kandoi, S.; Kunkes, E.; Dumesic, J. A.; Nørskov, J. K.; Mavrikakis, M. J. Am. Chem. Soc. **2009**, 131, 5809–5815.

[103] Liu, B.; Greeley, J. J. Phys. Chem. C **2011**, 115, 19702–19709.

[104] Salciccioli, M.; Vlachos, D. G. ACS Catal. **2011**, 1, 1246–1256.

[105] Salciccioli, M.; Edie, S. M.; Vlachos, D. G. J. Phys. Chem. C **2012**, 116, 1873–1886.

[106] Liu, B.; Greeley, J. Top. Catal. **2012**, 55, 280–289.

[107] Rangarajan, S.; Brydon, R. R. O.; Bhan, A.; Daoutidis, P. Green Chem. **2013**, 16, 813–823.

[108] Liu, B.; Greeley, J. Phys. Chem. Chem. Phys. **2013**, 15, 6457.

[109] Yu, W.; Salciccioli, M.; Xiong, K.; Barteau, M. A.; Vlachos, D. G.; Chen, J. G. ACS Catal. **2014**, 4, 1409–1418.

[110] Chen, Y.; Salciccioli, M.; Vlachos, D. G. J. Phys. Chem. C **2011**, 115, 18707–18720.

[111] Karp, E. M.; Silbaugh, T. L.; Campbell, C. T. J. Am. Chem. Soc. **2014**, 136, 4137–4140.

[112] Hammer, B.; Nørskov, J. K. Adv. Catal. **2000**, 45, 71–129.

[113] Nørskov, J. K.; Lang, N. D. Phys. Rev. B **1980**, 21, 2131–2136.

[114] Vojvodic, A.; Ruberto, C.; Lundqvist, B. I. J. Phys.: Condens. Matter **2010**, 22, 375504.

[115] Shustorovich, E. Russ. J. Phys. Chem. **2007**, 1, 307–329.

[116] Blanksby, S.; Ellison, G. Acc. Chem. Res. **2003**, 36, 255–263.

[117] Grabow, L.; Hvolbæk, B.; Nørskov, J. Top. Catal. **2010**, 53, 298–310.

[118] Howalt, J.; Vegge, T. Beilstein J. Nanotechnol. **2014**, 5, 111–120.

[119] İnoğlu, N.; Kitchin, J. Phys. Rev. B **2010**, 82, 045414.

[120] Miller, S.; İnoğlu, N.; Kitchin, J. J. Chem. Phys. **2011**, 134, 104709.

[121] An, W.; Gatewood, D.; Dunlap, B.; Turner, C. J. Power Sources **2011**, 196, 4724–4728.

[122] Peterson, A. A.; Abild-Pedersen, F.; Studt, F.; Rossmeisl, J.; Nørskov, J. K. Energy Env. Sci. **2010**, 3, 1311–1315.

[123] Hansen, H. A.; Varley, J. B.; Peterson, A. A.; Nørskov, J. K. J. Phys. Chem. Lett. **2013**, 4, 388–392.

[124] van Santen, R. A.; Markvoort, A. J.; Ghouri, M. M.; Hilbers, P. A. J.; Hensen, E. J. M. J. Phys. Chem. C **2013**, 117, 4488–4504.

[125] Cheng, J.; Hu, P.; Ellis, P.; French, S.; Kelly, G.; Lok, C. M. Top. Catal. **2010**, 53, 326–337.

[126] Rossmeisl, J.; Ferrin, P.; Tritsaris, G. A.; Nilekar, A. U.; Koh, S.; Bae, S. E.; Brankovic, S. R.; Strasser, P.; Mavrikakis, M. Energy Env. Sci. **2012**, 5, 8335–8342.

[127] Hummelshøj, J. S.; Abild-Pedersen, F.; Studt, F.; Bligaard, T.; Nørskov, J. K. Angew. Chem. **2012**, 124, 278–280.

[128] Lee, J.; Xu, Y.; Huber, G. Appl. Catal. B: Environ. **2013**, 140-141, 98–107.

[129] Nørskov, J. K.; Rossmeisl, J.; Logadottir, A.; Lindqvist, L.; Kitchin, J. R.; Bligaard, T.; Jónsson, H. J. Phys. Chem. B **2004**, 108, 17886–17892.

[130] Rossmeisl, J.; Karlberg, G. S.; Jaramillo, T.; Nørskov, J. K. Faraday Discuss. **2009**, 140, 337–346.

[131] Karlberg, G.; Rossmeisl, J.; Nørskov, J. K. Phys. Chem. Chem. Phys. **2007**, 9, 5158–5161.

[132] Greeley, J.; Stephens, I.; Bondarenko, A. S.; Johansson, T. P.; Hansen, H. A.; Jaramillo, T. F.; Rossmeisl, J.; Chorkendorff, I.; Nørskov, J. K. Nat. Chem. **2009**, 1, 552–556.

[133] Koper, M. T. M. J. Electroanal. Chem. **2011**, 660, 254–260.

[134] Liu, X.; Meng, C.; Han, Y. J. Phys. Chem. C **2013**, 117, 1350–1357.

[135] Jackson, A.; Viswanathan, V.; Forman, A. J.; Larsen, A. H.; Nørskov, J. K.; Jaramillo, T. F. ChemElectroChem **2014**, 1, 67–71.

[136] Stephens, I. E. L.; Bondarenko, A. S.; Perez-Alonso, F. J.; Calle-Vallejo, F.; Bech, L.; Johansson, T. P.; Jepsen, A. K.; Frydendal, R.; Knudsen, B. P.; Rossmeisl, J.; Chorkendorff, I. J. Am. Chem. Soc. **2011**, 133, 5485–5491.

[137] Halck, N.; Petrykin, V.; Krtil, P.; Rossmeisl, J. Phys. Chem. Chem. Phys. **2014**, DOI: 10.1039/c4cp00571f.

[138] Yoo, J.; Abild-Pedersen, F.; Nørskov, J.; Studt, F. ACS Catal. **2014**, 4, 1226–1233.

[139] Koper, M. T. M. Chem. Sci. **2013**, 4, 2710–2723.

[140] Yu, T. H.; Hofmann, T.; Sha, Y.; Merinov, B. V.; Myers, D. J.; Heske, C.; Goddard III, W. A. J. Phys. Chem. C **2013**, 117, 26598–26607.

[141] Xin, H.; Linic, S. J. Chem. Phys. **2010**, 132, 221101.

[142] Lee, K.; Lee, E.; Song, C.; Janik, M. J. Catal. **2014**, 309, 248–259.

[143] Marshall, S. T.; Medlin, J. W. Surf. Sci. Rep. **2011**, 66, 173–184.

[144] Akpa, B.; D'Agostino, C.; Gladden, L.; Hindle, K.; Manyar, H.; McGregor, J.; Li, R.; Neurock, M.; Sinha, N.; Stitt, E. H.; Weber, D.; Zeitler, J. A.; Rooney, D. W. J. Catal. **2012**, 289, 30–41.

[145] Zope, B.; Hibbitts, D.; Neurock, M.; Davis, R. Science **2010**, 330, 74–78.

[146] Kahsar, K.; Schwartz, D. K.; Medlin, J. W. J. Am. Chem. Soc. **2013**, 136, 520–526.

[147] Drakova, D.; Doyen, G. Surf. Sci. **1990**, 226, 263–185.

[148] Anderson, P. W. Phys. Rev. **1961**, 124, 41–53.

[149] Muscat, J.; Newns, D. Phys. Rev. Lett. **1979**, 43, 2025–2028.

[150] Muscat, J. P.; Newns, D. M. Prog. in Surf. Sci. **1978**, 9, 1–43.

[151] Grimley, T. Proc. Phys. Soc. **1967**, 90, 751–764.

[152] Grimley, T. Prof. Phys. Soc. **1958**, 72, 103–115.

[153] Newns, D. M. Phys. Rev. **1969**, 178, 1123–1135.

[154] Muscat, J.; Newns, D. Phys. Lett. A **1977**, 61, 481–484.

[155] Muscat, J.; Newns, D. Phys. Lett. A **1977**, 60, 348–350.

[156] Muscat, J.; Newns, D. Phys. Rev. B **1979**, 19, 1270–1282.

[157] Fassaert, D. J. M.; van der Avoird, A. Surf. Sci. **1976**, 55, 291–312.

[158] Muscat, J.; Newns, D. Surf. Sci. **1978**, 74, 355–364.

[159] Nørskov, J. Physica **1984**, 127B, 193–202.

[160] Nørskov, J. K. J. Less Common Met. **1987**, 130, 475–490.

[161] Nørskov, J. K. Rep. Prog. Phys. **1990**, 53, 1253–1295.

[162] Somorjai, G. A.; Li, Y. Top. Catal. **2010**, 53, 311–325.

[163] Nørskov, J. K. Prog. in Surf. Sci. **1993**, 44, 5–66.

[164] Nørskov, J. Phys. Rev. B **1982**, 26, 2875–2885.

[165] Nordlander, P.; Holloway, S.; Nørskov, J. Surf. Sci. **1984**, 136, 59–81.

[166] Nørskov, J. K.; Stoltze, P. Surf. Sci. **1987**, 189/190, 91–105.

[167] Jacobsen, K. W.; Nørskov, J. Phys. Rev. Lett. **1987**, 59, 2764–2766.

[168] Lang, N. D.; Holloway, S.; Nørskov, J. Surf. Sci. **1985**, 150, 24–38.

[169] Nørskov, J. J. Chem. Phys. **1989**, 90, 7461.

[170] Bengaard, H. J. Catal. **2002**, 209, 365–384.

[171] Larsen, A.; Kleis, J.; Thygesen, K.; Nørskov, J. K.; Jacobsen, K. W. Phys. Rev. B **2011**, 84, 245429.

[172] Jacobsen, K.; Stoltze, P.; Nørskov, J. K. Surf. Sci. **1996**, 366, 394–402.

[173] Ruban, A.; Hammer, B.; Stoltze, P.; Skriver, H. L.; Nørskov, J. K. J. Molec. Cat. A: Chem. **1997**, 115, 421–429.

[174] Schnur, S.; Groß, A. Phys. Rev. B **2010**, 81, 033402.

[175] Banerjea, A.; Smith, J. Physical Review B **1988**, 6632–6645.

[176] Hammer, B. Top. Catal. **2006**, 37, 3–16.

[177] Hammer, B.; Morikawa, Y.; Nørskov, J. K. Phys. Rev. Lett. **1996**, 76, 2141–2144.

[178] Hammer, B.; Nørskov, J. Nature **1995**, 376, 238–240.

[179] Hammer, B.; Nørskov, J. K. Surf. Sci. **1995**, 343, 211–220.

[180] Ruban, A.; Stensgaard, I.; Lægsgaard, E.; Nørskov, J. K. Surf. Sci. **1999**, 426, 395–409.

[181] Pallassana, V.; Neurock, M.; Hansen, L. B.; Hammer, B.; Nørskov, J. K. Phys. Rev. B **1999**, 60, 6146–6154.

[182] Hammer, B.; Nielsen, O. H.; Nørskov, J. K. Catal. Lett. **1997**, 46, 31–35.

[183] Mavrikakis, M.; Hammer, B.; Nørskov, J. K. Phys. Rev. Lett. **1998**, 81, 2819–2822.

[184] Liu, P.; Logadottir, A.; Nørskov, J. K. Electrochim. Acta **2003**, 48, 3731–3742.

[185] Kitchin, J.; Nørskov, J. K.; Barteau, M. A.; Chen, J. G. J. Chem. Phys. **2004**, 120, 10240.

[186] Nilsson, A.; Pettersson, L.; Hammer, B.; Bligaard, T. Catal. Lett. **2005**, 100, 111–114.

[187] Stamenkovic, V.; Mun, B. S.; Mayrhofer, K. J.; Ross, P. N.; Markovic, N. M.; Rossmeisl, J.; Greeley, J.; Nørskov, J. K. Angew. Chem. **2006**, 118, 2963–2967.

[188] Mason, S. E.; Grinberg, I.; Rappe, A. M. J. Phys. Chem. C **2008**, 112, 1963–1966.

[189] Goda, A. M.; ; Barteau, M. A.; Chen, J. G. J. Phys. Chem. B **2006**, 110, 11823–11831.

[190] Abild-Pedersen, F.; Nilsson, A.; Nørskov, J. K. J. Phys. Chem. C **2012**, 116, 24016–24026.

[191] Toyoda, E.; Jinnouchi, R.; Hatanaka, T.; Morimoto, Y.; Mitsuhara, K.; Visikovskiy, A.; Kido, Y. J. Phys. Chem. C **2011**, 115, 21236–21240.

[192] Xin, H.; Holewinski, A.; Linic, S. ACS Catal. **2012**, 2, 12–16.

[193] del Rosal, I.; Mercy, M.; Gerber, I. C.; Poteau, R. ACS Nano **2013**, 7, 9823–9835.

[194] Xin, H.; Vojvodic, A.; Voss, J.; Nørskov, J. K.; Abild-Pedersen, F. Phys. Rev. B **2014**, 89, 115114.

[195] Andriotis, A. N.; Mpourmpakis, G.; Broderick, S.; Rajan, K.; Datta, S.; Sunkara, M.; Menon, M. J. Chem. Phys. **2014**, 140, 094705.

[196] Ras, E.-J.; Louwerse, M. J.; Mittelmeijer-Hazeleger, M. C.; Rothenberg, G. Phys. Chem. Chem. Phys. **2013**, 15, 4436–4443.

[197] Rangan, M.; Yung, M. M.; Medlin, J. W. Catal. Lett. **2012**, 142, 718–727.

[198] Rangan, M.; Yung, M.; Medlin, J. J. Catal. **2011**, 282, 249–257.

[199] Ras, E.; Louwerse, M.; Rothenberg, G. Catal. Sci. Technol. **2012**, 2, 2456–2464.

[200] Shustorovich, E.; Baetzold, R. Science **1985**, 227, 876–881.

[201] Shustorovich, E. J. Phys. Chem. **1984**, 88, 1927–1929.

[202] Shustorovich, E. J. Phys. Chem. **1984**, 88, 3490–3493.

[203] Shustorovich, E.; Baetzold, R. C. J. Phys. Chem. **1983**, 87, 1100–1113.

[204] Shustorovich, E. J. Phys. Chem. **1982**, 86, 3114–3120.

[205] Haydock, R.; Heine, V.; Kelly, M. J. J. Phys. C: Solid State Phys. **1975**, 8, 2591–2605.

[206] Minot, C.; van Hove, M. A.; Somorjai, G. A. Surf. Sci. **1982**, 127, 441–460.

[207] Papoian, G.; Nørskov, J. K.; Hoffmann, R. J. Am. Chem. Soc. **2000**, 122, 4129–4144.

[208] Zheng, C.; Apeloig, Y.; Hoffmann, R. J. Am. Chem. Soc. **1988**, 110, 749–774.

[209] Hoffmann, R. Rev. Mod. Phys. **1988**, 60, 601–628.

[210] Hoffmann, R. Angew. Chem. Int. Ed. **1987**, 26, 846–878.

[211] Kua, J.; Goddard III, W. A. J. Phys. Chem. B **1998**, 102, 9481–9491.

[212] Kua, J.; Goddard III, W. A. J. Phys. Chem. B **1998**, 102, 9492–9500.

[213] Jackson, B.; Nave, S. J. Chem. Phys. **2011**, 135, 114701–114701–12.

[214] Chen, Y.; Vlachos, D. G. J. Phys. Chem. C **2010**, 114, 4973–4982.

[215] Yang, M.-L.; Zhu, Y.-A.; Fan, C.; Sui, Z.-J.; Chen, D.; Zhou, X.-G. J. Molec. Catal. A: Chem. **2010**, 321, 42–49.

[216] An, W.; Zeng, X. C.; Turner, C. H. J. Chem. Phys. **2009**, 131, 174702.

[217] Yang, M.-M.; Bao, X.-H.; Li, W.-X. J. Chem. Phys. **2007**, 127, 024705.

[218] Cao, D.; Li, Y.; Wang, J.; Jiao, H. Surf. Sci. **2006**, 600, 3226–3234.

[219] Kokalj, A.; Bonini, N.; de Gironcoli, S.; Sbraccia, C.; Fratesi, G.; Baroni, S. J. Am. Chem. Soc. **2006**, 128, 12448–12454.

[220] Bunnik, B.; Kramer, G. J. Catal. **2006**, 242, 309–318.

[221] Durand, W. J.; Peterson, A. A.; Studt, F.; Abild-Pedersen, F.; Nørskov, J. K. Surf. Sci. **2011**, 605, 1354–1359.

[222] Weimer, T.; Specht, M.; Bandi, A.; Schaber, K.; Maier, C. U. Energy Conv. Mgmt. **1997**, 38, S379–S384.

[223] Weimer, T.; Schaber, K.; Specht, M.; Bandi, A. Energy Conv. Mgmt. **1996**, 37, 1351–1356.

[224] Bandi, A.; Specht, M.; Weimer, T.; Schaber, K. Energy Conv. Mgmt. **1995**, 36, 899–902.

[225] Shibata, H.; Moulijn, J.; Mul, G. Catal. Lett. **2008**, 123, 186–192.

[226] Wang, G.-C.; Li, J.; Xu, X.-F.; Li, R.-F.; Nakamura, J. J. Comp. Chem. **2005**, 26, 871–878.

[227] Chen, Z.; Neyman, K.; Lim, K.; Rösch, N. Langmuir **2004**, 20, 8068–8077.

[228] Robinson, J.; Woodruff, D. Surf. Sci. **2002**, 498, 203–211.

[229] Michaelides, A.; Hu, P. J. Chem. Phys. **2001**, 114, 2523–2526.

[230] Pang, X.; Wang, C.; Zhou, Y.; Zhao, J.; Wang, G. J. Molec. Struc. **2010**, 948, 1–10.

[231] Paul, J.; Sautet, P. J. Phys. Chem. B **1998**, 102, 1578–1585.

[232] Xiao, H.; Xie, D. Surf. Sci. **2004**, 558, 15–22.

[233] Gajewski, G.; Pao, C.-W. J. Chem. Phys. **2011**, 135, 064707.

[234] Pascal, M.; Lamont, C.; Kittel, M.; Hoeft, J.; Constant, L.; Polcik, M.; Bradshaw, A.; Toomes, R.; Woodruff, D. Surf. Sci. **2002**, 512, 173–184.

[235] Yang, Q. Y.; Maynard, K.; Johnson, A.; Ceyer, S. J. Chem. Phys. **1995**, 102, 7734–7749.

[236] Sheppard, N.; de la Cruz, C. Adv. Catal. **1998**, 42, 181–313.

[237] Kua, J.; Goodard III, W. J. Phys. Chem. B **1998**, 102, 9492–9500.

[238] Lin, J.-L.; Bent, B. E. Chem. Phys. Lett. **1992**, 194, 208–212.

[239] Chuang, T.; Chan, Y.; Chuang, P.; Klauser, R. J. Electr. Spectr. Relat. Phenom. **1999**, 98-99, 149–173.

[240] Zaera, F. Acc. Chem. Res **1992**, 25, 260–265.

[241] Neurock, M.; van Santen, R. A. J. Phys. Chem. B **2000**, 104, 11127–11145.

[242] Miura, T.; Kobayashi, H.; Domen, K. J. Phys. Chem. B **2000**, 104, 6809–6814.

[243] Li, X.; Gellman, A.; Sholl, D. J. Chem. Phys. **2007**, 127, 144710.

[244] Li, M.; Guo, W.; Jiang, R.; Zhao, L.; Lu, X.; Zhu, H.; Fu, D.; Shan, H. J. Phys. Chem. C **2010**, 114, 8440–8448.

[245] Mei, D.; Sheth, P.; Neurock, M.; Smith, C. M. J. Catal. **2006**, 242, 1–15.

[246] Weaver, J.; Krzyzowski, M.; Madix, R. J. Chem. Phys. **2000**, 112, 396–407.

[247] Jenks, C.; Bent, B. E.; Bernstein, N.; Zaera, F. J. Phys. Chem. B **2000**, 104, 3008.

[248] Solymosi, F.; Klivényi, G. J. Electr. Spectr. Relat. Phenom. **1993**, 64/65, 499–506.

[249] Yang, H.; Whitten, J. Surf. Sci. **1991**, 255, 193–207.

[250] Chao-Ming, C.; Bent, B. E. Surf. Sci. **1992**, 279, 79–88.

[251] Schüle, J.; Panas, I.; Siegbahn, P.; Wahlgren, U. J. Molec. Struc. **1988**, 170, 151–153.

[252] Michaelides, A.; Hu, P. Surf. Sci. **1999**, 437, 362–376.

[253] Kresse, G.; Furthmüller, J. Comp. Mat. Sci. **1996**, 6, 15–50.

[254] Kresse, G.; Hafner, J. Phys. Rev. B **1993**, 47, 558–561.

[255] Blöchl, P. E. Phys. Rev. B **1994**, 50, 17953–17979.

[256] Perdew, J. P.; Chevary, J. A.; Vosko, S. H.; Jackson, K. A.; Pederson, M. R.; Sing, D. J.; Fiolhais, C. Phys. Rev. B **1992**, 46, 6671–6687.

[257] Bader, R. Atoms in Molecules: A Quantum Theory; Clarendon Press: New York, 1990.

[258] Manz, T.; Sholl, D. J. Chem. Theor. Comput. **2010**, 6, 2455–2468.

[259] Tarni, M.; Cignoni, P.; Montani, C. IEEE Trans. Vis. Comput. Graphics **2006**, 12, 1–8.

[260] Ferrighi, L.; xiang Pan, Y.; Gronbeck, H.; Hammer, B. J. Phys. Chem. C **2012**, 116, 7374–7379.

[261] Bryndza, H. E.; Fong, L. K.; Paciello, R. A.; Tam, W.; Bercaw, J. E. J. Am. Chem. Soc. **1987**, 109, 1444–1456.

[262] Lytken, O.; Lew, W.; Campbell, C. T. Chem. Soc. Rev. **2008**, 37, 2172–2179.

[263] Luo, Y.-R. Handbook of Bond Dissociation Energies in Organic Compounds; CRC Press: New York, 2003.

[264] Shultz, J. C.; Houle, F. A.; Beauchamp, J. L. J. Am. Chem. Soc. **1984**, 106, 3917–3927.

[265] Houle, F. A.; Beauchamp, J. L. J. Am. Chem. Soc. **1979**, 79, 4067–4074.

[266] Stowasser, R.; Hoffmann, R. J. Am. Chem. Soc. **1999**, 121, 3414–3420.

[267] Montemore, M. M.; Medlin, J. W. J. Chem. Phys. **2012**, 136, 204710.

[268] Bligaard, T.; Nørskov, J. K. In Chemical Bonding at Surfaces and Interfaces; Nilsson, A., Pettersson, L. G. M., Nørskov, J. K., Eds.; Elsevier, 2008; pp 255–321.

[269] Groß, A. J. Phys.: Condens. Matter **2009**, 21, 084205.

[270] Atkins, P.; Friedman, R. Molecular Quantum Mechanics; Oxford University Press: New York, 2005.

[271] Hudson, R. F. J. Molec. Struc. **1983**, 103, 153–162.

[272] Schmidt, M.; Baldridge, K.; Boatz, J. A.; Elbert, S. T.; Gordon, M. S.; Jensen, J. H.; Koseki, S.; Matsunaga, N.; Nguyen, K. A.; Su, S.; Windus, T. L.; Dupuis, M.; Jr, J. A. M. J. Comp. Chem. **1993**, 14, 1347–1363.

[273] Harrison, W. A. Electronic Structure and the Properties of Solids; W. H. Freeman and Company: San Francisco, 1980.

[274] Ciobîcă, I. M.; Frechard, F.; van Santen, R. A.; Kleyn, A. W.; Hafner, J. Chem. Phys. Lett. **1999**, 311, 185–192.

[275] Lin, J.-L.; Bent, B. E. Chem. Phys. Lett. **1992**, 194, 208–212.

[276] Henderson, M.; Mitchell, G. E.; White, J. M. Surf. Sci. Lett. **1987**, 184, L325–L331.

[277] Kecskés, T.; Barthos, R.; Raskó, J.; Kiss, J. Vacuum **2003**, 71, 107–111.

[278] Bol, C. W. J.; Friend, C. M. J. Am. Chem. Soc. **1995**, 117, 8053–8054.

[279] Lin, Y.; Fan, L.; Shafie, S.; Bertók, B.; Friedler, F. Comp. Chem. Eng. **2009**, 33, 1182–1186.

[280] Zaera, F. J. Molec. Catal. **1994**, 86, 221–242.

[281] Albers, P.; Angert, H.; Prescher, G.; Seibold, K.; Parker, S. F. Chem. Comm. **1999**, 1619–1620.

[282] Driessen, M. D.; Grassian, V. J. Am. Chem. Soc. **1997**, 119, 1697–1707.

[283] Lin, J. L.; Bent, B. E. J. Am. Chem. Soc. **1993**, 115, 6943–6950.

[284] Yang, H.; Whitten, J. J. Am. Chem. Soc. **1991**, 113, 6442–6449.

[285] Zaera, F. Langmuir **1991**, 7, 1998–1999.

[286] De Koster, A.; van Santen, R. A. J. Catal. **1991**, 127, 141–166.

[287] Liu, Z.-P.; Hu, P. J. Am. Chem. Soc. **2002**, 124, 11568–11569.

[288] Cheng, J.; Hu, P.; Ellis, P.; French, S.; Kelly, G.; Lok, C. M. J. Catal. **2008**, 257, 221–228.

[289] Chen, J.; Liu, Z.-P. J. Am. Chem. Soc. **2008**, 130, 7929–7937.

[290] Zhang, W.; Wu, P.; Li, Z.; Yang, J. J. Phys. Chem. C **2011**, 115, 17782–17787.

[291] Yang, M.-L.; Zhu, Y.-A.; Fan, C.; Sui, Z.-J.; Chen, D.; Zhou, X.-G. Phys. Chem. Chem. Phys. **2011**, 13, 3257–3267.

[292] Ge, Q.; Neurock, M.; Wright, H. A.; Srinivasan, N. J. Phys. Chem. B **2002**, 106, 2826–2829.

[293] Wang, W.; Gong, J. Front. Chem. Sci. Eng. **2011**, 5, 2–10.

[294] DeWulf, D.; Jin, T.; Bard, A. J. Electrochem. Soc. **1989**, 136, 1686–1691.

[295] Kaneco, S.; Iiba, K.; Suzuki, S.; Ohta, K.; Mizuno, T. J. Phys. Chem. B **1999**, 103, 7456–7460.

[296] Groß, A. Theoretical Surface Science: A Microscopic Perspective; Springer: New York, 2003.

[297] Nilsson, A., Pettersson, L. G. M., Nørskov, J. K., Eds. Chemical Bonding at Surfaces and Interfaces; Elsevier: Oxford, 2008.

[298] Schwank, J.; Linic, S. J. Am. Chem. Soc. **2009**, 131, 2747–2754.

[299] Mowbray, D. J.; Migani, A.; Walther, G.; Cardamone, D. M.; Rubio, A. J. Phys. Chem. Lett. **2013**, 4, 3006–3012.

[300] Shustorovich, E.; Sellers, H. Surf. Sci. Rep. **1998**, 31, 1–119.

[301] Moqadam, M.; Rahmani, M.; Karimi, Z.; Naderifar, A. Procedia Eng. **2012**, 42, 34–44.

[302] Karp, E.; Silbaugh, T.; Campbell, C. T. J. Am. Chem. Soc. **2013**, 135, 5208–5211.

[303] Kresse, G.; Joubert, D. Phys. Rev. B **1999**, 59, 1758–1774.

[304] Monkhorst, H.; Pack, J. Phys. Rev. B **1976**, 13, 5188–5192.

[305] Xin, H.; Holewinski, A.; Schweitzer, N.; Nikolla, E.; Linic, S. Top. Catal. **2012**, 55, 376–390.

[306] Calle-Vallejo, F.; Koper, M. T. M. Electrochim. Acta **2012**, 84, 3–11.

[307] Gavin, R. M.; Reutt, J.; Muetterties, E. Proc. Natl. Acad. Sci. **1981**, 78, 3981–3985.

[308] İnoğlu, N.; Kitchin, J. R. Molec. Sim. **2010**, 36, 633–638.

[309] Cheng, J.; Hu, P.; Ellis, P.; French, S.; Kelly, G.; Lok, C. M. J. Phys. Chem. C **2008**, 112, 6082–6086.

[310] Quiroga, M. M. B.; Luna, A. E. C. Ind. Eng. Chem. Res. **2007**, 46, 5265.

[311] Rezaei, M.; Alavi, S.; Sahebdelfar, S.; Yan, Z.-F. J. Nat. Gas Chem. **2006**, 15, 327–334.

[312] Bharadwaj, S.; Schmidt, L. J. Catal. **1995**, 155, 403–413.

[313] Yokoyama, C.; Bharadwaj, S.; Schmidt, L. Catal. Lett. **1996**, 38, 181–188.

[314] Bharadwaj, S.; Yokoyama, C.; Schmidt, L. App. Catal. A **1996**, 140, 73–97.

[315] Bhasin, M.; McCain, J.; Vora, B.; Imai, T.; Pujadó, P. R. App. Catal. A **2001**, 221, 397–419.

[316] Yang, M.; Zhu, Y.; Zhou, X.; Sui, Z.; Chen, D. ACS Catal. **2012**, 2, 1247–1258.

[317] Linic, S.; Jankowiak, J.; Barteau, M. J. Catal. **2004**, 224, 489–493.

[318] Kokalj, A.; Gava, P.; de Gironcoli, S.; Baroni, S. J. Catal. **2008**, 254, 304–309.

[319] Nguyen, N. L.; de Gironcoli, S.; Piccinin, S. J. Chem. Phys. **2013**, 138, 184707.

[320] Özbek, M.; van Santen, R. Catal. Lett. **2013**, 143, 131–141.

[321] Christopher, P.; Linic, S. J. Am. Chem. Soc. **2008**, 130, 11264–11265.

[322] Williams, F. J.; Bird, D. P. C.; Sykes, E. C. H.; Santra, A. K.; Lambert, R. M. J. Phys. Chem. B **2003**, 107, 3824–3828.

[323] Lambert, R. M.; Williams, F. J.; Cropley, R. L.; Palermo, A. J. Molec. Catal. A: Chem. **2005**, 228, 27–33.

[324] Gould, T. D.; Lubers, A. M.; Neltner, B. T.; Carrier, J. V.; Weimer, A. W.; Falconer, J. L.; Medlin, J. W. J. Catal. **2013**, 303, 9–15.

[325] Conrad, H.; Ertl, G.; Koch, J.; Latta, E. Surf. Sci. **1974**, 43, 462–480.

[326] Steininger, H.; Lehwald, S.; Ibach, H. Surf. Sci. **1982**, 123, 264–282.

[327] Tang, W.; Sanville, E.; Henkelman, G. J. Phys.: Condens. Matter **2009**, 21, 084204.

[328] Medlin, J. W. ACS Catal. **2011**, 1, 1284–1297.

[329] Monnier, J.; Hartley, G. J. Catal. **2001**, 203, 253–256.

[330] Torres, D.; Lopez, N.; a Francesc Illas,; Lambert, R. M. J. Am. Chem. Soc. **2005**, 127, 10774–10775.

[331] Marimuthu, A.; Zhang, J.; Linic, S. Science **2013**, 339, 1590–1593.

[332] Piccinin, S.; Zafeiratos, S.; Stampfl, C.; Hansen, T. W.; Hävecker, M.; Teschner, D.; Bukhtiyarov, V. I.; Girgsdies, F.; Knop-Gericke, A.; Schlögl, R.; Scheffler, M. Phys. Rev. Lett. **2010**, 104, 035503.

[333] Dellamorte, J.; Lauterbach, J.; Barteau, M. Catal. Today **2007**, 120, 182–185.

[334] Montemore, M. M.; Medlin, J. W. J. Phys. Chem. C **2014**, 118, 2666–2672.

[335] Schock, L.; Marks, T. J. Am. Chem. Soc. **1988**, 110, 7701–7715.

[336] Kristinsdóttir, L.; Skúlason, E. Surf. Sci. **2012**, 606, 1400–1404.

[337] Nilekar, A. U.; Greeley, J.; Mavrikakis, M. Angew. Chem. Int. Ed. **2006**, 45, 7046–7049.

[338] İnoğlu, N.; Kitchin, J. ACS Catal. **2011**, 1, 399–407.

[339] Stolbov, S.; Zuluaga, S. J. Phys. Chem. Lett. **2013**, 4, 1537–1540.

Appendix A

Details on surface properties screened in Chapter 7

A.1 The Surface Properties

The surface properties used in Chapter 7 are listed in Table A.1, along with their description and the other properties they correlate with. Where appropriate, values were taken from Mathematica's Element Database. Properties for the hollow site were calculated by simple averages of properties for the top site. Weighting averages by V_{ad}^2 was also tried, as suggested previously for the d-band center [297]. This resulted in very similar, but slightly worse, results. The Fermi energy is denoted as ϵ_f.

Table A.1: Description and correlations of the surface properties.

Variable	Description	Correlates with[a]
c	Constant (for comparison)	–
ϵ_d	d-Band center	ϵ_d(occ) [0.92], w_d [0.98], ϵ_d^2 [0.92]
ϵ_d(occ)	Center of occupied d states	ϵ_d [0.92], w_d [0.98], w_d(occ) [0.98], HP [0.80], ϵ_d^2 [0.83]
f_d(atom)	Filling of d shell of atom	f_d [0.97], HP [0.84], $w_p(\epsilon_p)$ [0.87], $w_s(\epsilon_s)$ [0.80], r_{cov} [0.81], ρ_p(occ1) [0.93], $\rho_p(2)$ [0.92], V_{ad}^2(OH) [0.86]
f_d	Idealized filling of d band	f_d(atom) [0.97], HP [0.84], $w_p(\epsilon_p)$ [0.90], $w_s(\epsilon_s)$ [0.84], r_{cov} [0.87], ρ_p(occ1) [0.90], $\rho_p(2)$ [0.91], V_{ad}^2(OH) [0.87]
f_d(DFT)	Filling of d band calculated by DFT	–
w_d	d-Band width about ϵ_f	ϵ_d [0.91], ϵ_d(occ) [0.98], w_d(occ) [0.97], HP [0.85]
w_d(occ)	Width of occupied d states about ϵ_f	ϵ_d(occ) [0.98], w_d [0.97]
$w_d(\epsilon_d)$	d-Band width about ϵ_d	w_d(occ, ϵ_d) [0.84]
w_d(occ, ϵ_d)	Width of occupied d states about ϵ_d(occ)	$w_d(\epsilon_d)$ [0.84]
HP	Hybridization parameter[339]	f_d(atom) [0.84], ϵ_d(occ) [0.80], f_d [0.84], w_d [0.85], ϵ_p(occ) [0.80], $w_p(\epsilon_p)$ [0.80], V_{ad}^2(OH) [0.86]
ϵ_p	p-Band center	f_p(DFT) [0.97], ϵ_s [0.87], ϵ_{sp} [0.96]
ϵ_p(occ)	Center of occupied p states	HP [0.80], w_p(occ) [0.98], $w_p(\epsilon_p)$ [0.80], w_p(occ, ϵ_p) [0.80], w_s(occ) [0.82], w_s(occ, ϵ_s) [0.94]
f_p(DFT)	p-Band filling calculated by DFT	ϵ_p [0.97], ϵ_s [0.86], ϵ_{sp} [0.94]
w_p	p-Band width about ϵ_f	–

Table A.1: Description and correlations of the surface properties (continued).

Variable	Description	Correlates with[a]
w_p(occ)	Width of occupied p states about ϵ_f	ϵ_p(occ) [0.98], w_p(occ, ϵ_p) [0.89], ϵ_s(occ) [0.84], w_s(occ) [0.88], w_s(occ, ϵ_s) [0.96]
$w_p(\epsilon_p)$	p-Band width about ϵ_p	f_d(atom) [0.87], f_d [0.90], HP [0.80], HP [0.80], ϵ_p(occ) [0.80], $w_s(\epsilon_s)$ [0.93], r_{cov} [0.84], ρ_p(occ1) [0.82], ρ_p(2) [0.83]
w_p(occ, ϵ_p)	Width of occupied p states about ϵ_p(occ)	ϵ_p(occ) [0.80], w_p(occ) [0.89], ϵ_s(occ) [0.87], w_s [0.88], w_s(occ) [0.90], w_s(occ, ϵ_s) [0.88]
ϵ_s	s-Band center	ϵ_p [0.87], f_p(DFT) [0.86], ϵ_{sp} [0.97]
ϵ_s(occ)	Center of occupied s states	w_p(occ) [0.84], w_p(occ, ϵ_p) [0.87], w_s [0.97], w_s(occ) [0.99], w_s(occ, ϵ_s) [0.83]
f_s(DFT)	Filling of s band calculated by DFT	$w_s(\epsilon_s)$ [0.84]
f_s(atom)	Filling of s shell of atom	–
w_s	s-Band width about ϵ_f	ϵ_s(occ) [0.97], w_s(occ) [0.97], w_s(occ, ϵ_s) [0.81]
w_s(occ)	Width of occupied s states about ϵ_f	ϵ_p(occ) [0.82], w_p(occ) [0.88], w_p(occ, ϵ_p) [0.90], ϵ_s(occ) [0.99], w_s [0.97], w_s(occ, ϵ_s) [0.88]
$w_s(\epsilon_s)$	s-Band width about ϵ_s	f_d(atom) [0.80], f_d [0.84], $w_p(\epsilon_p)$ [0.93], f_s(DFT) [0.84]
w_s(occ, ϵ_s)	s-Band width of occupied states about ϵ_s(occ)	ϵ_p(occ) [0.94], w_p(occ) [0.96], w_p(occ, ϵ_p) [0.88], ϵ_s(occ) [0.83], w_s [0.81]
ϵ_{sp}	Average of ϵ_s and ϵ_p	ϵ_p [0.96], f_p(DFT) [0.94], ϵ_s [0.97]
V_{ad}^2(LMTO)	Tabulated values of V_{ad}^2 (Ref. 112)	V_{ad}^2(OH) [0.80]
V_{ad}^2	Calculated value of matrix coupling element	r_{atom} [0.91]
n	Electron density at C atom in CH_3	n(avg1) [0.84]
n(avg1)	Integrated electron density .5 Å above and below C atom in CH_3	n [0.84]
n(avg2)	Integrated electron density 1 Å below C atom in CH_3	–
a	Lattice constant of base metal	a_{ads} [0.85]
E_{def}(const)	Geometrical deformation energy (constant as perturbation)	E_{def} [0.93]
E_{def}	Geometrical deformation energy (ratio of lattice constant as perturbation)	E_{def}(const) [0.93]
E_{EA}	Electron affinity	–
r_{atom}	Atomic radius	V_{ad}^2 [0.91]
r_{cov}	Covalent radius	f_d(atom) [0.81], f_d [0.87], $w_p(\epsilon_p)$ [0.84], ρ_p(2) [0.80], V_{ad}^2(OH) [0.89]
IA	Ionization energy	χ [0.82]
ρ_{mass}	Mass density	$\lvert V_{ad}^2(\text{OH}) f/(\epsilon_a(\text{OH}) - \epsilon_d)\rvert$ [0.81]
MP	Melting point	–
χ	Pauling electronegativity	IA [0.82], ρ_p(occ2) [0.85]
$\frac{V_{ad}^2 f}{\lvert(\epsilon_a - \epsilon_d)\rvert}$	Perturbation theory term	–
ϵ_d^2	Square of ϵ_d	ϵ_d [0.92], ϵ_d(occ) [0.83]
ϵ_p^2	Square of ϵ_p	–
$V_{ad}^2 f$	–	–
ρ_d(occ1)	Number of occupied d states within 1 eV of ϵ_f	ρ_d(2) [0.82]
ρ_d(occ2)	Number of occupied d states within 0.1 eV of ϵ_f	ρ_d(1) [0.87]
ρ_d(1)	Number of d states within 1 eV of ϵ_f	ρ_d(*occ*2) [0.87]
ρ_d(2)	Number of d states within 0.1 eV of ϵ_f	ρ_d(*occ*1) [0.82]
ρ_p(occ1)	Number of occupied p states within 1 eV of ϵ_f	f_d(atom) [0.93], f_d [0.90], $w_p(\epsilon_p)$ [0.82], ρ_p(occ2) [0.85], ρ_p(1) [0.81], ρ_p(2) [0.89]

Table A.1: Description and correlations of the surface properties (continued).

Variable	Description	Correlates with[a]
ρ_p(occ2)	Number of occupied p states within 0.1 eV of ϵ_f	χ [0.85], ρ_p(occ1) [0.85], $\rho_p(1)$ [0.94], $\rho_p(2)$ [0.89]
$\rho_p(1)$	Number of p states within 1 eV of ϵ_f	ρ_p(occ1) [0.81], ρ_p(occ2) [0.94], $\rho_p(2)$ [0.86]
$\rho_p(2)$	Number of p states within 0.1 eV of ϵ_f	f_d(atom) [0.92], f_d [0.91], $w_p(\epsilon_p)$ [0.83], r_{cov} [0.80], ρ_p(occ1) [0.89], ρ_p(occ2) [0.89], $\rho_p(1)$ [0.86]
ρ_s(occ1)	Number of occupied s states within 1 eV of ϵ_f	–
ρ_s(occ2)	Number of occupied s states within 0.1 eV of ϵ_f	–
$\rho_s(1)$	Number of s states within 1 eV of ϵ_f	–
$\rho_s(2)$	Number of s states within 0.1 eV of ϵ_f	–
a_{ads}	Lattice constant of bonding metal atom	a [0.85]
$\frac{V_{ad}^2(\text{OH})f}{\lvert(\epsilon_a(\text{OH})-\epsilon_d)\rvert}$	Perturbation theory term for OH	ρ_{mass} [0.81]
V_{ad}^2(OH)	Matrix coupling element for OH	f_d(atom) [0.86], f_d, [0.87], $w_p(\epsilon_p)$ [0.86], V_{ad}^2(LMTO) [0.80], r_{cov} [0.89]
$V_{ad}^2(\text{OH})f$	–	–
n_{o}	Electron density at O atom in OH	–
n_{o}(avg1)	Integrated electron density .5 Å above and below O atom in OH	–
n_{o}(avg2)	Integrated electron density 1 Å below O atom in OH	–
V_{dd}^2	d-d Coupling element	–

[a] Parameters that correlate with an $R^2 > 0.80$ are shown, with R^2 given in brackets.

Coupling elements were calculated as:

$$V_{dd}^2 \propto \frac{r_d^6}{d_m^{10}} \tag{A.1}$$

$$V_{ad}^2 \propto \frac{r_d^3}{d^7} \tag{A.2}$$

where r_d is the size of the metal orbitals (previously tabulated[273, 305]), d is the adsorbate-metal distance, and d_m is the metal-metal distance. The values were normalized so that the coupling elements for Cu were 1. We denote the coupling element from CH_3 as V_{ad} and explicitly label it when calculated from other species.

A.2 Single Term Expressions

The accuracy of a using linear fit of each property to predict adsorption energies of CH_3 and OH is shown in Table A.2.

Table A.2: The Accuracy of Using Each Property to Predict CH_3 and OH Adsorption Energies.

Variable	MAE for CH_3	MAE for OH	Variable	MAE for CH_3	MAE for OH	Variable	MAE for CH_3	MAE for OH
c	0.27	0.91	w_s	0.24	0.79	E_{def}(const)	0.25	0.92
ϵ_d	0.15	0.48	w_s(occ)	0.24	0.71	E_{def}	0.24	0.90
ϵ_d(occ)	0.18	0.55	$w_s(\epsilon_s)$	0.19	0.45	E_{EA}	0.21	0.54
f_d(atom)	0.20	0.22	w_s(occ, ϵ_s)	0.21	0.59	r_{atom}	0.22	0.79
f_d	0.20	0.22	ϵ_{sp}	0.21	0.77	r_{cov}	0.22	0.42
f_d(DFT)	0.16	0.42	V_{ad}^2(LMTO)	0.24	0.61	IA	0.23	0.46
w_d	0.19	0.46	V_{ad}^2	0.20	0.74	ρ_{mass}	0.26	0.78
w_d(occ)	0.20	0.59	n	0.24	0.91	MP	0.20	0.82
$w_d(\epsilon_d)$	0.26	0.71	n(avg1)	0.26	0.85	χ	0.23	0.35
w_d(occ, ϵ_d)	0.26	0.90	n(avg2)	0.26	0.65	$\frac{V_{ad}^2 f}{\lvert(\epsilon_a-\epsilon_d)\rvert}$	0.19	0.67
HP	0.18	0.43	a	0.24	0.76	ϵ_d^2	0.14	0.62
ϵ_p	0.21	0.74	ϵ_p^2	0.25	0.91	ρ_s(occ2)	0.27	0.85
ϵ_p(occ)	0.22	0.47	$V_{ad}^2 f$	0.26	0.78	ρ_s(1)	0.26	0.89
f_p(DFT)	0.20	0.72	ρ_d(occ1)	0.22	0.91	ρ_s(2)	0.21	0.86
w_p	0.22	0.85	ρ_d(occ2)	0.19	0.82	a_{ads}	0.25	0.81
w_p(occ)	0.22	0.54	ρ_d(1)	0.17	0.75	$\frac{V_{ad}^2(\mathrm{OH}) f}{\lvert(\epsilon_a(\mathrm{OH})-\epsilon_d)\rvert}$	0.26	0.93
$w_p(\epsilon_p)$	0.21	0.31	ρ_d(2)	0.16	0.85	V_{ad}^2(OH)	0.21	0.44
w_p(occ, ϵ_p)	0.24	0.77	ρ_p(occ1)	0.21	0.30	$V_{ad}^2 f$(OH)	0.22	0.88
ϵ_s	0.22	0.79	ρ_p(occ2)	0.23	0.41	n_{o}	0.25	0.73
ϵ_s(occ)	0.24	0.75	ρ_p(1)	0.22	0.43	n_{o}(avg1)	0.23	0.84
f_s(DFT)	0.17	0.51	ρ_p(2)	0.23	0.25	n_{o}(avg1)	0.27	0.75
f_s(atom)	0.21	0.75	ρ_s(occ1)	0.27	0.85	V_{dd}^2	0.24	0.81

A.3 Multiple Term Expressions

The most accurate multiple term expressions for a given number of non-constant terms are shown in Tables A.3 and A.4, as well as the proposed expressions in the main text and selected other expressions. Expressions were selected to give a sense of which parameters can be used to predict a given adsorbate with a given accuracy, not to show all possibilities. There are often several similar expressions that give similar results; in most of these cases, only one of these expressions was selected. The parameters that were used in the search for the most accurate 6 term expressions were those that were part of any of the 15 to 20 most accurate expressions for 1 to 5 terms.

The surface properties were also screened for their ability to predict C and O adsorption energies in expressions with up to four terms. As can be seen in Table A.4, C behaves similarly to CH_3 and O behaves similarly to OH.

A.4 Different Calculations of V_{ad}^2

Most of the reactivity metrics are adsorbate independent, but V_{ad}^2 is not. Since V_{ad}^2 is a useful metric in many cases, it is worth examining how much it varies between adsorbates. Examining different values for V_{ad}^2 on the homogeneous surfaces, we find that it is correlates strongly for C and CH_3 ($R^2 = 0.90$) as well as O and OH ($R^2 = 0.99$). However, the correlations are weaker for C and O ($R^2 = 0.72$) as well as for CH_3 and OH ($R^2 = 0.78$). The values for O and OH have moderate correlations with V_{ad}^2(LMTO) ($R^2 \approx 0.75$), while the values for C and CH_3 have weaker correlations with V_{ad}^2(LMTO) ($R^2 \approx 0.65$). The matrix coupling values for H in the top site correlate with those for CH_3 on late transition metals, but not on early transition meals, resulting in poor correlation overall. In fact, the values for H in the top site have little correlation with any other values ($R^2 < 0.25$). The values for H in the fcc hollow correlate with CH_3 ($R^2 < 0.62$) and C ($R^2 < 0.73$).

Values of V_{ad} calculated from CH_3 were used for both OH and CH_3, and replacing these with values calculated from OH significantly decreases the accuracy. Apparently CH_3 provides a better

Table A.3: MAEs (in eV) of Using Linear Fits of Multiple Parameters to Predict CH_3 and OH Adsorption Energies in the Top Site.

Number of Terms: Variables	MAE for CH_3	Number of Terms: Variables	MAE for OH
1: c	0.266	1: c	0.912
1[a]: ϵ_d^2	0.137	1[a]: f_d	0.217
2: ϵ_d, w_d(occ,ϵ_d)	0.093	2: f_d(atom), $\frac{V_{ad}^2 f}{\lvert(\epsilon_a-\epsilon_d)\rvert}$	0.154
2: f_d(DFT), ρ_d(occ2),	0.091	2: f_d(atom), IA	0.144
2[a]: w_d, w_d(occ, ϵ_d)	0.082	2[a]: f_d(atom), χ	0.143
3: w_d, w_d(occ,ϵ_d), $\frac{V_{ad}^2 f}{\lvert(\epsilon_a-\epsilon_d)\rvert}$	0.072	3: f_d(atom), ϵ_d^2, $V_{ad}^2 f$	0.120
3[a,b]: ϵ_d, ϵ_p, $V_{ad}^2 f$	0.065	3[a]: f_d, χ, a_{ads}	0.101
4: ϵ_d, ϵ_p, $V_{ad}^2 f$, ρ_d(occ2),	0.059	4[b]: ϵ_d, ϵ_p, $V_{ad}^2 f$, V_{ad}^2	0.095
4[a]: ϵ_d, ϵ_p, $V_{ad}^2 f$, V_{dd}^2	0.058	4: f_d, n_O(avg1), a_{ads}, $V_{ad}^2 f$	0.082
5: ϵ_d(occ), ρ_{mass}, ρ_d(occ1), $\rho_d(1)$, $\rho_d(2)$	0.050	4: HP V_{ad}^2(OH)f, ρ_p(occ2), $V_{ad}^2 f$	0.085
5: ϵ_d, w_d(occ,ϵ_d), w_p, V_{dd}^2, n_O(avg1)	0.048	4[a]: f_d, χ, ρ_d(occ1), $\rho_d(2)$	0.081
5[a]: ϵ_d(occ), ρ_{mass}, ρ_d(occ1), $\rho_d(1)$, $\rho_d(2)$	0.048	5: w_d, w_d(occ), IA, χ, $\rho_p(2)$	0.073
6: ϵ_d, n, ϵ_p, f_p(DFT), ρ_d(occ1), $\rho_p(2)$	0.045	5: f_d, n_o(avg2), $V_{ad}^2 f$, a_{ads}, V_{ad}^2	0.069
6[a]: n, ϵ_p, f_p(DFT), ϵ_d^2, $\rho_d(1)$, $\rho_d(2)$	0.043	5[a]: f_d, n_O(avg1), $\rho_p(1)$, $V_{ad}^2 f$, a_{ads}	0.068
		6: ϵ_d, r_{cov}, χ, ρ_d(occ1), ρ_d(occ2), ρ_p(occ1)	0.069
		6: f_d(atom), f_d(DFT), w_d(occ,ϵ_d), r_{cov}, IA, a_{ads}	0.062
		6[a]: w_d, r_{cov}, χ, ρ_d(occ1), $\rho_d(2)$, ρ_p(occ1)	0.056

[a] The most accurate form with a given number of terms.
[b] The expression proposed in the main text.

Table A.4: MAEs (in eV) of Using Linear Fits of Multiple Parameters to Predict Adsorption Energies of C and O in the FCC Hollow.

Number of Terms: Variables	MAE for C	Number of Terms: Variables	MAE for O
1: c	1.127	1: c	0.912
1: f_s(DFT)	0.675	1: ϵ_d	0.825
1: ϵ_d	0.644	1: χ	0.657
1: V_{ad}^2(C)	0.628	1: ρ_p(occ2)	0.527
1[a]: ϵ_d^2	0.594	1[a]: f_d	0.464
2: ϵ_d, w_d(occ, ϵ_d)	0.350	2: f_d(atom), w_d	0.309
2: ϵ_d, V_{ad}^2(O)f	0.333	2: ϵ_d^2, ρ_p(occ2)	0.306
2[a]: ϵ_d(occ), w_d(occ)	0.317	2[a]: f_d, χ	0.283
3[b]: ϵ_d, ϵ_p, $V_{ad}^2 f$	0.261	3: f_d, χ, $\frac{V_{ad}^2 f}{\lvert(\epsilon_a-\epsilon_d)\rvert}$	0.221
3: ϵ_d, ϵ_p, V_{ad}^2(C)f	0.242	3[a]: ϵ_d, χ, f_d	0.218
3: ϵ_d, a_{ads}, V_{ad}^2(C)	0.228	4[b]: ϵ_d, ϵ_p, $V_{ad}^2 f$, V_{ad}^2	0.208
3[a]: ϵ_d, f_p(DFT), V_{ad}^2(O)f	0.207	4: ϵ_d, f_d(atom), V_{ad}^2, $V_{ad}^2 f$	0.194
4: ϵ_d, MP, ρ_d(occ2), ρ_s(occ2)	0.196	4: f_d(atom), χ, $\frac{V_{ad}^2(O) f}{\lvert(\epsilon_a(O)-\epsilon_d)\rvert}$, V_{ad}^2(O)f	0.194
4[a]: ϵ_d, ρ(occ1), V_{ad}(C)^2, a_{ads}	0.184	4[a]: ϵ_d, f_d(atom), f_s, χ	0.186

[a] The most accurate form with a given number of terms.
[b] The expression proposed in the main text.

measure of the intrinsic adsorbate-metal coupling for a particular metal atom, likely because it only has the attractive term. A slight increase in accuracy for both CH_3 and OH is achieved by using V_{ad}(H, top) instead of V_{ad}, indicating that H may be the best measure of the adsorbate-metal coupling.